-48

NTACT STRESSES FOR CLOSELY NFORMING BODIES--APPLICATION TO CYLINDERS AND SPHERES

FINAL REPORT
UNDER CONTRACT DOT-OS-40093
DECEMBER 1976

This document is available to the U.S. Public through
the National Technical Information Service
Springfield, Virginia 22161

Prepared for

U.S. DEPARTMENT OF TRANSPORTATION
Office of the Secretary
Office of University Research
Washington D.C. 20590

NOTICE

This document is disseminated under the sponsorship of the Department of Transportation in the interest of information exchange. The United States Government assumes no liability for its contents or use thereof.

Technical Report Documentation Page

1. Report No.	2. Government Accession No.	3. Recipient's Catalog No.
DOT-TST-77-48		

4. Title and Subtitle	5. Report Date
CONTACT STRESSES FOR CLOSELY CONFORMING BODIES--APPLICATION TO CYLINDERS AND SPHERES	December 1976
	6. Performing Organization Code
7. Author(s) W. Woodward and B. Paul	8. Performing Organization Report No. MEAM Report 76-1
9. Performing Organization Name and Address Department of Mechanical Engineering and Applied Mechanics--University of Pennsylvania 111 Towne Building Philadelphia, Pennsylvania 19174	10. Work Unit No. (TRAIS)
	11. Contract or Grant No. DOT-OS-40093
12. Sponsoring Agency Name and Address Department of Transportation Program of University Research Office of the Secretary Washington, D. C. 20590	13. Type of Report and Period Covered Final Report
	14. Sponsoring Agency Code OST/TST-60

15. Supplementary Notes

OST Technical Monitor: Clifford Gannett, FRA, RA-43

16. Abstract

Since worn wheels and rails contact conformally, the existing contact stress theories for nonconformal contact are not adequate. In this report a general numerical method of solution for three dimensional, frictionless, conformal, elastic contact problems is presented for the first time. The method is used to analyze the conformal contact of a sphere indenting a spherical seat and a cylinder indenting a cylindrical seat. The results of the sphere-spherical seat problem compared well with experimental data. Results of the cylinder-cylindrical seat problem were in close agreement to a known analytic solution of this problem. For both analyses, results compared favorably with Hertzian theory for problems with small contact regions.

A method is given for defining the boundaries of the large contact regions, and for solving the associated governing singular integral equation of the first kind. A general iterative procedure is developed which converges to the true three dimensional contact region.

In addition the solution to a non-Hertzian contact problem with a multiply connected contact region is solved; namely, the case of two spheres in contact where one of them has a surface defect or pit.

17. Key Words	18. Distribution Statement
Rail wheel interaction, contact stress, conformal contact, elasticity, non-Hertzian contact, pitted sphere	Document is available to the public through the National Technical Information Service, Springfield, Virginia 22161

19. Security Classif. (of this report)	20. Security Classif. (of this page)	21. No. of Pages	22. Price
Unclassified	Unclassified	272	

Form DOT F 1700.7 (8-72) Reproduction of completed page authorized

EXECUTIVE SUMMARY

1. Introduction

This is the final report for Phase I (first year) of a two year effort on Contract DOT-OS-40093, "Improved Wheel and Rail Performance via Control of Contact Stress." The general state of the art prior to the beginning of the project has been summarized in the report "A Review of Rail-Wheel Contact Stress Problems," by B. Paul, FRA-OR&D 76-141, PB251238IAS, April 1975. The present report gives the detailed mathematical theory of a new approach to the higherto unsolved problem of finding the stresses between two closely fitted or "worn-in" metallic surfaces, such as a moderately worn wheel and rail. Before applying the general technique to the wheel-rail problem it is essential to check its validity with simpler geometries such as closely fitting cylinders and spheres, where previous experimental and approximate analytical solutions exist.

2. Problem Statement

The overall objective of the contact is to generate a method for calculating the contact stresses between arbitrarily profiled wheel and rails. In this report a general approach to the problem is formulated, and applied to two specific geometries: (a) a cylinder pressed against a closely fitted cylindrical seat and (b) a sphere pressed against a closely fitted spherical socket. In addition, the stress concentrations induced by the presence of a small defect such as a corrosion pit are calculated for the case of a sphere.

3. Results Achieved

Since worn wheels and rails contact conformally, the existing contact stress theories for nonconformal contact are not adequate. In this report a general numerical method of solution for three dimensional, frictionless, conformal, elastic contact problems is presented for the first time. The method is used to analyze the conformal contact of a sphere indenting a spherical seat and a cylinder indenting a spherical seat. The results of the sphere-spherical seat problem compared well with experimental data and are significantly more accurate than those of a previously published attempt to solve the problem. Results of the cylinder-cylindrical seat problem were in close agreement to a known approximate solution of this problem and agree well

with an existing photoelastic experiment. For both analyses, results compared favorably with Hertzian theory for the limiting case of small contact regions.

A method is given for defining the boundaries of the large contact regions, and for solving the associated governing singular integral equation of the first kind. A general iterative procedure is developed which converges to the true three-dimensional contact region.

In addition the solution to a non-Hertzian contact problem with a multiply connected contact region is solved; namely, the case of two spheres in contact where one of them has a surface defect or pit. The method developed was capable of detecting extremely steep gradients in stress at the defect.

4. Utilization of Results

Better understanding of the contact stress distribution at the interface of wheel and rail could lead to substantial advances in the solution of several key problems in railroad technology. Examples include wheel screech, flange impact noise, wheel and track wear and fatigue failures, deterioration of ride quality and possible derailment due to lateral and longitudinal slippage, increase of headway (and loss of economic capacity) due to adhesion limits in braking and acceleration.

The results of the research has potential for wheel and rail designers, and those doing research and development work in the areas of wheel and rail failures, rail-car dynamics, ride-comfort, and safety.

5. Conclusions

The objectives set for Phase I of the research have been achieved. In addition to the generation of a comprehensive survey report on wheel-rail contact stress phenomena, the work reported on herein successfully tested the validity of a new method for finding contact stresses between closely fitted curved surfaces such as cylinders and spheres. This work is a necessary precursor to the solution of the more complicated geometrical configuration of wheel-rail interfaces, which is the subject of Phase I of this research project.

CONTACT STRESSES FOR CLOSELY CONFORMING BODIES--APPLICATION TO CYLINDERS AND SPHERES

William Woodward and Burton Paul

Department of Mechanical Engineering and Applied Mechanics
University of Pennsylvania
Philadelphia, Pennsylvania

TABLE OF CONTENTS

1. INTRODUCTION

The very large contact stresses which exist between rails and conventional wheels may be calculated by Hertz's analysis when the wheels are new, and the area of contact is small. However, when the wheels are worn, or are initially fabricated with so-called preworn profiles, the contact area will be too large for the Hertzian analysis to be valid. In fact, for this latter case of so-called conformal elastic contact, there is no currently available method for accurately predicting contact stresses. We have therefore undertaken the task of developing general methods for the determination of contact regions, surface deformations, approach[1], and interfacial pressures in conformal (i.e. closely fitting) elastic bodies. In this work[2] we report upon the numerical method developed to date, and show how it may be applied to the case of conformal cylinders, or spheres.

Contact problems can be classified into the following two categories:

i) Problems where one body is elastic and the other is rigid

ii) Problems involving two elastic bodies

In the first class of problems, termed "punch" problems, the

---

[1]The approach" is defined in contact mechanics as the displacement of a point in one body relative to a point on the other body, where both points are far removed from the region of contact.

[2]The essentials of this work constitute the Ph.D. dissertation of W. Woodward at the University of Pennsylvania, 1976.

contact region is known a-priori. In the second class, termed elastic contact problems, the contact region is initially unknown and must be determined. The first widely acclaimed solution to a contact problem was that published by H. Hertz [1881] involving the elastic contact of frictionless bodies with quadratic surfaces. Hertz's solution is centered around the assumption that the dimensions of the contact region are small compared to the radii of curvature of the bodies. Problems for which this assumption is valid are termed "nonconformal" or "counterformal" contact problems. Most solutions that have been found to date are of this type. In contrast, problems not restricted to this assumption are termed "conformal." Following Hertz, solutions to punch problems were analyzed by several Russian authors such as Muskhelishvili [1963]. For detailed accounts of these problems the reader is referred to the excellent reviews of this work by L. A. Galin [1961] and A. I. Lure [1964]. Recently, elastic contact problems involving friction and dynamics have also been analyzed. In a recent publication, Kalker [1975] categorizes the solutions to date and identifies the areas within contact mechanics which need investigation. His comparison reveals that the areas involving friction, plasticity, visco-elasticity and large deformations are in most need of study. Kalker does not review the analysis of conformal contact problems in his survey. It should be noted that the uniqueness theorem of Kirchoff (not intended for contact problems) was extended only recently to include general frictionless, elastic contact problems by Kalker [1971].

This dissertation centers on providing a general numerical method of solution to conformal frictionless contact problems. The literature in the areas mentioned above is far too comprehensive to review in this brief introduction, instead the interested reader is referred to the aforementioned surveys. The remainder of this discussion will be devoted to a more detailed discussion of the existing numerical solutions and the limited literature on conformal contact problems.

With the advent of the digital computer several numerical techniques have been developed to analyze a more general class of contact problems. Conry and Seireg [1971] have examined elastic contact in terms of a linear programming model. Their method is general in scope, however, the only examples which were analyzed were Hertzian or one dimensional beam problems.

Kalker and van Randen [1972] derived a variational principle for both linear and non-linear elastic contact problems. For the case of linear elasticity the principle takes the form of an infinite dimensional convex quadratic programming problem. They successfully solved both a Hertzian and non-Hertzian problem. It was concluded that the solution yielded accurate values of approach, maximum pressure and applied force; however, the actual contact area was not determined with great accuracy.

Finite element techniques have also been adapted to solve contact problems by Chan and Tuba [1971] and more recently by Chaud, Haug and Rim [1974]. Both methods are general in that they are

reported to be able to handle problems which fall into the domain of finite element analysis such as analyzing non-isotropic, non-homogeneous media or problems with plasticity and creep, however, both works report only examples which are composed of isotropic materials stressed within the range of linear elasticity.

Tuba and Chan compare their computed results to photo elastic studies and concluded that trends were identical but the results lacked close agreement. Chaud et al, analyzed the non-Hertzian problem of a human knee joint and the contact between two half spaces where one half space has three bumps on the surface. The contact area in the latter case found in photo elastic studies had good general agreement with their computed results.

A general method of solution of non-Hertzian, non-conformal elastic contact problems was developed by Singh and Paul [1974]. They considered the classical contact criterion (which includes that of Hertz) for arbitrary surface geometries. In order to solve the governing integral equation of the first kind, which belongs to the class of "ill posed" or "Hadamard incorrect" problems, they introduced three different numerical schemes. The first "simply-discretized method" was found to be relatively unstable for the particular problems they investigated. In order to overcome this difficulty, Singh and Paul [1973-74] introduced two other methods of solving ill posed integral equations, called the "Redundant Field Point method" and the "Functional Regularization method"; the latter of which is based on Tychonov's regularization procedure.

In contrast to counterformal problems are those of the "conformal" type; i.e., those where the dimensions of the contact region can be large compared to the smallest radii of curvature of the contacting bodies. Relatively few solutions to conformal contact problems have been published. A brief summary of all elastic conformal problems, known to the author, follows.

An elastic sphere indenting an elastic seat has been solved by Goodman and Keer [1965]. They present results for the half angles of contact up to 20 degrees and provide experimental results which generally agree with their solutions. Improvements to the Hertzian theory are discussed--in particular, the problem which arises when one tries to include terms of higher order than those used in the "half space solution" (of Boussinesq) which is fundamental to the Hertzian solution. It is noted that there are higher order terms in the exact formulation of the sphere problem which do not appear in the formulation if the half space assumption is used without truncating terms. These terms are particular to the spherical geometry. Goodman and Keer justify their extension of the Hertzian theory through analysis of these second order terms.

The conformal contact of an elastic cylinder indenting a cylindrical seat was first analyzed by Sjtaerman [1940] and more recently by Persson [1964]. Sjtaerman and Persson derived the identical "contact criterion" but both proceeded in different ways to solve the equation. Sjtaerman formulated the displacements in terms of integrals of the influence functions and used finite difference

techniques to solve the resulting integral equation for the unknown pressure distribution. On the other hand, Persson assumed the contact region to be cylindrical in shape and formulated the criterion as an integro-differential equation from which he found analytic expressions for the pressure field. The earlier solution of Sjtaerman appears to be less accurate, possibly because he published before the digital computer was invented and may have been forced to use a too crude finite difference mesh.

Recently, a number of problems involving a disc in an infinite plate under tension have been solved by finite element techniques. Chan and Tuba [1971] analyzed a plate under tension with a shrink fit disc located in the center. They present results which show good agreement between their computed values of circumferential stress and the exact solution, however, there is a larger discrepancy between the computed value of compressive stress and the exact solution. In fact the compressive stress on each body for any one angle does not in general agree.

Chaud et al [1974] have analyzed the problem of a plate under tension with either a loose or full inclusion. They show good agreement between their predicted contact stress and experimental results for a contact angle of 20 degrees.

The goal of this research is to develop a general method of analysis for frictionless, conformal contact problems. In particular, the method developed is to be used in future research on the analysis of interfacial contact stresses between a railway wheel and rail. The

concepts of Hertz's classical geometric formulation of the contact criterion are extended to non-planar surfaces resulting in a singular integral equation of the first kind. The solution is dependent on identifying the influence functions for surface point displacements in the region of the contact area. A numerical appraoch to generating influence functions is developed and the accuracy of the generated functions is shown to be good for those cases where analytic solutions are known. The simply discretized method of Singh and Paul [1973] was used for solution of the integral equation. The solutions using this formulation were compared to Hertz's solutions for limiting cases involving small contact regions.

The results of the present general method are compared to available analytic solutions to specific problems involving the contact of an elastic cylinder in seat and a sphere in seat.

In addition, a solution was found to a noncomformal problem with a multiply connected contact region. The proper boundary iteration which is necessary to arrive at a unique solution is developed and discussed. The specific example analyzed is a pitted sphere in contact with a sphere. The significance of pit geometries on the contact stress are illustrated.

In summary, the main contributions of this disseration are:

1. A general numerical method for solution of frictionless conformal elastic contact problems is presented

2. Numerical influence functions needed for solutions of problems with cylindrical and spherical surface geometries were generated and their accuracy was verified by comparison to exact analytic solutions when they existed
3. In its application to the specific problems of a sphere indenting a spherical seat and a cylinder indenting a cylindrical seat, it was shown that this method produces accurate values of contact pressure approach, displacements, strains and applied force
4. The problem of a pitted sphere indenting a sphere was solved for the first time and the appropriate boundary iteration for multiply connected contact regions was established

Chapter 2 contains a brief review of the previous non-conformal methods of solution presented by Singh and Paul [1973-74]. The conformal contact theory which is the basis of this work is formulated in chapter 3. The generation of influence functions which are necessary to the solution of the sphere and cylinder problems is discussed in chapter 4. Chapters 5 and 6 contain solutions to the examples of a sphere indenting a conformal spherical seat and a cylinder indenting a conformal cylindrical seat respectively. A contact problem involving a multiply connected contact region is solved in chapter 7. The conclusions of this work are presented in chapter 8.

2. FORMULATION AND SOLUTIONS FOR NON-CONFORMAL CONTACT PROBLEMS

2.1 Introduction

The basic equation for non-conformal contact theory is developed in this chapter along with a method of solution. Hertz [1881] has shown that the governing equation is an integral equation of the first kind. Hertz found an analytical solution to this equation for the special case where the surfaces may be modelled as locally quadratic; however, the integral equation itself applies to any non-conformal contact problem and has been solved by Singh and Paul [1974] for non-conformal, non-Hertzian contact problems. The method of solution outlined here is that developed by Singh and Paul and is termed the "Simply-Discretized" or "S.D." method. They proved that the S.D. method can become unstable; they applied a stabilizing technique termed the "Functional Regularization" or "F.R." method, when the S.D. method proved unstable and successfully solved several problems. The "Functional Regularization" method is also summarized in this chapter.

In addition to presenting the basic integral equation for non-conformal contact, the material in this chapter introduces the concepts of contact theory which will be used in the development of the governing integral equation for conformal contact in chapter 3. Furthermore, the "Simply-Discretized" method of solution will be used

in solving the conformal contact problems presented in chapters 5 and 6 and in the non-conformal contact problem with a multiply connected contact region in chapter 7.

2.2 The Governing Equation for Non-conformal Contact Theory

Consider two frictionless non-conforming bodies initially in contact at a single point. Loading each body such that the resultant force acts through the initial point of contact produces deformations in the neighborhood of the initial point of contact. The area of contact between the bodies will increase from a single point to a finite area. In non-conformal contact theory it is assumed that the dimensions of the contact area are small compared to the local radii of curvature of the two contacting surfaces. After deformation, the two bodies undergo a localized elastic deformation and a rigid body displacement. The rigid body displacement is referred to as the "approach" in contact mechanics.

In general the geometry of the surfaces before deformation and the applied thrust is known, while the actual contact area, the pressure distribution within this area, and the approach δ are unknown. The governing equation for non-conformal contact relates the approach, the contact area, the surface geometry and the interfacial pressure distribution.

Consider body 1 and body 2 initially in non-conformal contact at a point O. (Fig. 2.1) Let a right-hand cartesian coordinate system $(\hat{x}_1, \hat{y}_1, \hat{z}_1)$ be constructed such that the x_1 - y_1 plane lies tangent to body 1 at point O and has point O as its origin. Let $\hat{z}_1$ be

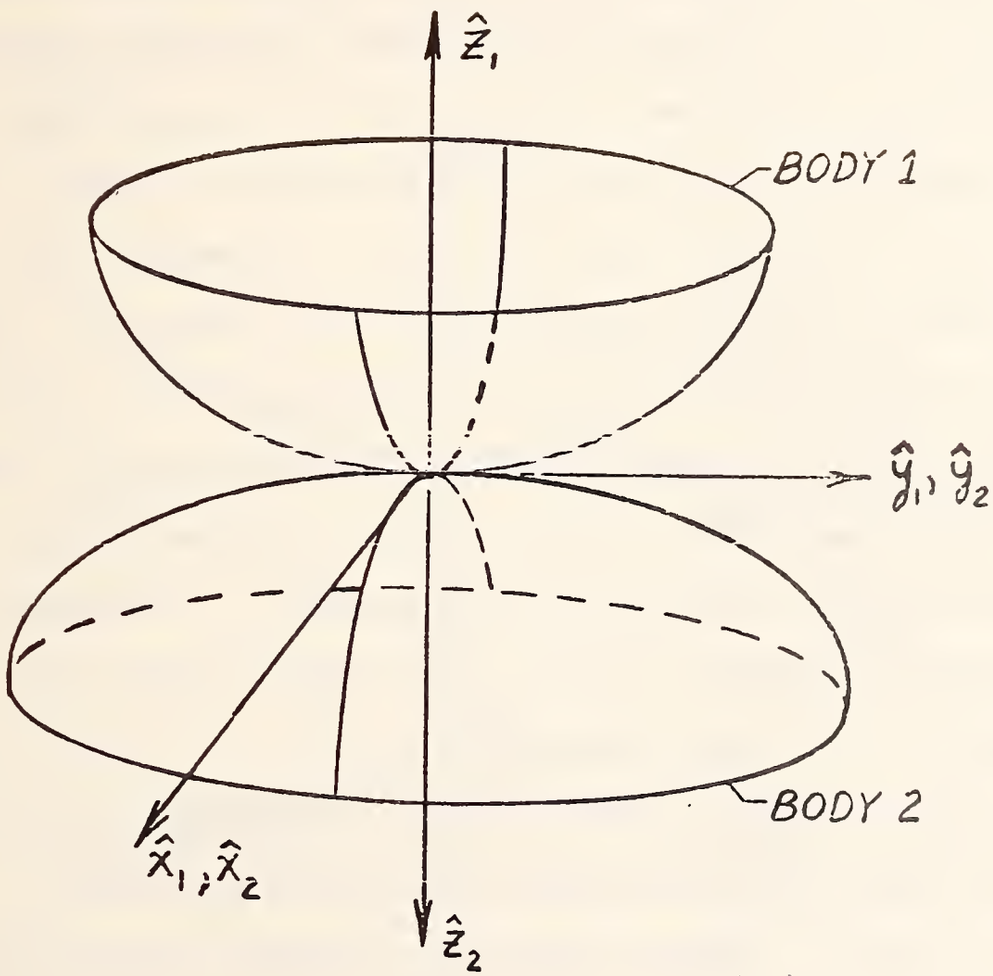

Fig. 2.1. Coordinate systems for non-conformal contact

the unit inward normal to body 1. Also define a left-handed coordinate system $(\hat{x}_2, \hat{y}_2, \hat{z}_2)$ such that $\hat{x}_2 = \hat{x}_1$, $\hat{y}_2 = \hat{y}_1$, and $\hat{z}_2 = -\hat{z}_1$. Now examine a cross section of the contacting bodies through the point O as shown in figure 2.2. It is assumed that points on the surfaces of bodies 1 and 2 which merge after deformation are located at the same (x, y) coordinates. The displacements due to the contact phenomena of a point A on body 1 and B on body 2 which merge after deformation, will be examined closely in the following paragraphs.

Consider the change in the position of point A on body 1 after a load F is applied. Due to the elastic deformation of the surface, point A moves the distance $\overline{A'A''}$ in the z_1 direction. This elastic deformation will be labeled w_1. Also point A moves a distance $\overline{AA'}$ due to rigid body motion, labeled Δ_1. Similarly on body 2 a point B displaces an amount $\overline{B'B''}$ or w_2 due to elastic deformation and displaces from B to B' due to a rigid body motion Δ_2. Therefore, considering the total motion of points A and B, point A moves a total distance $w_1 + \Delta_1$ and point B moves $w_2 + \Delta_2$.

Having traced the motion of points on the surfaces of the contacting bodies, these motions may be related to the surface geometry to obtain a necessary condition for contact of the two surfaces. Note that points A and B are initially separated by a distance equal to $f_1(x, y) + f_2(x, y)$ where $f_1(x, y)$ and $f_2(x, y)$ are termed the "profile functions" of the two surfaces. $f_1(x, y)$

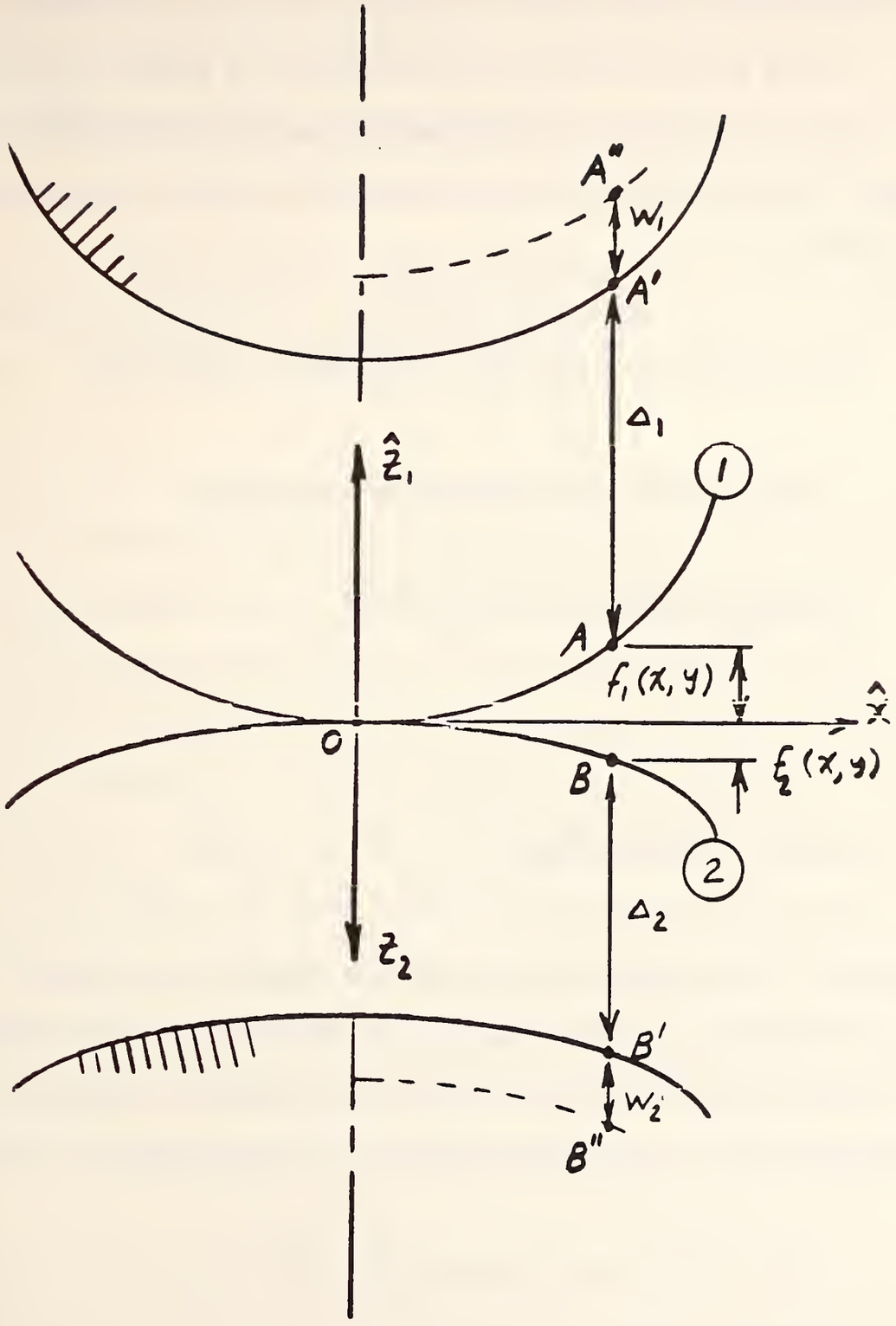

Fig. 2.2. Kinematics of surface point displacements in non-conformal contact.

represents the $\hat{z}_1$ coordinate of a point (x, y, z_1) on the surface of body 1, while $f_2(x, y)$ is the $\hat{z}_2$ coordinate of a point (x, y, z_2) on the surface of body 2. After deformation the initial separation changes. Consider the final separation, S, of points A and B after deformation

$$S = f_1(x, y) + f_2(x, y) + (W_1 + \Delta_1) + (W_2 + \Delta_2) \tag{2.1}$$

Define a function f (x, y) and a scalar δ such that

$$f(x, y) = f_1(x, y) + f_2(x, y) \tag{2.2}$$

and

$$\delta = -(\Delta_1 + \Delta_2) \tag{2.3}$$

The scalar δ is termed the "approach" and physically represents the distance that points on one body move parallel to the z_1 axis towards points on the other body due to rigid body movement. Rewriting equation (2-1) by substituting equations (2-2) and (2-3),

$$S = f(x, y) + (W_1 + W_2) - \delta \tag{2.4}$$

By assumption in non-conformal contact theory, the contact area is small compared to the local radii of curvature of the contacting

bodies. Therefore, it is appropriate to replace these displacements with the displacement field of an elastic half space due to some pressure distribution p (x, y) over an area Ω_i. Hence,

$$W_i(x,y) = \frac{(1-\nu_i^2)}{\pi E_i} \int_{\Omega_i} \frac{P(x',y')\,dx\,dy}{\sqrt{(x-x')^2+(y-y')^2}} \qquad (2.5)$$

where E_i and ν_i are the Young's modulus and Poisson's ratio for body i. It is reasonable to neglect the displacements in the $(x_1 - y_1)$ plane and assume that points A and B, located at equal $\hat{x}_1, \hat{y}_1$ coordinates, will merge after deformation since the displacements in the $(x_1 - y_1)$ plane on each body are nearly equal in magnitude and direction. The pressure distribution in equation (2.5) is over the contact region Ω_i on body i, however $\Omega_1 = \Omega_2$. Furthermore, since the radii of curvature of the bodies are large compared to the dimensions of the contact area and the radius of curvature of the contact patch is still larger owing to the non-conformal nature of the contact, the contact area may be represented by Ω, the projection of Ω_1 onto the $x_1 - y_1$ plane. Substituting equation (2.5) into equation (2.4) the separation

becomes:

$$S = f(x,y) + k\int_{\Omega}\frac{P(x',y')\,dx'dy'}{\sqrt{(x-x')^2+(y-y')^2}} - \delta \qquad (2.6)$$

where

$$k = \frac{(1-\nu_1^2)}{\pi E_1} + \frac{(1-\nu_2^2)}{\pi E_2}$$

If Ω is known then equation (2.6) is an integral equation of the first kind and is the governing equation for non-conformal contact. The separation of two points within the contact region has to be zero while the pressure has to be positive, i.e., the bodies can only exert compressive forces on one another within the contact region. Outside the contact region, S must be positive while the pressure distribution must equal zero.

These boundary conditions may be summarized as follows:

$$S = 0 \qquad \text{INSIDE } \Omega \qquad (2.7a)$$

$$S > 0 \qquad \text{OUTSIDE } \Omega \qquad (2.7b)$$

$$P(x,y) > 0 \qquad \text{INSIDE } \Omega \qquad (2.7c)$$

$$P(x,y) = 0 \qquad \text{OUTSIDE } \Omega \qquad (2.7d)$$

The solution of a non-conformal contact problem for a given thrust requires the determination of the unknown contact region Ω, the pressure distribution p (x, y), and the approach δ. These quantities must all satisfy equation (2.6) and the boundary conditions (2.7). General numerical solutions to equation (2-6) are explained in sections 2.3 and 2.4.

2.3 The "Simply-Discretized" Method of Solution of Singh and Paul

The general non-conformal contact problem as posed in equation (2.6) and boundary conditions (2.7) has been solved by Singh and Paul by the "Simply-Discretized" method. This method is a semi inverse solution which will be explained in the following paragraphs.

Given that two bodies of known shape are brought into contact with one another and held there by a force F, the task remains to locate the boundary of the contact region Ω and to find the interfacial pressure distribution p (x, y) and the approach δ. The "Simply-Discretized" method is called a semi inverse method because the contact area is assumed to be some logical "candidate" region whereupon the pressure distribution and approach are then found via equation (2.6). The force F is then calculated from the integral of the pressure distribution over the area Ω. The initial guess of the logical "candidate" contact region Ω is then checked to see if the values of the separation satisfy equation (2.7a) and (2.7b). If they do not, the "candidate" region can be modified to better approximate the true

contact region and the solution procedure is repeated. Now consider the details of this solution.

The first step in solving equation (2.6) by the "Simply-Discretized" method is to find an approximation to the contact region Ω. Singh and Paul used the $x_1 - y_1$ plane projection of an "interpenetration curve" formed by the intersection of the two surfaces when one body was allowed to mathematically interpenetrate the other. Increasing the depth of interpenetration would increase the contact area. Each interpenetration depth would provide one "candidate" contact area corresponding to one loading F on the bodies. This concept of interpenetration is physically meaningless in a contact problem since the bodies can not actually interpenetrate one another; it is only a method which enables one to find an approximation to the contact area.

Having found a "candidate" contact region the next task is to find the pressure distribution and approach in equation (2.6). A "Simply-Discretized" solution is obtained by assuming a piecewise constant pressure distribution over the area Ω. Dividing up the contact area Ω into N cells and assuming the pressure p (x, y) to be constant within each cell equation (2.6) becomes

$$\sum_{i=1}^{N} k P_i \int_{\Omega_i} \frac{dx'dy'}{\sqrt{(x-x')^2+(y-y')^2}} - \delta + f(x+y) = 0 \qquad (2.8)$$

where

$$k = \frac{(1-\nu_1^2)}{\pi E_1} + \frac{(1-\nu_2^2)}{\pi E_2} \tag{2.9}$$

and

P_i is the constant pressure in cell i.

In equation (2.8) there are N unkown P_i's and 1 unknown δ, thus a total of N + 1 unknowns. However, equation (2.8) applies to every point (x, y) inside Ω, thus it can be written for N + 1 "field points" inside the contact region. Singh and Paul chose the centroids of the N cells as N of the field points and picked a last field point at the intersection of several cells. The integrals in equation (2.8) can be evaluated numerically to provide the coefficients for this set of linear equations. Thus equation (2.8) can be expanded to the form

$$b_{ij} P_j - \delta = -f_i \quad (i, j = 1, N) \tag{2.10}$$

where

$$b_{ij} = k \int_{\Omega} \frac{dx'\, dy'}{\sqrt{(x_i - x')^2 + (y_i - y')^2}}$$

P_j is the pressure in cell j

f_i is the initial separation of the centroid of cell i

Ω_j is the area of cell j

(x_i, y_i) are the coordinates of the centroid cell i

and

$$V_i P_i - \delta = -f_{N+1} \qquad (i = 1, N) \tag{2.11}$$

where

$$V_i = \int_{\Omega_i} \frac{dx'\, dy'}{\sqrt{(x_0 - x')^2 + (y_0 - y')^2}}$$

(x_0, u_0) are the coordinates of the N + 1 field point

f_{N+1} is the initial separation of the N + 1 field point

Combining equations (2.10) and (2.11) into one set of linear equations in P_i and δ, the unknown P_i and δ can be found, in principle, by using standard Gaussian elimination. This is done by first substracting equation (2.11) from equation (2.10), thus eliminating δ from all equations. The new set of N equations formed can be written as

$$\sum_{j=1}^{N} B_{ij} P_j = f_i' \qquad (i = 1, N) \tag{2.12}$$

where

$$f_i' = -f_i + f_0 \qquad (i = 1, N)$$

$$B_{ij} = b_{ij} - V_j \qquad (i, j = 1, N)$$

Equation (2.12) is a set of N linear equations in N unknown P_i's. After solving this set of equations for the pressure field, the approach δ may be found by back substitution of these pressures into equation (2.11).

Having obtained the pressure distribution and approach the original "candidate" contact region Ω can be verified via the boundary conditions (2.7a, b). The "candidate" contact region can be reduced if the pressure is less than zero at the boundary of Ω or it can be extended if the separation is negative outside the boundary of Ω. The problem can be solved again if necessary to find the pressure distribution in the connected region Ω. When the true contact area is found the total force applied to the bodies can be computed by integrating the pressure over the contact area, i.e.,

$$F = \int_{\Omega} P(x, y)\, dx\, dy = \sum_{i=1}^{N} P_i A_i \qquad (2.13)$$

where

A_i is the area of cell i.

In applying the S.D. method to a variety of problems, Singh and Paul found that it was numerically unstable in the general case. For small cell densities the solutions obtained were good; however, as the cell density was increased, the solutions broke down. The pressure distribution became very erratic, changing from positive values to

negative values from cell to cell. The details of these results were recorded by Singh [1972] and Singh and Paul [1973] [1974]. One method for eliminating the problem of ill-conditioning is known as the "Functional Regularization" method which will be explained in section 2.4.

2.4 "Functional Regularization"

The "Functional Regularization" method is a technique of stabilizing an ill-conditioned set of linear equations. This method was developed by Singh and Paul [1973] in order to extract a sensible solution from the unstable "Simply-Discretized" method of solving non-conformal contact problems.

The "Simply-Discretized" method yields solutions which have wide variations in the pressure fields. Furthermore, it was observed that small perturbations in the coefficient matrix B of equation (2.12) produce completely different pressure fields which also vary radically from cell to cell. Although the determinant of the coefficient matrix was not singular, it appeared that there were many solutions to the set of equations generated by the "Simply-Discretized" method of solution. In order to find the correct solution vector of a large number of vectors that satisfy the linear equation set, the F.R. method exploits the "smoothness" property of the pressure distribution. The F.R. method seeks to approximately solve the original set of equations while it simultaneously minimizes the difference between the pressure in neighboring cells. This is accomplished by introducing a function Φ

such that

$$\Phi = \sum_i (P_i - P_{i+1})^2 \tag{2.14}$$

Solving the equation set (2.12) is equivalent to finding a solution to equation (2.15) which produces an ε^2 of exactly zero.

$$\varepsilon^2 = \sum_{i,j,k} [B_{ij} P_j - f_i][B_{ik} P_k - f_i] \tag{2.15}$$

"Functional Regularization" seeks an approximate solution to equation (2.15) such that both ε^2 and Φ are small quantities. Mathematically, this is equivalent to minimizing a functional

$$\psi(P_i) = [B_{ij} P_j - f_i]^2 + \upsilon \Phi(P_i) \tag{2.16}$$

where

υ is a small parameter which controls the influence of the constraint function Φ. Minimizing ψ implies finding the vector P_i such that $\frac{d\psi}{d P_i}(P_j) = 0$ or solving the equation set

$$B_{ij} B_{il} P_j + \frac{\upsilon}{2} \frac{d\Phi(P_i)}{d P_i} = B_{il} F_i \quad (l = 1, N) \tag{2.17}$$

Bounds for the parameter υ have been given by Singh and Paul [1973].

The solution to equation (2.17) is stable in that it yields a smoothly varying positive pressure distribution which is physically realistic. Singh and Paul [1973-74] have shown that it closely agrees with the exact solution for several Hertzian contact problems.

3. FORMULATION OF CONFORMAL CONTACT PROBLEM

3.1 Introduction

The development of nonconformal contact theory was based on the assumption that the dimensions of the contact area are small compared to the local radii of curvature of the contacting surfaces. This assumption is no longer valid in conformal contact. By its very nature, conformal contact can produce contact areas with dimensions as large as the radii of curvature of the surfaces. Because of this assumption in the nonconformal theory it was appropriate to approximate the contacting surfaces by two elastic half spaces and to use the Boussinesq displacement function for a point load on a plane as the influence function[1] necessary for the calculation of the displacement field. In conformal contact theory the contact region cannot be approximated by a plane, and alternative influence functions for the surfaces must be found.

Furthermore, no longer can the displacements tangent to the surface be considered small as was the case in nonconformal theory. A solution procedure must incorporate both the normal and tangential displacements of the contacting surfaces in the solution.

Presented in the following sections of this chapter is a

---

[1] The "influence function" relates the surface tractions to the displacement field. It may be sometimes referred to as a "Green's function."

formulation for conformal contact theory which not only incorporates the true influence function for conformal surfaces but also accounts for the surface displacements both normal and tangent to the surface.

3.2 Assumptions in Conformal Contact Theory

Consider two contacting bodies, labeled 1 and 2, which have closely conforming surfaces, i.e., they exhibit conformal contact. The initial point of contact will be labeled 0. Figure 3.1 represents a cross section through 0 of the two surfaces. A coordinate system is constructed such that $\hat{z}$ is the inward unit normal to body 1 at 0 and unit normal $\hat{y}$ lies in the plane of the cross section at 90° clockwise of $\hat{z}$. The intersection of the surfaces of body 1 and 2 with planes through the $\hat{z}$ axis will be termed the "contour curves" of the respective surfaces. The following assumptions will be made:

1. The surfaces are assumed to be frictionless
2. The line of the applied load on the bodies in contact passes through 0 (fig. 3.1)

Considering only frictionless surfaces reduces the complexity of the contact problem significantly, yet it does not destroy the usefulness of the solution. It is often desirable to have frictionless surfaces in contact applications. For example, in the situations involving bearing surfaces, such as ball bearings or ball joints, the surfaces are machined and lubricated to minimize surface friction. This assumption dictates that no shear tractions can be applied to the surface of either body within the contact region.

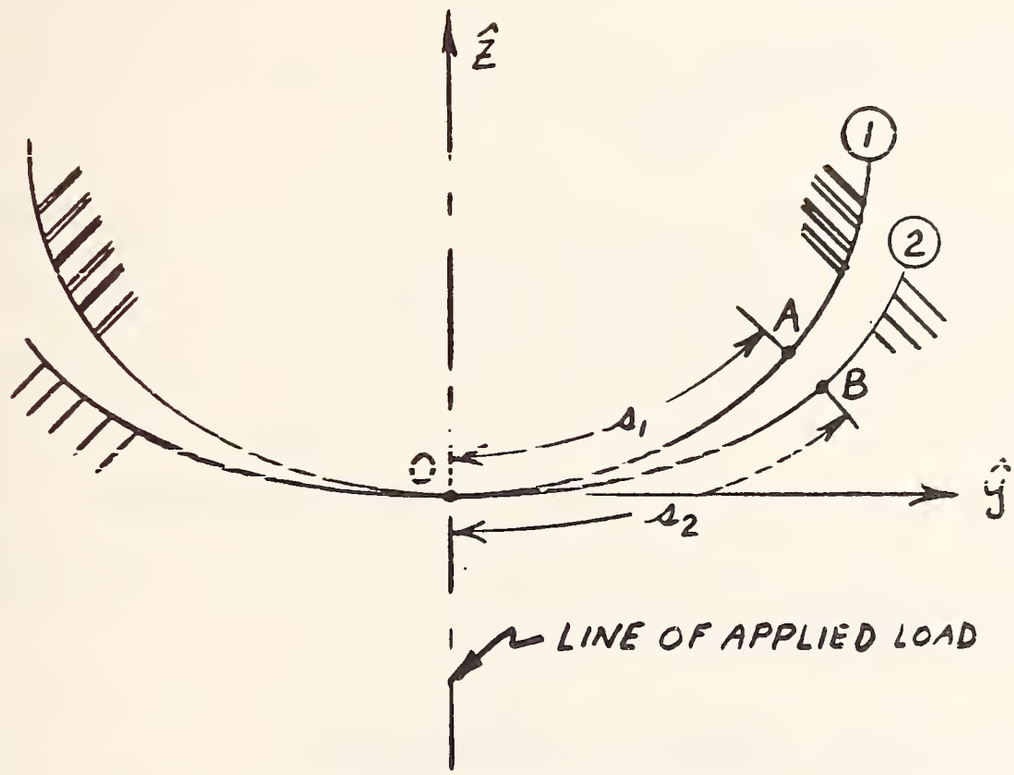

Fig. 3.1. Cross section of bodies in conformal contact

Hence, the normal interfacial pressures will be the only surface tractions allowed within the contact area.

Assumption (2) requires that the resultant applied force passes through O. Mathematically this assumption requires that the following relationship hold:

$$\int_{\Omega_i} \vec{r} \times (-p\hat{n}_i)\, dA = 0 \qquad (i=1,2) \tag{3.1}$$

Where Ω_i is the contact area on body i, $\vec{r}$ is a vector extending from the origin, O, to a point within the contact area, $\hat{n}_i$ is the unit normal to body i of the point defined by $\vec{r}$, and p is the interfacial pressure at the point located by $\vec{r}$. This assumption is not required in the analysis, rather it is made to simplify the analysis. It should be possible to extend the present analysis to include moments and rigid body notations.

3.3 Formulation of Conformal Contact Criterion

Consider two conforming frictionless bodies in contact. Body 1 will be called the "indentor" while body 2 will be termed the "seat." In the undeformed state these bodies contact at a point O. Figure 3.2 represents a cross section through O of typical conformal contact surfaces. A global coordinate system $(\hat{x},\hat{y},\hat{z})$ is constructed such that the x-y plane is tangent to point O on body 1 with O as its origin and $\hat{z}$ is directed inside body 1.

One of the difficulties in this class of problems is the

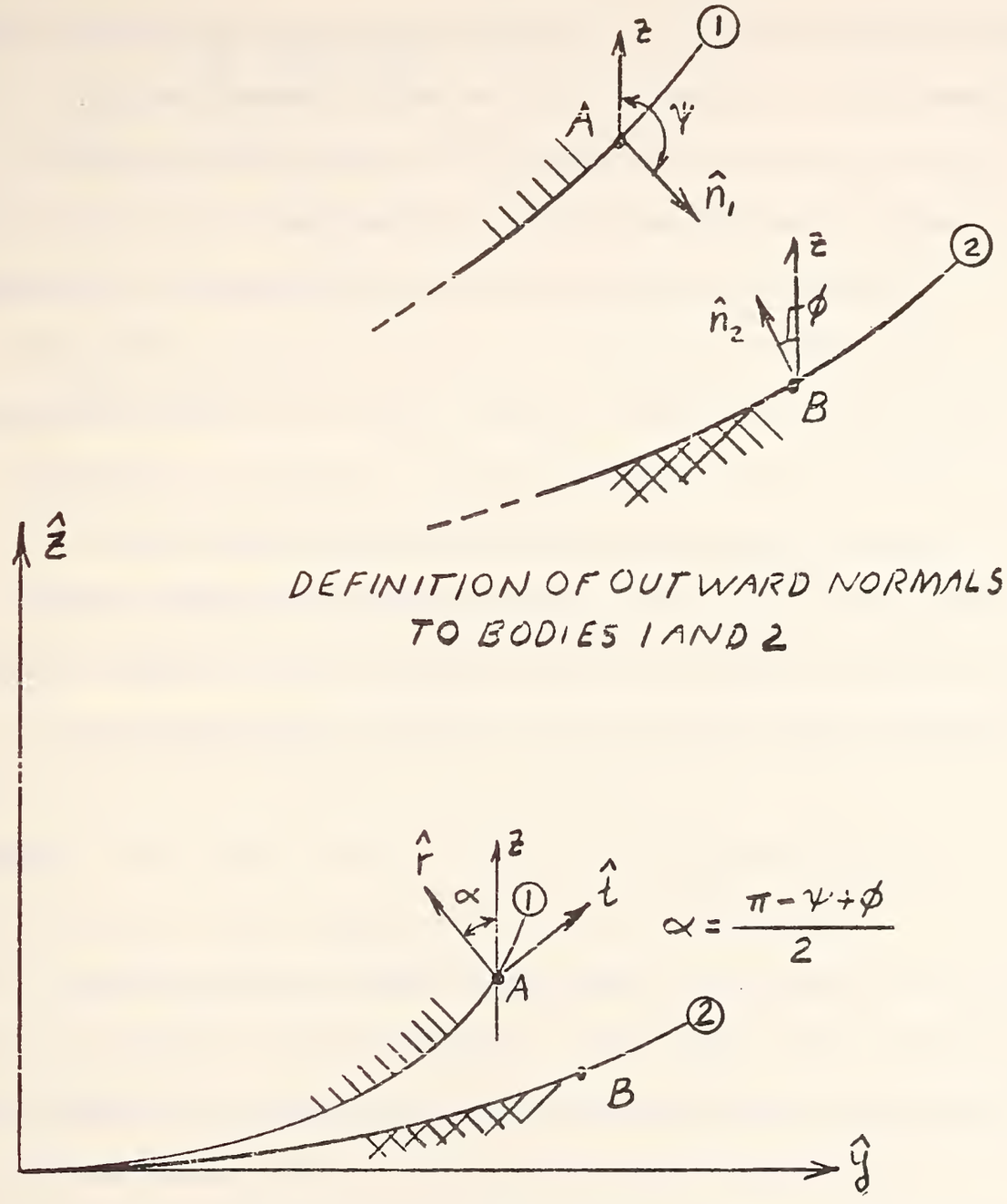

Fig. 3.2 Definition of coordinate systems in conformal contact theory.

identification of points on each body which come into contact in the deformed state. In order to find the sets of mating points we introduce an iterative scheme termed the "point-mating procedure." The details of this scheme will be discussed later.

Consider two points, A on body 1 and B on body 2, which come into contact after deformation. It will be initially assumed that points A and B lie at equal distances along their respective contour curves from the initial point of contact. Figure 3.1 illustrates this concept. The distance between O and A measured along the contour curve of body 1 is s_1 while the distance between O and B measured along the contour curve of body 2 is s_2. In order to formulate the contact criterion it will be initially assumed that

$$s_1 = s_2 \tag{3.2}$$

Let $\hat{n}_1$ and $\hat{n}_2$ define the outward unit normals to the surfaces of bodies 1 and 2 respectively. Shown in figure 3.2 are the normal vectors at points A and B. $\hat{n}_1$ is directed ψ degrees clockwise of the $\hat{z}$ direction while $\hat{n}_2$ is directed ϕ degrees counter clockwise of the $\hat{z}$ direction. For extremely conforming bodies $\hat{n}_2 \approx -\hat{n}_1$. A local coordinate system will be assigned to each set of points which contact after deformation. This local coordinate system will have a unit vector $\hat{r}$ defined as the mean of $\hat{n}_2$ and $-\hat{n}_1$, i.e., the angle between $\hat{r}$ and $\hat{z}$ is defined by α measured counter clockwise, where

$$\alpha = \frac{\pi - \psi + \phi}{2} \tag{3.3a}$$

A unit vector $\hat{t}$ will be defined as being 90° clockwise of $\hat{r}$ in the y-z plane, and a $\hat{\omega}$ unit vector will be defined by

$$\hat{\omega} = \hat{t} \times \hat{r} \tag{3.3b}$$

The displacement of point A (and B) due to conformal contact as illustrated in figure 3.3 will be traced. Point A (B) undergoes a rigid body translation Δ_1 (Δ_2) which carries it in the direction of $\hat{z}$ ($-\hat{z}$) to point A' (B'). As shown in figure 3.3, point A displaces an amount w_1 in the $-\hat{n}_1$ direction (from A' to A") due to elastic deformation. Not shown in figure 3.3 are the elastic displacements of points A and B in the tangent plane. These displacements will be initially neglected in the formulation of the contact criterion.

Similarly point B displaces to B" due to an elastic displacement w_2 in the $-\hat{n}_2$ direction. The original vector separation of points A and B is labeled $\vec{f}$ and is a function of the geometry of the contour curves. The vector separation $\vec{S}$, between A" and B" (in the deformed state) is therefore given by the vector relation

$$\vec{S} = \vec{f} + \Delta_1 \hat{z} - w_1 \hat{n}_1 + w_2 \hat{n}_2 - \Delta_2 \hat{z} \tag{3.4}$$

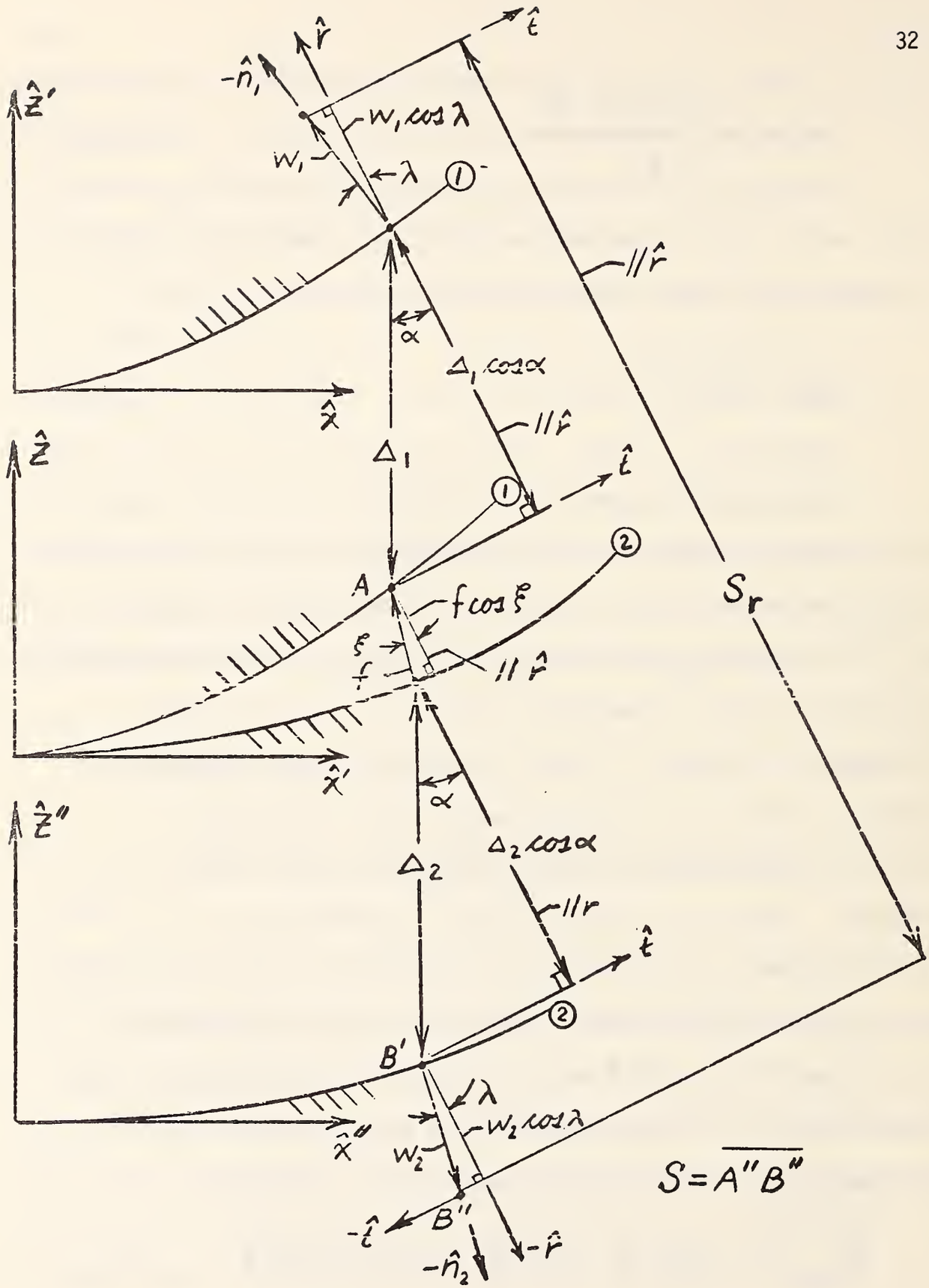

Fig. 3.3 Kinematics of surface point displacements in conformal contact.

Only the components of displacement along the $\hat{r}$ axis will be considered in the formulation of the contact criterion. The elastic displacements, w_1 and w_2 form angles of λ and $\pi-\lambda$ respectively with the $\hat{r}$ direction where

$$\lambda = \frac{\pi - \psi - \phi}{2} \tag{3.5}$$

The rigid body displacements Δ_1 and Δ_2 form angles $-\alpha$ and $\pi-\alpha$ respectively with the $\hat{r}$ direction while $\vec{f}$ forms an angle ξ with the $\hat{r}$ direction. ξ is determined by the shape of the contour curve at points A and B. The projections of $\vec{S}$ in the $\hat{r}$ direction may be written as

$$S_r = |\vec{f}| \cos\xi - \delta \cos\alpha + (w_1 + w_2)\cos\lambda \tag{3.6}$$

where $\delta = -(\Delta_1 + \Delta_2)$. δ is termed the approach and represents the distance that points on one body move along the z axis towards points on the other body due to rigid body movement.

In general the displacement w_1 and w_2 may be written in terms of the interfacial pressure $p(x',y',z')$ and an influence function $G_1(x,x',y,y',z,z')$ as

$$w_i = \int_{\Omega_i} p(x',y',z')\, G_i(x,x',y,y',z,z')\, dx'dy'dz' \tag{3.7}$$

where Ω_i is the area of contact of body i. Physically the function $G_i(x,x'y,y'z,z')$ represents the elastic displacement in the $-\vec{n}_i$ direction at point (x,y,z) due to a unit load at point (x',y',z') in the $-\vec{n}_i$ direction. In the most general form equation (3.6) may be written as.

$$S_r = |\vec{f}| \cos\xi - \delta\cos\alpha +$$

$$+ \cos\lambda \int_{\Omega_1} P(x',y',z')\, G_1(x,x',y,y',z,z')\, dx'dy'dz' +$$

$$+ \cos\lambda \int_{\Omega_2} P(x',y',z')\, G_2(x,x',y,y',z,z')\, dx'dy'dz' \qquad (3.8)$$

In order to solve the conformal contact problem it is necessary to find the interfacial pressure $P(x',y',z')$, the approach δ, and the final contact area Ω, all of which satisfy equation (3.8) and the following boundary conditions:

$$S_r = 0 \qquad \text{INSIDE } \Omega \qquad (3.9a)$$

$$P(x,y,z) \geq 0 \qquad \text{INSIDE } \Omega \qquad (3.9b)$$

$$S_r > 0 \qquad \text{OUTSIDE } \Omega \qquad (3.9c)$$

$$P(x,y,z) = 0 \qquad \text{OUTSIDE } \Omega \qquad (3.9d)$$

Furthermore, it is required to verify the accuracy of equation (3.2), i.e., that the points within the contact area satisfy the relationships:

$$S_t = 0 \qquad \text{INSIDE } \Omega \tag{3.9e}$$

$$S_\omega = 0 \qquad \text{INSIDE } \Omega \tag{3.9f}$$

where S_t and S_ω represent the separation in the $\hat{t}$ and $\hat{\omega}$ directions respectively.

Conditions (3.8) and (3.9a-f) represent the contact criterion for conformal contact. They are analogous to equations (2.6) and (2.7a-d) for nonconformal contact. Equations (3.8) and (3.9a-d) may be solved in a similar manner as equations (2.6) and (2.7a-d) using the "Simply-Discretized" method of solution. However, this solution only guarantees the displacements be compatible in the $\hat{r}$ direction since only S_r was involved in equation (3.8). Therefore it is necessary to examine the components of the displacements in the $\hat{t}$ and $\hat{\omega}$ directions to insure that A and B merge as originally assumed. An iterative scheme, termed the "point-mating procedure," is outlined which shows how successive "Simply-Discretized" solutions may be utilized to converge upon a final solution in which merging points on each body have been identified.

Consider the "point-mating procedure" on the first attempt at solution. As shown in figure 3.1

$$a_2 = k_1 a_1 \tag{3.10}$$

where $k_1 = 1$. With the "Simply Discretized" method of solution, equation (3.8) is written for N + 1 field points, thus for each

field point equation (3.10) must be assumed. This can be restated as

$$\Delta_2^i = k_1 \Delta_1^i \qquad (i = 1, N+1) \tag{3.11}$$

The first solution of equation (3.8) yields a pressure field, approach and a contact region Ω. The elastic displacements w_1 and w_2 at each field point may be calculated via equation (3.7). Now it remains to see if indeed the field points on each body merge. In order to check the final separation it is necessary to compute the displacements in both the $\hat{\omega}$ and $\hat{t}$ direction. Denoting the displacements of a field point on body i in the tangential plane of body i by u_i and v_i respectively, they may be determined as in equations (3.12a,b), where u_i lies in the plane of the contour curve and v_i is in the direction of $\hat{\omega}$.

$$u_i = \int_{\Omega_i} P(x',y',z') H_i(x,x',y,y',z,z') dx'dy'dz' \tag{3.12a}$$

$$v_i = \int_{\Omega_i} P(x',y',z') I_i(x,x',y,y',z,z') dx'dy'dz' \tag{3.12b}$$

In equations (3.12a,b) H_i and I_i represent the influence functions for body i which relate the displacements u_i and v_i respectively at a point (x,y,z) to the normal pressures exerted at a point (x',y',z'). The pressure field $P(x',y',z')$ and the contact areas Ω_i are known from the solution of equation (3.8).

Examining one set of points, A on body 1 and B on body 2,

which are assumed to merge after deformation, the total separation may be written as:

$$\vec{S} = S_r \hat{r} + S_t \hat{t} + S_\omega \hat{\omega} = (W_1+W_2)\cos\lambda \hat{r} +$$

$$+(u_1-u_2)\cos\lambda \hat{t} + (v_1-v_2)\hat{\omega} + f_r \hat{r} + f_t \hat{t} + f_\omega \hat{\omega} - \delta_r \hat{r} - \delta_t \hat{t} \qquad (3.13a)$$

where

$$\vec{f} = f_r \hat{r} + f_t \hat{t} + f_\omega \hat{\omega} \qquad (3.13b)$$

and

$$\delta \hat{z} = -(\Delta_1+\Delta_2)\hat{z} = \delta_r \hat{r} + \delta_t \hat{t} + 0\,\hat{\omega} \qquad (3.13c)$$

Equation (3.8), which was originally solved by the "Simply-Discretized" method represents the $\hat{r}$ components of equation (3.13).

In the first solution of equation (3.8) it was assumed that $u_1 = u_2$, $v_1 = v_2$, $f_\omega = 0$. However, the first solution has now provided values for u_1, u_2, v_1, v_2, and δ. $\vec{f}$ is a function of the geometry of the undeformed surfaces and δ may be decomposed into δ_r and δ_t. Therefore all the quantities in equation (3.13) are known to a first approximation after the first simply discretized solution. The separation after the first solution may be computed and in general it will be non-zero. It will be shown how the separation may be utilized to better approximate equation (3.11) so that the separation of a second solution to the same problem will be much smaller.

In order to simplify the illustration of the point-mating procedure, it will be assumed that for the problem at hand v_1 and v_2 are zero for all field points. This is the case for axisymmetric bodies. Furthermore, consider the seat to be fixed at some point well removed from the contact area (where the elastic deformation is negligible), thus after the deformation the indentor will have displaced the entire amount δ due to rigid body displacement. Typical displacements for points A and B, including the u_1 and u_2 displacements found via the first simply discretized solution, are illustrated in figure 3.4. The solution to equation (3.8) guaranteed only that the separation S_t in the $\hat{r}$ direction would be zero. As shown, the points A and B will in general be separated by a distance S_t'. Equation (3.11) may now be modified such that

$$\Delta_2^i = k_j^i \Delta_1^i \qquad (i=1,N+1) \tag{3.14}$$

where

$$k_j^i = \left(\frac{\Delta_2^i - S_t'}{\Delta_1^i} \right) \tag{3.15}$$

and subscript j refers to the number of the iteration.

This modification compensates for the error in the original assumption (3.11). Using relationship (3.14), the calculation may be performed a second time. The value of S_t' in the second solution will be much smaller than that of the first, however, if it is

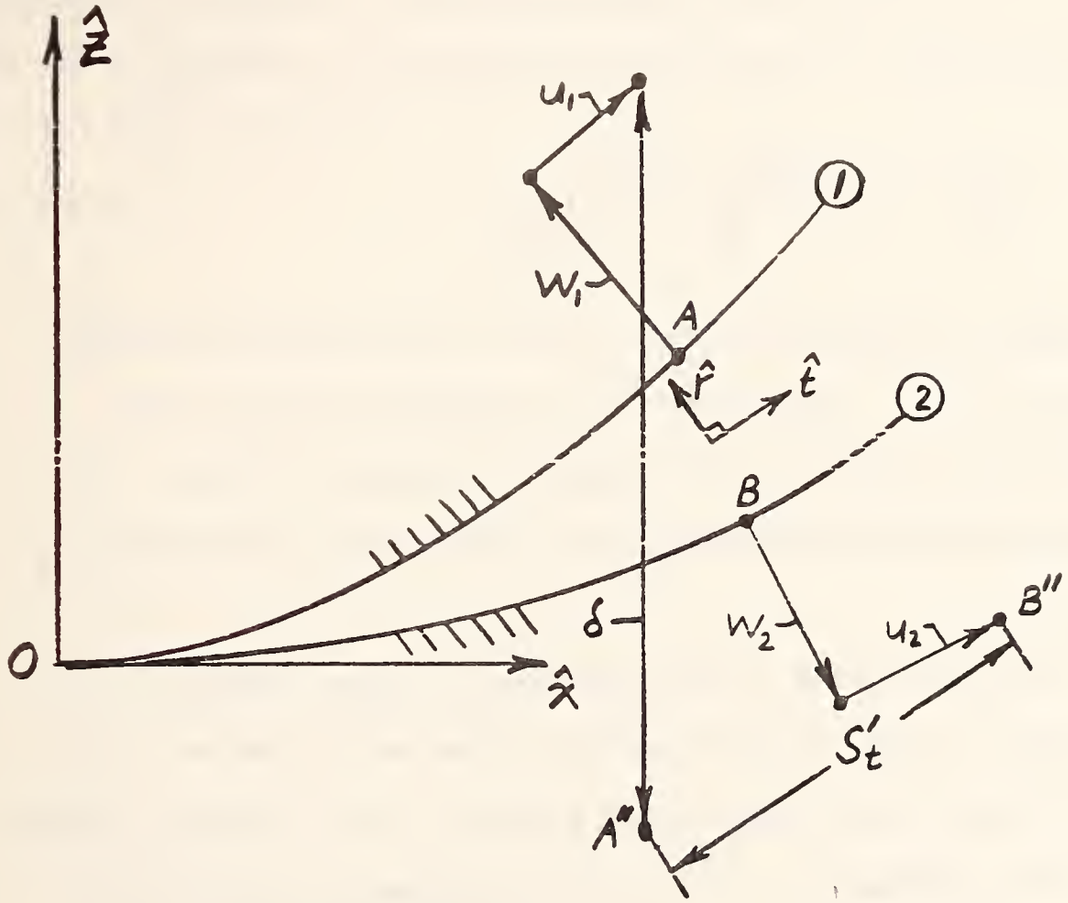

Fig. 3.4. Displacements of typical field points in conformal contact.

still too large, a new value of k_2, may be computed following equation (3.15).

Equations (3.14) and (3.15) may be generalized as

$$s_2^i = k_j^i \, s_1^i \tag{3.16a}$$

where

$$k_j^i = \left(\frac{s_2^i - S_t'}{s_1^i} \right)_{j-1} \tag{3.16b}$$

and j denotes values associated with the j th "Simply Discretized" solution [$k_1 = 1$]. The value of k_j^i in equation (3.16) is used in place of k_{j-1}^i for the j th "Simply Discretized" solution. The iterative scheme can be repeated until the desired tolerances on S_t' are met.

Also of concern is the separation in the $\hat{\omega}$ direction. It was assumed that points along contour curves merge, however, if v_1 and v_2 are not equal, points A and B may not lie on the same contour curve after deformation. This can be determined by examining the separation, S_ω', in the ω direction. It must be remembered that the solution at hand is an iterative one and therefore, the separation of field points will in general never be zero. The separation can only be reduced to an acceptable amount.

In summary, a mathematical model of frictionless conformal contact theory has been presented. The model takes the form of

equations (3.8) and (3.9a-d). Since there is no knowledge a priori of which points on each surface merge, initially points located by equation (3.11) are assumed to merge. The contact criterion of equations (3.8) and (3.9a-d) only insure that two field points, assumed to merge, have zero separation in the $\hat{r}$ direction. In order to guarantee the absence of separation between two field points in the contact region, the iterative scheme termed the "point-mating procedure" must be applied.

4. GENERATION OF INFLUENCE FUNCTIONS

4.1 Introduction

In the formulation of both the nonconformal and conformal contact theories, the influence function plays a crucial role.

Physically the influence function relates the elastic displacement at a given point to the applied force at some other point. The elastic displacements due to a given pressure distribution can be found by integrating the product of pressure and the influence function over the contact area. This is illustrated by equation 3.7.

In any given problem it is necessary to know the influence functions which are appropriate for the given surfaces in contact. In nonconformal theory the contact area is approximated by a plane making it appropriate to use the Boussinesq influence function, for a point load on a half space, as the influence function for all surface geometries. However, in conformal theory, where the contact surface can not be approximated by a plane, it is necessary to find the influence functions explicitly for each of the bodies in contact.

For some problems analytic influence funtions may be found; however, in the event that no analytic functions are available, they may be generated numerically. The following two sections, 4.2 and 4.3, present the classical solutions of a half space loaded under a point load and line load respectively. In section 4.4 the principles

involved in the numerical generation of influence functions are developed. The remainder of chapter 4 contains examples of influence functions generated with finite element techniques. Wherever feasible, analytic solutions are compared to the numerical influence functions.

4.2 Influence Function for a Point Load on a Half Space

The problem of a half space loaded with a normal concentrated load was first solved by J. Boussinesq [1885].[1] Consider the half space and coordinate system illustrated in figure 4.1.

A concentrated load F is applied at point O and point A is located on the surface of the half space at a distance $|\vec{r}|$ from O. u represents the elastic displacement of point A in the direction of $\hat{r}$ while w represents the elastic displacement in the $\hat{z}$ direction. Boussinesq found u and w to be given by

$$u = -\frac{(1-2\nu)(1+\nu)F}{2\pi E |\vec{r}|} \tag{4.1}$$

$$w = \frac{(1-\nu^2)F}{\pi E |\vec{r}|} \tag{4.2}$$

where E and ν are Young's modulus and Poisson's ratio respectively for the half space.

Equation (4.2) forms the basis of the influence function used

[1] See Timoshenko and Goodier [1970], pp. 398-402.

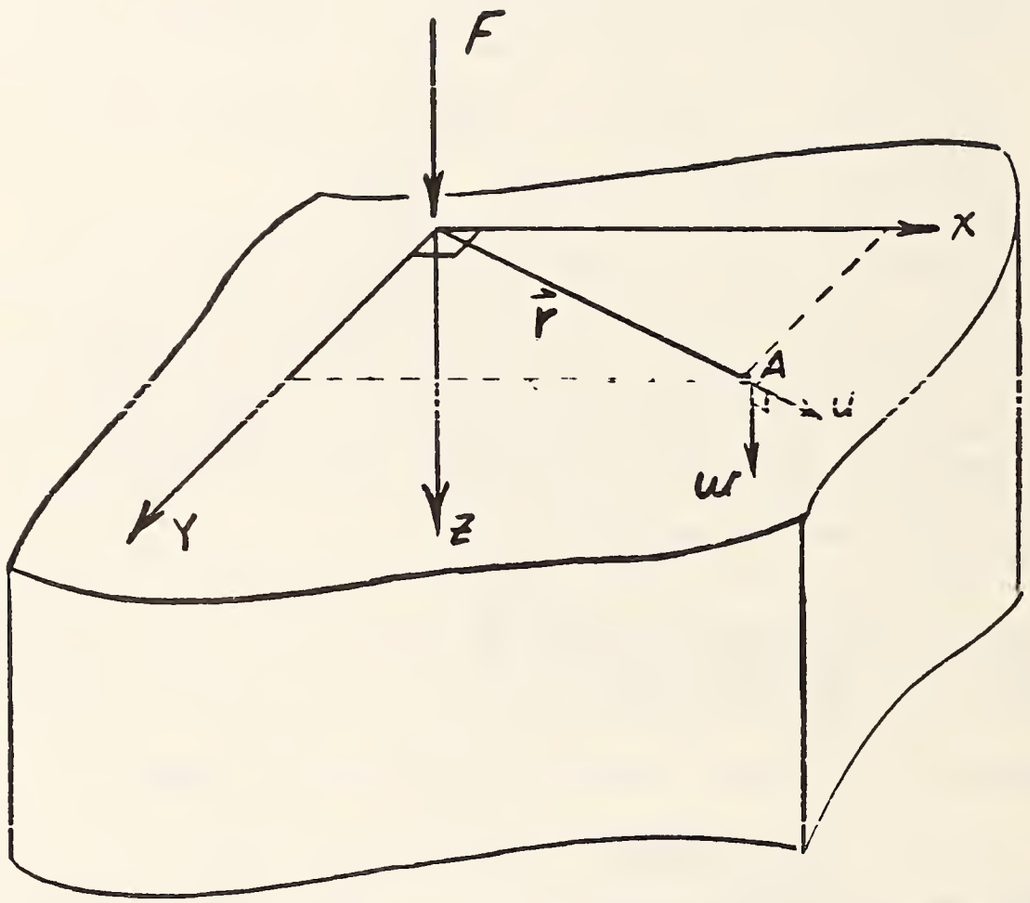

Fig. 4.1. Point load on half space

in nonconformal contact theory. We wish to generate a function $G(x, x', y, y')$ which relates the normal displacement at (x, y) to a unit load at (x', y'). Noting that in equation (4.2) w is proportional to $1/|\vec{r}|$, where $|\vec{r}|$ is the distance between points (x, y) and (x', y'), the influence function for the normal surface displacement on a half space may be written as

$$G(x,x',y,y') = \frac{(1-\nu^2)}{\pi E} \frac{1}{\sqrt{(x-x')^2+(y-y')^2}} \tag{4.3}$$

Similarly, for the displacements tangent to the surface, a function $H(x, x', y, y')$ may be defined as

$$H(x,x',y,y') = \frac{-(1-2\nu)(1+\nu)}{2\pi E} \frac{1}{\sqrt{(x-x')^2+(y-y')^2}} \tag{4.4}$$

If a pressure field $p(x', y')$ were considered to act over the surface of a half space within a region Ω, the displacements w and u due to this pressure field can be calculated by the following equations:

$$w = \int_{\Omega} P(x',y') G(x,x',y,y') dx'dy' \tag{4.5}$$

$$u = \int_{\Omega} P(x',y') H(x,x',y,y') dx'dy' \tag{4.6}$$

Both G and H play an important role in the generation of numerical influence functions which will be explained in section 4.4.

4.3 Analytic Solution for a Line Load on a Plane

Consider a line load acting on the edge of a semi-infinitely plate. It is desired to find the displacement field in the plate due to the given loading. (see fig. 4.2)

As posed the problem is one of plane stress and was originally solved by Flamant [1892]. For boundary conditions, it is assumed that points along the y axis have no motion in the x direction while a point A, located along the y axis at a distance d from the surface, is fixed rigidly. The displacement field then becomes[1]

$$v = -\frac{2F}{\pi E}\cos\theta \log r - \frac{(1-\nu)F}{\pi E}\theta \sin\theta + \\ + \frac{2F}{\pi E}\log d \cos\theta \qquad (4.7)$$

$$u = -\frac{2\nu F}{\pi E}\sin\theta - \frac{2F}{\pi E}\log r \sin\theta + \frac{(1-\nu)F}{\pi E}\theta\cos\theta \\ - \frac{(1-\nu)}{\pi E}\sin\theta + \frac{2F}{\pi E}\log d \sin\theta \qquad (4.8)$$

where E and ν are the Young's modulus and Poisson's ratio respectively of the plate. The solution is not unique in that it is dependent on the value of d chosen in the boundary condition.

---

[1] See Timoshenko and Goodier [1970], p. 103.

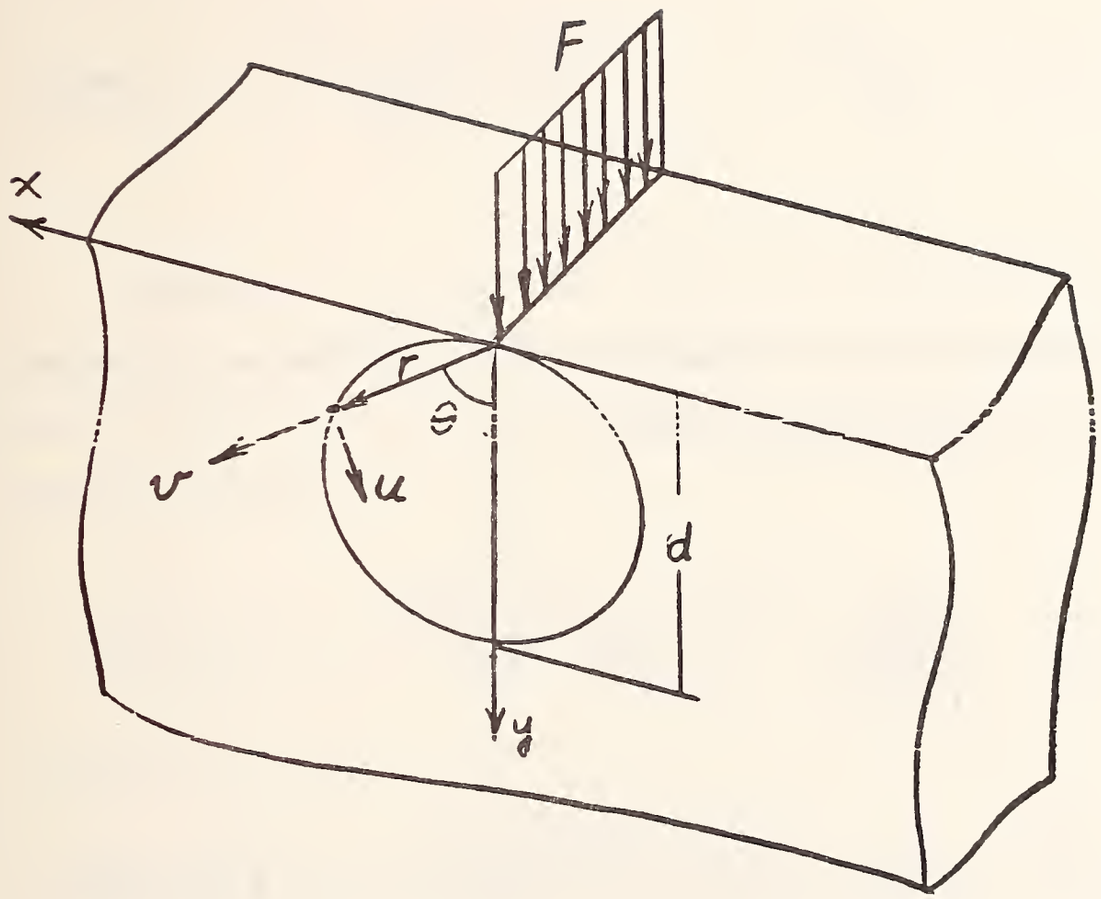

Fig. 4.2. Plate loaded under line load

Let θ be $\pi/2$. The surface displacements for the plane stress problem become

$$u = +\frac{2F}{\pi E} \log \frac{d}{r} - \frac{(1+\nu)}{\pi E} F \tag{4.9}$$

$$v = -\frac{(1-\nu)}{2E} F \tag{4.10}$$

For the case of plane strain equations (4.9) and (4.10) may be written substituting ν by $\bar{\nu}$ and $\bar{E}$ by E where

$$\bar{\nu} = \frac{\nu}{(1-\nu)}$$

$$\bar{E} = \frac{E}{(1-\nu^2)} \tag{4.11}$$

The proof of this substitution is shown in appendix 1. For plane strain the surface displacements at $\theta = \pi/2$ become

$$u = -\frac{2F(1-\nu^2)}{\pi E}\log\frac{r}{d} - \frac{(1+\nu)}{\pi E}F \tag{4.12}$$

$$v = -\frac{(1-2\nu)(1+\nu)F}{2E} \tag{4.13}$$

Equations (4.12) and (4.13) form the basis of an influence function for a line load on a plane. Consider a unit line load. Parallel to the z axis at x', then the displacements along a line at coordinate x becomes

$$G(x,x') = -\frac{2(1-\nu^2)}{\pi E}\log\frac{|x-x'|}{d} - \frac{(1+\nu)}{\pi E} \tag{4.14}$$

$$H(x,x') = -\frac{(1-2\nu)(1+\nu)}{2E}\frac{x-x'}{|x-x'|} \tag{4.15}$$

where $G(x, x')$ and $H(x, x')$ represent the influence functions for displacements u and v respectively for $\theta = \pi/2$. Equations (4.14) and (4.15) are essential to the numerical generation of influence functions when line loads are involved. These results will be used in sections 4.7 and 4.8 for line loads on bodies with cylindrical surfaces.

4.4 Numerical Generation of Influence Functions

Consider a three dimensional body whose surface is defined by $z = \phi(x, y)$, as illustrated in figure 4.3. For a linear isotropic material, the influence function for the surface point displacements will be of the form

$$G(x, x', y, y', \nu, E) = \frac{F}{E}\, g(x, x', y, y', \nu) \qquad (4.16)$$

where F is a unit load acting normal to the surface at point (x', y', z') and (x, x', y, y') represents the displacement in a defined direction at some other surface point (x, y, z). E is the Young's modulus of the material and ν is Poisson's ratio. The function $g(x, x', y, y', \nu)$ depends on the geometry of the body and has dimensions of [1/L]. In some cases g may be found analytically however for more complicated geometries the task may be impossible. When g can not be derived by analytic means, it can in principle be constructed from a set of finite element solutions. A simple example follows which demonstrates this numerical procedure.

Consider the region $(z < 0)$ defined by the curvilinear coordinate system illustrated in figure 4.4.

A unit load F is applied to point (x', y') normal to the surface and it is desired to find the displacement G in a specified direction at a point (x, y). For the purpose of finding finite

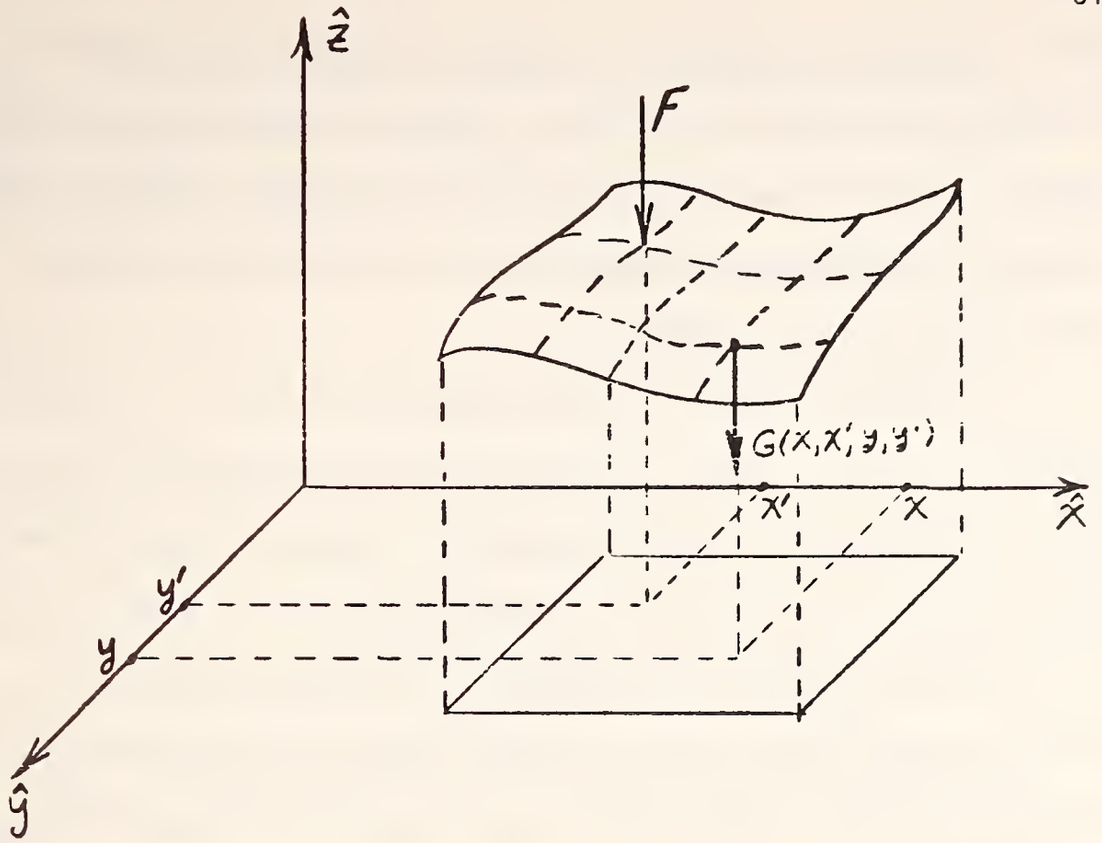

Fig. 4.3. Three dimensional surface ϕ (x, y) under point load

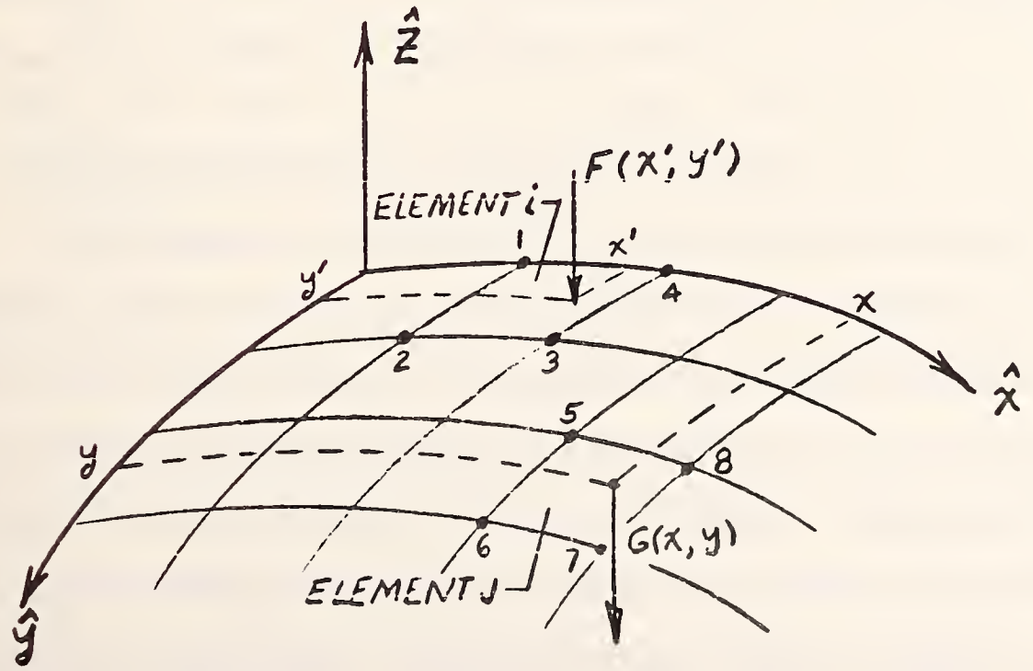

Fig. 4.4. Curvilinear coordinate system on three dimensional surface

element solutions, a model of the body is divided into "elements." The surface of the body is defined by the top sides of some of those elements. The intersection of more than two elements defines a node. Figure 4.4 illustrates a typical discretization of the surface of some typical body into elements.

In order to find G at (x, y) due to F at (x', y') it will be necessary to solve a number of finite element problems with the above model. Consider that a set of solutions is known via finite element techniques within the region of interest around (x, y) and (x', y'). Each solution corresponds to a problem where the point load is applied to a different node. Thus from these solutions the displacement at each node is known due to a point load at any of the other nodes.

Now consider in further detail elements i and j which contain points (x', y') and (x, y) respectively. (see fig. 4.4)

Let us approximate element 1, 2, 3, 4 as a plane facet, then a set of four forces located at nodes 1, 2, 3 and 4 may be found which is equipollent to F at (x', y') i.e., if it is required that the forces at nodes 1, 2, 3 and 4 sum to F and that their moment about (x', y') is zero then F may be replaced by forces F_1, F_2, F_3, and F_4 at nodes 1, 2, 3, 4 respectively. By superposition of the finite element solutions, the displacement at node 5 may be found due to the set of forces F_1, F_2, F_3, F_4. Similarly the displacement at nodes 6, 7, 8 may be found. One final interpolation may be made between these displacements at nodes 5, 6, 7 and 8 to obtain the displacement G at (x, y)

due to F. The above scheme, involving the interpolation between finite element solutions, illustrates how an influence function can be generated numerically for arbitrary surfaces.

It must be noted that finite element solutions for a point load applied to a node will yield a finite displacement directly under the load. This is inconsistent with, at least, equations (4.1) and (4.2) which predict infinite displacements under a point load on a plane. The finite element displacement function is only valid away from the point load. In the neighborhood of the load, the appropriate singularities must be identified as described in sections 4.5--4.8.

The following sections contain examples of the generation of influence functions via the method described above. They deal with both point and line loading on spherical and cylindrical surfaces respectively. In all but one of the examples analytic solutions are compared to the numerically generated influence functions.

4.5 Influence Function for a Point Load on a Sphere

Sternberg and Rosenthal [1952] have found the solution for the stress distribution in an elastic sphere under two equal and diametrically opposed point loads. Guerrero and Turteltaub [1972] have analyzed a similar problem of a sphere under a finite number of concentrated surface loads of arbitrary orientation. Both of these solutions are useful in providing an analytic influence function for a point load on a sphere. The results that follow are from the analysis of Sternberg and Rosenthal.

Consider a sphere compressed by two concentrated forces F as

shown in figure 4.5. From dimensional considerations, symmetry considerations and the fact that the displacements must be proportional to loads in classical problems of elasticity, it follows that displacements on the surface of a sphere must be of the form

$$\frac{u}{R} = \frac{F}{ER^2}\, g(\theta, \nu) \tag{4.17}$$

It is shown in Lure' [1964] that the displacements u_r (radial) and u_θ (meridional) on the surface of the sphere are as follows:

$$u_r = \frac{(m-2)F}{4G(m+1)\pi R} + \frac{F}{4\pi GR}\left\{\frac{m-1}{m}\left(\frac{1}{\sin\frac{\theta}{2}} + \frac{1}{\cos\frac{\theta}{2}} - 4\right)\right.$$

$$+ \frac{(m-2)^2}{m^2}\left(\log\left(\cot\frac{\theta}{4}\cot\frac{\pi-\theta}{4}\right) - 2\right)$$

$$- \frac{3m^2-20m+16}{m^3}\left(\sin^2\frac{\theta}{2}\log\frac{1+\sin\frac{\theta}{2}}{\sin\frac{\theta}{2}} + \cos^2\frac{\theta}{2}\log\frac{1+\cos\frac{\theta}{2}}{\cos\frac{\theta}{2}}\right.$$

$$\left.\left. + \frac{1}{2} - \sin\frac{\theta}{2} - \cos\frac{\theta}{2}\right) + \sum_{k=1}^{\infty} A_{2k} P_{2k}(\cos\theta)\right\} \tag{4.18}$$

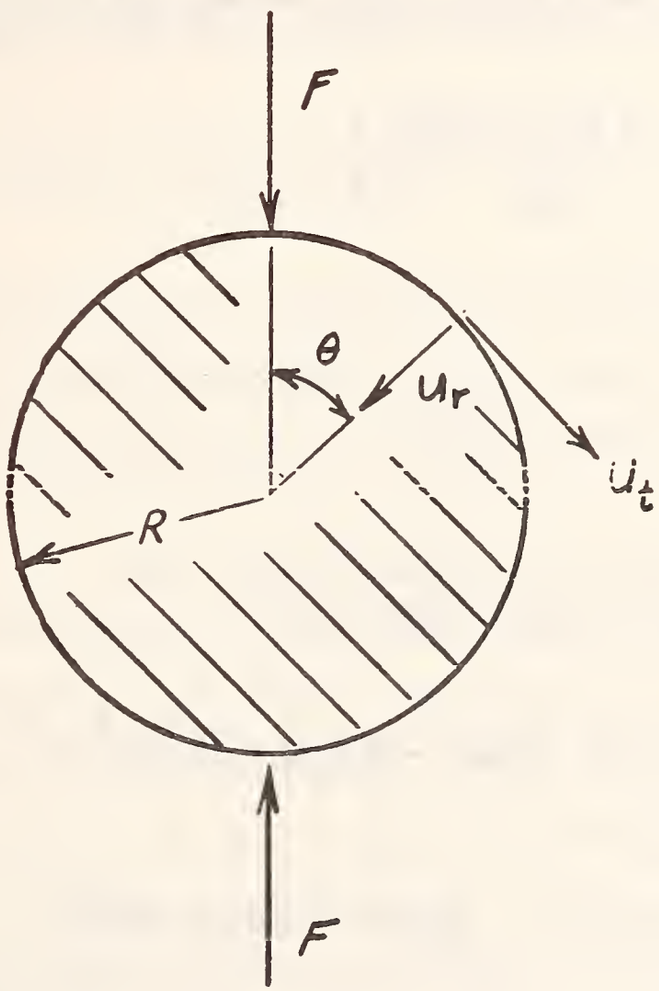

Fig. 4.5. Sphere under diametrically opposed point loads

$$U_\theta = \frac{-F}{4\pi GR}\left\{\frac{m-2}{m}\,\frac{\cos\frac{\theta}{2}-\sin\frac{\theta}{2}}{\sin\theta}+\frac{m^2+8m-8}{m^2}\times\right.$$

$$\times\left[\left(1-\cos\tfrac{\theta}{2}-\sin\tfrac{\theta}{2}\right)\cot\theta+\tfrac{1}{2}\sin\theta\log\cot\tfrac{\theta}{2}\,\frac{1+\sin\frac{\theta}{2}}{1+\cos\frac{\theta}{2}}\right]$$

$$\left.+\sum_{k=1}^{\infty}B_{2k}\,\frac{dP_{2k}(\cos\theta)}{d\theta}\right\} \qquad (4.19)$$

where m is the reciprocal of Poisson's ratio, G is the modulus of rigidity and P_{2k} (cos θ) are the Legendre polynomials in cos θ. The coefficients are given as

$$A_n = \frac{1}{m^4(n-1)(n+1)(n+2)\Delta'}\times$$

$$\times\left[(m^4+7m^3+30m^2-64m+32)n^2+\right.$$

$$+(7m^4+22m^3-39m^2+44m-16)n$$

$$\left.+10m^4-11m^3+9m^2+20m-16\right] \qquad (4.20)$$

$$B_n = \frac{1}{m^3(n-1)(n+1)(n+2)\Delta'} \times$$

$$\left[(7m^3+11m^2-28m+16)(n+2)^2\right.$$

$$+ \ (-18m^3-48m^2+132m-72)(n+2)$$

$$\left. + \ 9(m-1)(m^2+8m-8)\right] \qquad (4.21)$$

where

$$\Delta' = n(n-1) + (2n+1)\frac{m+1}{m} \qquad (4.22)$$

The influence functions for a point load on a sphere may be obtained by considering a unit load F in equations (4.18, 4.19) and letting θ represent the angle between the vectors describing the position of the load and the point A where the displacements are desired. This is illustrated in figure 4.6.

Consider points A and B on the surface of a sphere. A cartesian coordinate system ($\hat{\eta}$, $\hat{\zeta}$, $\hat{\gamma}$,) is constructed with the origin, O, at the center of the sphere. The vectors $\vec{OA}$ and $\vec{OB}$ form an angle θ between them.

If loads F are applied at point B and at a point diametrically opposite D then the displacements u_r and u_θ at A are defined by equations (4.18) and (4.19) respectively. It is important to note

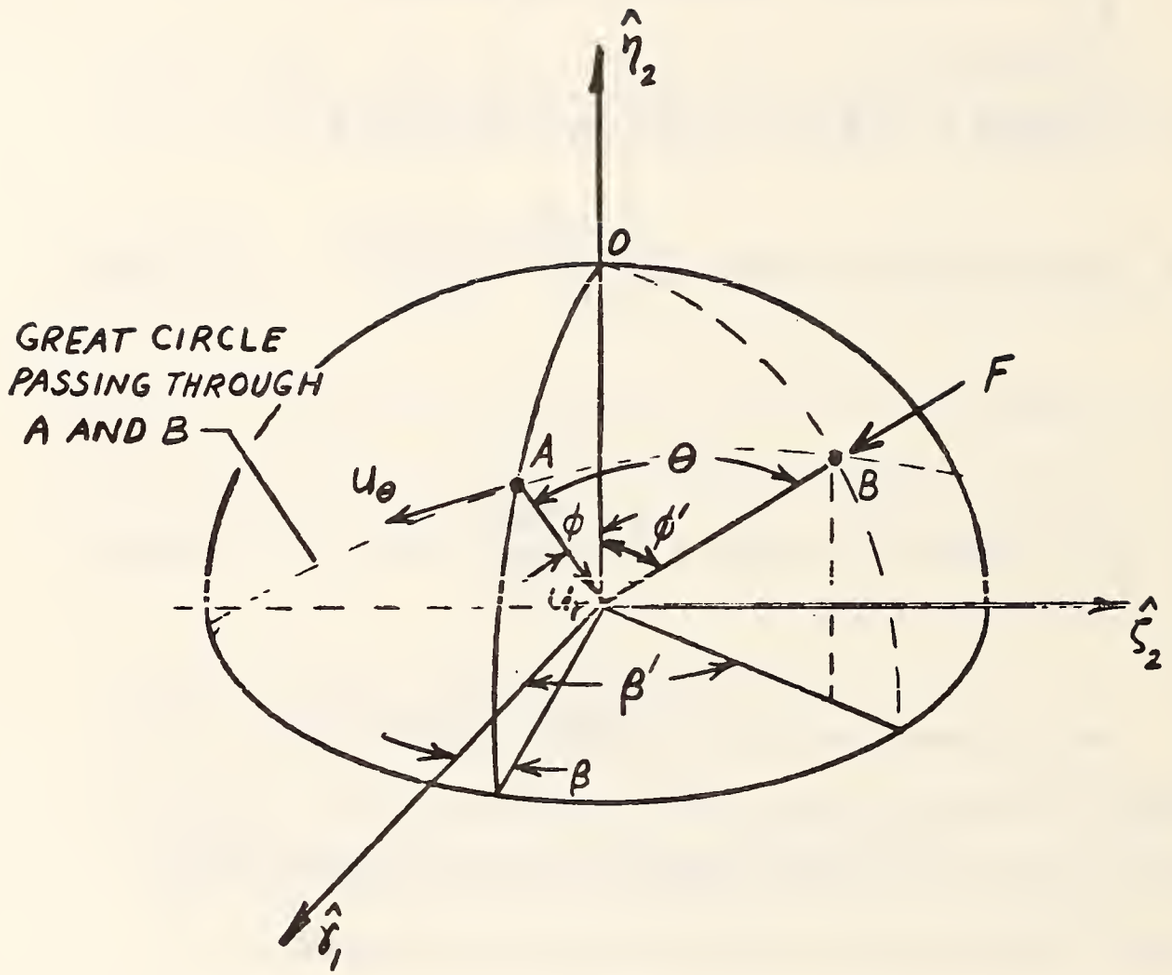

Fig. 4.6. Coordinate system for influence functions for a point load on a sphere.

that the direction of u_θ is not only a function of θ but also of the spherical coordinates (ψ, β) of D and those (ψ', β') of A. u_θ is measured along the tangent to the great circle at D which passes through point A.

The influence functions for a point load on a sphere may be written as

$$G(\psi, \beta, \psi', \beta', \nu, E, R) = \frac{1}{ER} g_r(\theta, \nu) \tag{4.23}$$

and

$$H(\psi, \beta, \psi', \beta', \nu, E, R) = \frac{1}{ER} g_\theta(\theta, \nu) \tag{4.24}$$

where[1]

$$\theta(\psi, \beta, \psi', \beta') = \arccos(\sin\psi \sin\psi' \cos\beta \cos\beta' + \sin\psi \sin\psi' \sin\beta \sin\beta' + \cos\psi \cos\psi') \tag{4.25}$$

---

[1] From spherical law of cosines or from $\cos\theta = \overrightarrow{OA} \cdot \overrightarrow{OD} / |\overrightarrow{OA}| \cdot |\overrightarrow{OD}|$.

G and H represent the influence functions for u_r and u_θ respectively which are given by equations (4.18) and (4.19) respectively. The displacements u_r (ψ, β) and u_θ (ψ, β) at point (ψ, β) due to a distributed load p (ψ', β') over region Ω can be calculated respectively

$$u_R(\psi,\beta) = \int_\Omega p(\psi',\beta')\, G(\psi,\beta,\psi',\beta',\nu,E,R)\, R^2 \sin\psi'\, d\beta'\, d\psi' \qquad (4.26)$$

and

$$u_\theta(\psi,\beta) = \int_\Omega p(\psi',\beta')\, H(\psi,\beta,\psi',\beta',\nu,E,R)\, R^2 \sin\psi'\, d\beta'\, d\psi' \qquad (4.27)$$

Now consider the numerical generation of these influence functions. It is known from symmetry that the magnitudes of G and H are related to R, θ, ν and E. Furthermore the orientation of positive G is always radially inward whereas that of H is tangent to the surface in the direction away from the unit load. Therefore it is necessary to find functions g_r (θ, ν) and g_θ (θ, ν) in equations (4.23) and (4.24). These functions can be constructed if desired[1] from one finite element solution of a point load on a sphere.

---

[1] The analytic solution of Sternberg and Rosenthal [1952] will serve as a check on the finite element development which will then be applied to the spherical seat and other problems without analytic solutions.

Consider the sphere under the loading in figure 4.5. This problem can be modeled for finite element analysis with the grid shown in figure 4.7. The present analysis was made with the computer program for axisymmetric problems, described in Wilson [1965]. The grid in figure 4.7 represents a cross section of ring elements which are axisymmetric about the z axis. Because of the symmetry of the loading, points located on the x axis were restricted to move only in the x direction while points on the z axis were fixed from moving in the x direction. The output data of interest are the displacements of the surface points. Consider the finite element analysis of a sphere where $E = 30 \times 10^6$ psi, $\nu = 0.3$, $R = 1$ in. which is compressed between two forces F, where $F = 30 \times 10^7$ lb. From equation (4.17) it follows that

$$u_r = \frac{F}{ER} h_r(\theta, \nu) \tag{4.28}$$

$$u_\theta = \frac{F}{ER} h_\theta(\theta, \nu) \tag{4.29}$$

and the function h_r and h_θ are exactly those, g_r and g_θ, in equations (4.23) and (4.24).

The functions h_r (θ, ν) and h_θ (θ, ν) are non-dimensional functions of displacement which are known at the nodes in figure 4.7 from the finite element analysis. Knowing the displacements at the

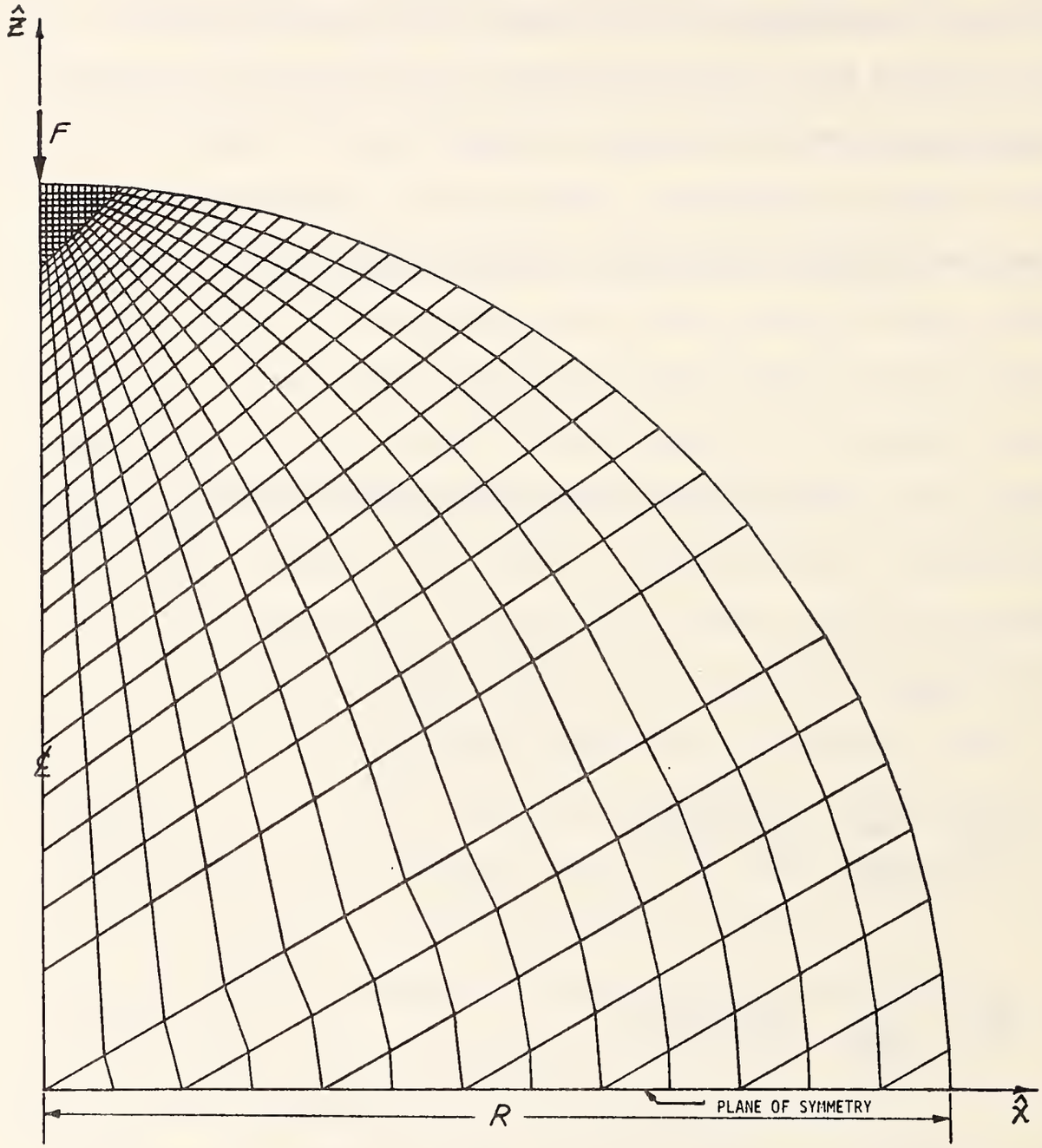

Fig. 4.7. Axisymmetric finite element model of a sphere under two diametrically opposed point loads.

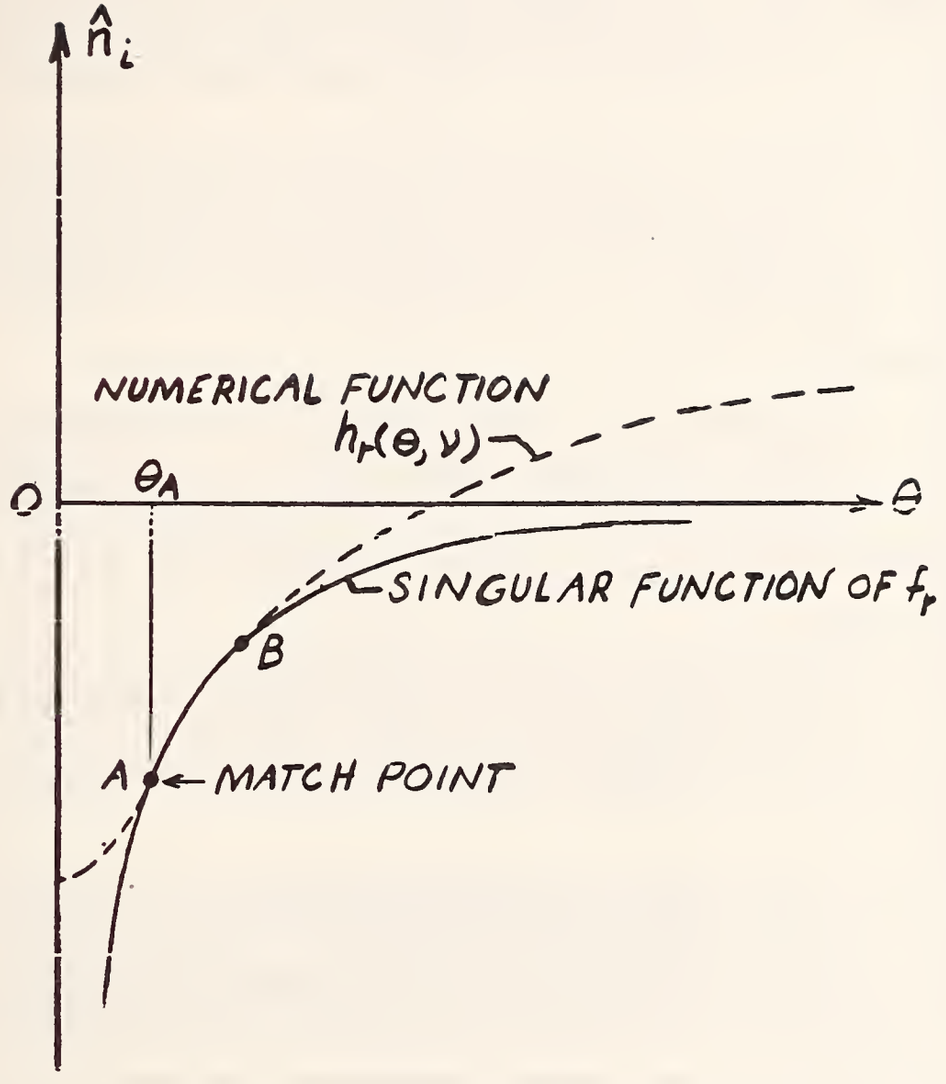

Fig. 4.8. Matching of analytic singularity to numerical (finite element) influence function.

TABLE 4.1

COMPARISON OF INFLUENCE FUNCTIONS GENERATED USING FINITE ELEMENTS
TO THE ANALYTIC SOLUTIONS FOR POINT LOADS ON A SPHERE

	DIMENSIONLESS RADIAL DISPLACEMENT			DIMENSIONLESS TANGENTIAL DISPLACEMENT		
THETA (DEG.)	ANALYTICAL SOLN.	FINITE ELEM. SOLN	PERCENT DIFF.	ANALYTICAL SOLN.	FINITE ELEM. SOLN	PERCENT DIFF.
0.2045459330-02	0.8113861710+04	0.1649658480+03	-0.9796686390+02	-0.2317904220+04	0.5889280760-02	0.1000002540+03
0.4088203330+00	0.4050229290+02	0.3424065740+02	-0.1545995300+02	-0.1128314630+02	-0.1346815630+01	0.8806347450+02
0.8176615050+00	0.2018073170+02	0.1955843050+02	-0.3083640570+01	-0.5483855840+01	-0.3067182390+01	0.4406887270+02
0.1226544310+01	0.1340073160+02	0.1327690670+02	-0.9240160070+00	-0.3549897840+01	-0.2747853170+01	0.2289345780+02
0.1634548950+01	0.1000761980+02	0.9980322290+01	-0.2727675410+00	-0.2581926800+01	-0.2283654620+01	0.1155230970+02
0.2044518310+01	0.7969822320+01	0.7949410310+01	-0.2561162160+00	-0.2000188000+01	-0.1872729940+01	0.6372303820+01
0.2453651170+01	0.6609952610+01	0.6587216510+01	-0.3439706630+00	-0.1611486740+01	-0.1544148870+01	0.4178617330+01
0.2862909090+01	0.5637618950+01	0.5613547550+01	-0.4269779930+00	-0.1333058110+01	-0.1288278370+01	0.3359173570+01
0.3272313500+01	0.4907583620+01	0.4884419400+01	-0.4720005640+00	-0.1123541590+01	-0.1087976000+01	0.3165488470+01
0.3681885030+01	0.4339138730+01	0.4317871900+01	-0.4901165430+00	-0.9599750950+00	-0.9288008800+00	0.3247398300+01
0.4091645720+01	0.3883844690+01	0.3865758380+01	-0.4656806220+00	-0.8285923850+00	-0.7993873720+00	0.3524653730+01
0.4501615330+01	0.3510870270+01	0.3494378570+01	-0.4697323920+00	-0.7206423620+00	-0.6943374240+00	0.3650207030+01
0.4911816050+01	0.3199653910+01	0.3188319170+01	-0.3542488570+00	-0.6302968740+00	-0.6012479590+00	0.4604876030+01
0.5322269900+01	0.2935957340+01	0.2924116640+01	-0.4032995640+00	-0.5535260160+00	-0.5341638920+00	0.3497961080+01
0.5732006630+01	0.2710116070+01	0.2697217450+01	-0.4759433900+00	-0.4876034150+00	-0.4709389020+00	0.3417636620+01
0.6140391690+01	0.2428193480+01	0.2416261470+01	-0.4913945240+00	-0.4050903530+00	-0.3910677700+00	0.3461593840+01
0.7011554080+01	0.2173410740+01	0.2162647990+01	-0.4952006010+00	-0.3303510690+00	-0.3191046970+00	0.3470436967D+01
0.7751680470+01	0.1943042310+01	0.1933417010+01	-0.4953725350+00	-0.2627320800+00	-0.2542312640+00	0.3235545650+01
0.8567392140+01	0.1734660670+01	0.1726101110+01	-0.4934428040+00	-0.2016939410+00	-0.1957632230+00	0.2940454250+01
0.9465900630+01	0.1546061850+01	0.1538490820+01	-0.4896978050+00	-0.1467837930+00	-0.1430783380+00	0.2524430870+01
0.1045485860+02	0.1375279140+01	0.1368626290+01	-0.4837456820+00	-0.9762612310-01	-0.9563768020-01	0.2036793880+01
0.1154264810+02	0.1220508760+01	0.1214702160+01	-0.4757522640+00	-0.5387856760-01	-0.5299491570-01	0.1640080580+01
0.1273818360+02	0.1080135040+01	0.1075098600+01	-0.4662787980+00	-0.1520723370-01	-0.1474498870-01	0.3039639010+01
0.1405108330+02	0.9526901920+00	0.9483501280+00	-0.4555587370+00	0.1876235080-01	0.1945897370-01	-0.3712876580+01
0.1549147380+02	0.8368604080+00	0.8331417750+00	-0.4443551900+00	0.4847635380-01	0.4987088140-01	-0.2932414510+01
0.1707019480+02	0.7314493370+00	0.7282762950+00	-0.4338020590+00	0.7447136670-01	0.7682138200-01	-0.3155595840+01
0.1879864970+02	0.6353769800+00	0.6326703590+00	-0.4259866690+00	0.9733475040-01	0.1004347090+00	-0.3184842760+01
0.2068886300+02	0.5476614040+00	0.5453520630+00	-0.4215271650+00	0.1176008930+00	0.1208954930+00	-0.2801508930+01
0.2275341160+02	0.4674128080+00	0.4654500330+00	-0.4199231530+00	0.1355839960+00	0.1383292320+00	-0.2029474860+01
0.2500532320+02	0.3938322860+00	0.3921841360+00	-0.4184904730+00	0.1512143940+00	0.1528158010+00	-0.1059031080+01
0.2745811070+02	0.3262119290+00	0.3248657750+00	-0.4126622650+00	0.1640088700+00	0.1644011630+00	-0.2391901350+00
0.3012565570+02	0.2639441660+00	0.2628910800+00	-0.3989805280+00	0.1733079980+00	0.1730968760+00	0.1218188850+00
0.3302203970+02	0.2065251000+00	0.2057405350+00	-0.3798888370+00	0.1787668320+00	0.1788827350+00	-0.6483504870-01
0.3616148380+02	0.1535411680+00	0.1529821720+00	-0.3640691860+00	0.1807648940+00	0.1817111500+00	-0.5234731990+00
0.3956821160+02	0.1046485240+00	0.1042747220+00	-0.3571973680+00	0.1801834590+00	0.1815133380+00	-0.7340692660+00
0.4322627520+02	0.5956783770-01	0.5936401960-01	-0.3421613900+00	0.1774147530+00	0.1782058930+00	-0.4459266560+00
0.4717937680+02	0.1811762430-01	0.1812070990-01	0.1703046730-01	0.1715957450+00	0.1717280980+00	-0.7713050450-01
0.5143069640+02	-0.1973798290-01	-0.1955554740-01	-0.9242861940+00	0.1615035440+00	0.1620946960+00	-0.3660305160+00
0.5999999990+02	-0.7917790840-01	-0.7941958170-01	0.3052281300+00	0.1338512810+00	0.1337398730+00	0.8323306990-01
0.6441173180+02	-0.1025410770+00	-0.1027311190+00	0.1853328120+00	0.1177611360+00	0.1173972980+00	0.3049624080+00
0.6884988940+02	-0.1217635980+00	-0.1218932530+00	0.1064808740+00	0.9951902460-01	0.9925398130-01	0.2663242960+00
0.7334237030+02	-0.1371503850+00	-0.1372089590+00	0.4270848570-01	0.7919041600-01	0.7957801210-01	-0.4899481630+00
0.7792021610+02	-0.1488552030+00	-0.1488710230+00	0.1062750030-01	0.5798489550-01	0.5852349810-01	-0.9248669630+00
0.8261987610+02	-0.1569066380+00	-0.1568753240+00	-0.1995727790-01	0.3616023180-01	0.3616165310-01	-0.3930419610-02
0.8748643490+02	-0.1611339470+00	-0.1609373460+00	-0.1220113080+00	0.1258548560-01	0.1255620210-01	0.2326770240+00
0.9000000000+02	-0.1616888830+00	-0.1611866960+00	-0.3105882850+00	-0.4691003500-07	0.7533453190-14	0.1000000160+03

surface nodes, the displacement at any surface point may be obtained through interpolation.

The computed displacements under the load are finite and the numerical results must be matched at some point near the load with the singularity of the function. It is shown in appendix A that the dominant singularities in the displacements under a point load on a sphere are indeed those of equations (4.1) and (4.2).

It was found that with an appropriately dense mesh, such as that shown in figure 4.7, the numerical influence function $h_r(\theta, \nu)$ would merge with its analytic singularity over a region near the load. This is illustrated in figure 4.8 where the numerical influence function h_r merges with the singular function in the region between A and B. The singularity was matched to the numerical function at A, thus between 0 and θ_A the behavior of the generated influence function was taken to be that of the singularity while for θ greater than θ_A the numerical values of h_r were utilized to describe the influence function $g_r(\theta, \nu)$. Similar treatment was used to generate $g_\theta(\theta, \nu)$.

A comparison of the displacement functions given by "analytic" equations (4.18) and (4.19) with the displacement function $h_r(\theta, \nu)$ at the node points of finite element analysis are given in table 4.1. It can be concluded that the numerical influence functions are accurate representations of the analytic ones.

4.6 Influence Function for a Point Load on a Spherical Cavity

The displacements due to a point load on a spherical cavity

have not been published to date. An investigation by Sternberg et al [1951], which deals with the solution to the axisymmetric problem of a region bounded by two concentric spheres, could be used under certain limiting conditions to produce the influence function; however, the limit process is very involved and has not been performed. For the purposes of the present research, the influence function for a point load on a spherical cavity is derived numerically as outlined in this section.

Consider a spherical cavity of Radius R under two diametrically opposed point loads, F. The material has elastic moduli E and ν. (see fig. 4.9)

The displacements u_r and u_θ are desired as a function of R, θ, E, ν, and F. From equation (4.17) which is also valid for a spherical seat, we note that the displacements must be at the form

$$u_r = \frac{F}{ER} g_r(\theta, \nu) \tag{4.30a}$$

and

$$u_\theta = \frac{F}{ER} g_\theta(\theta, \nu) \tag{4.30b}$$

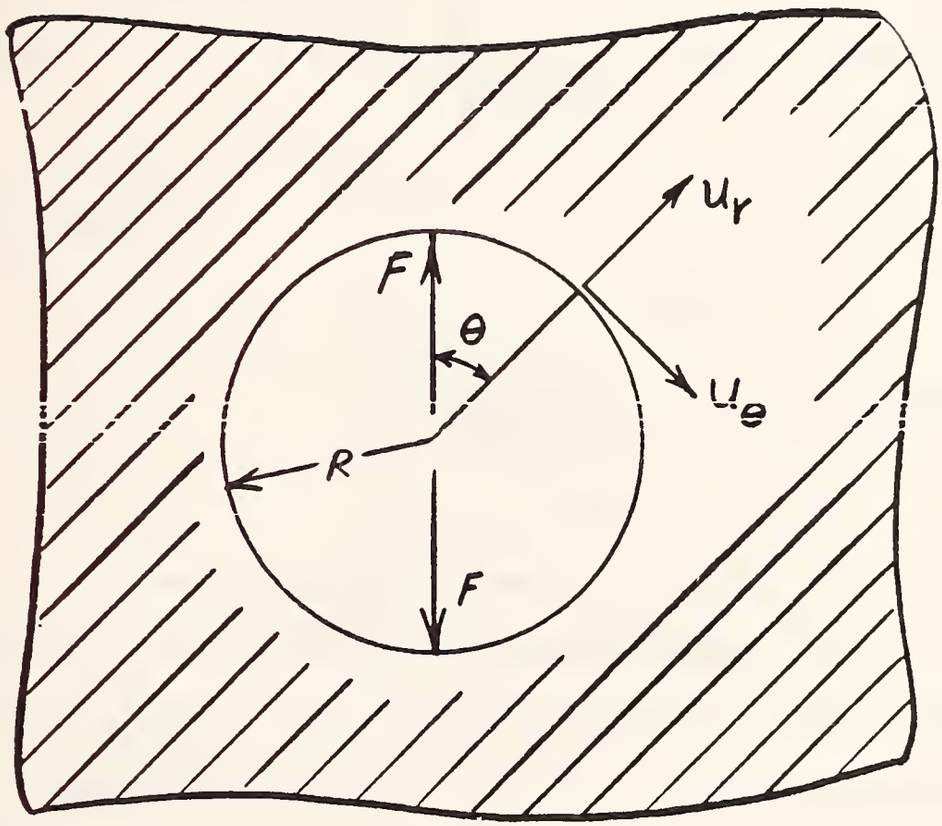

Fig. 4.9. Spherical cavity under diametrically opposed point loads

Now consider a $(\eta_2, \zeta_2, \gamma_2)$ coordinate system as shown in figure 4.11.

The influence function for radial and tangential displacements respectively due to loads, diametrically opposed on a spherical cavity, may be expressed in terms of a $(\eta_2, \zeta_2, \gamma_2)$ spherical coordinate system as

$$G(\phi,\beta,\phi',\beta',\nu,E,R) = \frac{1}{ER}\, g_r(\theta,\nu) \tag{4.31}$$

and

$$H(\phi,\beta,\phi',\beta',\nu,E,R) = \frac{1}{ER}\, g_\theta(\theta,\nu) \tag{4.32}$$

We seek to find the functions g_r and g_θ which are the displacements on the internal spherical boundary surface of an infinite region under a loading condition such that F/ER = 1. These displacement functions can be easily found using a single finite element analysis.

Consider the discretized model of a spherical cavity in an infinite medium as shown in figure 4.11. The model represents the loading illustrated in figure 4.9. Each element is a ring, axisymmetric about the z axis. The boundary conditions for the model restrict the nodes on the z axis to move only in the z direction while those on the x axis are allowed to move only in the x direction. The

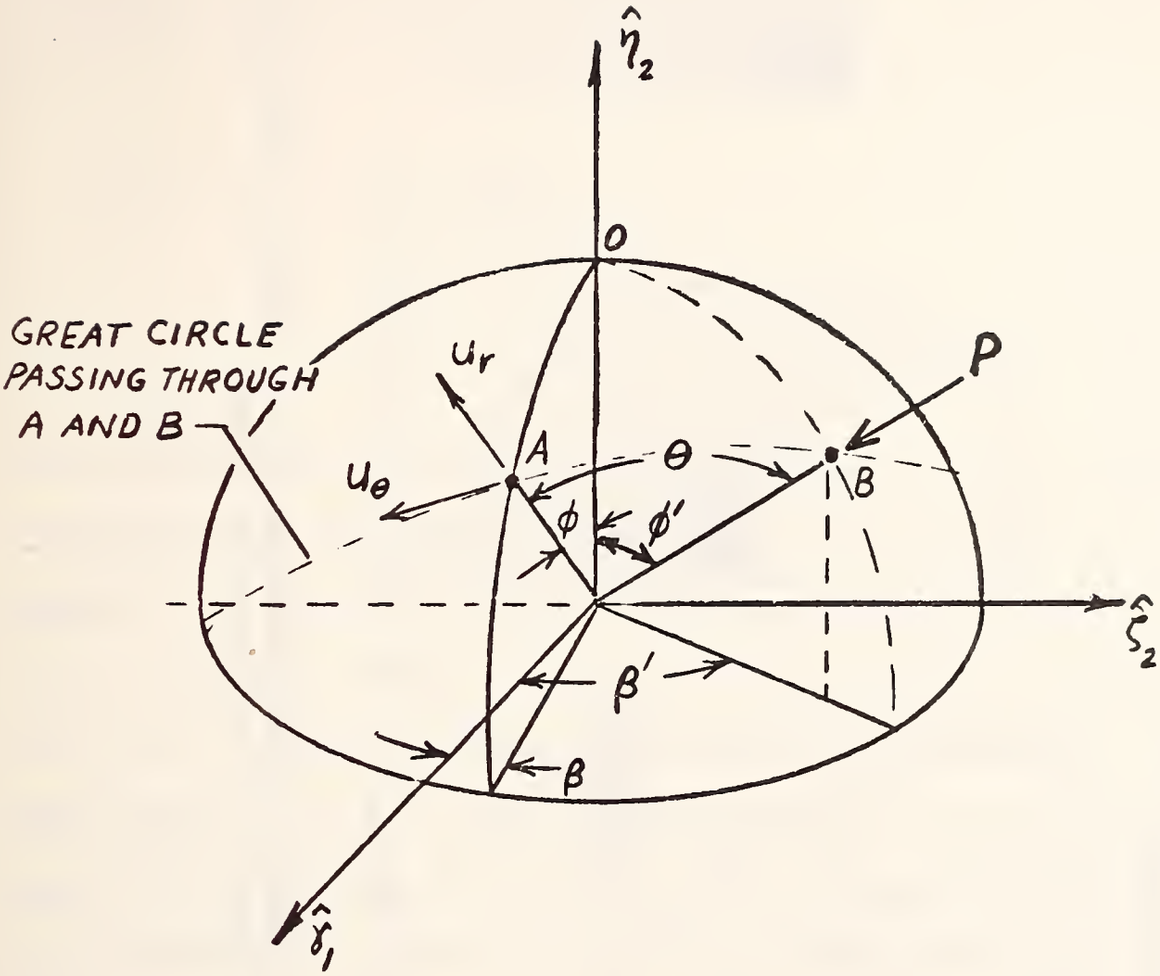

Fig. 4.10. Coordinate system for influence functions for a point load on a spherical seat.

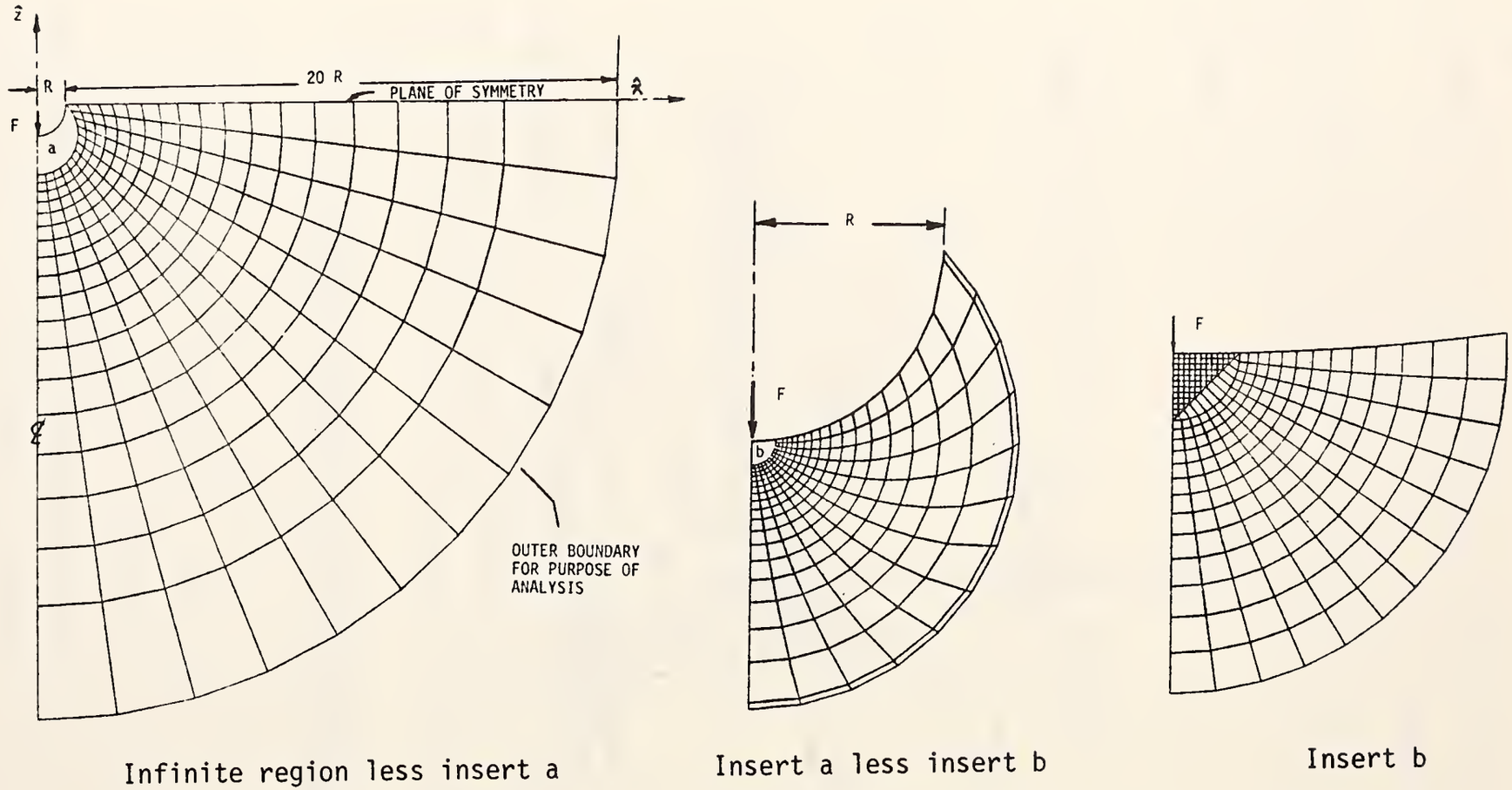

Infinite region less insert a

Insert a less insert b

Insert b

Fig. 4.11. Axisymmetric finite element model of a spherical cavity in an infinite region under diametrically opposed point loads.

nodes on the outer boundary were free. The values of the Force F, radii, Poisson's Ratio and Young's modulus used in the finite element analysis were as follows

$$F = 30 \times 10^7 \text{ lb.}$$
$$R = 10 \text{ in.}$$

$$R_o = 200 \text{ in.}$$
$$\nu = 0.3 \text{ and } 0.25$$
$$E = 30 \times 10^6 \text{ psi} \qquad (4.33)$$

The solution of the finite element analysis gives the values of the displacements on the surface of the cavity at the nodal points in figure 4.11. These displacements, u_r and u_θ, under conditions where F/ER = 1, actually represent the values of the functions $g_r(\theta, \nu)$ and $g_\theta(\theta, \nu)$. Therefore by interpolating between these values an approximation of $g_r(\theta, \nu)$ and $g_\theta(\theta, \nu)$ is known for all θ. As with the influence functions for the sphere, the singularities of equations (4.31) and (4.32) near the point load were represented by equations (4.1) and (4.2).

4.7 Influence Functions for a Cylinder Under Concentrated Line Loads

Consider a long cylinder under two concentrated line loads as shown in figure 4.12.

The problem is one of plane strain and has been solved in Muskhelishvili [1963]. The displacements at the point Q, in terms of

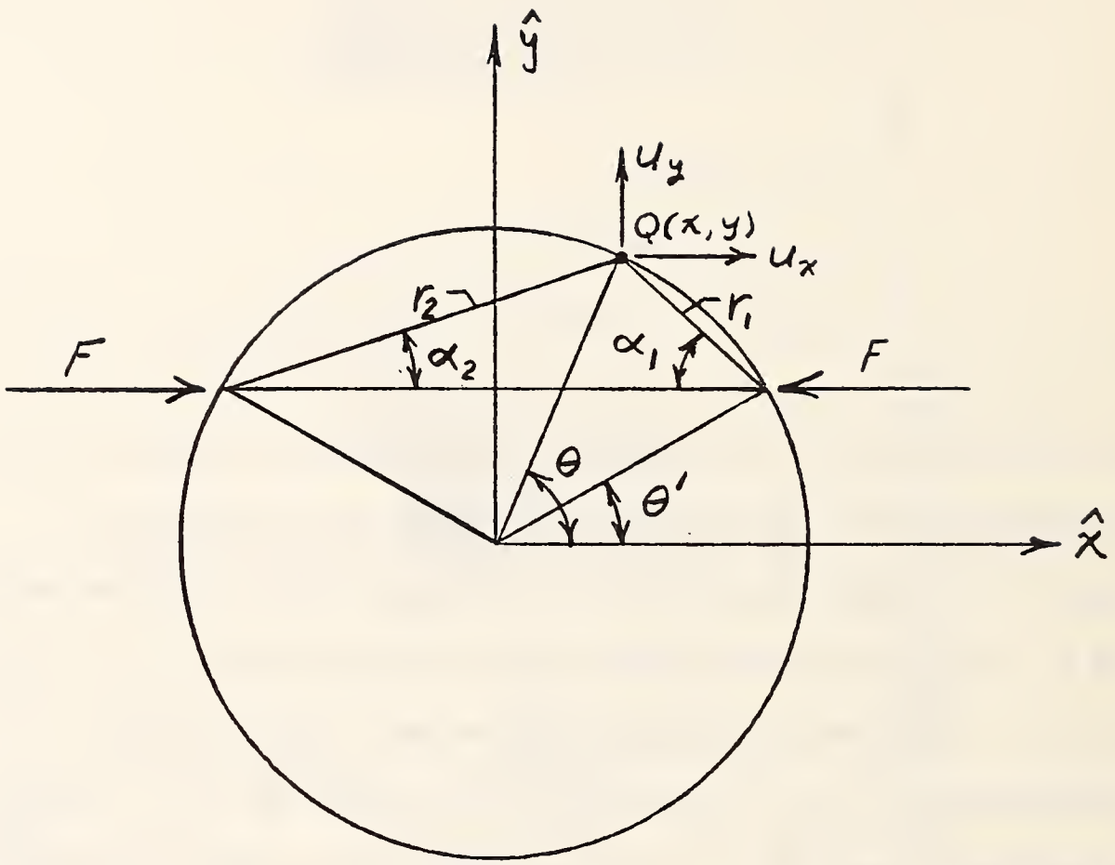

Fig. 4.12. Geometry of a cylinder under two line loads

quantities labeled in figure 4.12, are

$$u_x(x,y) = -\frac{F}{4\pi\mu}\left\{\frac{2(\lambda+2\mu)}{(\lambda+\mu)}\ln\frac{r_2}{r_1} + \right.$$

$$\left. + (\cos 2\alpha_1 - \cos 2\alpha_2) - \frac{2\mu\cos\theta'}{(\lambda+\mu)R}\,x\right\} \qquad (4.34)$$

and

$$u_y(x,y) = -\frac{F}{4\pi\mu}\left\{\frac{2\mu}{(\lambda+\mu)}(\alpha_1+\alpha_2) - \right.$$

$$\left. - (\sin 2\alpha_1 + \sin 2\alpha_2) - \frac{2\mu\cos\theta'}{(\lambda+\mu)R}\,y\right\} \qquad (4.35)$$

where F is a line load expressed in units of force/length, u_x and u_y are the displacements in the x and y directions respectively, and λ and μ are the Lame' constants of the cylinder. Equations (4.34) and (4.35) may be combined to find the displacement field in polar cordinates of a cylinder under two diametrically opposed line loads, as illustrated in figure 4.13.

The derivation of u_r and u_θ is performed in appendix B. The results are as follows:

$$u_r = -F K_1\left\{\cos\theta \ln\tan\frac{\theta}{2} + 1\right\} + F\,\frac{K_2}{\pi}\sin\theta \qquad (4.36)$$

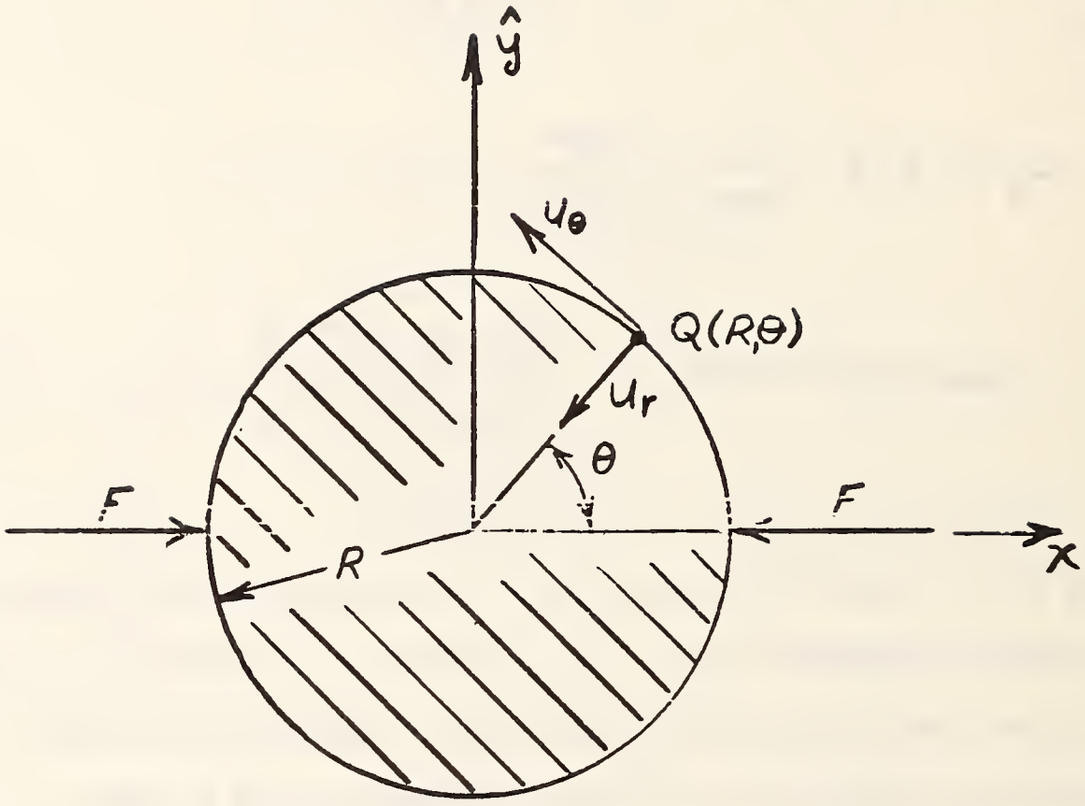

Fig. 4.13. Polar coordinate system for a cylinder under two diametrically opposed line loads.

and

$$u_\theta = -F K_1 \sin\theta \ln \tan \frac{\theta}{2} - F \frac{K_2}{\pi} \cos\theta \tag{4.37}$$

where

$$K_1 = \frac{2(1-\nu^2)}{\pi E} \tag{4.38}$$

and

$$K_2 = \frac{(1+\nu)(1-2\nu)}{2E} \tag{4.39}$$

The influence function for a line load on a cylinder may be formed from equations (4.36) and (4.37) by considering θ to be the angle between the vector describing the position of the unit load F and the point Q. The influence functions in the radial and tangential directions respectively are

$$G(\theta, \theta', \nu, E) = -K_1 \left\{ \cos(\theta-\theta') \ln \tan \frac{\theta-\theta'}{2} + 1 \right\} + \frac{K_2}{\pi} \sin(\theta-\theta') \tag{4.40}$$

and

$$H(\theta,\theta';\nu,E) = -K_1 \sin(\theta-\theta') \ln \tan\left[\frac{\theta-\theta'}{2}\right] + \frac{1}{\pi} K_2 \cos(\theta-\theta') \tag{4.41}$$

where θ and θ' are illustrated in figure 4.14.

It is important to note that equations (4.40) and (4.44) represent the influence function for two diametrically opposed line loads. They may be integrated as shown below to find the displacements u_r (θ, R) and u_θ (θ, R) due to two symmetric loadings p (θ), where $p(\theta) = p(\theta + \pi)$. The displacements may be calculated by

$$u_r(\theta,R) = \int_\Omega G(\theta,\theta';\nu,E)\, p(\theta')\, R\, d\theta' \tag{4.42}$$

and

$$u_\theta(\theta,R) = \int_\Omega H(\theta,\theta';\nu,E)\, p(\theta')\, R\, d\theta' \tag{4.43}$$

Now consider the numerical generation of equations (4.40) and (4.41). It is known that the displacements u_r and u_θ due to diametrically opposed point loads, F are functions of θ, F, E, ν and R, where

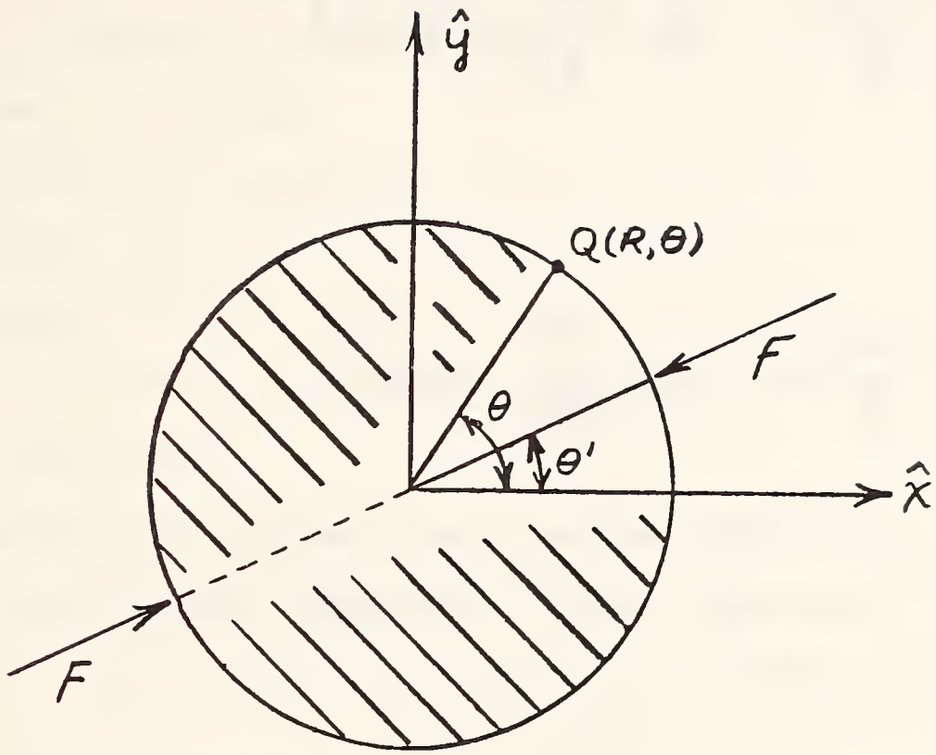

Fig. 4.14. Coordinate system for the influence functions of a cylinder under two diametrically opposed line loads.

E and ν are the elastic constants of the cylinder of radius R. From dimensional analysis the displacements u_r and u_θ may be expressed in the forms

$$\frac{u_r}{R} = g_r\left(\frac{F}{ER}, \theta, \nu\right) \tag{4.44}$$

and

$$\frac{u_\theta}{R} = g_\theta\left(\frac{F}{ER}, \theta, \nu\right) \tag{4.45}$$

Furthermore, because of the linearity of the problem, the ratio $\frac{F}{ER}$ must appear linearly in the above equations; hence u_r and u_θ may be expressed in the form:

$$u_r = \frac{F}{E} g_r(\theta, \nu) \tag{4.46}$$

and

$$u_\theta = \frac{F}{E} g_\theta(\theta, \nu) \tag{4.47}$$

We therefore seek to find the dimensionless functions $g_r(\theta, \nu)$ and

g_θ (θ, ν) which represent the displacements u_r and u_θ under the conditions that F/E = 1. These functions may be found with one finite element analysis of a cylinder under two diametrically opposed line loads.

Consider the model of a cylinder given by the finite element representation in figure 4.15. The elements are plane stress elements. The line load per unit thickness, F, is applied and due to the symmetry of loading only the upper-right quarter of the cylinder is considered. Nodes on the x axis are restricted to move only along the x axis and nodes on the z axis are restricted to move only along the z axis. For the solution at hand the values of the parameters P, E, ν and R were taken as

$$\begin{aligned} P &= 3 \times 10^7 \text{ lb/in.} \\ E &= 32.967 \times 10^6 \text{ psi} \\ \nu &= 0.42857 \\ R &= 1 \text{ in.} \end{aligned} \qquad (4.48)$$

The values of E and ν used above represent the moduli in plane stress which are equivalent to the values of $E = 30 \times 10^6$ psi and $\nu = 0.3$ in plane strain. These values were determined via equation (4.11) and the results are appropriate for the plane strain model with the noted values of E and ν. The solution yields the values of the displacements, u_r and u_θ at the surface nodes in figure 4.15. These

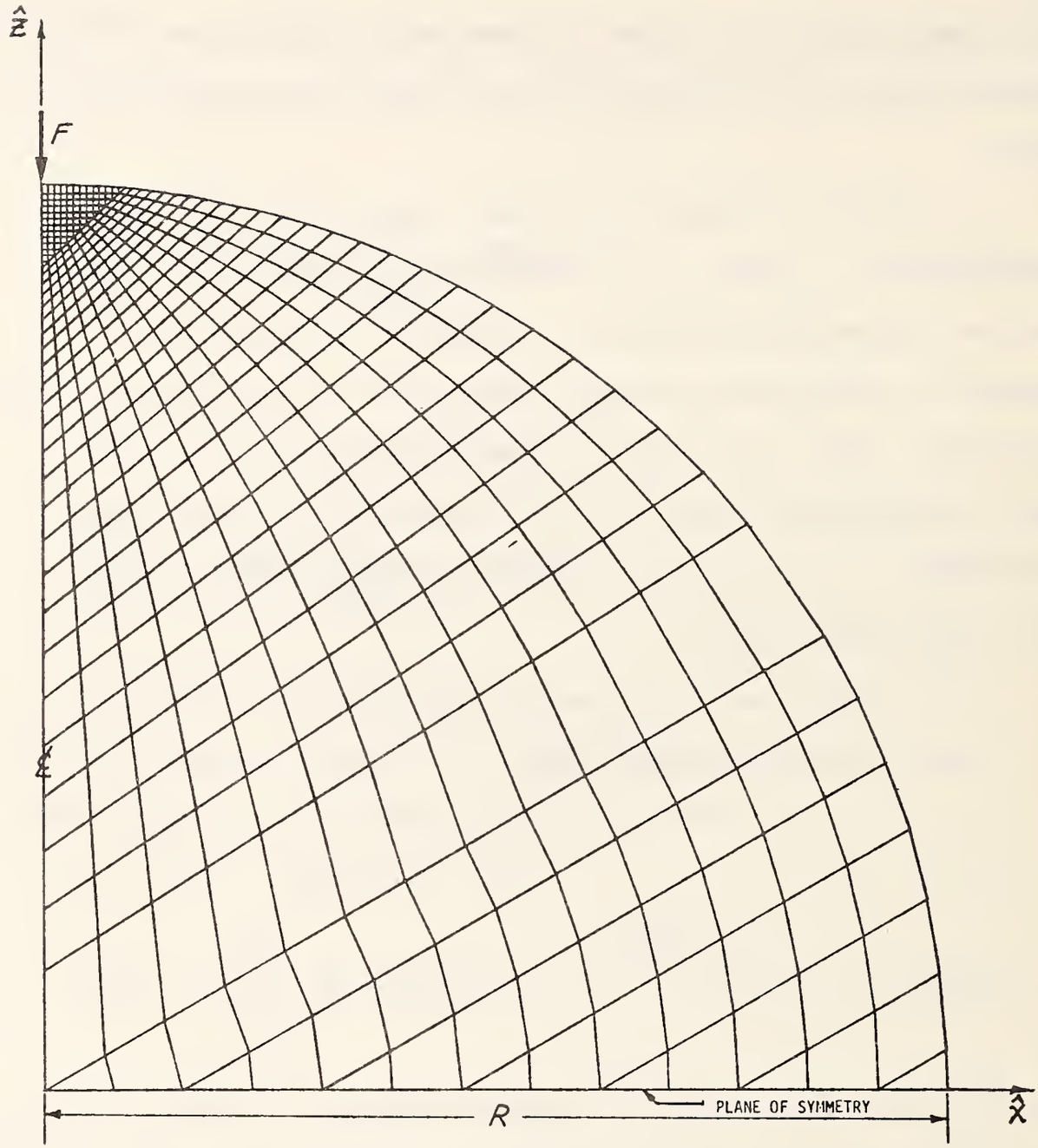

Fig. 4.15. Plane stress finite element model of a cylinder under line loads.

TABLE 4.2

COMPARISON OF INFLUENCE FUNCTIONS GENERATED USING FINITE ELEMENTS TO THE ANALYTIC SOLUTIONS FOR LINE LOADS ON A CYLINDER

	DIMENSIONLESS RADIAL DISPLACEMENT			DIMENSIONLESS TANGENTIAL DISPLACEMENT		
THETA (DEG.)	ANALYTICAL SOLN.	FINITE ELEM. SOLN	PERCENT DIFF.	ANALYTICAL SOLN.	FINITE ELEM. SOLN	PERCENT DIFF.
0.57295836A0-04	0.7825A89220+01	0.3755788930+01	0.5200815110+02	-0.2599915950+00	0.375579269D-05	0.1000014450+03
0.4088090790+00	0.2687446730+01	0.2651919940+01	0.1321953290+01	-0.2366976030+00	-0.1349376020+00	0.4299156400+02
0.8176394880+00	0.2287514100+01	0.2292281890+01	-0.2084264090+00	-0.2191124830+00	-0.1892381260+00	0.1363425590+02
0.1226510920+01	0.2054126170+01	0.2057000060+01	-0.1390082400+00	-0.2036776150+00	-0.1949983360+00	0.4261282570+01
0.1635446860+01	0.1888068060+01	0.1889710280+01	-0.4501228730-01	-0.1896350010+00	-0.1840954920+00	0.8118274400+00
0.2044465750+01	0.1760901390+01	0.1760008780+01	0.5069031740-01	-0.1766246880+00	-0.1769242590+00	-0.1696093280+00
0.2453639970+01	0.1656483290+01	0.1654646670+01	0.1109474100+00	-0.1644335910+00	-0.1648926290+00	-0.2791632080+00
0.2862888770+01	0.1568314640+01	0.1566043660+01	0.1448040200+00	-0.1529248050+00	-0.1529704250+00	-0.2983150150-01
0.3272280810+01	0.1492011690+01	0.1489662340+01	0.1574619870+00	-0.1419975430+00	-0.1415290510+00	0.3299296160+00
0.3681842970+01	0.1424755500+01	0.1422498080+01	0.1584424960+00	-0.1315774730+00	-0.1306428530+00	0.7103125630+00
0.4091593060+01	0.1364623460+01	0.1362614360+01	0.1472272890+00	-0.1216071750+00	-0.1202348370+00	0.1128500710+01
0.4501608860+01	0.1310237190+01	0.1308382810+01	0.1415300970+00	-0.1120394710+00	-0.1104489950+00	0.1419567350+01
0.4911796650+01	0.1260599860+01	0.1259274090+01	0.1051696440+00	-0.1028395900+00	-0.1005623190+00	0.2194944260+01
0.5322239390+01	0.1214934940+01	0.1213553370+01	0.1137153440+00	-0.9397494310-01	-0.9232799910-01	0.1752535320+01
0.5731978150+01	0.1172743120+01	0.1171196700+01	0.1318638760+00	-0.8543932210-01	-0.8378584440-01	0.1935253720+01
0.6340394220+01	0.1115359220+01	0.1113940600+01	0.1264728210+00	-0.7329592010-01	-0.7154059820-01	0.2383927890+01
0.7011536440+01	0.1058117170+01	0.1056865290+01	0.1183117440+00	-0.6057185530-01	-0.5877594070-01	0.2964932350+01
0.7751631430+01	0.1001001560+01	0.9999011840+00	0.1099279920+00	-0.4727907510-01	-0.4548512070-01	0.3794394040+01
0.8567369240+01	0.9440016350+00	0.9430463150+00	0.1011990250+00	-0.3343996080-01	-0.3166441340-01	0.5309657460+01
0.9465929830+01	0.8871089590+00	0.8862878400+00	0.9256120850-01	-0.1908875140-01	-0.1734917650-01	0.9113089030+01
0.1045486240+02	0.8303223340+00	0.8296249290+00	0.8399203020-01	-0.4274851270-02	-0.2581724650-02	0.3960667900+02
0.1154263240+02	0.7736223650+00	0.7730377350+00	0.7557047760-01	0.1094181810-01	0.1257548460-01	-0.1493048420+02
0.1273817820+02	0.7169901850+00	0.7165056490+00	0.6757926380-01	0.2648416870-01	0.2805779080-01	-0.5941746390+01
0.1405109860+02	0.6604085060+00	0.6600078990+00	0.6066056440-01	0.4225541530-01	0.4376342310-01	-0.3568791730+01
0.1549150900+02	0.6038637010+00	0.6035381610+00	0.5390956850-01	0.5813627630-01	0.5958184960-01	-0.2486525450+01
0.1707016650+02	0.5473423680+00	0.5470846630+00	0.4708293770-01	0.7398387140-01	0.7536549980-01	-0.1867472460+01
0.1879862610+02	0.4908290450+00	0.4906265800+00	0.4124970170-01	0.8963048080-01	0.9094732360-01	-0.1469190860+01
0.2068889740+02	0.4343213560+00	0.4341641760+00	0.3618981140-01	0.1048776820+00	0.1061381120+00	-0.1201809360+01
0.2275343930+02	0.3778316540+00	0.3777108470+00	0.3197371930-01	0.1194949280+00	0.1207015200+00	-0.1009742880+01
0.2500531170+02	0.3213867830+00	0.3212964290+00	0.2811387520-01	0.1332193340+00	0.1343787890+00	-0.8703353280+00
0.2745809160+02	0.2650368800+00	0.2649721220+00	0.2443360720-01	0.1457539680+00	0.1468729360+00	-0.7677101610+00
0.3012557470+02	0.2088693120+00	0.2088250630+00	0.2115092000-01	0.1567666040+00	0.1578509070+00	-0.6916672710+00
0.3302207330+02	0.1530107650+00	0.1529848950+00	0.1690771010-01	0.1658929110+00	0.1669502710+00	-0.6373754970+00
0.3616147350+02	0.9765590410-01	0.9764839780-01	0.7686428070-02	0.1727373280+00	0.1737778030+00	-0.6023453610+00
0.3955816420+02	0.4306107420-01	0.4307293310-01	-0.2753960730-01	0.1768829010+00	0.1779182720+00	-0.5853422630+00
0.4322624420+02	-0.1042671440-01	-0.1039603710-01	0.2942179550+00	0.1778948700+00	0.1789491420+00	-0.5903756750+00
0.4717938500+02	-0.6235373610-01	-0.6228734260-01	0.1064786730+00	0.1753555840+00	0.1764833900+00	-0.6431537440+00
0.5143071080+02	-0.1121427570+00	-0.1120333500+00	0.9756016670-01	0.1688444680+00	0.1702268670+00	-0.8187408950+00
0.5600000940+02	-0.1950443520+00	-0.1953718770+00	-0.1679232120+00	0.1455919660+00	0.1455503970+00	0.2855192770-01
0.6091173870+02	-0.2291693740+00	-0.2294546760+00	-0.1244976050+00	0.1292236380+00	0.1295359930+00	-0.2417166360+00
0.6616989550+02	-0.2578633600+00	-0.2581288540+00	-0.1029589800+00	0.1103246580+00	0.1107749330+00	-0.4081358330+00
0.7334234890+02	-0.2812599910+00	-0.2814726430+00	-0.7560685150-01	0.8915197590-01	0.8964069420-01	-0.5481856170+00
0.7792023340+02	-0.2993290210+00	-0.2994915370+00	-0.5429354050-01	0.6591907570-01	0.6640278580-01	-0.7337938090+00
0.8261989560+02	-0.3118660960+00	-0.3119855540+00	-0.3830449650-01	0.4081104650-01	0.4125568390-01	-0.1089502520+01
0.8748648520+02	-0.3184592290+00	-0.3183417930+00	0.3687644600-01	0.1399581390-01	0.1445070720-01	-0.3250209500+01
0.9000000000+02	-0.3193239930+00	-0.3187125000+00	0.1914959000+00	0.1491805540-13	0.1489580570-13	0.1491461420+00

displacements represent the values of $g_r(\theta, \nu)$ and $g_\theta(\theta, \nu)$ at the nodal points in the finite element model. The functions $g_r(\theta, \nu)$ and $g_\theta(\theta, \nu)$ can therefore be approximated by interpolating between these values.

The singularities for the functions g_r and g_θ are given by equations (4.14) and (4.15), that is, those singularities appropriate to the line load on a plane. It is shown in Appendix C that these are indeed the correct singularities since the functions in equations (4.12) and (4.13) approach infinity in exactly the same manner as equations (4.36) and (4.37), respectively.

It may be concluded that by knowing values of $g_r(\theta, \nu)$ and $g_\theta(\theta, \nu)$ at the nodal points in figure 4.15 and by having correctly identified the singularities of those functions, the influence functions for line loads on a cylinder have been determined. As a final check on the accuracy of such a function the values of the displacements g_r and g_θ from the finite element analysis have been compared to those of equations (4.12) and (4.13) in table 4.2. It is clearly indicated that the finite element solution gives a very accurate representation of the displacements up to within a half degree from the applied force.

4.8 Influence Function for a Line Load on a Cylindrical Cavity

Consider a cylindrical cavity within an infinite solid body. Given that two line loads, F, diametrically opposed, are applied to the cavity surface, the displacements u_r and u_θ are derived from known elasticity solutions in Appendix D. (see figure 4.16)

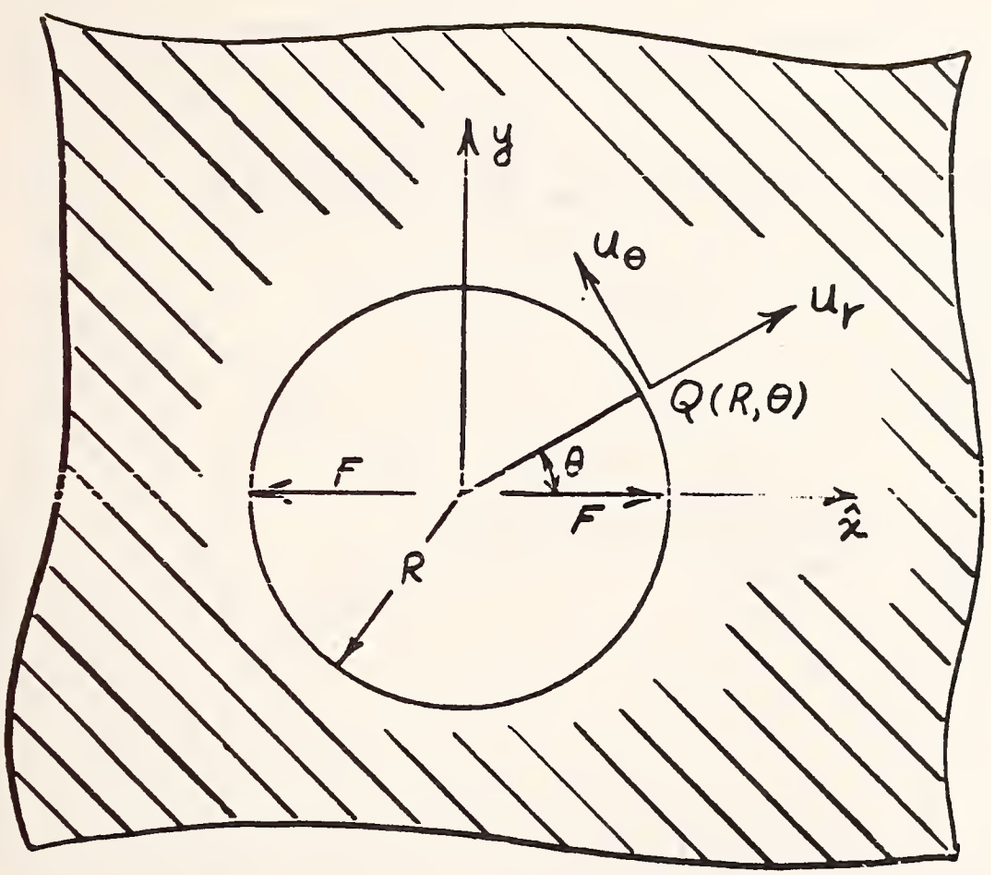

Fig. 4.16. Cylindrical cavity under two diametrically opposed line loads.

They are as follows:

$$u_r = F\left\{ K_1 \cos\theta \ln \tan\frac{\theta}{2} + K_2 \sin\theta \right\} \tag{4.49}$$

and

$$u_\theta = F\left\{ K_1 \sin\theta \ln \tan\frac{\theta}{2} - K_2 \cos\theta \right\} \tag{4.50}$$

where

$$K_1 = \frac{2(1-\nu^2)}{\pi E} \tag{4.51}$$

and

$$K_2 = \frac{(1-2\nu)(1+\nu)}{2E} \tag{4.52}$$

The influence functions for u_r and u_θ can be derived simply from equations (4.49) and (4.50). By considering F to be a unit load per unit width and by replacing θ by $\theta-\theta'$ as illustrated in figure 4.17.

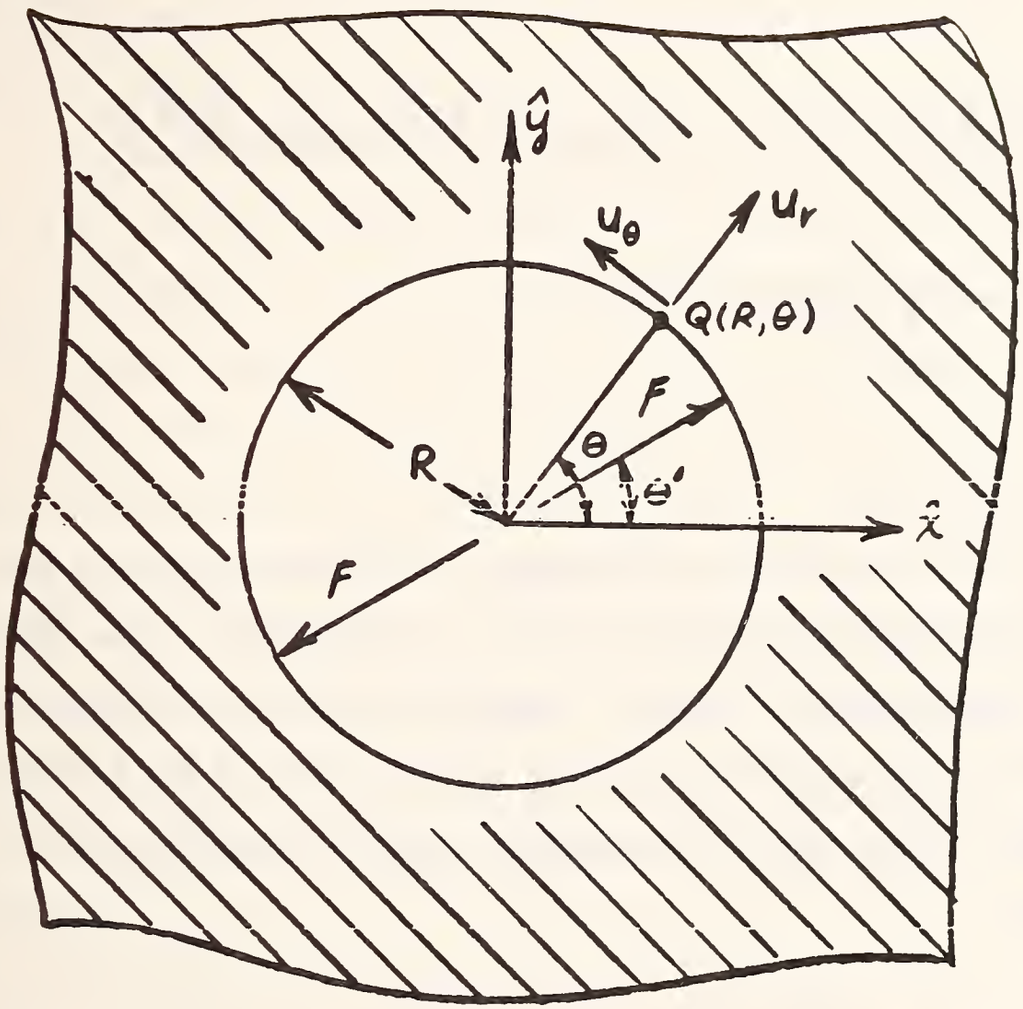

Fig. 4.17. Coordinate system for the influence functions of a cylindrical cavity under two diametrically opposed line loads.

the influence function for two line loads on a cylinder become

$$G(\theta,\theta',\nu,E) = -K_1 \cos(\theta-\theta') \ln \tan\left|\frac{\theta-\theta'}{2}\right| \qquad (4.53)$$

$$- K_2 \sin|(\theta-\theta')|$$

and

$$H(\theta,\theta',\nu,E) = K_1 \sin(\theta-\theta') \ln \tan\left|\frac{\theta-\theta'}{2}\right|$$

$$- K_2 \cos(\theta-\theta') \qquad (4.54)$$

It is interesting to note that the influence functions for both the cylinder and cylindrical seat are independent of the radius R, since the dimensional analysis leading to equations (4.44) and (4.45) are valid for the cylindrical cavity as well as for the solid cylinder. Accordingly, the displacement functions for the cylindrical seat are:

$$u_r = \frac{F}{E} g_r(\phi,\nu) \qquad (4.55)$$

and

$$u_\theta = \frac{F}{E} g_\phi(\phi,\nu) \qquad (4.56)$$

where ϕ represents the difference between the angular position of the force and the displacement, i.e., θ-θ' in figure 4.17. The functions $g_r(\phi, \nu)$ and $g_\theta(\phi, \nu)$ represent the displacement on a cylinder where the ratio $F/E = 1$. An approximation to these functions may be obtained through finite element analysis. From equations (4.55) and (4.56) we see that the required influence functions are found by dividing g_r and g_ϕ by E.

Consider the model of a cylindrical cavity as illustrated in figure 4.18. The model represents the loadings illustrated in figure 4.17. The points along the z axis are restricted to move only along the z axis and likewise the points on the x axis are restricted to move on the x axis. The outside radius is thought to be sufficiently removed from the cavity to consider it at infinity. In the mathematical problem both the stresses and displacements vanish at infinity. Therefore, two cases of boundary conditions will be considered at the outside radius in the discretized model. In the first case those points are free while in the second they will be fixed rigidly.

For the example at hand the values of $\bar{E}$, $\bar{\nu}$, R, R_o and F were as follows:

$$
\begin{aligned}
F &= 3 \times 10^7 \text{ lb} \\
\bar{E} &= 32.967 \times 10^6 \text{ psi} \\
\bar{\nu} &= 0.42857 \\
R &= 1 \text{ in} \\
R_o &= 20 \text{ in}
\end{aligned}
\qquad (4.57)
$$

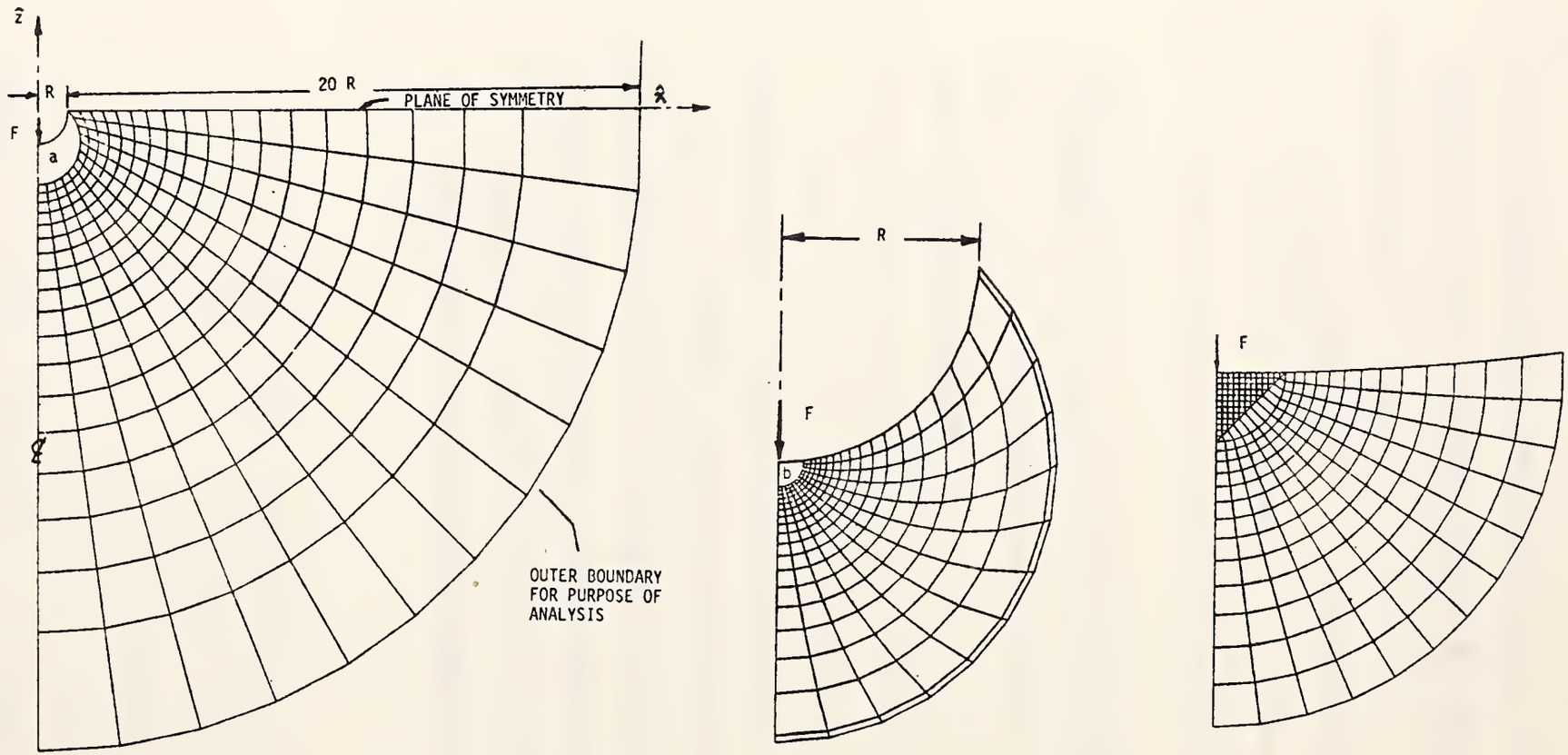

Fig. 4.18. Plane stress finite element model of a cylindrical cavity in an infinite region under two diametrically opposed line loads.

The results of the surface nodal point displacement for the free and fixed boundary conditions are compared to the analytic solutions in tables 4.3 and 4.4 respectively. The results indicate that the boundary condition at the outside radius which most closely models the true condition is when those points are considered to be free. The finite element data in table 4.3 shows good agreement between the numerical and analytic solutions. While the data in table 4.4 also indicates a close correspondence it does not agree as well as the results in table 4.3.

Again there is the problem of finding the appropriate singularity. As might be expected, the Flamant solution for a line load on a plane, represents the singularity for the case of a line load on a cylindrical cavity. This is proven in appendix E.

From the above finite element analysis, the functions $g_r(\phi, \nu)$ and $g_\phi(\phi, \nu)$ may be evaluated away from the applied loads by interpolating between the nodal displacements. The Flamant singularity, given by equation (4.14), may be used as the singularity of the function (4.55), while the constant in equation (4.15) may be substituted for the limit of equation (4.56) near the applied loads. Having constructed equations (4.55) and (4.56), the displacements u_r and u_θ due to distributed line loads $p(\theta)$ and $p(\theta + \pi)$, where $p(\theta) = p(\theta + \pi)$, may be calculated from equations (4.42) and (4.43) respectively.

TABLE 4.3
COMPARISON OF INFLUENCE FUNCTIONS GENERATED USING FINITE ELEMENTS TO THE ANALYTIC SOLUTIONS FOR LINE LOADS ON A CYLINDRICAL CAVITY
(OUTER BOUNDARY OF FINITE ELEMENT MODEL FREE)

	DIMENSIONLESS RADIAL DISPLACEMENT			DIMENSIONLESS TANGENTIAL DISPLACEMENT		
THETA (DEG.)	ANALYTICAL SOLN.	FINITE ELEM. SOLN	PERCENT DIFF.	ANALYTICAL SOLN.	FINITE ELEM. SOLN	PERCENT DIFF.
0.5729572220-04	0.8405213850+01	0.5145587900+01	0.387A099960+02	-0.2600084050+00	-0.51455P2760-05	0.9999802100+02
0.1192897600+00	0.3978000200+01	0.3890324400+01	0.2204017090+01	-0.2682827680+00	-0.2242413560+00	0.1641604210+02
0.2386372120+00	0.3575738730+01	0.3554582870+01	0.5916500380+00	-0.2748953110+00	-0.2723745810+00	0.9169783070+00
0.3579858160+00	0.3340217680+01	0.3312160090+01	0.8399930160+00	-0.2808751310+00	-0.2772214500+00	0.1300817520+01
0.4773358480+00	0.3172942550+01	0.3147527840+01	0.8009822870+00	-0.2864436800+00	-0.2831359600+00	0.1154753A30+01
0.5967455940+00	0.3042997820+01	0.3018482170+01	0.8056413510+00	-0.2917006050+00	-0.2880443960+00	0.1256119580+01
0.7161012220+00	0.2936760970+01	0.2913485580+01	0.7925533570+00	-0.2967268100+00	-0.2928290420+00	0.1313588020+01
0.8354582740+00	0.2846835300+01	0.2824767190+01	0.7751806470+00	-0.3015417080+00	-0.2974500060+00	0.1356661970+01
0.9548212030+00	0.2768843460+01	0.2747831610+01	0.7588674110+00	-0.3061825290+00	-0.3021600880+00	0.1313478100+01
0.1074243400+01	0.2699935660+01	0.2679792150+01	0.7460739280+00	-0.3106729590+00	-0.3067166560+00	0.1273462200+01
0.1193613540+01	0.2638249200+01	0.2618430580+01	0.7512032980+00	-0.3150256720+00	-0.3113511730+00	0.1166412550+01
0.1312932390+01	0.2582400810+01	0.2563326360+01	0.7386323700+00	-0.3192543340+00	-0.3149905370+00	0.1333042950+01
0.1432312410+01	0.2531324060+01	0.2511941230+01	0.7657191070+00	-0.3233739220+00	-0.3198832420+00	0.1079456310+01
0.1621340970+01	0.2458448740+01	0.2439226970+01	0.7818655600+00	-0.3296912480+00	-0.3260924510+00	0.1091567220+01
0.1835497590+01	0.2385353140+01	0.2366307750+01	0.7984305590+00	-0.3365755480+00	-0.3325A29290+00	0.1186247440+01
0.2078285510+01	0.2311970810+01	0.2293416000+01	0.8025539600+00	-0.3440698810+00	-0.3397333310+00	0.1260368910+01
0.2353566630+01	0.2238272580+01	0.2220317920+01	0.8021659090+00	-0.3522138720+00	-0.3475989390+00	0.1310264510+01
0.2665673460+01	0.2164235590+01	0.2146932920+01	0.7994814700+00	-0.3610449410+00	-0.3562780570+00	0.1320301930+01
0.3019909460+01	0.2089750520+01	0.2073136460+01	0.7950257410+00	-0.3706089170+00	-0.3657120990+00	0.1321289820+01
0.3421958440+01	0.2014782070+01	0.1998841870+01	0.7911622820+00	-0.3809394150+00	-0.3759384660+00	0.1312793660+01
0.3878561320+01	0.1939238530+01	0.1923976950+01	0.7869883670+00	-0.3920719060+00	-0.3869862530+00	0.1297122510+01
0.4397466140+01	0.1863016990+01	0.1848428730+01	0.7830448710+00	-0.4040361290+00	-0.3988561150+00	0.1282067030+01
0.4987532430+01	0.1786007960+01	0.1772094790+01	0.7790096920+00	-0.4168520420+00	-0.4115707530+00	0.1266945600+01
0.5659020570+01	0.1708077790+01	0.1694849440+01	0.7744585010+00	-0.4305284390+00	-0.4251473400+00	0.1249880380+01
0.6423806400+01	0.1629069830+01	0.1616538370+01	0.7692399450+00	-0.4450576050+00	-0.4395591230+00	0.1235453060+01
0.7295860810+01	0.1548783960+01	0.1536963740+01	0.7631935320+00	-0.4604123200+00	-0.4548003950+00	0.1218891100+01
0.8291235590+01	0.1467009440+01	0.1455904380+01	0.7569867020+00	-0.4765306180+00	-0.4707906420+00	0.1204534560+01
0.9428921140+01	0.1383480790+01	0.1373117520+01	0.7490725760+00	-0.4933121110+00	-0.4874464620+00	0.1189034120+01
0.1073138310+02	0.1297881240+01	0.1288283550+01	0.7394886200+00	-0.5106016540+00	-0.5046025940+00	0.1174900370+01
0.1222520480+02	0.1209844390+01	0.1201041840+01	0.7275773440+00	-0.5281676380+00	-0.5220370590+00	0.1160725820+01
0.1394212410+02	0.1118942440+01	0.1110969270+01	0.7125626360+00	-0.5456756620+00	-0.5394225680+00	0.1145936000+01
0.1592051040+02	0.1024671250+01	0.1017547080+01	0.6952635170+00	-0.5626524490+00	-0.5562803870+00	0.1132504160+01
0.1820687240+02	0.9264597160+00	0.9202159330+00	0.6739400790+00	-0.5784306570+00	-0.5719551570+00	0.1119494630+01
0.2085871340+02	0.8236525800+00	0.8183074220+00	0.6489796300+00	-0.5920776370+00	-0.5855061840+00	0.1109897210+01
0.2394757870+02	0.7155427670+00	0.7111224270+00	0.6177604440+00	-0.6022857080+00	-0.5956364950+00	0.1103930030+01
0.2756479960+02	0.6013865670+00	0.5979037090+00	0.5791379680+00	-0.6072191730+00	-0.6005151930+00	0.1104046190+01
0.3182817510+02	0.4805282350+00	0.4779827990+00	0.5297161790+00	-0.6042816820+00	-0.5975484100+00	0.1114260510+01
0.3689486710+02	0.3525684490+00	0.3509344080+00	0.4634676420+00	-0.5897727840+00	-0.5830526590+00	0.1139443090+01
0.4298087860+02	0.2177978410+00	0.2169827390+00	0.3742470690+00	-0.5583584800+00	-0.5517330180+00	0.1186596570+01
0.5039644730+02	0.7809530600-01	0.7784482650-01	0.3207356440+00	-0.5022502920+00	-0.4958970010+00	0.1264965190+01
0.5961475840+02	-0.6104543500-01	-0.6140671320-01	-0.5918185830+00	-0.4099145440+00	-0.4042452390+00	0.1383045770+01
0.7142301980+02	-0.1855363740+00	-0.1881412020+00	-0.1403944610+01	-0.2640816140+00	-0.2600453240+00	0.1528425250+01
0.8732824110+02	-0.2584576620+00	-0.2664785160+00	-0.3103353030+01	-0.3911453450-01	-0.4142897840-01	-0.5917094250+01
0.9000000000+02	-0.2600000000+00	-0.2731110750+00	-0.5042721150+01	-0.3922152310-13	-0.1276451190-13	0.6745533860+02

TABLE 4.4

COMPARISON OF INFLUENCE FUNCTIONS GENERATED USING FINITE ELEMENTS TO THE ANALYTIC SOLUTIONS FOR LINE LOADS ON A CYLINDRICAL CAVITY (OUTER BOUNDARY OF FINITE ELEMENT MODEL FIXED)

	DIMENSIONLESS RADIAL DISPLACEMENT			DIMENSIONLESS TANGENTIAL DISPLACEMENT		
THETA (DEG.)	ANALYTICAL SOLN.	FINITE ELEM. SOLN	PERCENT DIFF.	ANALYTICAL SOLN.	FINITE ELEM. SOLN	PERCENT DIFF.
0.5729572220-04	0.8405213850+01	0.5121700750+01	0.3906519400+02	-0.2600084050+00	-0.5121695630-05	0.9999803020+02
0.1192697600+00	0.3978000200+01	0.3866436880+01	0.2804507710+01	-0.2682827680+00	-0.2241601510+00	0.1644631070+02
0.2386372120+00	0.3575738730+01	0.3530697140+01	0.1259644300+01	-0.2744953110+00	-0.2722107230+00	0.9765858420+00
0.3579058160+00	0.3340217680+01	0.3288273050+01	0.1555127130+01	-0.2804751310+00	-0.2769749320+00	0.1388508120+01
0.4773358480+00	0.3172942550+01	0.3123644020+01	0.1553716360+01	-0.2864436800+00	-0.2828077510+00	0.1269334700+01
0.5967455940+00	0.3042997820+01	0.2994597030+01	0.1590562900+01	-0.2917086050+00	-0.2876353930+00	0.1396328910+01
0.7161012220+00	0.2936760970+01	0.2889600740+01	0.1605858680+01	-0.2967268100+00	-0.2923411880+00	0.1478000100+01
0.8354582740+00	0.2846835300+01	0.2800884360+01	0.1614106110+01	-0.3015417080+00	-0.2968817350+00	0.1545382480+01
0.9548212030+00	0.2768843460+01	0.2723954390+01	0.1621221040+01	-0.3061825290+00	-0.3015087540+00	0.1526466950+01
0.1074243400+01	0.2699935660+01	0.2655917880+01	0.1630327120+01	-0.3106729590+00	-0.3059833070+00	0.1509513910+01
0.1193613540+01	0.2638249200+01	0.2594556160+01	0.1656137770+01	-0.3150256720+00	-0.3105370440+00	0.1424843670+01
0.1312932390+01	0.2582400810+01	0.2539456310+01	0.1662968160+01	-0.3192543340+00	-0.3141033360+00	0.1613446600+01
0.1432312410+01	0.2531324060+01	0.2488073850+01	0.1708600030+01	-0.3233739220+00	-0.3189079190+00	0.1381064660+01
0.1621340970+01	0.2458448740+01	0.2415363870+01	0.1752522320+01	-0.3296912480+00	-0.3249886870+00	0.1426352740+01
0.1835497590+01	0.2385353140+01	0.2342450320+01	0.1795844100+01	-0.3365755480+00	-0.3313322670+00	0.1557871970+01
0.2074828551D+01	0.2311970810+01	0.2269569330+01	0.1833997290+01	-0.3440698810+00	-0.3383157800+00	0.1672364060+01
0.2353566630+01	0.2238272580+01	0.2196486110+01	0.1866907030+01	-0.3522138720+00	-0.3459938350+00	0.1765902940+01
0.2665673460+01	0.2164235590+01	0.2123116950+01	0.1899914920+01	-0.3610449410+00	-0.3544599070+00	0.1823882050+01
0.3019909460+01	0.2089750520+01	0.2049343900+01	0.1933561860+01	-0.3706089170+00	-0.3636514400+00	0.1877309750+01
0.3421958440+01	0.2014782070+01	0.1975081310+01	0.1970474320+01	-0.3809394150+00	-0.3736032440+00	0.1925810370+01
0.3878561320+01	0.1939238530+01	0.1900253060+01	0.2010349470+01	-0.3920719060+00	-0.3843402490+00	0.1971999870+01
0.4397466140+01	0.1863016990+01	0.1824756590+01	0.2053679690+01	-0.4040361290+00	-0.3958581370+00	0.2024074460+01
0.4987532430+01	0.1786007960+01	0.1748487580+01	0.2100795960+01	-0.4168520420+00	-0.4081726510+00	0.2082127430+01
0.5659020570+01	0.1709077790+01	0.1671326510+01	0.2151616600+01	-0.4305284390+00	-0.4212968930+00	0.2144236130+01
0.6423806400+01	0.1629069830+01	0.1593125860+01	0.2206410510+01	-0.4450576050+00	-0.4351962790+00	0.2215741530+01
0.7295860810+01	0.1548783960+01	0.1513691390+01	0.2265814290+01	-0.4604123200+00	-0.4498571880+00	0.2292538940+01
0.8291235590+01	0.1467009440+01	0.1432814720+01	0.2330913660+01	-0.4765306180+00	-0.4651904800+00	0.2379729070+01
0.9428921140+01	0.1383480790+01	0.1350265400+01	0.2400856580+01	-0.4933121110+00	-0.4811037570+00	0.2476772930+01
0.1073138310+02	0.1297881240+01	0.1265740120+01	0.2476429980+01	-0.5106016540+00	-0.4974225040+00	0.2591102230+01
0.1222520480+02	0.1209044390+01	0.1178901490+01	0.2557593680+01	-0.5281676380+00	-0.5139163660+00	0.2698247800+01
0.1394212410+02	0.1118942440+01	0.1089343810+01	0.2646960400+01	-0.5456756620+00	-0.5302488030+00	0.2827111560+01
0.1592051040+02	0.1024671250+01	0.9966060020+00	0.2738951220+01	-0.5626524490+00	-0.5459354470+00	0.2971070680+01
0.1820687240+02	0.9264597160+00	0.9001581010+00	0.2838937850+01	-0.5784306570+00	-0.5603204960+00	0.3130913090+01
0.2085871340+02	0.8236525800+00	0.7993993240+00	0.2944597810+01	-0.5920776370+00	-0.5724718620+00	0.3311351990+01
0.2394757870+02	0.7155427670+00	0.6937124390+00	0.3050876760+01	-0.6022857080+00	-0.5811184600+00	0.3514486290+01
0.2756479980+02	0.6013865670+00	0.5823916400+00	0.3150619640+01	-0.6072191730+00	-0.5844806680+00	0.3744694840+01
0.3182817510+02	0.4805282350+00	0.4650343610+00	0.3224342120+01	-0.6042816820+00	-0.5800662230+00	0.4007213770+01
0.3689486710+02	0.3525684490+00	0.3412140380+00	0.3220488040+01	-0.5897727840+00	-0.5643704930+00	0.4307131700+01
0.4298087860+02	0.2177978410+00	0.2113404230+00	0.2964867820+01	-0.5583584800+00	-0.5323999190+00	0.4649085190+01
0.5039644730+02	0.7809530600-01	0.7720953860-01	0.1134213330+01	-0.5022502920+00	-0.4769633440+00	0.5034730400+01
0.5961475840+02	-0.6104543500-01	-0.5623269600-01	0.7883863860+01	-0.4099145440+00	-0.3875551800+00	0.5454640300+01
0.7142301980+02	-0.1855363740+00	-0.1770235420+00	0.4582280800+01	-0.2640816140+00	-0.2486058550+00	0.5860521310+01
0.8732824110+02	-0.2584576620+00	-0.2513583930+00	0.2746782350+01	-0.3911453450-01	-0.3956634740-01	-0.1155102150+01
0.X00000000D+02	-0.2600000000+00	-0.2576689120+00	0.8965721150+00	-0.3922152310-13	-0.1204278480-13	0.6929546880+02

5. CONFORMAL ELASTIC CONTACT OF A SPHERE INDENTING A SPHERICAL CAVITY

5.1 Introduction

Hertz [1881] provides an analytic solution to the problem of two contacting bodies with quadratic surfaces. In his theory, Hertz assumed non-conformal contact, i.e., that all of the dimensions of the contact patch were small compared to the radii of curvature of the bodies, hence justifying the approximation of the surfaces in the contact region, by elastic half spaces. Hertzian theory may be applied to the problem of a sphere indenting a spherical cavity, however, it is restricted in its application to the analysis of cases where the contact patch remains small. If the sphere and seat are closely conforming, i.e., their radii are nearly equal, then Hertzian analysis can only be applied for very small loads for which the contact patch remains small.

Goodman and Keer [1965] have analyzed the conformal problem of a sphere and seat with nearly equal radii. They present results for areas of contact larger than those that could be analyzed by Hertzian theory. As in the theory of Hertz, Goodman and Keer assumed that points on surfaces of the sphere and seat respectively which lie along a line parallel to the line of applied load will merge after deformation. Furthermore, the basic equation in their formulation enforces this constraint. It will be shown that this

assumption in conformal theory can lead to erroneous strains and displacements when large areas of contact are analyzed.

In section 5.2 the problem of an elastic sphere indenting an elastic spherical seat will be formulated, using the conformal contact model discussed in chapter 3. The numerical procedures used in the solution will be reviewed in section 5.3 and the numerical results will be presented in section 5.4.

5.2 Formulation

Consider the conformal contact problem of an elastic sphere of radius R_1 indenting an elastic spherical seat of radius R_2 ($R_2 > R_1$). It is assumed that the sphere and seat are equilibrated by pressure distributions equal to the interfacial contact pressure and diametrically opposite the contact region. Contact regions will be therefore limited to hemispherical contact. A cross section of a sphere, body 1, and spherical seat, body 2, in point contact at O is illustrated in figure 5.1.

Let us establish a global coordinate system $(\hat{x}, \hat{y}, \hat{z})$ whose origin will be fixed at the initial point of contact, O, such that the x - y plane is tangent to the sphere at O and z is directed into the sphere. The cross section of the sphere and seat in the x - z plane represent the "contour curves" of the sphere and seat and each curve is a circle.

It is initially assumed that two points which will merge after deformation, A on body 1 and B on body 2, are defined such that their distances from the origin along their respective contour curves

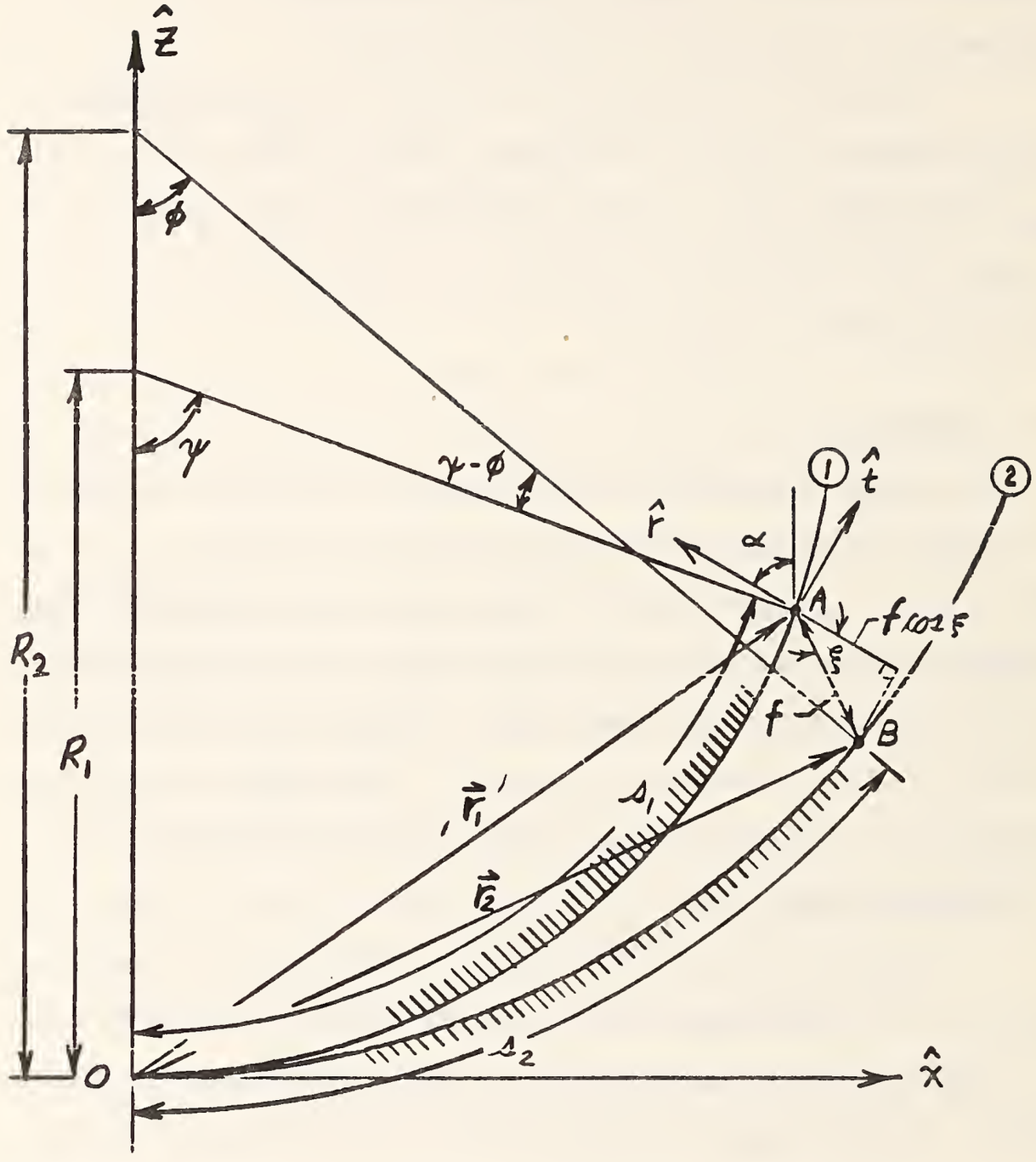

Fig. 5.1. Conformal contact between a sphere and spherical seat or a cylinder and a cylindrical seat.

are equal, i.e., $s_1 = s_2$ (Fig. 5.1). Points A and B are defined by vectors $\vec{r}_1$ and $\vec{r}_2$, and the vector difference between them is defined by $\vec{f}$, the vector valued profile function. Alternatively, points A and B may be located on their respective contour curves by angles measured at the center of the contour curves from the z axis as shown in figure 5.1. Point A is defined by angle ψ and point B is defined by angle ϕ. In the notation to follow in this chapter all angles ψ will refer to locations of points on the sphere while all angles ϕ will denote points on the seat.

A local coordinate system $(\hat{r}, \hat{t}, \hat{\omega})$ will be constructed at point A such that unit vector $\hat{r}$, which represents the "mean normal" forms an acute angle α with the z axis, where

$$\alpha = \frac{\psi + \phi}{2} \tag{5.1}$$

unit vector t is defined to be $\pi/2$ radians clockwise of $\hat{r}$ and $\hat{\omega}$ is such that

$$\hat{\omega} \quad \hat{t} \times \hat{r} \tag{5.2}$$

The contact criterion can then be formulated by examining the displacements of points A and B. Consider the following displacements as illustrated in figure 5.2. Point A moves through a rigid body translation Δ_1, parallel to the z axis, to A', and through an elastic

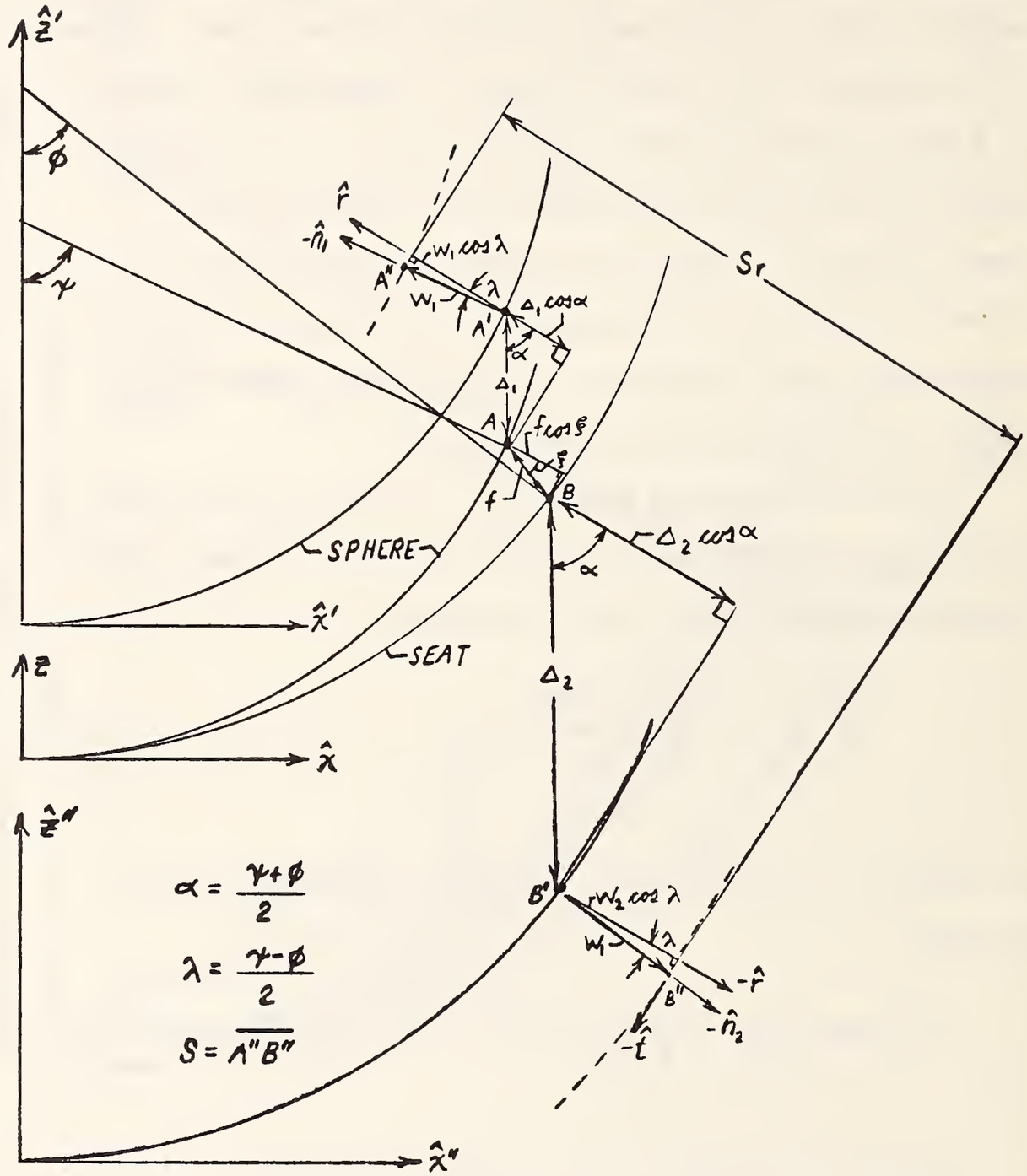

Fig. 5.2. Displacements on sphere and spherical seat

displacement w_1 along the inward normal of the sphere to A". Similarly point B undergoes a rigid body translation Δ_2 parallel to the z axis to B' and an elastic displacement w_2 directed along the inward normal of the seat to B". Because of the symmetry of the contacting surfaces about the z axis, there will be no displacements on either body in the ω direction.

We now impose the contact criterion, i.e., that the projection of the separation (S = A" B") in the direction of the mean normal $\hat{r}$ must vanish. Following equation (3.6) this criterion may be expressed in the form:

$$S_r = f\cos\xi - \delta\cos\alpha + (w_1 + w_2)\cos\lambda \qquad (5.3)$$

where

$$\lambda = \frac{\psi - \phi}{2} \qquad (5.4)$$

$$\delta = -(\Delta_1 + \Delta_2) \qquad (5.5)$$

and

$$\xi = \alpha - \arctan\left(\frac{r_{2x} - r_{1x}}{r_{1z} - r_{2z}}\right) \qquad (5.6)$$

ξ is derived in appendix F and r_{1x}, r_{2x}, r_{1z}, r_{2z} are the x and z components of vectors $\vec{r}_1$ and $\vec{r}_2$ as shown in figure 5.2. f and δ are the profile function and approach respectively.

It should be noted that the peak strains will remain small (as required by the assumption of linear elasticity theory) only if the initial separation f (see fig. 5.1) is small compared to the local radii of curvature. Therefore some additional but consistent approximations are possible in the derivation of equation (5.3), (see appendix H). However, these approximations result in no significant reduction of computational effort.

Consider now the $(\eta_1, \zeta_1, \gamma_1)$ coordinate fixed to the sphere as shown in figure 4.7. Point A can be located in spherical coordinates by (ψ, β, R_1). The elastic displacement w_1 at A, shown as u_r in figure 4.7, can be expressed in terms of the pressure distribution $p(\psi', \beta')$ in the form

$$w_1(\psi, \beta, \nu_1, E_1) = R_1^2 \int_{\Omega_1} p(\psi', \beta') G_1(\psi, \beta, \psi', \beta', \nu_1, E_1) \sin\psi' d\beta' d\psi' \qquad (5.7)$$

where $G(\psi, \beta, \psi', \beta', \nu_1, E_1)$ is given by G in equation (4.22) and Ω_1 is the contact surface defined on the sphere.

Similarly in terms of the $(\eta_2, \zeta_2, \gamma_2)$ coordinate system in figure 4.11, w_2 can be expressed in terms of $p(\phi, \beta)$ by

$$w_2(\phi, \beta, \nu_2, E_2) = R_2^2 \int_{\Omega_2} p(\phi', \beta') G_2(\phi, \beta, \phi', \beta', \nu_2, E_2) \sin\phi' d\beta' d\phi' \qquad (5.8)$$

where G_2 (ϕ, β, ϕ', β', ν_2, E_2) is defined by equation (4.35) and Ω_2 is the contact are defined on the spherical seat. The integrands in equations (5.7) and (5.8) may be simplified by utilizing the symmetry of the pressure field. Because of the symmetry about the z axis of the contact surfaces in figure 5.1, the pressure distribution must also be symmetric about z. Hence, p (x, β) may be replaced by p (x) in equation (5.7), (see fig. 5.3) and p (ϕ, β) in equation (5.8) may be replaced by p (ϕ). Making these substitutions and combining equations (5.3), (5.7) and (5.8) the contact criterion, equation (5.3) becomes

$$S = f\cos\xi - \delta\cos\alpha +$$

$$+ \cos\lambda R_1^2 \int_{\Omega_1} p(\psi') G_1(\psi, \beta, \psi', \beta', \nu_1, E_1) \sin\psi' d\beta d\psi' +$$

$$+ \cos\lambda R_2^2 \int_{\Omega_2} p(\phi') G_2(\phi, \beta, \phi', \beta', \nu_2, E_2) \sin\phi' d\beta d\phi' \qquad (5.9)$$

The boundary conditions require that the separation, S_r, be zero with positive pressure inside the contact regions Ω_1 and Ω_2. Also, the separation must be positive with zero pressure outside the contact

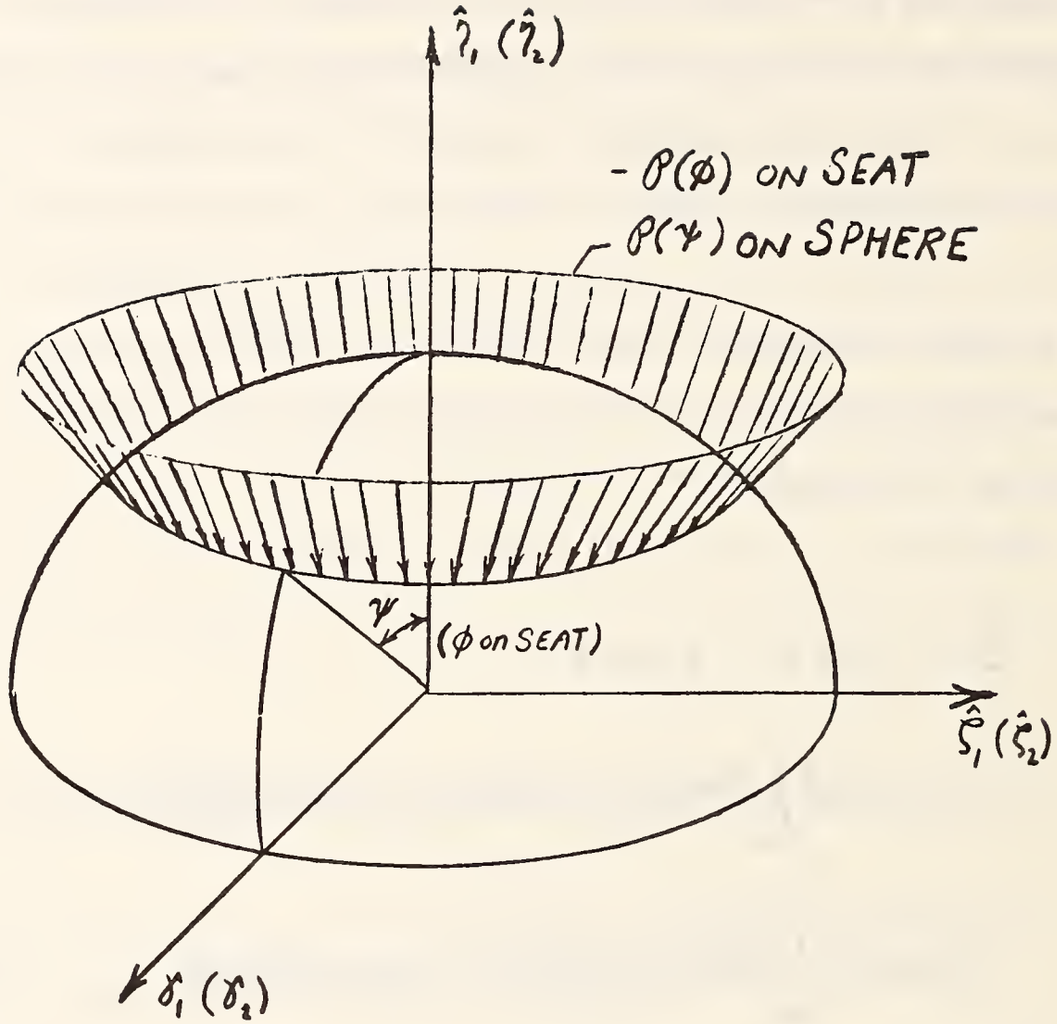

Fig. 5.3. Axisymmetric pressure loading on sphere

regions. In symbolic terms

$$S_r = 0 \qquad \text{INSIDE } \Omega \tag{5.10a}$$

$$p(\phi), p(\psi) \geq 0 \qquad \text{INSIDE } \Omega \tag{5.10b}$$

$$S_r > 0 \qquad \text{OUTSIDE } \Omega \tag{5.10c}$$

$$p(\phi), p(\psi) = 0 \qquad \text{OUTSIDE } \Omega \tag{5.10d}$$

It is required to determine the contact regions, Ω_1 and Ω_2, the pressure distributions p (ψ) and p (ϕ), and the approach, δ, such that relationships (5.9) and (5.10) are satisfied.

The determination of the contact regions, Ω_1 and Ω_2, poses a major problem in the solution of equation (5.9). However, choosing some tentative "candidate" regions, Ω_1^* and Ω_2^*, will establish equation (5.9) as an integral equation of the first kind which can be solved using the "Simply Discretized" method of Singh and Paul [1974]. In the conformal contact problem of a sphere indenting a spherical seat, it is known a priori, that the boundary of Ω_1 will always be a circle on the sphere defined by ψ_{max}. Also, the boundary, ϕ_{max}, of Ω_2^* may be chosen such that $s_2 = s_1$ for the boundaries of Ω_1 and Ω_2^*. Thus

$$\phi_{max} = \frac{R_1}{R_2} \psi_{MAX} \tag{5.11}$$

The region Ω_1 is written without an asterisk since it can be defined as the exact contact region on the sphere corresponding to some unknown force F. Ω_2^* is denoted with the asterisk since it is chosen according to equation (5.11). Further details on the refinement of the tentative region Ω_2^* are discussed later.

A "Simply Discretized" solution is found by subdividing Ω_1 and Ω_2^* into a large number of small cells. The normal pressure is replaced by a piecewise constant pressure field (pressure p_i and cell i). Thus Ω_1 and Ω_2^* are divided into N cells apiece, such that the centroid of cell i of Ω_1 merges with the centroid of cell i of Ω_2^*. This is achieved by first choosing the cells on Ω_1 and then using the relation $s_2 = s_1$ to determine the corresponding cells on Ω_2^*.

Because of the known symmetry of p (ϕ) and p (ψ), the cells on each surface will be chosen as rings symmetric about the η_1 axis as shown in figure 5.4 for the sphere. Cell i will be located on the sphere between ψ_1 and ψ_{i+1} while that on the seat will be between ϕ_i and ϕ_{i+1}. N field points are chosen on each surface such that the location of the j^{th} field point is within the j^{th} cell. Equation (5.9) may be written in discretized form for field point j as,

$$
\begin{aligned}
S_1 = {} & f\cos\xi - \delta\cos\alpha + \\
& + \cos\lambda \sum_{i=1}^{N} P_i \int_{\Omega_{1i}} G_1(\psi_j, \beta_j, \psi', \beta', \nu_1, E_1) \sin\psi' d\beta' d\psi' \\
& + \cos\lambda \sum_{i=1}^{N} P_i \int_{\Omega_{2i}} G_2(\phi_j, \beta_j, \phi', \beta', \nu_2, E_2) \sin\phi' d\beta' d\phi'
\end{aligned}
\qquad (5.12)
$$

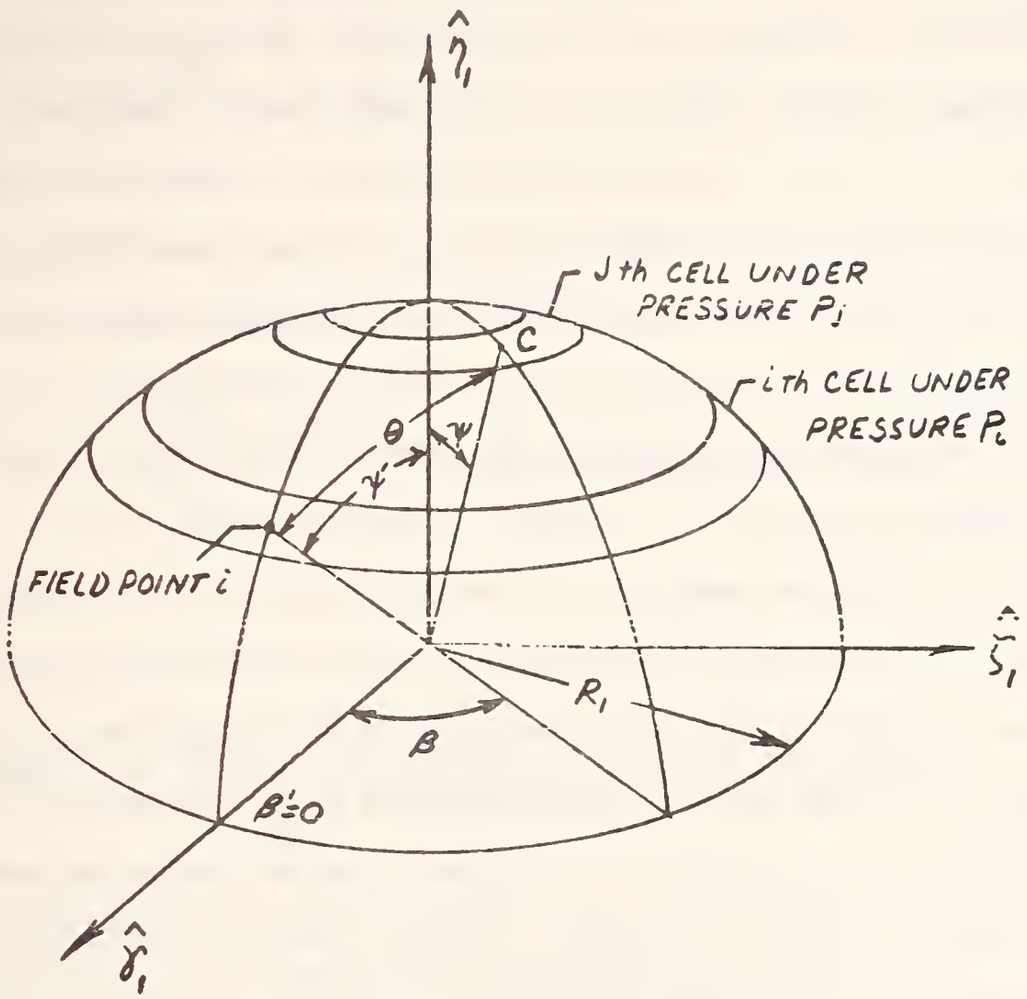

Fig. 5.4. Axisymmetric cells on sphere

The integrals in equation (5.12) may be evaluated numerically. The location of all the field points will be along the contour curve located in the η_1 - γ_1 and η_2 - γ_2 planes so that β'_j will always be considered zero. Equation (5.12) may be written for each field point. Thus N linear algebraic equations are generated in N + 1 unknown (N values of P_i, and δ). One additional equation is needed to produce a unique solution of the unknown variables. The last equation is generated by writing equation (5.12) for one additional field point. The location of this field point is, in theory, arbitrary but, as will be discussed later, the results are sensitive to this choice.

Having generated N + 1 linear algebraic equations in N + 1 unknowns the piecewise constant pressure distribution, P_i, and δ may be found. It now remains to check the validity of the method used to determine Ω_2^* and the location of two points A and B which merge after deformation. In each case, the merging points or boundaries were initially chosen such that $s_2 = s_1$. It will now be illustrated how the "point-mating" procedure, described in chapter 3 may be utilized to refine the choice of the outer boundary of Ω_2^* and of points on the seat such that they merge with the appropriate points on the sphere.

The total separation after deformation of points A and B may be computed from equation (3.13a). For the case of a sphere indenting a spherical seat, the value of S_θ is zero. Furthermore, the contact criterion required that S_r is zero. Therefore, the only non-zero component of separation is S_t where

$$S_t = \cos\lambda\,(u_1 - u_2) + f_t - \delta_t \qquad (5.13a)$$

and

$$\delta_t = \delta \cos(\pi - \alpha) \tag{5.13b}$$

$$f_t = |\bar{F}| \sin \xi \tag{5.13c}$$

The components of displacements u_1 and u_2 may be computed using the pressure distribution (P_i) of the "Simply Discretized" solution by

$$U_1(\psi_j, \beta_j) = \sum_{i=1}^{N} P_i R_1^2 \int_{\Omega_{1i}} H_1(\psi_j, \beta_j, \psi', \beta', \nu_1, E_1) \sin\psi' \, d\beta' d\psi' \tag{5.14a}$$

and

$$U_2(\phi_j, \beta_j) = \sum_{i=1}^{N} P_i R_2^2 \int_{\Omega_{2i}} H_2(\phi_j, \beta_j, \phi', \beta', \nu_2, E_2) \sin\phi' \, d\beta' d\phi' \tag{5.14b}$$

where H_1 and H_2 are the influence functions for displacements in the tangential direction on the sphere and seat respectively. H_1 is defined by H in equation (4.24) and H_2 is defined by H in equation (4.32). Having evaluated S_t, at all field points, the "point-mating procedure" may be used to find coordinates for a new set of field points on the seat which upon repeating the solution procedure just described will give rise to new values of S_t which are smaller than those previously calculated. Originally, mating points on the sphere and seat were located by assuming that the distances along their respective contour curves were equal, i.e., $s_2 = s_1$ as illustrated in

figure 3.1. The "point-mating procedure" discards this relation after the initial solution and replaces it with relations (3.16 a,b). Repeated iterations yield values of S_t which become smaller if the process converges. The limits on the final values of S_t depend largely on the cell density and the values of ψ_{max}. Numerical experiments have shown that for large values of ψ_{max} ($> 10^o$), with few cells (< 10), the final value of S_t which can be achieved is of the order of $\varepsilon\ (w_1 + w_2)$ where $\varepsilon = 0.1$. For problems with up to 15 cells values of $\varepsilon = 0.01$ can be achieved. Considering, essentially Hertzian problems ($\psi_{max} < .1^o$), $\varepsilon = 0.01$ may be achieved on the first solution. The location of ϕ_{max} defining Ω_2^* may also be refined using the "point-mating procedure." In most cases this was performed automatically since ϕ_{max} was chosen as the additional field point.

Having generated the displacements w_1, w_2, u_1 and u_2 via equations (5.7), (5.8) and (5.14) at field points along a contour curve, the strains $\varepsilon_{\beta\beta}$, $\varepsilon_{\psi\psi}$ on the sphere and $\varepsilon_{\beta\beta}$ and $\varepsilon_{\phi\phi}$ on the seat may be formulated. These quantities will be needed later for accuracy analysis. It can be shown[1] that the strains on the surface of a sphere for the axisymmetric set of displacements are

$$\varepsilon_{\beta\beta}(\psi_i) = \frac{-w_1(\psi_i)}{R_1} + \frac{u_1(\psi_i)}{R_1}\cot(\psi_i) \qquad (5.15)$$

---

[1] Sokolnikoff, 2d ed., 1956, p. 184.

and

$$\varepsilon_{\psi\psi}(\psi_i) = \frac{1}{R_1}\frac{dU_1(\psi_i)}{d\psi} - \frac{W_1(\psi_i)}{R_1} \qquad (5.16)$$

where ψ_i is the coordinate of the i^{th} field point. Similarly, for the spherical seat

$$\varepsilon_{\beta\beta}(\phi_i) = \frac{W_2(\phi_i)}{R_2} + \frac{U_2(\phi_i)}{R_2}\cot(\phi_i) \qquad (5.17)$$

and

$$\varepsilon_{\phi\phi}(\phi_i) = \frac{1}{R_2}\frac{dU_2(\phi_i)}{d\phi} + \frac{W_2(\phi_i)}{R_2} \qquad (5.18)$$

where ϕ_i is the coordinate of the i^{th} field point on the seat. These strains may be computed using finite difference approximations for the derivatives in equations (5.16) and (5.18)[1].

5.3 Numerical Procedures

In each "Simply Discretized" solution the boundaries on Ω_1 and Ω_2 are defined by ψ_{max} and ϕ_{max} respectively. Each contact region was divided into N cells by first subdividing ψ_{max} and ϕ_{max} into N equal intervals subtending equal arc lengths. The cells were then

---

[1] Carnahan, [1969] p. 431.

defined by the surface generated by revolving the arc lengths about the η_1 and η_2 axis. Typical cells on the sphere are illustrated in figure 5.4. All field points were located on the contour lines defined by the $\eta_1 - \gamma_1$ and $\eta_2 - \gamma_2$ planes. (see fig. 5.4)

The integrals in equations (5.12) and (5.14a, b) were evaluated in part by analytic means. Consider the integration of an influence function corresponding to the i_{th} field points at ψ_i (ϕ_i) over the region Ω_{1j} (Ω_{2j}). For all cases where $i \neq j$, the integration was performed by Gaussian quadrature. When $i = j$, i.e., when the field point is located within the cell of integration, the integrand is singular within the region of integration and the singularity is located at the field point. Integration over the singularity is performed analytically while that over the remaining portion of the cell is performed numerically using Gaussian quadrature.

Consider the portion of a cell on a sphere of radius R_1 near the field point at (ψ_c, 0) as shown in figure 5.5. The region is bounded by arcs defined by $\beta = \pm\Delta$, $\psi = \psi_c - \Delta$ and $\psi = \psi_c + \Delta$ ($\Delta << 1$). Similarly, consider a region on the seat. For both the sphere and seat when small cells are used, the boundaries of the cell fall within the limits of this region. In this case the values of ψ_i and ϕ_i defining the cell boundaries were used to bound the region. For small Δ, taken in this analysis to be 1/4 degree, the region around the singularity on the sphere will be approximated by a small

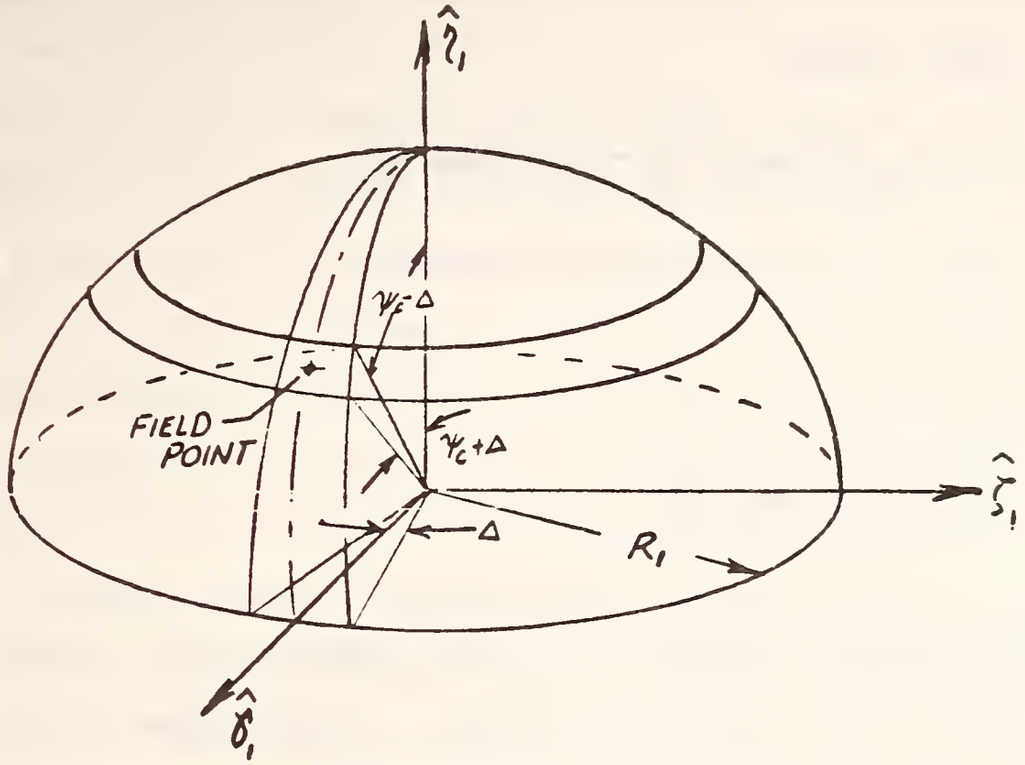

Fig. 5.5. Small region surrounding a field point on a spherical surface.

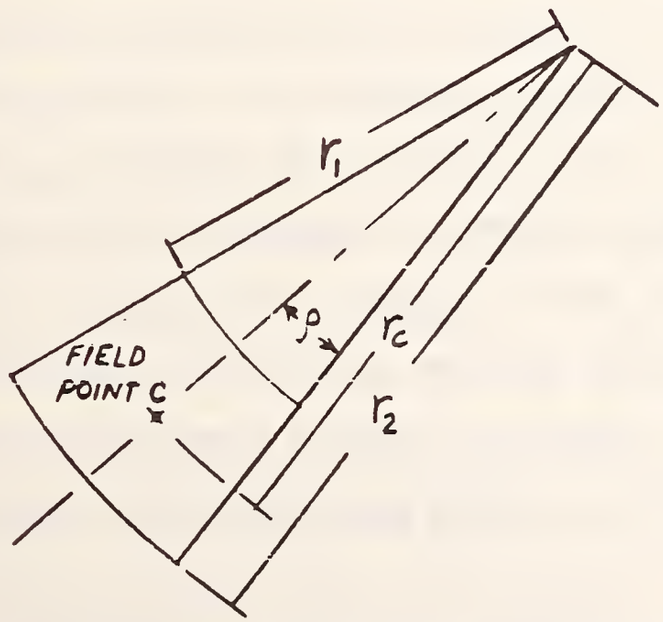

Fig. 5.6. Planar approximation to a region surrounding a field point on a spherical surface.

planar annular element with inner radius r_1, outer radius r_2, and half angle ρ where

$$r_1 = R_1 \sin(\psi_c - \Delta)/\cos\psi_c \tag{5.19a}$$

$$r_2 = R_1 \sin(\psi_c + \Delta)/\cos\psi_c \tag{5.19b}$$

and

$$\rho = \Delta \cos\psi_c \tag{5.19c}$$

Similar relations in terms of ϕ_c, R_2 and Δ may be written for the definition of r_1, r_2 and ρ for the seat. The derivation of r_1, r_2 and ρ is shown in appendix P. The displacement at the field point C due to a constant force applied to a general point A within the region is governed by the Boussinesq influence function as shown in appendix A. The integration of the Boussinesq influence function over an annular element is derived in appendix G. Therefore, the integration over a cell i for field point i was performed in two parts. First a small annular element surrounding the singularity (field point) was defined, and the integral within that region was computed using the analytical solutions in appendix G. Second the remaining portion of the integral was computed using 2-dimensional 10 point Gaussian quadrature. Similar approximations were made for the spherical seat.

The "point-mating procedure" was employed to identify the set

of field points on the seat which merge with the field points on the sphere. The iteration was terminated when values of S_t for all field points were within their respective values of $[(w_1 + w_2)\varepsilon]_i$. ε was taken to be 0.1 for preliminary results while accurate solutions were obtained by choosing ε to be 0.01.

For all cases that follow, the extra field point was located at the outer boundary of the contact region. With this location, the final determination of ϕ_{max} on the seat is automatically performed, i.e., ϕ_{max} is the final coordinate of the extra field point. The "Simply Discretized" method of solution always provided stable pressure distributions even though Singh and Paul [1973] noted that for the problems they treated, this method generated an ill-conditioned set of equations which resulted in unstable (widely varying and negative) pressure distributions. This stability can possibly be attributed to the choice of axisymmetric cell distributions which had not previously been attempted in the work of Singh and Paul. The solutions will be termed "quasi stable" because the solution becomes unstable if the location of the extra field point is moved within the contact region. The success achieved when the extra field point is located on the boundary of the contact region can possibly be attributed to the fact that the location is farthest from all other field points, on the average, than any location inside the contact region. This choice could yield the most independent extra equation thus providing a more stable solution.

Having generated N + 1 equations in N + 1 unknowns

(N values of P_i and δ) as described in section 5.2, the set was first reduced to N equations in N unknowns by subtracting the equation written for the extra field point from the others thus eliminating δ from the set. The remaining N equations were solved using Gaussian elimination. The approach, δ, was then computed from the $N + 1^{st}$ equation.

The strains corresponding to equations (5.17), (5.18), (5.19) and (5.20) were computed, from equations (5.15) - (5.18), using the values of w_1, w_2, u_1 and u_2 at each field point on the sphere and seat. The required derivatives $du_1/d\psi$ and $du_2/d\phi$ were evaluated using central difference formulae for field points i where $i \neq 1$ or N. For $i = 1$ forward difference formulae were used while for $i = N$ backward difference formulae were used.[1]

The total force applied to the sphere can be calculated from the pressure distribution found in the analysis. Consider the discretized pressure distribution P_i on cell i. The force in the $-\eta_1$ direction from P_i applied to a small sector area $2\pi R_1^2 \sin\psi d\psi$ is $2\pi R_1^2 P_i \cos\psi \sin\psi d\psi$. Integrating this between ψ_i and ψ_{i+1}, the force in the $-\eta_1$ direction due to P_i on cell i is $\pi R_1^2 P_i \cdot (\sin^2 \psi_{i+1} - \sin^2 \psi_i)$. Thus the total force applied to the sphere can be computed as

$$F = \sum_{i=1}^{N} \pi R_1^2 P_i (\sin^2 \psi_{i+1} - \sin^2 \psi_i) \qquad (5.20)$$

---

[1] See Carnahan [1969] p. 431.

5.4 Numerical Results

A computer program termed CONSPHERE was written to analyze the conformal contact between an elastic sphere and seat. The following numerical example was considered

$$
\begin{aligned}
R_1 &= 1 \text{ in} \\
R_2 &= 1.01 \text{ in} \\
\nu_1 &= \nu_2 = 0.25 \\
E_1 &= E_2 = 30 \times 10^6 \text{ psi} \\
\psi_{max} &= 0.5 \text{ degrees}
\end{aligned}
\tag{5.21}
$$

In this example and the ones to follow, the value of Poisson's ratio was chosen to be 0.25 so that the results could be compared to those of Goodman and Kerr [1965]. The results are presented in dimensionless form. Let,

$$R = \frac{2 R_1 R_2}{R_2 - R_1} \tag{5.22}$$

and

$$k = \frac{(1-\nu_1^2)}{\pi E_1} + \frac{(1-\nu_2^2)}{\pi E_2} \tag{5.23}$$

Then define

$$\text{Dimensionless Pressure in cell i, } P_i^* = P_i k \tag{5.24a}$$

$$\text{Dimensionless Load, } F^* = F \frac{R^k}{R_m^2} \tag{5.24b}$$

$$\text{Dimensionless Radii, } R_1^* = \frac{R_1}{R_m} \tag{5.24c}$$

$$R_2^* = \frac{R_2}{R_m} \tag{5.24d}$$

$$\text{Dimensionless Approach, } \delta^* = \frac{\delta}{R_m} \tag{5.24e}$$

$$\text{Dimensionless Ratio of Radii} = \frac{R_2}{R_1} \tag{5.24f}$$

The contact region was divided into 15 cells such that $\psi_{j+1} - \psi_j = 0.033$ degrees. The pressure distribution obtained from CONSPHERE is compared in figure 5.7 to the pressure distribution predicted by Hertzian theory for the same applied force of $F^* = 0.7294 \times 10^{-14}$. The approach δ^* was found to be 0.3858×10^{-8} in. while the value predicted by Hertzian theory is $\delta^* = 0.3895 \times 10^{-8}$ in. This problem falls within the domain of Hertzian theory, and the comparison of these results indicates that the solution produced by CONSPHERE is in general agreement with those of Hertz.

Now consider the non-Hertzian problem where $\psi_{max} = 30$ degrees

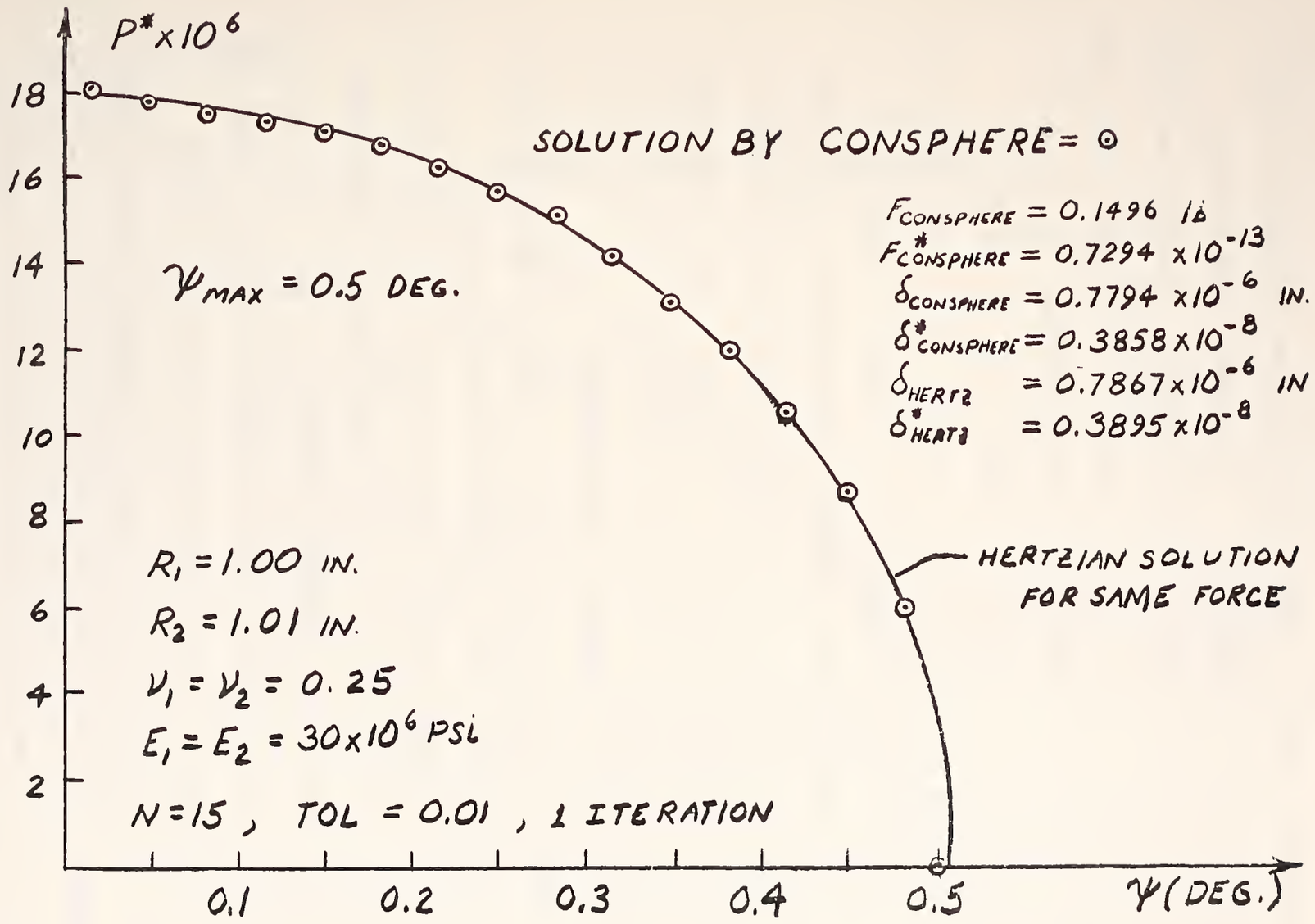

Fig. 5.7. Pressure distributions between sphere and seat, $\psi_{max} = 0.5^{0}$.

and the dimensions and elastic constants are the same values as used in the previous example. Figure 5.8 illustrates the pressure distribution between the sphere and seat. Also shown is the Hertzian pressure distribution for the same applied force. It should be noted that the conformal contact solution predicts a higher peak stress and a smaller contact region than the Hertzian solution. The approach for the conformal solution is $\delta^* = 0.1281 \times 10^{-4}$ and the total compressive force was found to be $F^* = 0.1780 \times 10^{-7}$. The radial and tangential displacements are tabulated in tables 5.1 and 5.2. It is interesting to note that the tangential displacements on the sphere are all positive (increasing ψ is positive direction) while those on the seat are negative (increasing ϕ is positive). This can be understood if one considers the sphere to be flattened out while the seat is a depression which elongates or grows deeper.

Additional problems were solved in order to compare the load-approach relationship to that obtained with the solutions of Hertz [1881] and Goodman and Keer [1965]. Figure 5.9 illustrates the load-approach curves for Hertzian theory, the theory of Goodman and Keer and experimental data reported by Goodman and Keer. The results are plotted for half angles of contact between 0^o and 20^o. Figure 5.9 clearly illustrates a strong correspondence between the present theory and the experimental data reported by Goodman and Keer. The load-approach curve for the Hertzian theory indicates more compliance than that of the other theories while the load-approach relation of the Goodman and Keer theory is less compliant than the others. All

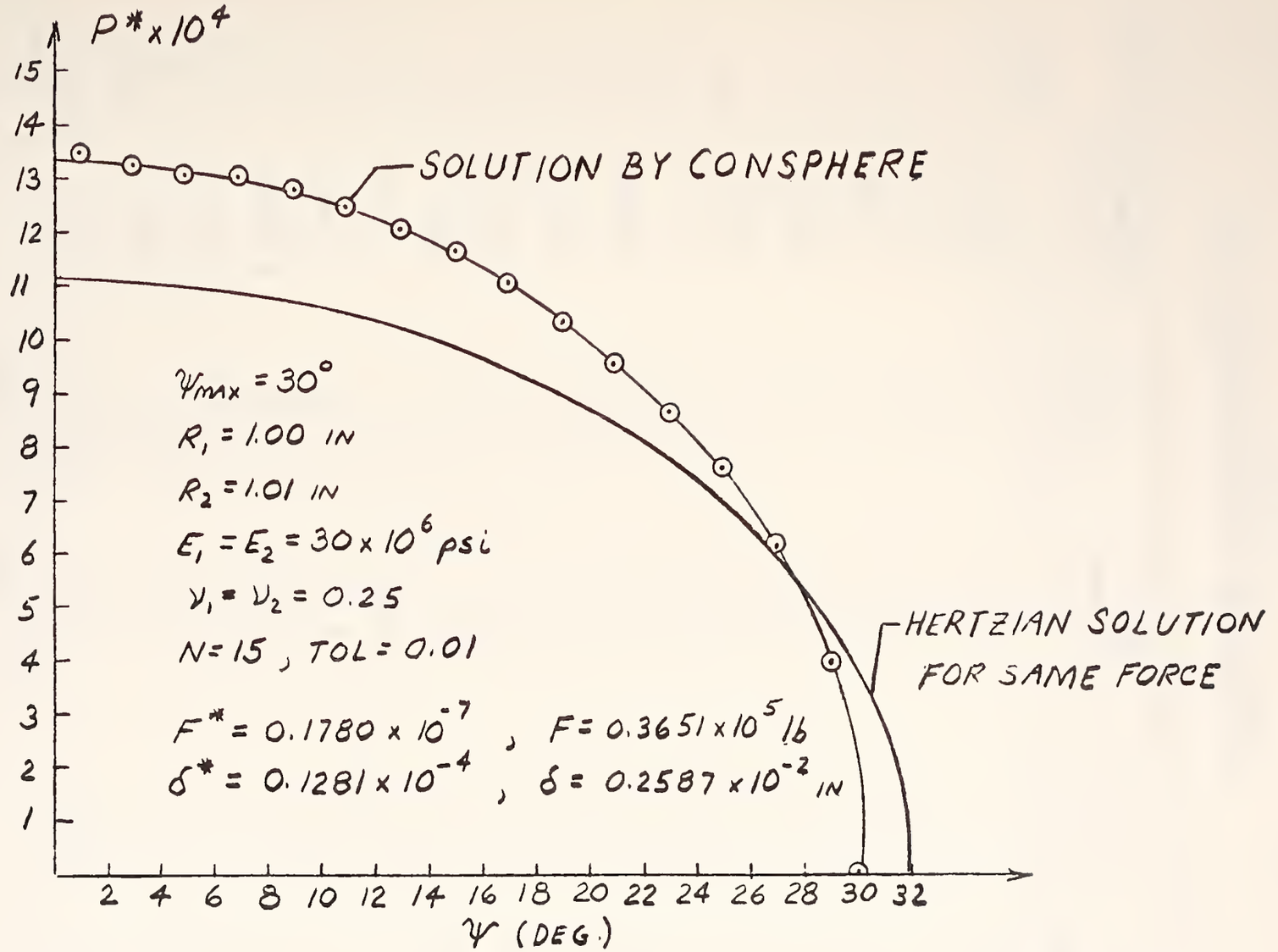

Fig. 5.8. Pressure distribution between sphere and seat, $\psi_{max} = 30°$.

TABLE 5.1

SURFACE DISPLACEMENTS ON SPHERE

ψ [Deg]	Radial Displacements $w_1 \times 10^4$ in	Tangential Displacements $u_1 \times 10^4$ in
1.0	14.12	0.03869
3.0	14.04	0.1194
5.0	13.87	0.2035
7.0	13.62	0.2841
9.0	13.29	0.3578
11.0	12.88	0.4300
13.0	12.39	0.4968
15.0	11.82	0.5580
17.0	11.16	0.6123
19.0	10.43	0.6635
21.0	9.627	0.7116
23.0	8.745	0.7562
25.0	7.792	0.7998
27.0	6.766	0.8475
29.0	5.672	0.9165
30.0	5.099	0.9711

$\psi_{max} = 30^o$, $R_1 = 1.00$ in, $R_2 = 1.01$ in,

$E_1 = E_2 = 30 \times 10^6$ psi, $\nu_1 = \nu_2 = 0.25$

TABLE 5.2

SURFACE DISPLACEMENTS ON SPHERICAL SEAT

ϕ [Deg]	Radial Displacements $w_2 \times 10^4$ in	Tangential Displacements $u_2 \times 10^4$ in
0.9888	11.73	- 0.1789
2.966	11.66	- 0.5307
4.944	11.53	- 0.8735
6.922	11.32	- 1.211
8.899	11.04	- 1.542
10.88	10.70	- 1.858
12.85	10.29	- 2.158
14.83	9.812	- 2.439
16.81	9.267	- 2.699
18.79	8.654	- 2.929
20.77	7.974	- 3.125
22.74	7.228	- 3.286
24.72	6.414	- 3.404
26.70	5.534	- 3.470
28.68	4.587	- 3.463
29.67	4.089	- 3.418

$\psi_{max} = 30^o$, $R_1 = 1.00$ in, $R_2 = 1.01$ in,

$E_1 = E_2 = 30 \times 10^6$ psi, $\nu_1 = \nu_2 = 0.25$

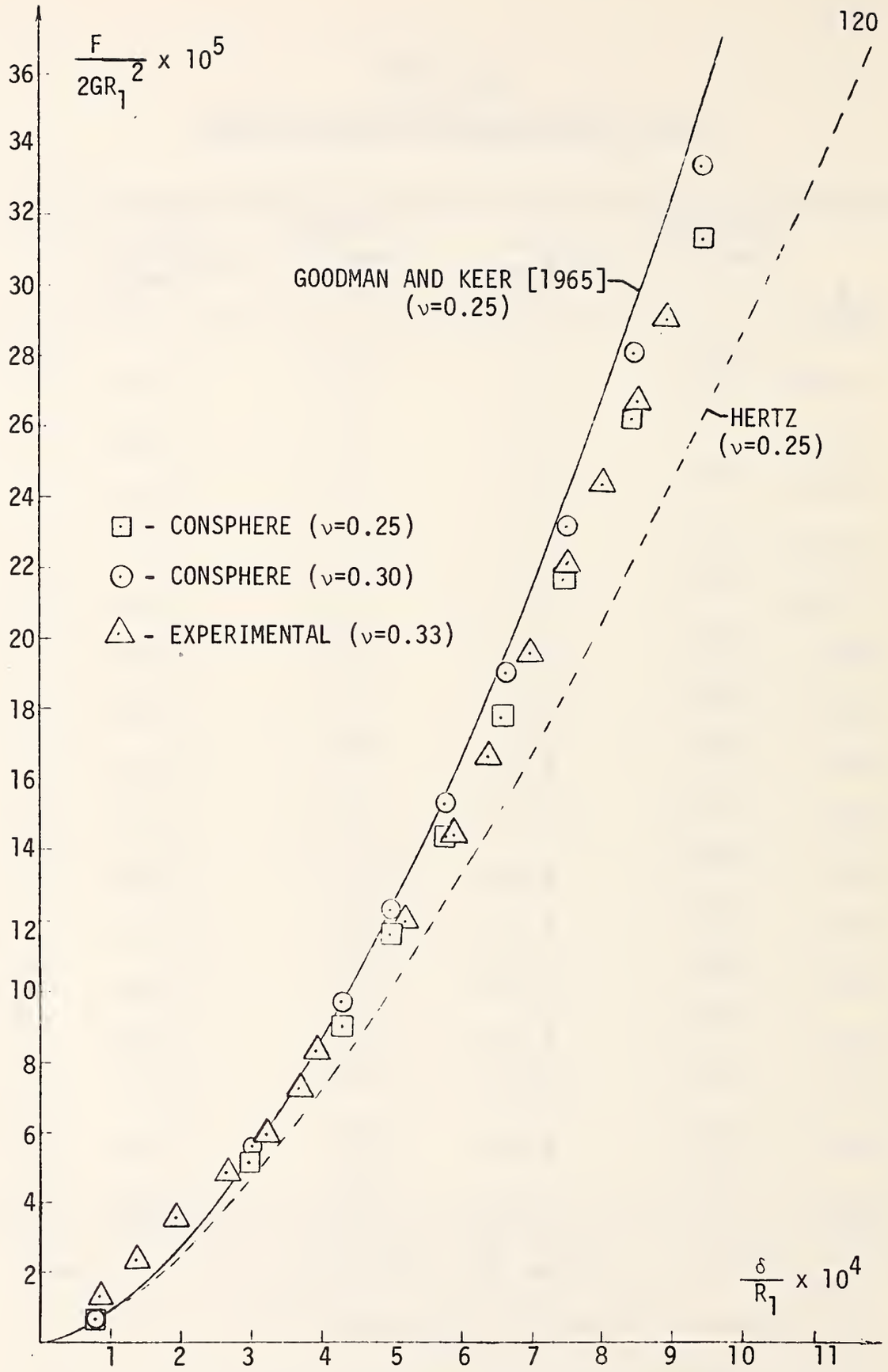

Fig. 5.9 Load-approach relationship for conformal contact of a sphere and spherical seat.

of the theories agree for loads less than $F (1 - \nu) / R_1^2 E = 2$ while the experimental data near this region deviates from the theories. Goodman and Keer [1965] attribute this discrepancy to experimental error.

The effect of Poisson's ratio on the load-approach curve was also studied. The variation of force and approach for values of Poisson's ratio of $\nu = 0.25$ and $\nu = 0.30$ were plotted together in figure 5.9. With increasing Poisson's ratio the materials were found to be less compliant.

A comparison was made of the values, predicted by the various theories, of the radius of the contact region $a^* = \sin(\psi)$ and δ^*. Figure 5.10 illustrates the results of Hertz, Goodman and Keer, and the present theory. The results from CONSPHERE fall much closer to the Hertzian theory than those of Goodman and Keer.

Knowledge of the displacements at discrete points, namely, the field points, enables one to also calculate the surface strains given in equations (5.15) - (5.18). Both the displacements and strains for several problems will be compared to those obtained in the analysis of Goodman and Keer [1965]. It will be shown through this comparison that the assumptions used by Goodman and Keer can produce erroneous displacements and strains in problems where the contact angle exceeds $\psi_{max} = 60^o$.

In the derivation of the contact criterion used by Goodman and Keer (see appendix L) it is assumed that points on both bodies, which are initially equidistant from the axis of symmetry come into

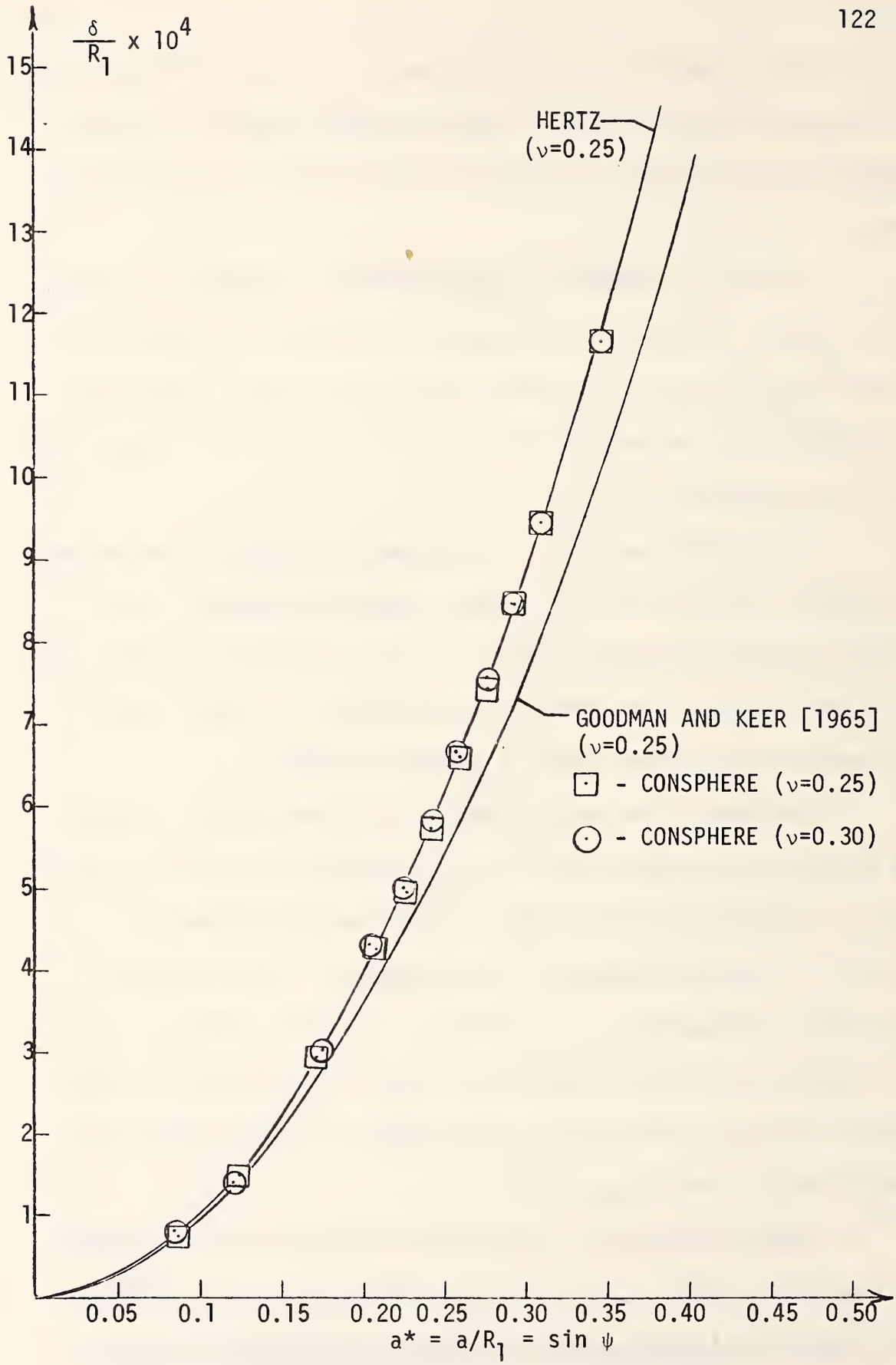

Fig. 5.10. Approach vs. radius of contact boundary for conformal contact of sphere and spherical seat.

contact after deformation. To show that this assumption can not be true for large angles of contact, consider the contact of an elastic sphere in a rigid seat, as shown in figure 5.11. According to Goodman and Keer points A and B which merge after deformation, are located such that $R_1 \sin \psi = R_2 \sin \phi$. Since the seat is rigid, point A on the sphere will merge with point B on the seat solely due to a displacement u_z of point A. This displacement may be viewed as having components in the $\hat{r}$ and $\hat{t}$ directions, i.e., w_1 and u_1, where $\hat{r}$ is directed radially inward on the sphere and $\hat{t}$ is perpendicular to $\hat{r}$, i.,e.,

$$\vec{u}_z = w_1 \hat{r} + u_1 \hat{t} \tag{5.25}$$

where (see appendix M for derivation):

$$|\vec{u}_z| = R_2 (1 - \cos\phi) - R_1 (1 - \cos\psi) + \delta \tag{5.26}$$

$$w_1 = |\vec{u}_z| \cos\psi \tag{5.27}$$

$$w_2 = |\vec{u}_z| \sin\psi \tag{5.28}$$

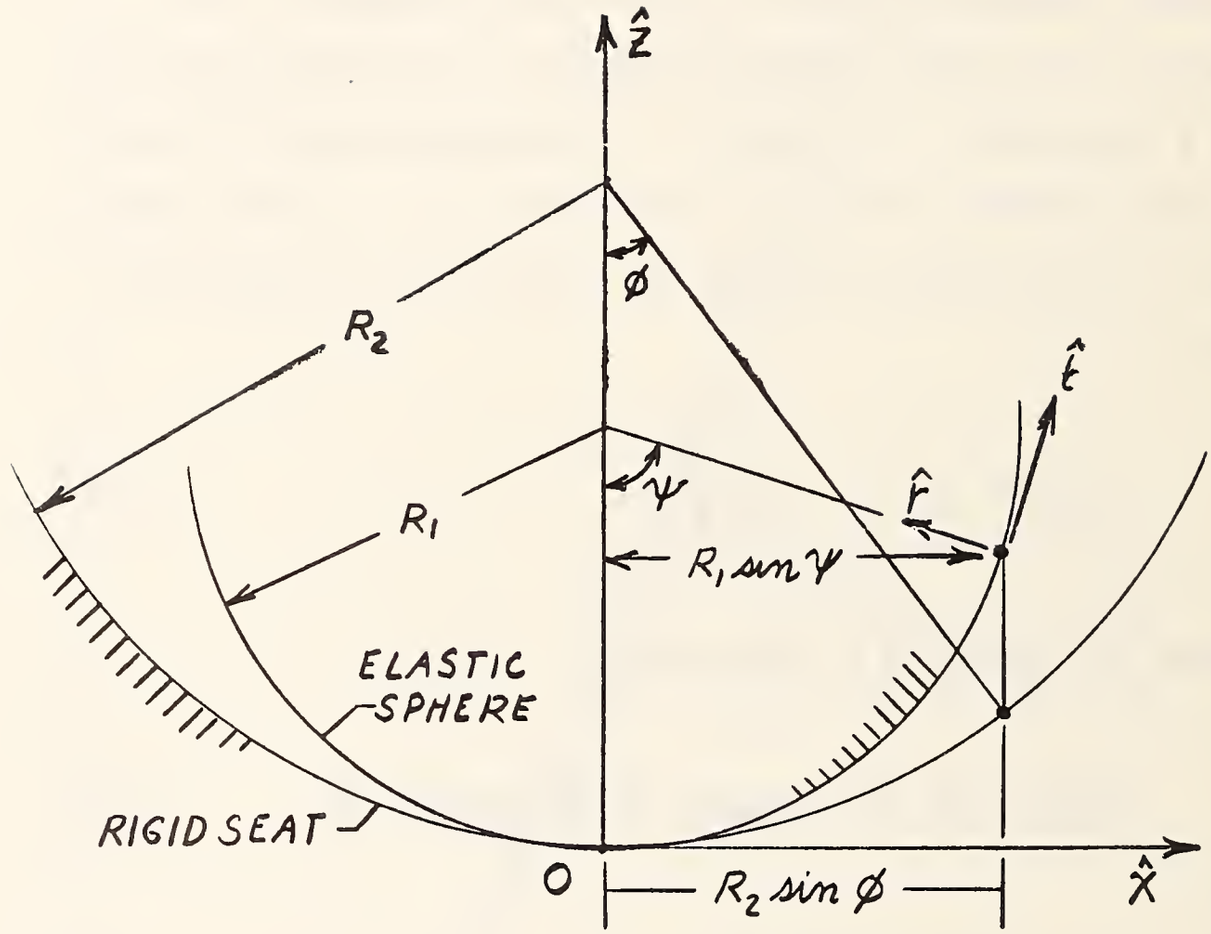

Fig. 5.11. Sphere in contact with seat (displacements of points A and B constrained).

and

$$\phi = \arcsin\left(\frac{R_1}{R_2}\sin\psi\right) \tag{5.29}$$

Now consider the case where

$$\begin{aligned} &R_1 = 1.0 \text{ in.} \\ &R_2 = 1.001 \text{ in.} \\ &E_1 = 30 \times 10^6 \text{ psi}, \; E_2 = 30 \times 10^{10} \text{ psi} \\ &\nu_1 = 0.25, \; \nu_2 = 0.25 \\ &\psi_{max} = 60^o \end{aligned} \tag{5.30}$$

Since $E_2 >> E_1$ the seat will be considered completely rigid and equations (5.27) and (5.28) will be used to compute w_1 and u_1 for results obtained in the Goodman and Keer analysis. The displacements for the present conformal theory of section 5.2 were computed using equations (5.7), (5.8) and (5.14). The displacement results for the problem at hand are compared in tables 5.3 and 5.4. Also tabulated are the displacements that are obtained when the pressure distribution obtained through CONSPHERE was applied to a finite element model of the sphere.[1] The radial displacements of all solutions agree well. The tangential displacements obtained through the Goodman and Keer analysis are much higher than those of CONSPHERE

---

[1]The paper of Goodman and Keer [1965] did not provide any data for angles of contact above 20 degrees. Therefore no comparable finite element model could be analyzed using their pressure distribution.

TABLE 5.3

COMPARISON OF RADIAL DISPLACEMENTS w_1

ψ [Deg]	Goodman and Keer $w_1 \times 10^3$ in	CONSPHERE $w_1 \times 10^3$ in	Finite Element $w_1 \times 10^3$ in
3.0	1.171	1.166	1.184
9.0	1.147	1.142	1.157
15.0	1.100	1.095	1.109
21.0	1.029	1.025	1.040
27.0	0.9368	0.9330	0.9480
33.0	0.8231	0.8197	0.8315
39.0	0.6895	0.6864	0.6965
45.0	0.5374	0.5348	0.5364
51.0	0.3686	0.3663	0.3535
57.0	0.1850	0.1828	0.1738

$\psi_{max} = 60^o$, $R_1 = 1.000$ in, $R_2 = 1.001$ in,

$E_1 = 30 \times 10^6$ psi, $E_2 = 30 \times 10^{10}$ psi, $\nu_1 = \nu_2 = 0.25$

TABLE 5.4

COMPARISON OF TANGENTIAL DISPLACEMENTS u_1

ψ [Deg]	Goodman and Keer $u_1 \times 10^4$ in	CONSPHERE $u_1 \times 10^4$ in	Finite Element $u_1 \times 10^4$ in
3.0	0.6135	0.2001	0.2065
9.0	1.816	0.5972	0.6160
15.0	2.946	0.9737	1.002
21.0	3.951	1.306	1.338
27.0	4.773	1.576	1.607
33.0	5.345	1.770	1.806
39.0	5.584	1.881	1.910
45.0	5.374	1.892	1.915
51.0	4.552	1.811	1.858
57.0	2.849	1.657	1.718

$\psi_{max} = 60°$, $R_1 = 1.000$ in, $R_2 = 1.001$ in,

$E_1 = 30 \times 10^6$ psi, $E_2 = 30 \times 10^{10}$ psi, $\nu_1 = \nu_2 = 0.25$

or the finite element solution.

Having computed the displacement fields, the strains $\varepsilon_{\beta\beta}$ and $\varepsilon_{\psi\psi}$ may be calculated using relations (5.15 - 5.18). They are tabulated in tables 5.5 and 5.6 for the analysis by Goodman and Keer, CONSPHERE and finite element theory. It can be seen that the $\varepsilon_{\beta\beta}$ strains are zero for the analysis of Goodman and Keer which is expected since the circle defined by ψ does not enlarge or shrink after deformation. The strains $\varepsilon_{\beta\beta}$ from CONSPHERE are in general agreement with those produced through finite element analysis. The computation of $\varepsilon_{\psi\psi}$ reveals that near the boundary of the contact region, those strains predicted by the Goodman and Keer analysis are much larger than the solutions of CONSPHERE and the finite element analysis. Furthermore, the results of CONSPHERE agree with those of the finite element analysis.

Both $\varepsilon_{\beta\beta}$ and $\varepsilon_{\psi\psi}$ decrease as ψ increases according to CONSPHERE and the finite element analysis. This is to be expected since the pressure diminishes when ψ increases. On the other hand the values of $\varepsilon_{\psi\psi}$ predicted by the Goodman and Keer model increase as ψ increases. Finally, the values of $\varepsilon_{\beta\beta}$ and $\varepsilon_{\psi\psi}$ are nearly equal for small ψ in the solution of CONSPHERE and finite element analysis which is expected in this axisymmetric case.

5.5 Conclusions

The problem of a sphere indenting a spherical seat has been solved. The pressure distribution for $\psi_{max} = 0.50^{o}$ has been shown to compare closely with the Hertzian solution. (fig. 5.7) For $\psi_{max} = 30^{o}$,

TABLE 5.5

CONPARISON OF STRAINS $\varepsilon_{\psi\psi}$

ψ [Deg]	Goodman and Keer $\times 10^3$ in/in	CONSPHERE $\times 10^3$ in/in	Finite Element $\times 10^3$ in/in
3.0	- 0.002744	- 0.7868	- 0.7894
9.0	- 0.02506	- 0.7730	- 0.7692
15.0	- 0.07172	- 0.7567	- 0.7563
21.0	- 0.1472	- 0.7377	- 0.7355
27.0	- 0.2593	- 0.7115	- 0.7121
33.0	- 0.4210	- 0.6741	- 0.6626
39.0	- 0.6545	- 0.6280	- 0.6181
45.0	- 0.9975	- 0.5681	- 0.5437
51.0	- 1.520	- 0.4788	- 0.4171
57.0	- 2.360	- 0.3299	- 0.2873

$\psi_{max} = 60^o$, $R_1 = 1.000$ in, $R_2 = 1.001$ in,

$E_1 = 30 \times 10^6$ psi, $E_2 = 30 \times 10^{10}$ psi, $\nu_1 = \nu_2 = 0.25$

TABLE 5.6

COMPARISON OF STRAINS $\varepsilon_{\beta\beta}$

ψ [Deg]	Goodman and Keer in/in	CONSPHERE $\times 10^3$ in/in	Finite Element $\times 10^3$ in/in
3.0	0.0	- 0.7842	- 0.7900
9.0	0.0	- 0.7653	- 0.7680
15.0	0.0	- 0.7318	- 0.7354
21.0	0.0	- 0.6849	- 0.6912
27.0	0.0	- 0.6237	- 0.6325
33.0	0.0	- 0.5471	- 0.5535
39.0	0.0	- 0.4542	- 0.4604
45.0	0.0	- 0.3455	- 0.3444
51.0	0.0	- 0.2196	- 0.2029
57.0	0.0	- 0.07525	- 0.06036

$\psi_{max} = 60^o$, $R_1 = 1.000$ in, $R_2 = 1.001$ in,

$E_1 = 30 \times 10^6$ psi, $E_2 = 30 \times 10^{10}$ psi, $\nu_1 = \nu_2 = 0.25$

the resulting pressure distribution has a higher peak stress and smaller contact area than the Hertzian solution for the same applied force. The load-approach curve was plotted and was found to agree closely with the experimental results reported by Goodman and Keer. The plot of approach vs. contact area indicates that the results are nearly equal to those of the Hertzian theory for angles up to 20^{o}. The displacement field and resulting strains were found to be reproduced when a finite element analysis was made of the sphere under the pressure field predicted by CONSPHERE for $\psi_{max} = 60^{o}$ (the seat being rigid). It was shown that in using the constraint imposed by Goodman and Keer in their analysis, larger tangential displacements and $\varepsilon_{\psi\psi}$ strains will be produced. In view of the fact that the uniqueness theorem for contact theory (proven by J. J. Kalker 1971) guarantees a unique pressure field and displacement field for a given contact area, it can be concluded that the total solution predicted by CONSPHERE is correct since the finite element model reproduces the same displacement field as CONSPHERE when subjected to the interfacial pressure predicted by CONSPHERE.

6. CONFORMAL ELASTIC CONTACT OF A CYLINDER INDENTING A CYLINDRICAL CAVITY

6.1. Introduction

The solution of the two dimensional contact problem of two cylinders in contact or the problem of a cylinder indenting a cylindrical seat can be obtained from Hertzian theory by allowing the radii of curvature of each body to become infinite in one direction.[1] However, such a solution is only valid within the assumptions of Hertz, i.e., the in plane dimensions of the contact area must remain small compared to the in plane radii of curvature. Therefore, Hertz's solution is not appropriate for moderate loads, when the difference in the radii of the cylinder and cylindrical seat is small.

A more recent theory, pertaining specifically to the problem of a cylinder indenting a cylindrical seat has been published by Sjtaerman [1949] for the problem where the contact pressure on the cylinder and seat are equilibrated by identical pressures located at π radians from the contact region. Sjtaerman's solution is based on the formulation of a contact criterion in the radial direction of a polar coordinate system fixed at the center of the cylinder. He does not consider displacements tangential to the surface. In order to compute the radial displacements within the contact area, Sjtaerman forms the

---

[1] Timoshenko and Goodier, 3d. ed. [1970], pp. 418-20.

integral of the unknown pressure distribution times the influence function for the cylinder and seat. These integrals are incorporated into the contact criterion and the unknown pressure field is determined using a finite difference technique.

A third theory specific to the problem of a disc contacting a hole in an infinite plate has been published by Persson [1964]. In contrast to the work of Sjtaerman and the present analysis, Persson considers the disc to be equilibrated by a force located at the center of the disc with the seat being fixed at infinity. Persson initially assumes the existence of both tangential and radial displacements of surface points. He found that by assuming the contact region to be circular and neglecting second order quantities, the contact criterion was independent of tangential displacements and is identical to that derived by Sjtaerman. Persson proceeds to develop the final form of the contact criterion in terms of a singular integro-differential equation which he solves.

The problem of an elastic cylinder indenting an elastic cylindrical seat is solved in this chapter using the conformal theory developed in chapter 3. No assumptions pertaining to the tangential displacements are retained in the final solution. The loading conditions applied are the same as those used in the Sjtaerman analysis.

Section 6.2 contains the formulation of the problem and the numerical procedures are discussed in section 6.3. The results are compared to those of Hertz, Sjtaerman and Persson in section 6.4.

6.2 Formulation

Consider the conformal contact of an elastic cylinder of radius R_1 indenting an elastic cylindrical seat of radius R_2 ($R_2 > R_1$). It is assumed that the bodies are equilibrated by pressure distributions equal to the interfacial contact pressures and applied at π radians relative to the contact region. (see fig. 6.1). This assumption is not inherent in the method of analysis but it does effect the form of the influence functions used in the analysis to follow. Therefore the contact region will be limited to contact over half the cylinder, i.e., a half angle contact of $\frac{\pi}{2}$ radians (which should cover all cases of practical interest). A cross section of the cylinder, body 1, and cylindrical seat, body 2, is shown in figure 6.2-a.

The contour curves are the same as those obtained in the analysis of the sphere and seat, therefore much of the development takes the same form. The reader is referred to chapter 5 for the details of the formulation omitted in this section. It must be remembered that the problem of a cylinder and seat in contact is two dimensional and the force applied at any point on either body represents a line load with units [lbs/in].

Surface points on the cylinder and seat will be described as in the last chapter, i.e., coordinates ψ pertain to points on the cylinder and coordinates ϕ defines points on the seat. The initial location of points A and B on the contour curves are chosen in the same way as those on the sphere and spherical seat, $s_1 = s_2$. The local coordinate system $(\hat{r}, \hat{t}, \hat{\omega})$ is fixed at point A as before, however, the

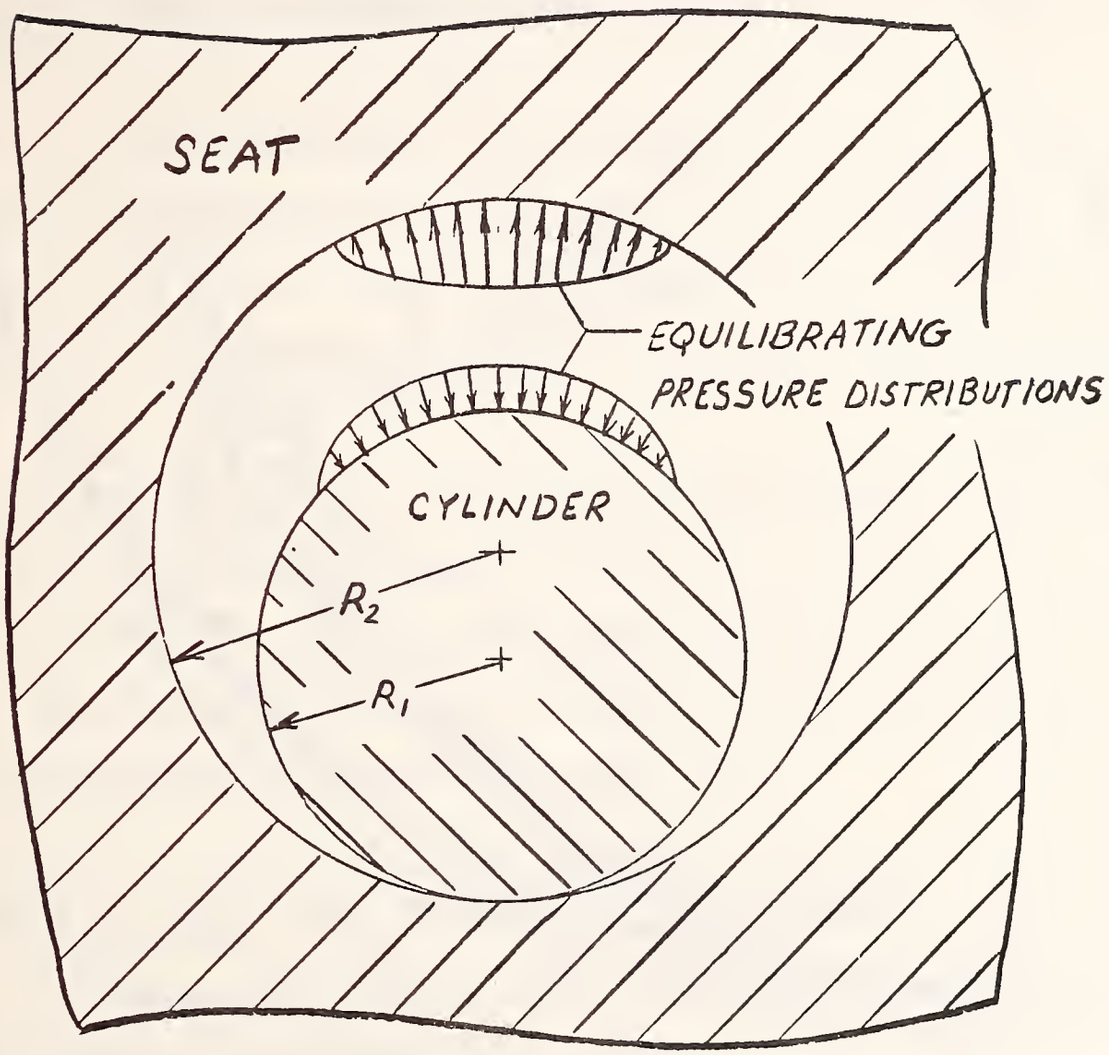

Fig.6.1. Cross section of cylinder and cylindrical seat in conformal contact.

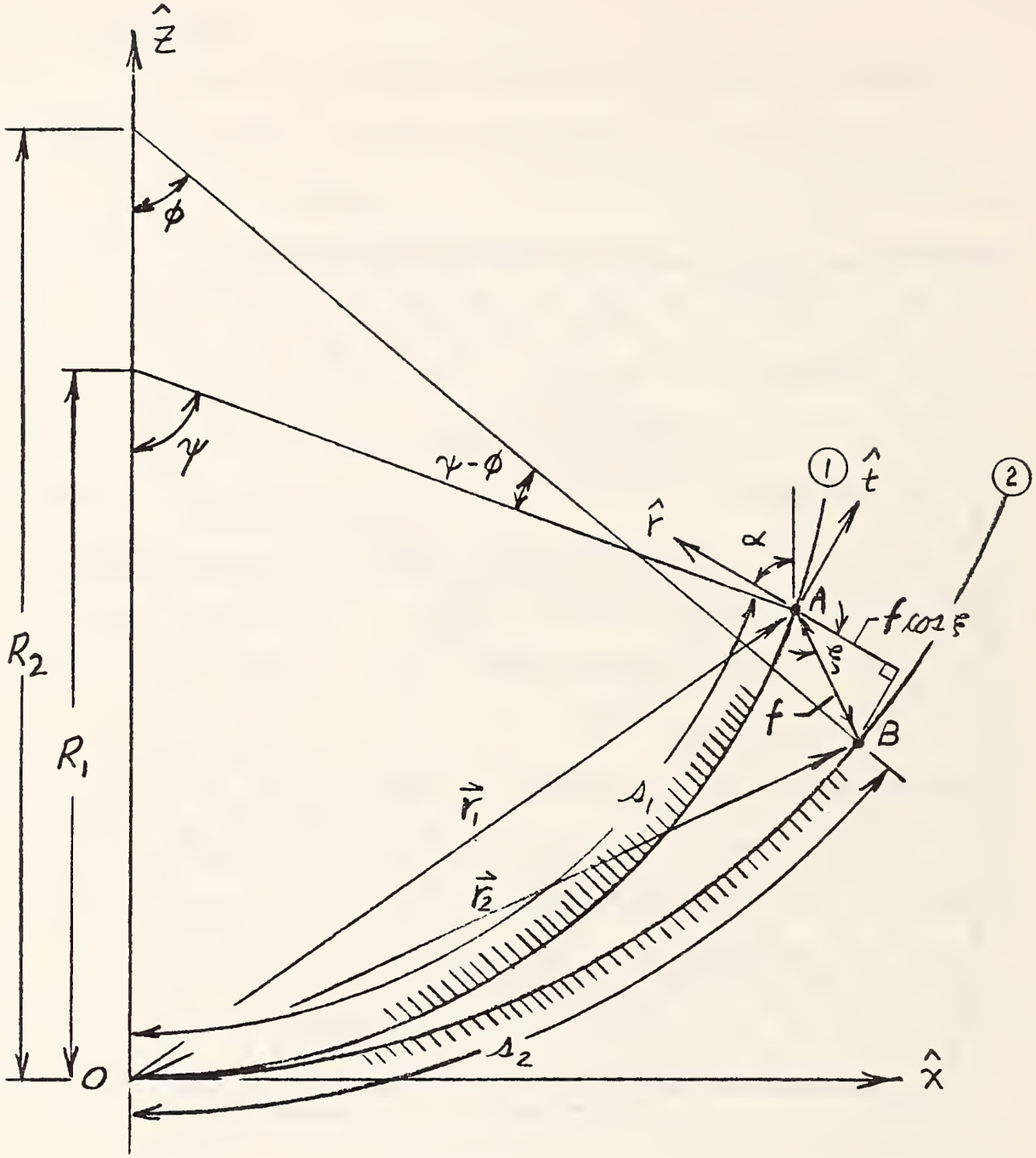

Fig. 6.2-a. (repeated) Conformal contact between a sphere and spherical seat or a cylinder and cylindrical seat.

unit vector $\hat{\omega}$ is parallel to the axis of the cylinder.

The contact criterion of equation (5.3) exactly represents the criterion needed for the solution of this problem, i.e.,

$$S_r = f\cos\xi - \delta\cos\alpha + (w_1+w_2)\cos\lambda \qquad (5.3)$$

where f is the profile function, δ is the approach and w_1 and w_2 represent the displacements in the radial directions of points A and B on the cylinder and seat respectively. The quantities α, λ, δ and ξ are defined by equations (5.1), (5.4), (5.5) and (5.6) respectively.

Now consider the $(\hat{\eta}_1, \hat{\zeta}_1)$ and $(\hat{\eta}_2, \hat{\zeta}_2)$ cartesian coordinate systems fixed to the cylinder and seat respectively as illustrated in figure 6.2. Point A is located on the cylinder by polar coordinates (ψ, R_1). The elastic displacement w_1 at point A, can be expressed as a function of the pressure distribution p (ψ) by

$$W_1(\psi, \nu_1, E_1) = R_1\int_{\Omega_1} p(\psi')G_1(\psi, \psi', \nu_1, E_1)d\psi' \qquad (6.1)$$

where G_1 $(\psi, \psi', \nu_1, E_1)$ is given by G in equation (4.40) and Ω_1 is the contact surface on the cylinder. Similarly, on the cylindrical seat, the elastic displacement w_2 may be defined by

$$W_2(\phi, \nu_2, E_2) = R_2\int_{\Omega_2} p(\phi')G_2(\phi, \phi', \nu_2, E_2)d\phi' \qquad (6.2)$$

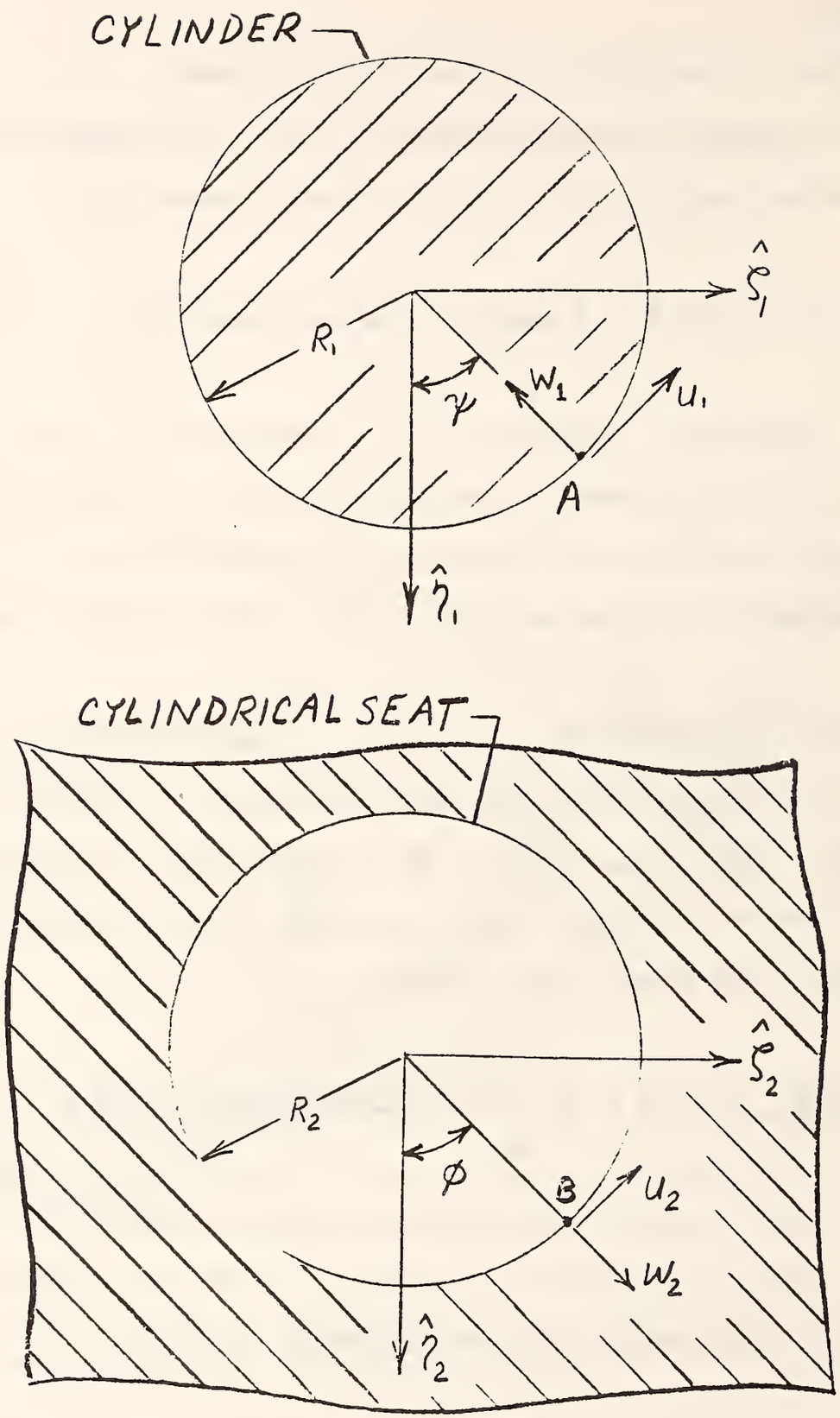

Fig. 6.2. Coordinate systems for cylinder and cylindrical seat

where $G_2(\phi, \phi', \nu_2, E_2)$ is defined by equation (4.53) and Ω_2 is the contact region on the cylindrical seat.

Combining equations (6.1), (6.2) and (5.3) the contact criterion may be written

$$S_r = f\cos\xi - \delta\cos\alpha +$$

$$+\cos\lambda\, R_1 \int_{\Omega_1} p(\psi')\, G_1(\psi, \psi', \nu_1, E_1)\, d\psi' +$$

$$+\cos\lambda\, R_2 \int_{\Omega_2} p(\phi')\, G_2(\phi, \phi', \nu_2, E_2)\, d\phi' \qquad (6.3)$$

The supplementary conditions associated with equation (6.3) are equations (5.10 a-d).

The initial choice of the tentative contact region Ω_2^* is based on the same assumptions used in the previous chapter, i.e., $s_1 = s_2$ so that

$$\phi_{max} = \frac{R_1}{R_2}\,\psi_{max} \qquad (6.4)$$

A simply discretized solution of equation (6.3) is found by first subdividing Ω_1 and Ω_2^* into a large number (N) of infinitely long cells which are oriented such that the infinite dimensions of the cells are parallel to the axis of the cylinder. The normal pressure distribution is then approximated with a piecewise constant pressure distribution such that the pressure in each cell is constant. The

i^{th} cell on the cylinder will be denoted Ω_{1i} while that on the seat will be termed Ω_{2i}. The choice of Ω_{2i}^{*} is such that it merges with Ω_{1i}. This is achieved by first choosing the cells on Ω_1 and then using the point mating procedure to determine the cell boundaries on Ω_2^{*}. Cell i will be located on the cylinder between ψ_i and ψ_{i+1} while cell i on the seat will be defined between ϕ_i and ϕ_{i+1}. N field points are chosen on each body such that one lies within each cell. The N + 1 field point was located on the boundary of the contact region on each body. The location of the i^{th} field point on the seat is determined using the point mating procedure so that it is assumed to merge with the i^{th} field point on the cylinder. Equation (6.3) may be written in discretized form as

$$S_r = f\cos\xi - \delta\cos\alpha + \tag{6.5}$$

$$+ \cos\lambda \sum_{i=1}^{N} P_i \int_{\Omega_{1i}} G_1(\psi_j, \psi_j' \nu_1, E_1)\, d\psi' +$$

$$+ \cos\lambda \sum_{i=1}^{N} P_i \int_{\Omega_{2i}} G_2(\phi_j, \phi_j', \nu_2, E_2)\, d\phi' \quad (j=1,N+1)$$

The integrals in equation (6.5) may be evaluated analytically as described in the following section. Thus N + 1 equations are generated in N + 1 unknowns which may be solved for by Gaussian elimination as discussed in section 5.2.

It remains to check the validity of the assumption used to determine the location of merging points. This is done in precisely the same manner as described in section 5.2 using the point mating procedure. The separation in the tangential direction is determined using equation (5.13a), however, the tangential displacements u_1 and u_2 used in equation (5.13a) are now defined by

$$U_1(\psi_j) = \sum_{i=1}^{N} P_i \, R_1 \int_{\Omega_{1i}} H_1(\psi_j, \psi', \nu_1, E_1) \, d\psi' \tag{6.6}$$

and

$$U_2(\phi_j) = \sum_{i=1}^{N} P_i \, R_2 \int_{\Omega_{2i}} H_2(\phi_j, \phi', \nu_2, E_2) \, d\phi' \tag{6.7}$$

with H_1 and H_2 defined by H in equations (4.41) and (4.54) respectively. The remaining steps in the point mating procedure are performed as described in section 5.2.

For the two dimensional problem of plane strain, the only meaningful strains which can be calculated (from the surface displacements) are $\varepsilon_{\psi\psi}$ for the cylinder and $\varepsilon_{\phi\phi}$ for the seat. The strains $\varepsilon_{\omega\omega}$, $\varepsilon_{r\omega}$, $\varepsilon_{\psi\omega}$ and $\varepsilon_{\phi\omega}$ are all identically zero while $\varepsilon_{r\psi}$, $\varepsilon_{r\phi}$ and ε_{rr} can not be calculated with only knowledge of the surface point displacements. $\varepsilon_{\psi\psi}$ and $\varepsilon_{\phi\phi}$ can be calculated using equations (5.16) and (5.18) respectively.

6.3 Numerical Procedures

In each simply discretized solution the boundaries on Ω_1 and Ω_2 were defined by ψ_{max} and ϕ_{max} respectively. The contact region on each body was partitioned into N cells by dividing ϕ_{max} or ψ_{max} by N and defining the i^{th} cell to lie between ψ_i and ψ_{i+1} where $\psi_{i+1} - \psi_i = \frac{\psi_{max}}{N}$ and $\psi_{i+1} = i*(\psi_{max} / N)$ (see fig. 6.3). The pressure distribution between $\psi = 0$ and $\psi = -\psi_{max}$ was assumed to be symmetric with respect to the η_1 axis. The i^{th} field point on the cylinder was located on the contour curve at an angle of $\frac{\psi_i + \psi_{i+1}}{2}$. The N + 1 field point was located at ψ_{N+1}. Similar locations for the field points on the seat were chosen in terms of ϕ_i, ϕ_{i+1} and ϕ_{N+1}.

The integrals in equations (6.5), (6.6) and (6.7) were evaluated using the analytic formulations derived in appendix O. Since the pressure distribution is symmetric about the η_1 axis (fig. 6.3), the integral over the i^{th} cell on the cylinder (or seat) consisted of two parts, the region between ψ_i and ψ_{i+1} (or ϕ_i and ϕ_{i+1}) and between $-\psi_i$ and $-\psi_{i+1}$ (or $-\phi_i$ and $-\phi_{i+1}$). In evaluating the tangential displacements in equations (6.6) and (6.7) the integrals were multiplied by either + 1 or - 1 depending on the relative positions of the field point and regions of integration. If the region of integration was located to the left (in the $-\psi$ or $-\phi$ direction) of the field point the integral was multiplied by - 1; otherwise it was multiplied by 1. This procedure accounted for the sign of the direction of the displacement due to the position of the loading. The

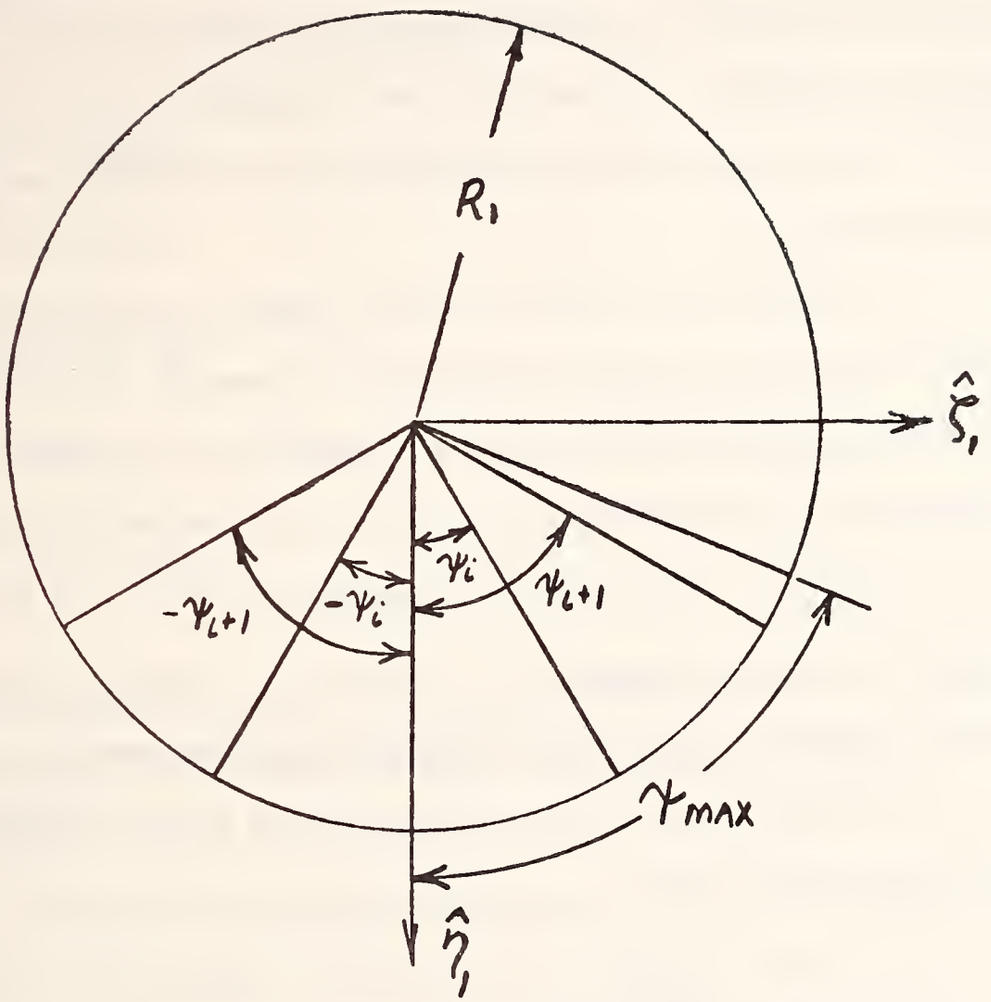

Fig. 6.3. Cell boundaries on cylinder

integrals when evaluated at their singularities present no problem since the results are finite as shown in appendix O.

The point mating procedure was employed in the same manner as described in section 5.3, to converge on the coordinates of a set of merging field points. Also as described in section 5.3, N + 1 equations were generated and the variables were solved for using Gaussian elimination.

The total applied force per unit length can be calculated from the discretized pressure distribution determined in the analysis. Consider the constant normal pressure P_i over cell i on the cylinder. The component of incremental force in the $-\eta_1$ direction at angle ψ is $P_i \cos\psi \, R_1 \, d\psi$. Integrating this between ψ_1 and ψ_{i+1} the force per length over cell i becomes $P_i \, R_1 \, (\sin\psi_{i+1} - \sin\psi_i)$. Recalling that the pressure P_i acts over an identical region between $-\psi_i$ and $-\psi_{i+1}$, the total force on the cylinder may be found by summing the forces on each cell, i.e.,

$$F = 2R_1 \sum_{i=1}^{N} P_i (\sin\psi_{i+1} - \sin\psi_i) \qquad (6.8)$$

Finally the approach δ may be calculated by back substitution of the $P_{i's}$ in the $N+1^{st}$ equation written at the N + 1 field point (see chapter 2 for a description of the complete simply discretized method of solution).

6.4 Numerical Results

The following numerical example in plane stress was considered:

$$R_1 = 1.00 \text{ in}$$

$$R_2 = 1.01 \text{ in}$$

$$\psi_{max} = 40 \text{ Deg} \qquad (6.9)$$

$$E_1 = E_2 = 30 \times 10^6 \text{ psi}$$

$$\nu_1 = \nu_2 = 0.3$$

A program CONCYL was written using the analysis of section 6.3. The results for the above problem were compared to those of Persson [1964].

The pressure distributions obtained by Persson and CONCYL are plotted in figure 6.4. A close correspondence exists between the two solutions. The displacements calculated in CONCYL are tabulated in tables 6.1 and 6.2 as functions of the angles ψ and ϕ.

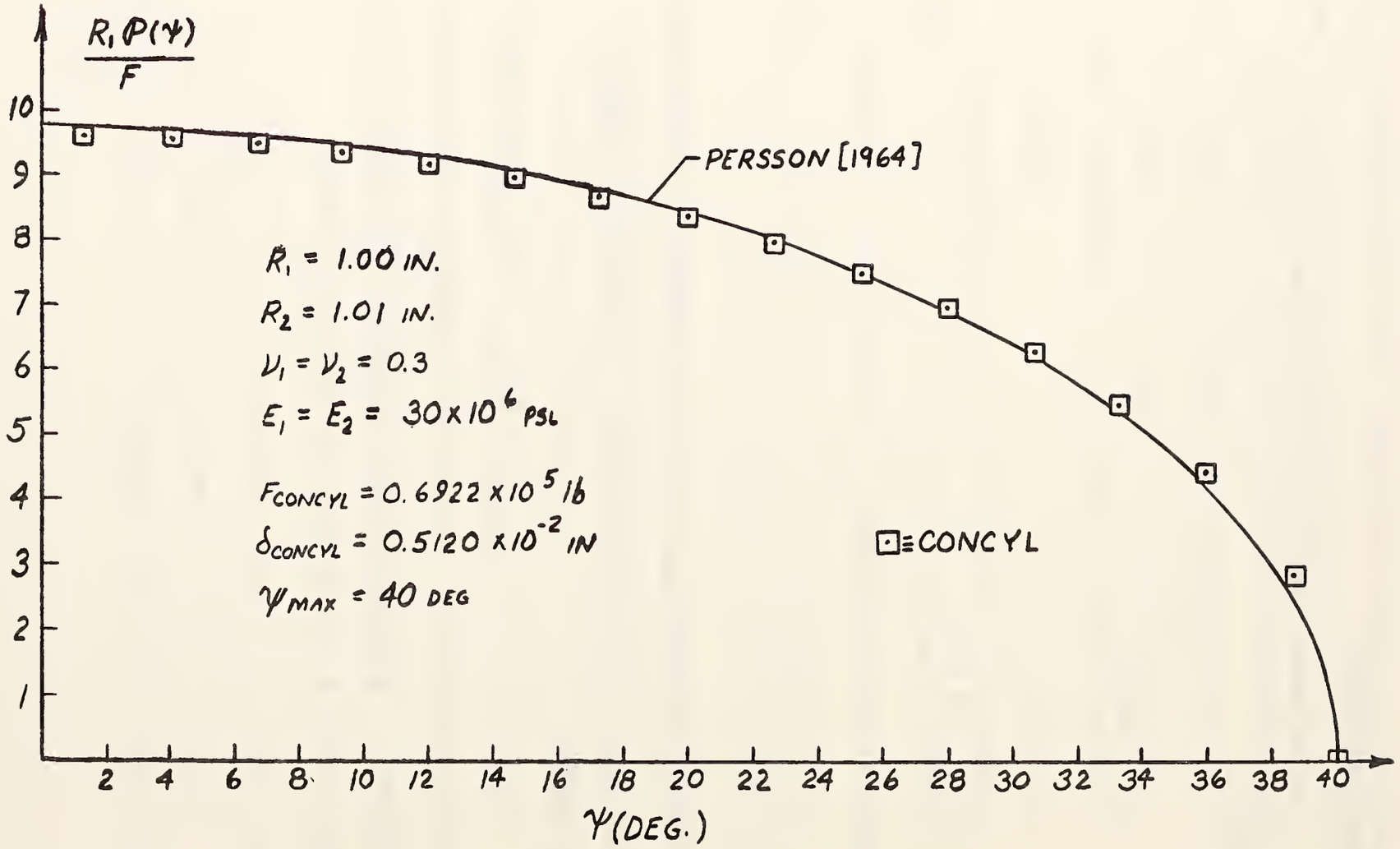

Fig. 6.4. Pressure distribution between a cylinder and cylindrical seat, ψ_{max} =40°.

TABLE 6.1

DISPLACEMENTS ON CYLINDER

ψ [Deg]	Radial Displacement $\times 10^3$ [in]	Tangential Displacement $\times 10^3$ [in]
1.33	2.019	0.1101
4.00	2.006	0.3288
6.67	1.979	0.5429
9.33	1.939	0.7492
12.00	1.886	0.9450
14.67	1.819	1.127
17.33	1.739	1.294
20.00	1.646	1.443
22.67	1.540	1.573
25.33	1.422	1.682
28.00	1.290	1.771
30.67	1.146	1.841
33.33	0.9885	1.896
36.00	0.8189	1.945
38.67	0.6368	2.010
40.00	0.5409	2.039

PLANE STRESS RESULTS FOR:

$\psi_{max} = 40^{\circ}$, $R_1 = 1.00$ in, $R_2 = 1.01$ in,

$E_1 = E_2 = 30 \times 10^6$ psi, $\nu_1 = \nu_2 = 0.3$

TABLE 6.2

DISPLACEMENTS ON CYLINDRICAL SEAT

ϕ [Deg]	Radial Displacement $\times 10^3$ [in]	Tangential Displacement $\times 10^3$ [in]
1.31	0.3097	-0.07100
3.93	0.3078	-0.2124
6.55	0.3040	-0.3521
9.17	0.2984	-0.4889
11.79	0.2910	-0.6216
14.41	0.2817	-0.7490
17.04	0.2706	-0.8700
19.66	0.2577	-0.9834
22.28	0.2431	-1.088
24.91	0.2268	-1.182
27.54	0.2089	-1.265
30.16	0.1894	-1.334
32.79	0.1683	-1.389
35.43	0.1458	-1.427
38.06	0.1219	-1.444
39.38	0.1094	-1.446

PLANE STRESS RESULTS FOR:

$\psi_{max} = 40^o$, $R_1 = 1.00$ in, $R_2 = 1.01$ in,

$E_1 = E_2 = 30 \times 10^6$ psi, $\nu_1 = \nu_2 = 0.3$

The radial displacements on the seat are larger by a factor of 1.5 to 2.0 than those on the cylinder. As in the case of the sphere and seat, the tangential displacements on the cylindrical seat were found to be negative while the tangential displacements on the cylinder were positive. The physical interpretation of this result is the same as that expressed in section 5.4 for the sphere and seat. The values of force and approach for this problem were found to be $F = 0.6922 \times 10^{5}$ lbs/in and $\delta = 0.5120 \times 10^{-2}$ in.

In order to correlate results with Hertzian theory, the problem for $\psi_{max} = 0.1$ degree was analyzed. The resulting pressure distribution is plotted in figure 6.5 along with the results of Persson and Hertz. There is close agreement between all solutions as would be expected for this case of small contact area.

Figure 6.6 illustrates the relation between the load F, radial difference ΔR,[1] and the maximum angle of contact, ψ_{max}. Along with the results of CONCYL are plotted the solutions of Hertz, Sjtaerman [1949] and Persson.

There is close agreement between all solutions for angles of contact less than 15 degrees. For larger angles of contact there is a close correspondence between the results of CONCYL and those of Persson. The curves corresponding to Hertz's theory and that of Sjtaerman deviate significantly.

Figure 6.7 illustrates the variation of maximum pressure with

---

[1] ΔR equals $R_2 - R_1$.

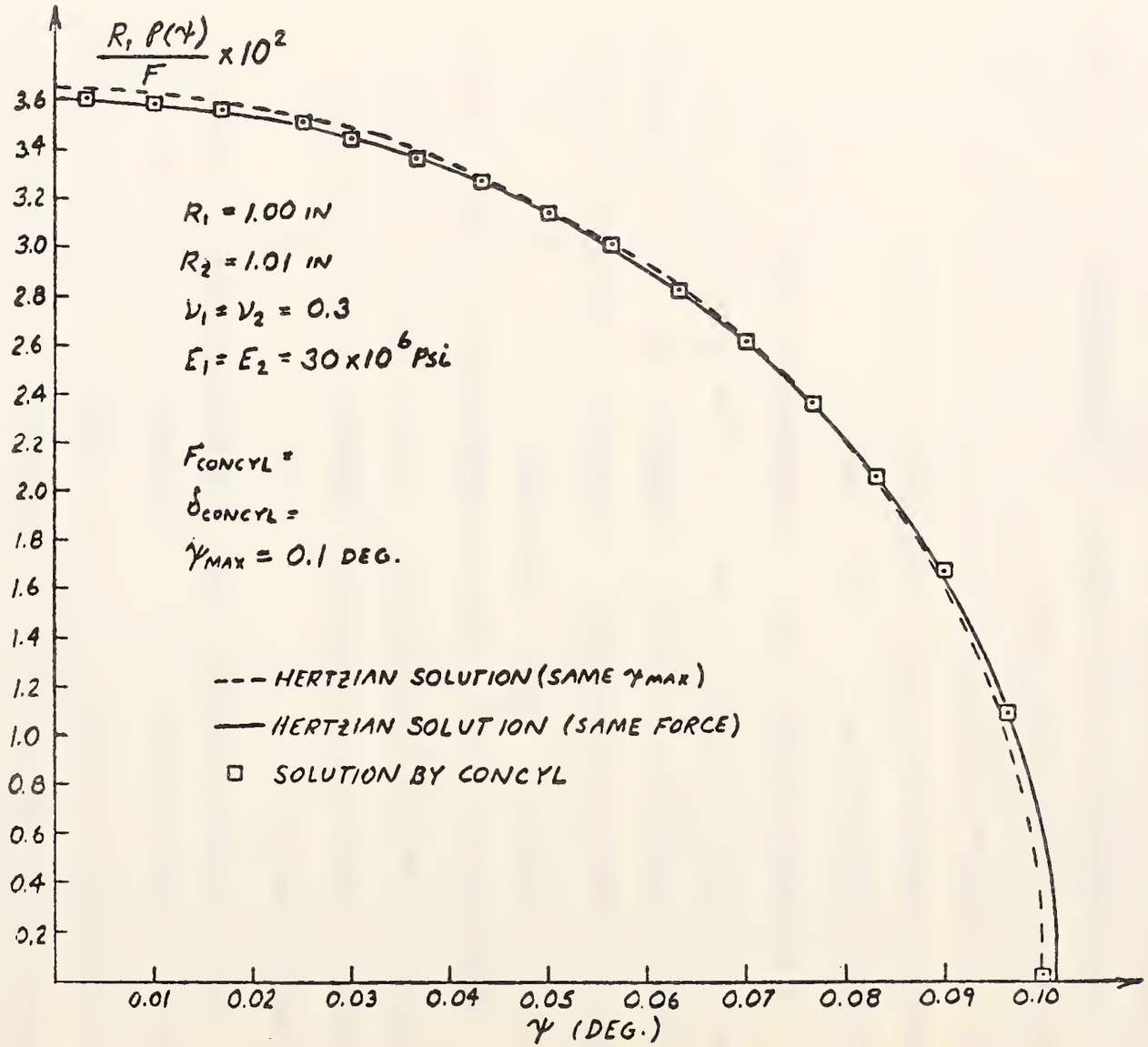

Fig. 6.5. Pressure distribution between a cylinder and cylindrical seat, $\psi_{max} = 0.10^{o}$.

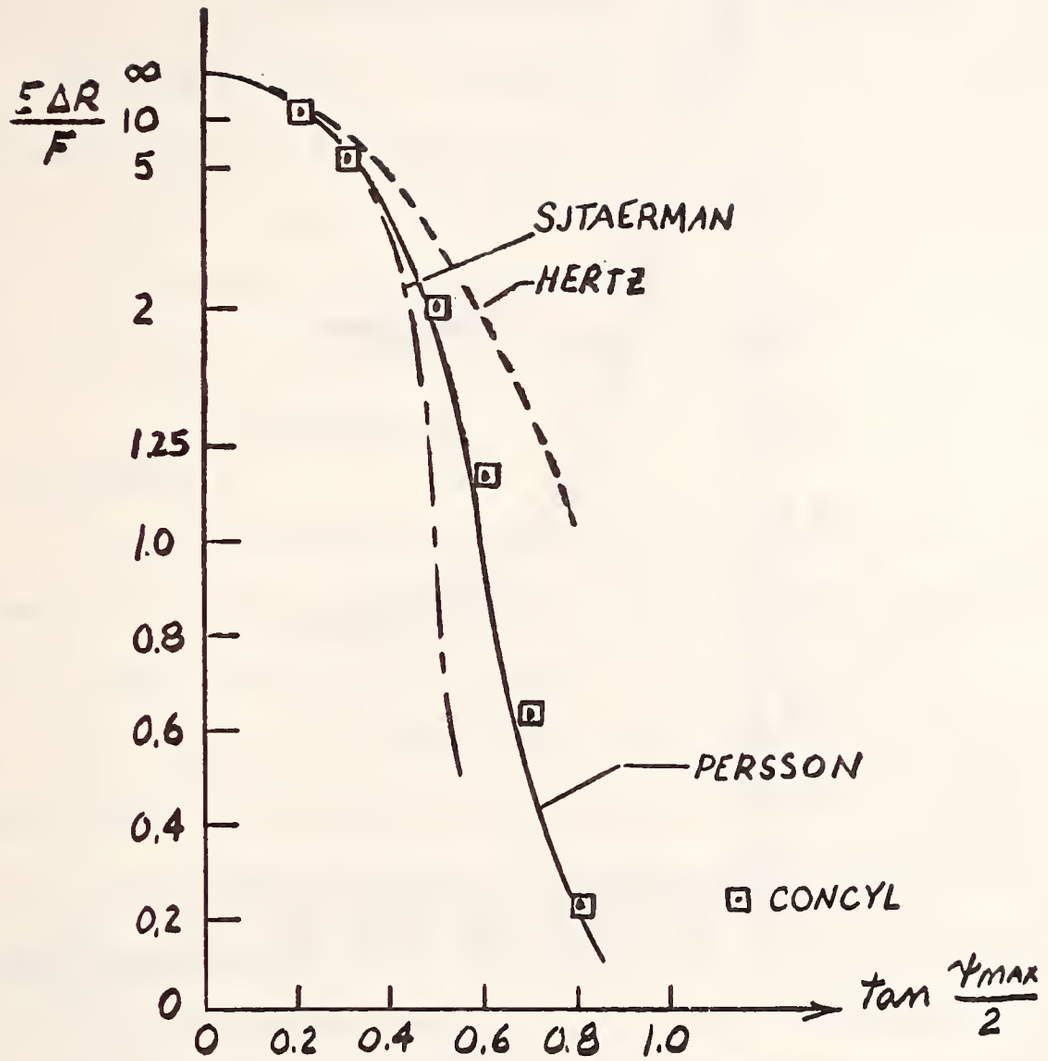

Fig. 6.6. Relationship between $\frac{E\Delta R}{F}$ and tangent of $\frac{\psi_{max}}{2}$

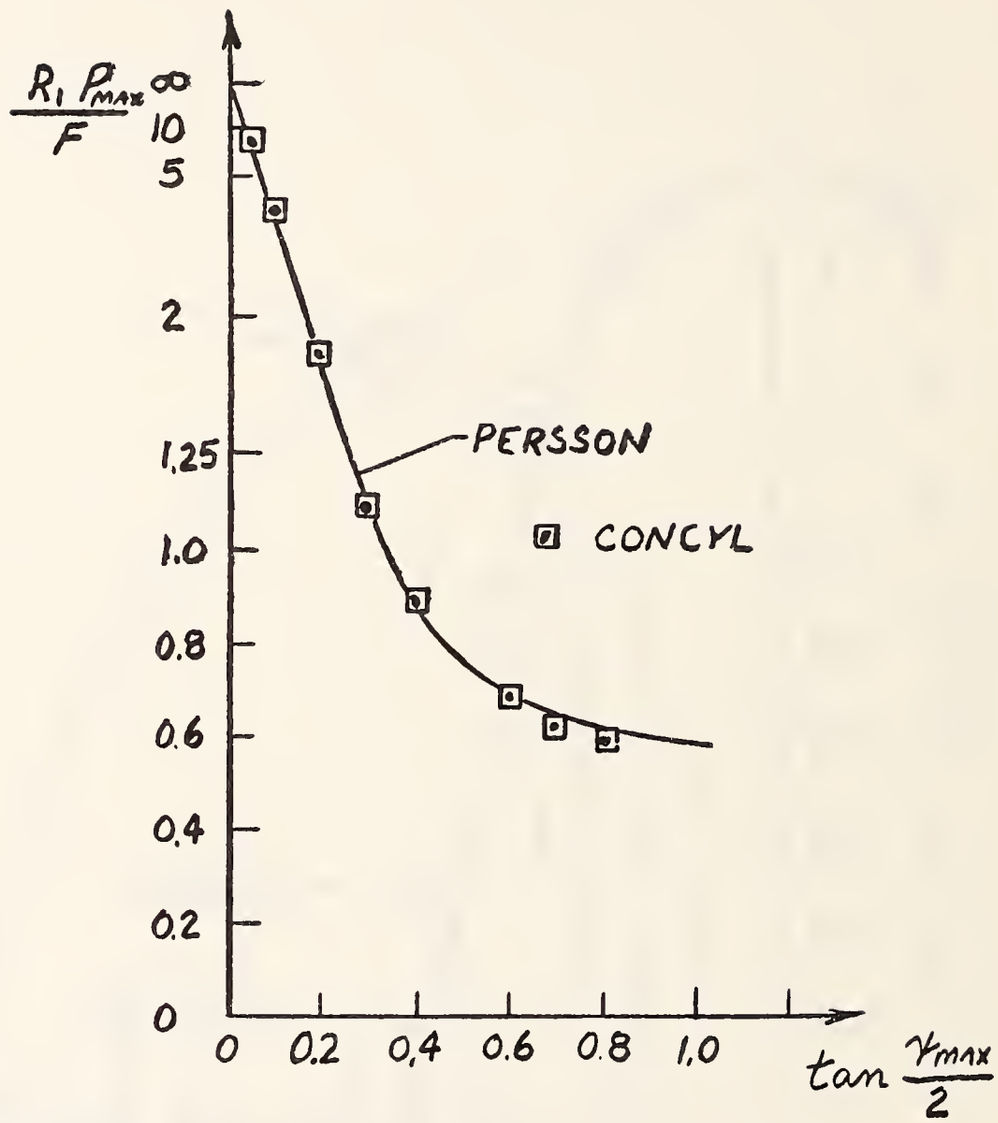

Fig. 6.7. Relationship between $\frac{R_1 P_{max}}{F}$ and tangent of $\frac{\psi_{max}}{2}$

maximum contact angle for both the present theory and that of Persson. Figure 6.8 relates the variation between the maximum pressure, radial difference and load. In each of the last two figures the results of CONCYL show close agreement with the results of Persson.

The computer costs in running CONCYL were minimal, being about twenty-three cents for a fifteen node case. This corresponds to about five seconds of CPU time on the IBM 360/65 computer. The low costs in CONCYL can be attributed to the fact that all integration was performed analytically rather than numerically as in CONSPHERE.

6.5 Conclusions

It can be concluded that the problem of a cylindrical seat has been successfully solved using the conformal theory presented in chapter 3. The pressure distributions for the problems where $\psi_{max} = 40^{o}$ and $\psi_{max} = 0.1^{o}$ were found to agree with the results of Persson [1964]. In addition the latter results also corresponded to the solution of Hertzian theory. The displacements were calculated for the case where $\psi_{max} = 40^{o}$. The tangential components were found to be of opposite sign on each body. The load vs. subtended angle relationship was found to agree with the solution of Persson, however, the solution of Sjtaerman [1949] deviates significantly for angles greater than 20 degrees. The results of maximum pressure vs. contact angle also agreed well with that of Persson.

In general there was strong agreement with the Persson solution. This close agreement supports Persson's assumption that the contour curve of the contact region is circular. The correlation

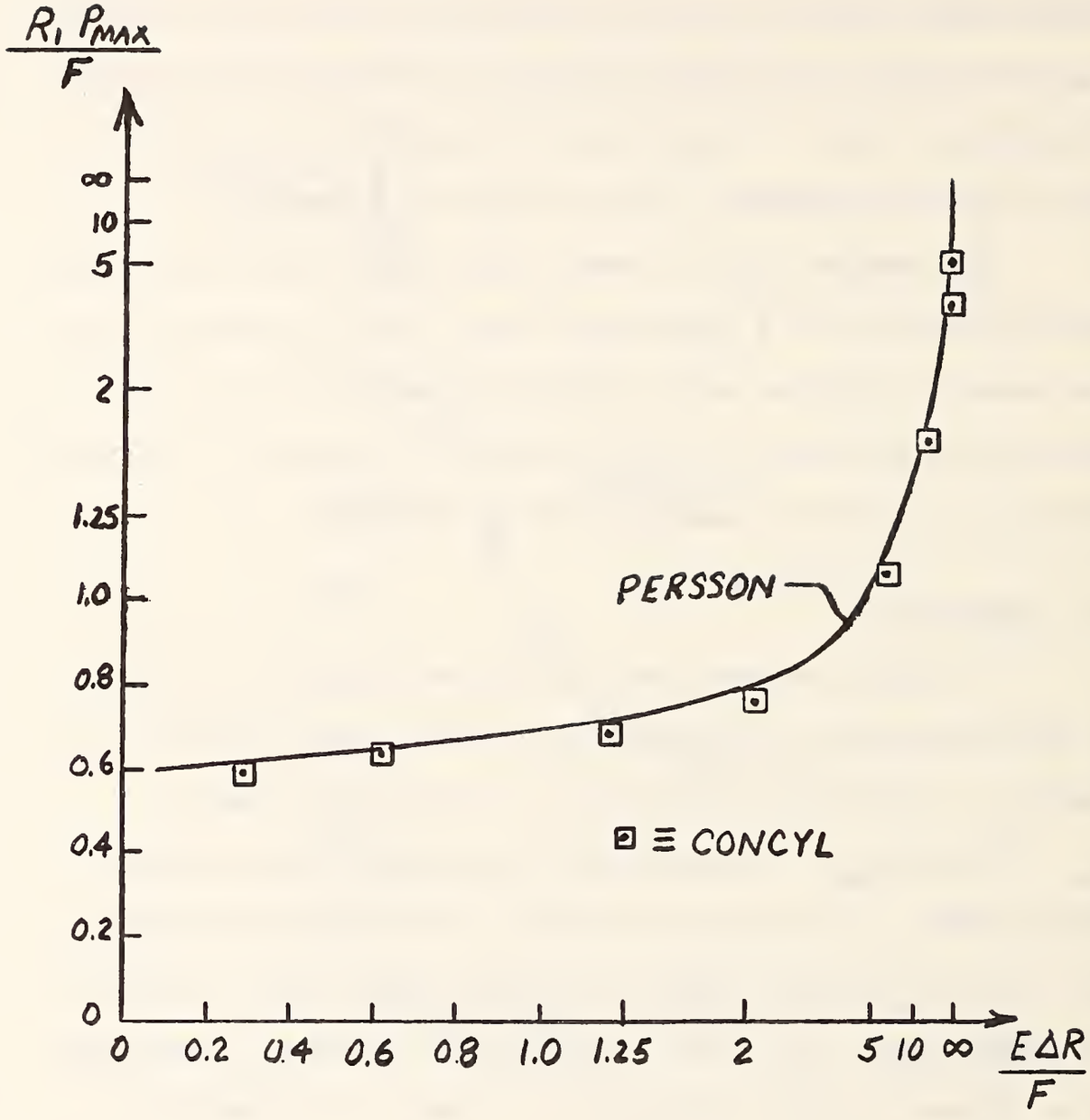

Fig. 6.8. Relationship between $\frac{R_1 P_{max}}{F}$ and $\frac{E\Delta R}{F}$

between the solutions presented and the Hertzian solutions broke down for large angles as expected. The results of Sjtaerman also deviated from those of the present theory which may be explained by the fact that Sjtaerman may have used an extremely crude finite difference scheme since he could not take advantage of modern computational aids at the time of publication.

7. CONTACT STRESSES FOR MULTIPLY CONNECTED REGIONS

7.1 Introduction

Contact problems involving multiply-connected contact regions have received little attention in the literature, possibly because of the non-Hertzian nature of such problems. Such problems arise, for example, whenever either of the contacting bodies have surface pits (e.g., casting defects, corrosion pits, machining faults, etc.). Barely perceptible surface flaws can cause high stress concentrations, and consequently, rapid fatigue failure. Experimental observations by Tallian [1967], Martin and Eberhardt [1967] and Littman and Widner [1966] indicate that such surface defects may be potential nuclei of microcrack propagation and can produce rapid destruction of rolling surfaces.

Based on the degree of difficulty associated with their solution, these problems may be divided into the following two categories:

(i) Contact region known a priori:

When the indentor contact surface is flat (or almost flat) it will be called a "stamp," and the contact surface is defined a priori by the stamp boundary. When the indentor surface is not flat, but the indentor has a substantially higher elastic modulus than the indented body, the indentor can be

treated as rigid, and the shape of the contact region becomes known for any given depth of penetration relative to the indentor tip. These are also termed "punch" problems.

(ii) Elastic Contact Problems:

When the indentor is not a stamp, and the two bodies have comparable elastic moduli, then the geometry of the contact region is unknown a priori, and it must be determined by solving the appropriate Elasticity problem.

To the best of our knowledge, only one recent solution by Chaud et al. [1974] for three dimensional elastostatics with multiply-connected regions, has been reported in the literature. However, solution of a few special cases of rigid indentor problems (category [i]) have been found by Olesiak [1965], Parlas and Michalpoulos [1972] and Chiu [1969].

Olesiak [1965] solved the problem of an annular flat faced-stamp pressed on an elastic half space. Parlas et al. proposed the solution for a "bolt shaped" indentor pressed into an elastic half space with a cylindrical hole. The cylindrical (bolt) section of the indentor was assumed to be rigidly bonded to the wall of the cylindrical hole while the bottom face of the bolt head presses against the half space.

Chiu [1969] solved the problem of an infinitely long rigid cylinder in contact with an elastic half space, where the rigid cylinder has a groove running parallel to its axis.

In this chapter, results indicate that problems of

both categories (i) and (ii) may be successfully solved by an extension of the method introduced by Singh and Paul [1974].

A brief synopsis of the formulation and application of the "simply discretized" method of solution are given with some limitations and advantages of this method in section 7.2. The example problem of a pitted sphere in contact with a complete sphere is described in section 7.3. Techniques devised for an accurate numerical solution and rapid convergence are described in section 7.4. Results for an example are given in section 7.5, and conclusions are reviewed in section 7.6.

7.2 Formulation

We will restrict our attention to "nonconformal" contact problems where the dimensions of the contact region are small compared to appropriate radii of curvature of the undeformed bodies. Therefore, we may assume that the contact surfaces do not deviate significantly from a reference plane in which we imbed fixed cartesian axes (x,y). Furthermore, we shall consider only those cases where the two bodies undergo a relative rigid body translation of amount δ, in a direction normal to the reference plane, plus an elastic deformation. The translation δ is called the "relative approach" and is positive if it moves the bodies towards one another. We will also assume that the applied load consists of a force F, acting normal to the reference plane, and that the contacting surfaces have a sufficient degree of symmetry that the resultant of the contact pressures on each body is a force of magnitude F which acts through the

origin O of the reference plane and equilibrates the applied force F.

The fundamental integral equation governing nonconformal contact problems was shown in chapter 2 to be

$$S(x,y) = k\int_{\Omega}\frac{p(x',y')dx'dy'}{\sqrt{(x-x')^2+(y-y')^2}} - \delta + f(x,y) \qquad (7.1)$$

where the "elastic parameter" k is defined as

$$k = \frac{(1-\nu_1^2)}{\pi E_1} + \frac{(1-\nu_2^2)}{\pi E_2} \qquad (7.2)$$

In the foregoing equations, ν_1, ν_2, and E_1, E_2 denote the Poisson's ratio and Young's modulus respectively for body 1 (indentor) and body 2 (indented); p(x',y') is the normal pressure over the contact surface; Ω is the projection of the contact surface on the (x,y) reference plane; f(x,y) represents the initial separation (or gap) between surface points on the two bodies, located at the same (x,y) coordinates, before the load F is applied; S(x,y) is the separation of the opposed surface points after the load is applied. Figure 7.1 illustrates the initial separation f for a case of axial symmetry where f is a function f(r) of the radial coordinate r.

The condition of impenetrability of matter requires that S(x,y) should vanish inside Ω and it should be positive outside of Ω. Conversely, the interfacial contact pressure p(x,y) should be positive inside Ω, and it should vanish identically outside of it.

In symbolic terms,

$$S = 0 \qquad \text{FOR } (x,y) \text{ INSIDE AND ON } \Omega \tag{7.3a}$$

$$S > 0 \qquad \text{FOR } (x,y) \text{ OUTSIDE } \Omega \tag{7.3b}$$

$$P(x,y) = 0 \qquad \text{FOR } (x,y) \text{ OUTSIDE } \Omega \tag{7.4a}$$

$$P(x,y) \geq 0 \qquad \text{FOR } (x,y) \text{ INSIDE AND ON } \Omega \tag{7.4b}$$

In short, a solution of the problem requires the determination of the boundaries of region Ω, a pressure field $p(x,y)$, and an approach δ which satisfy relations (7.1)-(7.4). The associated load may be found from the expression

$$F = \int_{\Omega} p(x,y)\,dx\,dy \tag{7.5}$$

The absence of foreknowledge of the contact region Ω is a major impediment to a mathematical solution. This obstacle is overcome by postulating a tentative contact region Ω^*. Singh and Paul [1974] proposed that the "interpenetration curve" described by

$$f(x,y) = d \tag{7.6}$$

be used as a tentative contact region. Equation (7.6) defined the contour of the curve formed by interpenetration (without deformation) of the two surfaces through an arbitrary distance d. Picking a suitable value of d establishes the candidate contact region Ω^*. Using this as a preliminary estimate of Ω, equation (7.1) is readily

recognized to be an integral equation of the first kind.

Equation (7.1) can be solved using the "simply discretized" method of Singh and Paul which is reviewed in chapter 2. A "simply discretized" numerical solution of equation (7.1) is found by subdividing Ω into a large number of small cells. The pressure function $p(x,y)$ is replaced by a piecewise constant pressure field (pressure P_i in cell i). Thus if Ω is subdivided into N cells, equation (7.1) becomes

$$\sum_{i=1}^{N} k P_i \int_{\Omega_i} \frac{dx'dy'}{\sqrt{(x-x')^2+(y-y')^2}} - \delta + f(x,y) = S \qquad (7.7)$$

where Ω_i is the region of cell i. In equation (7.7), N values of p_i and the constant δ are unknowns to be determined. The centroids (x_i,y_i) of the cells are taken as field points (x,y) and equation (7.7) is written for each field point. The integrals in equation (7.7) are evaluated by numerical quadrature. Thus N linear algebraic equations are generated. An additional independent linear equation, essential for a unique solution, is generated by picking up a field point other than the cell centroids. The choice of this additional field point is otherwise arbitrary, however, it does affect the quality of the results, as discussed in section 7.4.

Having thus generated a set of N + 1 linear equations, the N unknown pressures, P_i, and the approach δ, are obtained through

Gaussian elimination. The next step in the solution is to determine whether the tentatively selected region of integration Ω^* is indeed the true contact region. This is done by utilizing the inequalities (7.3) and (7.4) and systematically adjusting the boundaries of Ω until these inequalities are satisfied.

Singh and Paul [1974] showed that the "simply discretized" method was unstable in the general case and was incapable of predicting the proper stress distribution. For such problems they found it necessary to introduce stabilizing techniques known as the "Redundant Field Point Method," and the "Functional Regularization Method" (see Singh [1972], Singh and Paul [1973]).

The amount of numerical computation required for either of the two last methods exceeds that of the Simply Discretized Method. Accordingly, it is desirable to use the latter whenever circumstances permit.

In this chapter we will focus on a problem with complete axisymmetry, and it will be shown that the Simply Discretized Method provides an excellent solution, provided that the maximum possible use is made of the symmetry of the problem.

In other words, we recognize that all cells located at the same radius from the axis of symmetry have the same contact pressure at their centroids, and the number of unknown pressures P_i is reduced from the number of cells to N (the number of annular rings formed by an axisymmetric distribution of cells). By using the Simply Discretized Method, we are able to utilize Inequality (7.4) to

iteratively refine the region of contact Ω. Upon satisfying Inequality (7.4), it was invariably found that Inequality (7.3) was satisfied.

The nature of the Functional Regularization Method prohibits the use of Inequality (7.4) as a basis for refining Ω.

Numerical experiments have indicated that iteration procedures based on Inequality (7.4) converge much faster than those based upon Inequality (7.3). Further details of the iteration procedures will be found in sections 7.4 and 7.5.

7.3 Pitted Sphere Geometry

As a typical example, contact of a pitted elastic sphere of radius R_1 with an unpitted elastic sphere of radius R_2 is considered. A section of the pitted surface by a plane through the axis of symmetry is shown in figure 7.1. The local contour of the pitted surface is idealized as a torus smoothly blended into a sphere. The blending point P, where the pit joins the main surface, is located at a distance r_b from the load line. The center of curvature O' of the pit blending arc lies on the conical surface of semivertex angle τ. The meridional radius of curvature of the torus is r_c.

Note that the discontinuity in curvature which occurs at P does not preclude the use of the method of solution being used. A tentative contact region, Ω, is established by a hypothetical interpenetration of the two spheres through a distance d. The annulus of contact so formed is bounded by an inner radius r_I and an outer radius

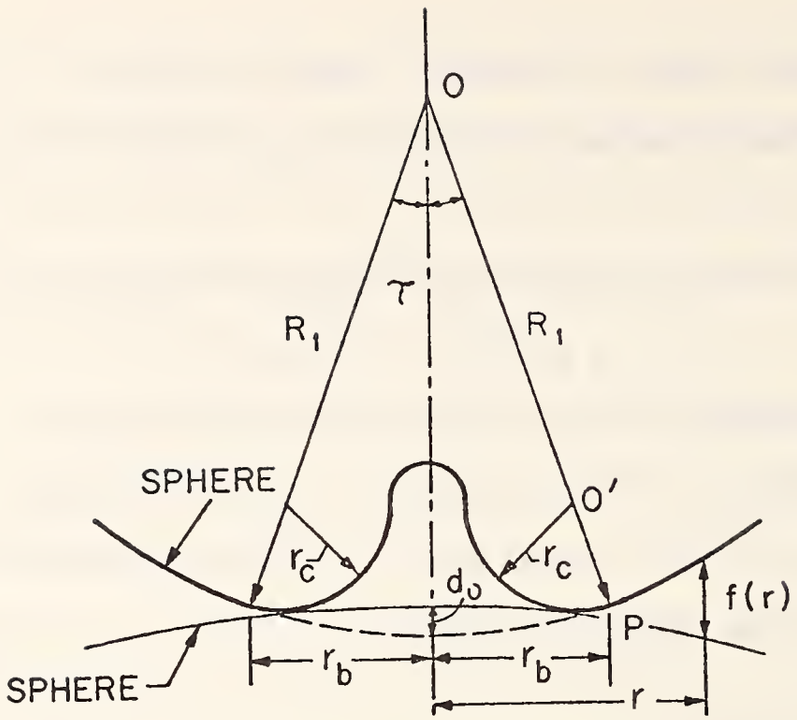

Fig. 7.1. Geometry of pitted surface

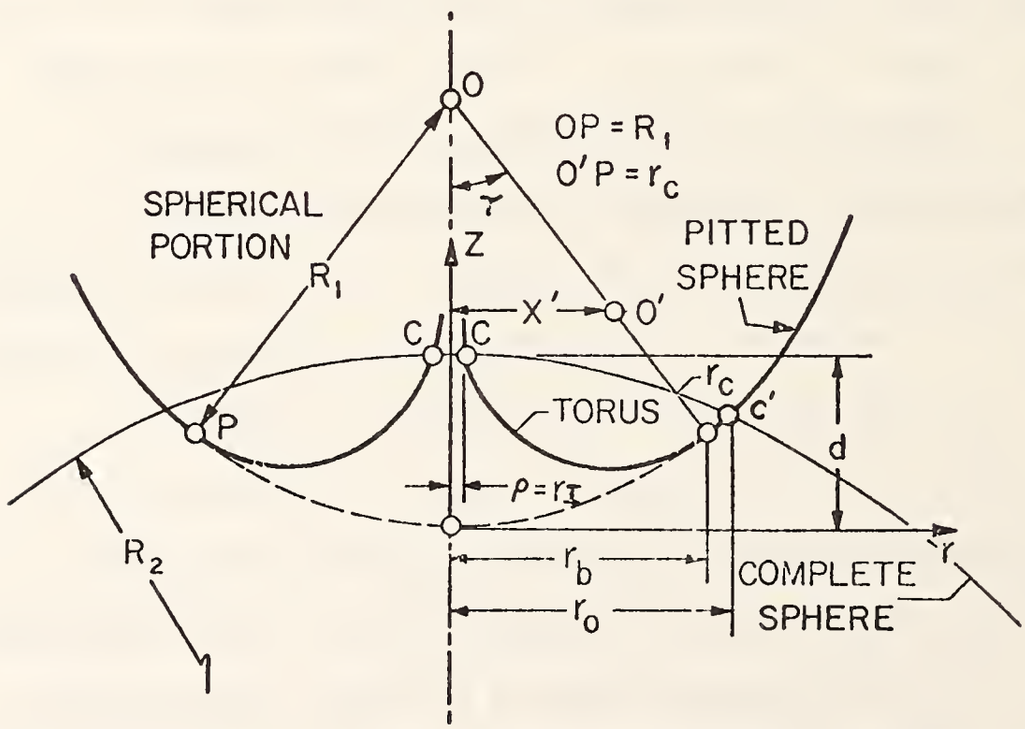

Fig. 7.2. Generation of annular interpenetration

r_o as shown in figure 7.2, where suitable coordinate axes r, and z are indicated. The values of r_I and r_o for a given problem are determined as follows. The z coordinate of a point $C(\rho, z_1)$ located at a distance ρ from the z-axis on the toroidal portion of body 1 (see fig. 712), where

$$\rho < r_b \tag{7.8a}$$

is:

$$z_1 = R_1 - (R_1 - r_c)\cos\tau - \sqrt{r_c^2 - (l-\rho)^2} \tag{7.8b}$$

where

$$l = \frac{(R_1 - r_c) r_b}{R_1} \tag{7.8c}$$

$$\tau = \sin^{-1}\frac{r_b}{R_1} \tag{7.9}$$

The z-coordinate of a point on sphere 2, located at a distance ρ from the z-axis is given by

$$z_2 = d - \left[R_2 - (R_2^2 - \rho^2)^{1/2}\right] \tag{7.10}$$

Since point C lies on both the torus and the lower sphere, $z_1 = z_2$; thus equations (7.8b) and (7.10) require that

$$d = R_1 - (R_1 - r_c)\cos\tau - [r_c^2 - (\rho - \ell)^2]^{1/2} + R_2 - (R_2^2 - \rho^2)^{1/2}$$

$$\rho < r_b \tag{7.11a}$$

Furthermore, the z-coordinate of a material point C' located on the spherical portion of body 1, at a distance ρ from the z-axis, is given by

$$z_1 = R_1 - (R_1^2 - \rho^2)^{1/2} \tag{7.12}$$

where

$$\rho > r_b \tag{7.12a}$$

Hence, for a given interpenetration d, the radius ρ of a point on the intersection of sphere 2 and spherical region of body 1 is given by

$$d = R_1 - (R_1^2 - \rho^2)^{1/2} + R_2 - (R_2^2 - \rho^2)^{1/2} \tag{7.13a}$$

$$\rho > r_b \tag{7.13b}$$

The geometry of the toroidal surface indicates that for $r_c < R_1$, equation (7.11) has two solutions for ρ. Let ρ_1 and ρ_2 ($\rho_1 < \rho_2$) be roots of equation (7.11). Two cases are readily identified.

Case (i). When both inner and outer radii of the assumed contact region lie inside the blending radius, i.e.,

$$\rho_2 < r_b \tag{7.14}$$

In this case the contact is assumed to be completely confined to the toroidal segment of body 1, in which case

$$r_I = \rho_1$$
$$r_o = \rho_2 \tag{7.15}$$

Case (ii). When the outer boundary of Ω lies beyond the blending radius (as shown in fig. 7.2), i.e.,

$$\rho_2 > r_b \tag{7.16a}$$

In this case

$$r_I = \rho_1 \tag{7.16b}$$

and the outer radius r_o is determined from solution of equation (7.13). Note that equations (7.11) and (7.13) are transcendental in ρ, which can be found by an iterative procedure (e.g., Newton Raphson).

In order to find the initial separation f(r), shown in figure 7.1, it is only necessary to find

$$f(r) = z_1 - z_2 \tag{7.16c}$$

where z_2 is found from equation (7.10) with $\rho \equiv r$ and $d \equiv d_o$; d_o is the value of d corresponding to initial contact as shown in figure 7.1.

To find z_1, set $\rho \equiv r$ and use equation (7.8b) for points on the torus ($r < r_b$), or equation (7.12) for points on the upper sphere ($r > r_b$).

In order to find the initial separation d_0, it is necessary to note from figure 7.1, that when $d = d_0$, the slope of the torus matches that of the lower sphere at the contact point; i.e.,

$$\frac{dz_1}{d\rho} = \frac{dz_2}{d\rho} \tag{7.17}$$

where the derivatives are found from equation (7.8b) and equation (7.10). Equation (7.17), together with equations (7.8b) and (7.10), suffice to find d_0, and the two coordinates (r,z) of the initial contact point.

Having found the boundaries (r_I and r_o) of the contact region Ω and the initial separation function $f(r)$, we may proceed to solve the governing integral equation (7.1).

7.4 Numerical Solution Procedure

The contact region Ω is subdivided into N annular rings. Since a steep pressure gradient is expected near the pit, the annular rings near the inner boundary are very narrow in width. It was also learned from experience that the peak pressure always occurs at some radius r where $r < r_b$. Guided by this consideration, a majority of the rings are clustered in the region $r_I \leq r \leq r_b$. Exploiting the axisymmetry of the problem, we assume that the pressure is constant in each ring. The rings are numbered sequentially from 1 to N, from

the inside out, and the pressure in the i-th ring is assumed to be an unknown constant p_i. Let r_i and r_{i+1} be the inner and outer bounding radii for cell i; thus $r_1 \equiv r_I$ and $r_{N+1} \equiv r_o$. Each ring is further subdivided circumferentially into m equal sectors by drawing (m) equispaced radial rays from the center of Ω; the angle $\Delta\phi$ between two adjacent rays is $2\pi/m$. The sector, bounded by radial rays 1 and 2, is shown in figure 7.3.

The region of the sector located in the i-th ring, between ray j and ray (j+1), is identified as S_{ij}; and its centroidal radius by β_{ij}. Elementary calculations show that

$$\beta_{ij} = \frac{4 \sin \frac{\Delta\phi}{2}}{3\,\Delta\phi} \frac{(r_{i+1}^2 + r_i^2 + r_{i+1} r_i)}{(r_{i+1} + r_i)} \qquad (7.18)$$

The centroids of the first sector shown in figure 7.3 (i.e., where j = 1) are selected as field points.

Thus for the field point ℓ, equations (7.7) and (7.3a) reduce to

$$k \sum_{i=1}^{N} P_i \sum_{j=1}^{m} \int_{S_{ij}} \frac{dA_{ij}}{c_{ij\ell}} - \delta + f(\beta_{\ell 1}) = 0 \qquad (7.19)$$

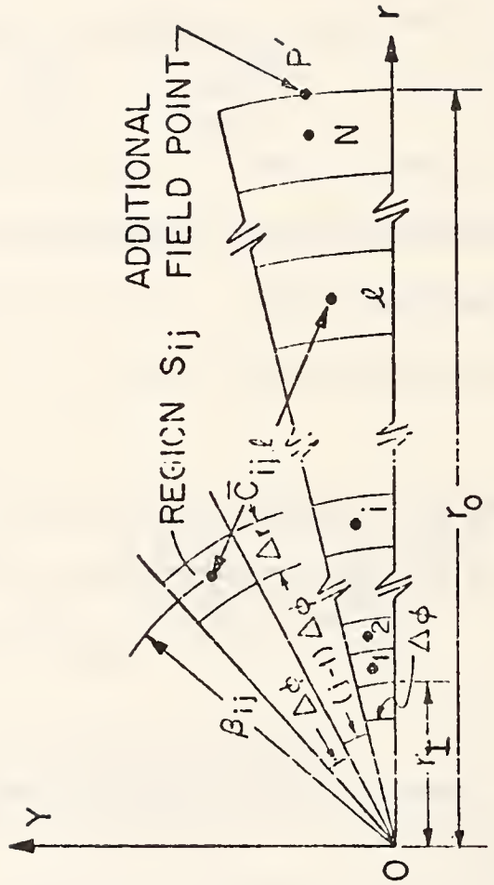

Fig. 7.3. Subdivided and labeled contact region (portion)

where $f(r)$ is calculated for $r = \beta_{\ell 1}$ from equation (7.16c). $c_{ij\ell}$ is the radial distance from field point ℓ to the elemental area dA_{ij} located in S_{ij}. For most cells, the integral in equation (7.19) may be replaced by the approximation

$$I_{ij\ell} = \int_{S_{ij}} \frac{dA_{ij}}{c_{ij\ell}} \doteq \frac{A_{ij}}{\bar{c}_{ij\ell}} \tag{7.20}$$

where $\bar{c}_{ij}$ is the distance between field point ℓ and the centroid of the region S_{ij}, whose area is denoted by A_{ij}. It was shown in Singh [1972] that, in general, equation (7.20) is a very useful approximation which results in a significant reduction of computation time, without compromising the accuracy of results. However, for regions located in the immediate vicinity of the field point ℓ, the errors due to the approximation (7.20) may be unacceptable. To avoid such errors, $I_{ij\ell}$ is evaluated by numerical quadrature within cells located near the field point. The criterion which must be satisfied in order to use equation (7.20) is

$$\bar{c}_{ij\ell} > \max(r\Delta\phi, \Delta r) \tag{7.21}$$

In equation(7.21), $r\Delta\phi$ and Δr are the side lengths of a typical cell. Notice that when the field point ℓ lies inside the region S_{ij} (i.e., $j = 1$, $i = \ell$), $\bar{c}_{ij\ell} = 0$, and hence the integrand in equation (7.15) has a singularity. However, for such cases, an approximate analytical

solution for the integral is readily constructed as shown in Appendix G.

In this manner, N linear equations corresponding to the N field points are generated. An additional linearly independent equation is generated by selecting point P' at the outermost boundary of the contact region as field point (N + 1). The location of this additional field point has a pronounced affect on the solution, which deteriorates as P' is moved inside the boundary. It is plausible to assume that this behavior is due to the gradual increase in cell width Δr with r (see fig. 7.3) which was introduced to keep the aspect ratio of the cells from becoming excessive. With the cells so designed, the location of P' shown in figure 7.3 maximizes the distance between P' and its nearest neighboring field point. This in turn tends to maximize the amount of independent information supplied by the equation written for field point P', and should tend to minimize ill-conditioning effects on the coefficient matrix generated.

Thus (N + 1) equations in (N + 1) unknowns are generated, and equation (7.19) assumes the form

$$b_{ij} P_j = -f_i + \delta \qquad (7.22)$$

and the equation using P' as a field point becomes,

$$V_j P_j = -f_{N+1} + \delta \qquad (7.23)$$

where f_i is the value of the "initial separation" function f(r) at the field point i. f_{N+1} is the value of f(r) at P'; and summation from 1 to N is henceforth implied over repeated subscripts. From equations (7.22) and (7.23), δ may be eliminated to yield

$$B_{ij} P_j = f_i' \tag{7.24}$$

where

$$B_{ij} = b_{ij} - V_j \tag{7.25}$$

and

$$f_i' = f_{N+1} - f_i \tag{7.26}$$

When equation (7.24) is solved for P_i, using Gaussian elimination, the resulting pressure distribution is usually found to predict negative contact pressures in the immediate vicinity of the inside boundary, $r = r_I$. The axisymmetry of the problems enables us to maintain the outside boundary fixed, and iterate on the inside boundary where the predicted pressure is incorrect. The iteration scheme is best explained with the aid of the numerical example given in section 7.5.

7.5 A Numerical Example

The following example problem was considered.

$R_1 = R_2 = 1$ in

$\nu_1 = \nu_2 = 0.3$

$E_1 = E_2 = 30 \times 10^6$ lb/in^2

r_c = .006 in

r_b = .00025 in

The results are presented in dimensionless form. Let

$$R_m = \frac{2R_1R_2}{R_1+R_2} \tag{7.27}$$

Then, we define

Dimensionless pressure in ring i, $P_i^* = k\,P_i$ (7.28)

Dimensionless load, $F^* = \frac{kF}{R^2_m}$ (7.29)

Dimensionless distance from origin of Ω, $r^* = r/R_m$ (7.30a)

Dimensionless approach, $\delta^* = \delta/R_m$ (7.30b)

$r_b^* = r_b/R_m$ (7.31a)

$r_c^* = r_c/R_m$ (7.31b)

Figure 7.4 shows the pressure distribution near the inside boundary for the uniterated solution. The pressure distribution far from the pit agrees closely with the Hertzian solution for unpitted spheres (not shown in the figure). However, the pressure in cell #1 is highly negative. The pressures in the successive cells are less and less

negative, until at point Q_1 the pressure curve crosses the r*-axis. The shape of the pressure curve readily suggests the iteration scheme. The new region of integration is assumed to have inner radius $r_I = OQ_1$. The discretized equation set (7.24) is generated corresponding to this new region Ω, and thus a new pressure vector is generated (see first iteration, fig. 7.4). This new curve also has a negative peak (weaker than that of the uniterated solution) at the innermost field point. The new point of intersection is Q_2, which defines the inner boundary of Ω for the next iteration. The process is thus continued until all pressures are positive. In figure 7.4, the third iteration yields the desired solution. It is found that this solution also satisfies Inequality (7.3), thus qualifying as the "true" solution of the contact problem. The complete pressure distribution is shown in figure 7.5. Notice the essentially Hertzian pressure distribution (corresponding to contact of unpitted spheres) at $r^* > 6 \times 10^{-4}$. Thus the effect of the cavity is of a strictly localized nature. However, as the cavity is made larger (e.g., $r_I/r_o \geq 0.3$) the pressure curve departs completely from the Hertzian case. For example, figure 7.6 shows a typical pressure distribution for $r_I/r_o = 0.623$, along with the Hertzian solution for unpitted spheres corresponding to identical values of thrust F.

In order to establish confidence in the solution, it is necessary to study its convergence with change in the number of cells used. It must be recognized that it is necessary for the cells to be densely concentrated only in that region where a high pressure

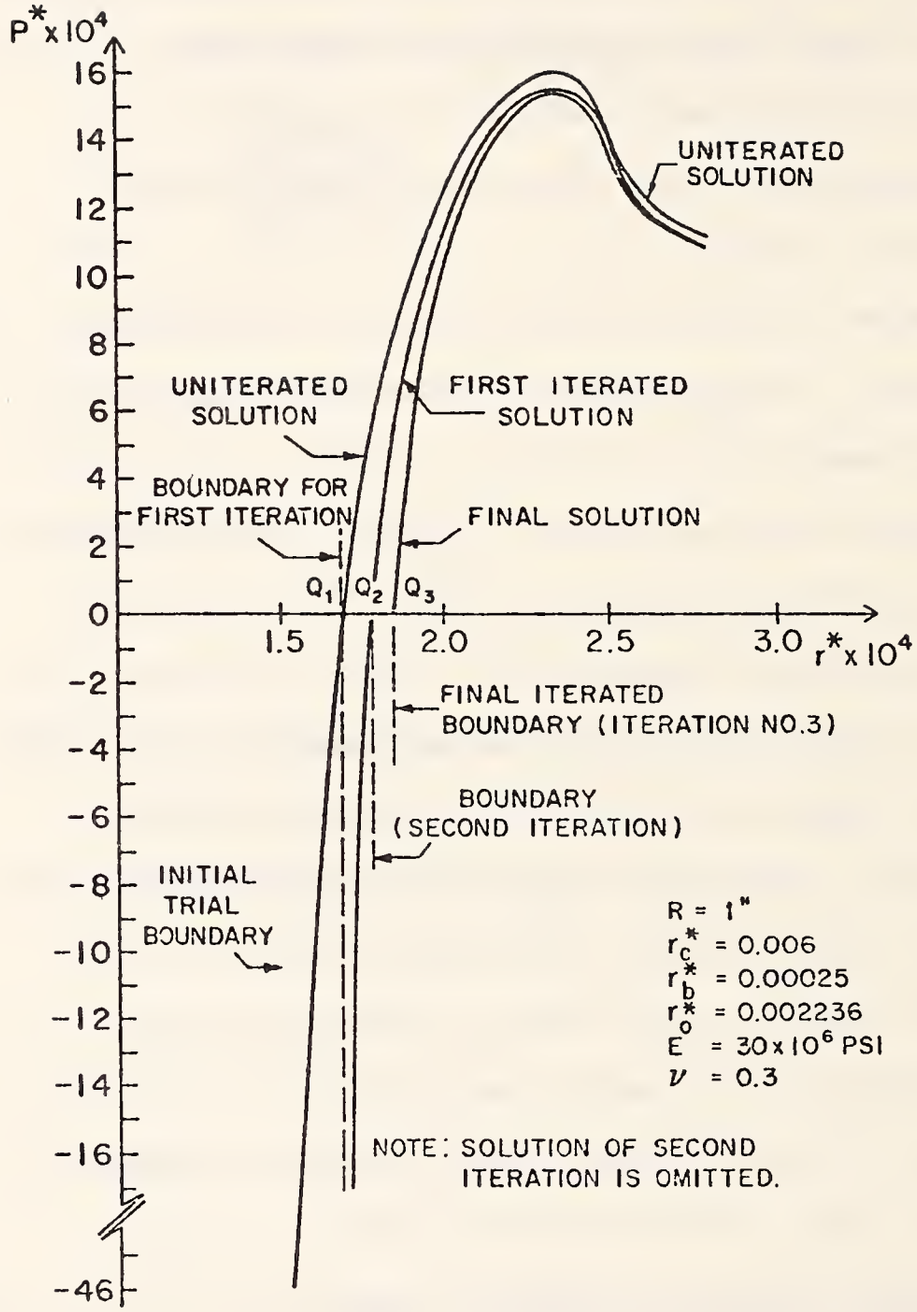

Fig. 7.4. Boundary iteration sequence

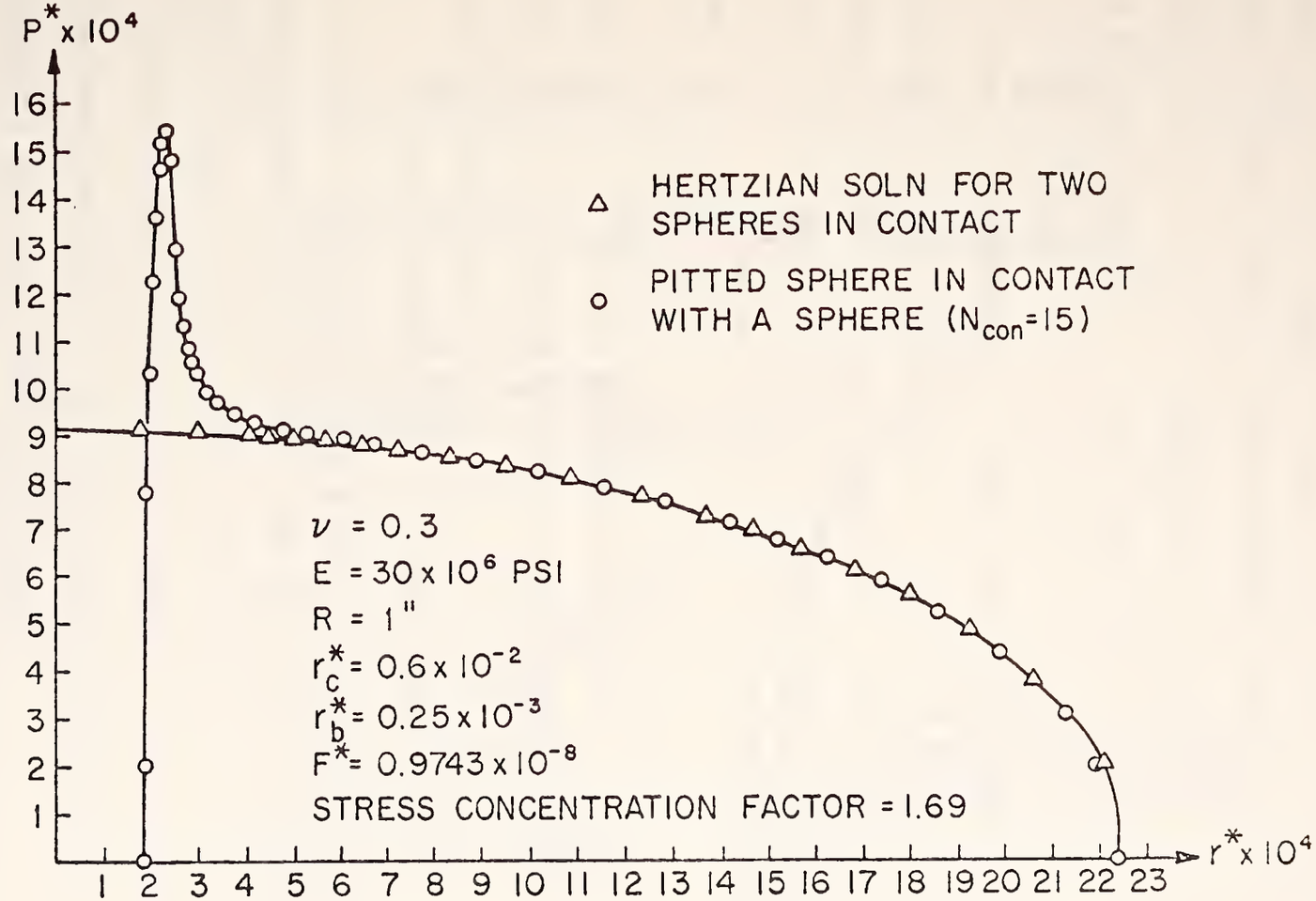

Fig. 7.5. Pressure distribution for pitted sphere pressed against a sphere

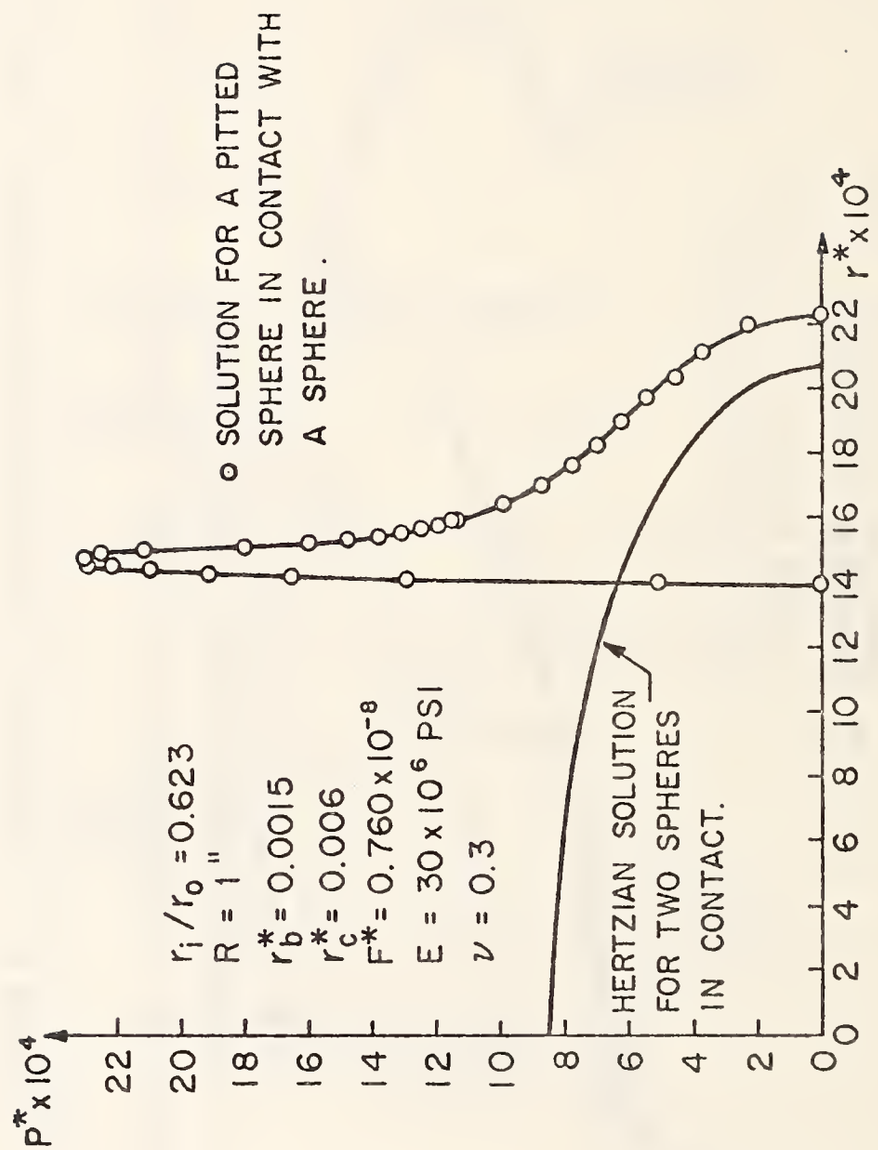

Fig. 7.6. Pressure distribution for a large pit diameter

gradient exists. Therefore, for purposes of convergence studies, we have systematically varied the number of cells within a fixed radius r_{con}. This radius is chosen arbitrarily for each problem in such a way that the major area of stress concentration lies inside the radius r_{con}. For the example problem considered, $r_{con} = .0003$. Let N_{con} be the number of rings located within radius r_{con}. Figure 7.7 illustrates the convergence of the peak pressure, P^*_{max}. Figure 7.8 shows the convergence of stress concentration factor with N_{con}. Stress Concentration Factor (SCF) is defined as the ratio of the peak computed pressure to the peak pressure for unpitted spheres under equal thrust. Notice both figures 7.7 and 7.8 exhibit convergence for $N_{con} > 8$.

The load-approach curve is shown in figure 7.9. It is obvious from figure 7.9 that the compliance characteristics of the balls (with small pits) remain essentially the same as that predicted by the Hertzian solution.

Figure 7.10 shows SCF as a function of cavity edge radius r^*_c. Smaller values of r^*_c cause greater stress concentration. Due to the nonlinearity of the problem, the SCF is also a function of the applied load F*. Table 7.1 shows the variation of SCF with the size of the pit (measured by blend point radius). Notice that SCF increases with increasing value of r^*_b. This variation of SCF with r^*_b may be related to the loss of load carrying area.

The computer program developed to solve this problem is moderately efficient. For example, the nine cases, needed to generate

TABLE 7.1

DEPENDENCE OF STRESS CONCENTRATION FACTOR ON r_b

Case No.	$r_b^* \times 10^3$	SCF	$F^* \times 10^8$	$\delta \times 10^4$	$r_I^* \times 10^3$
1	0.25	1.692	0.9743	0.1023	0.1845
2	0.35	1.856	0.9737	0.1029	0.2753
3	0.50	2.049	0.9702	0.1041	0.4166

$R_m = 1"$, $r_c^* = 0.006$, $r_o^* = 0.002236$, $E = 30 \times 10^6$ psi, $\nu = 0.3$.

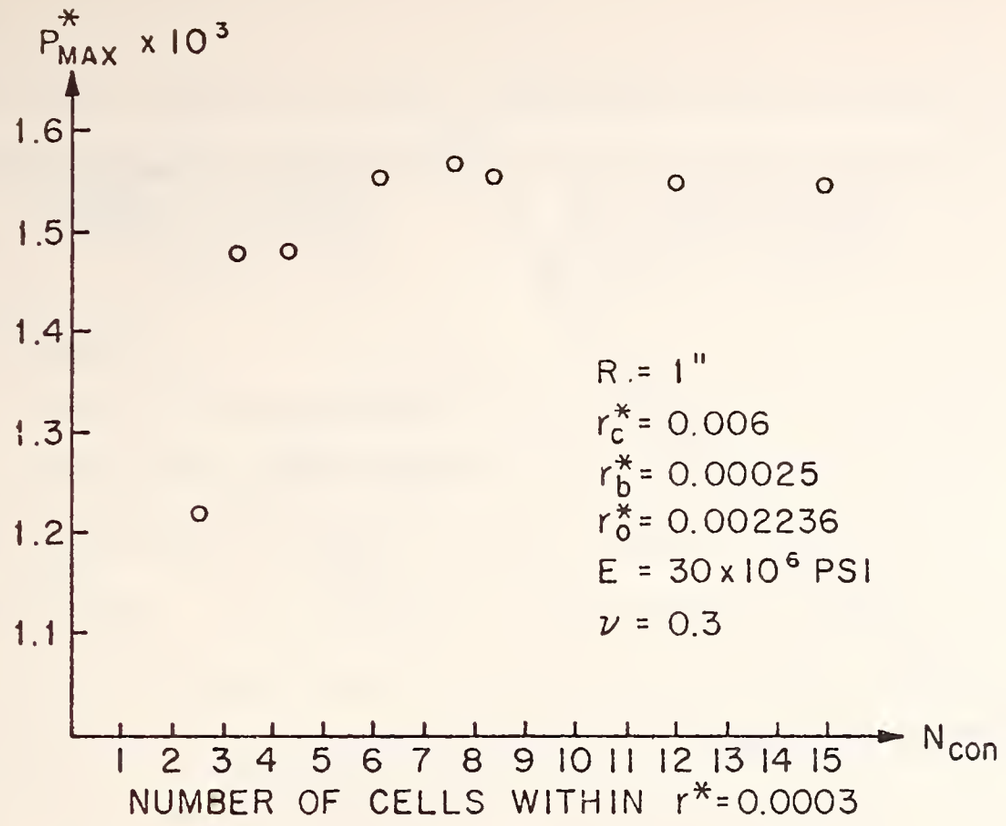

Fig. 7.7. Convergence of peak pressure with increasing number of cells.

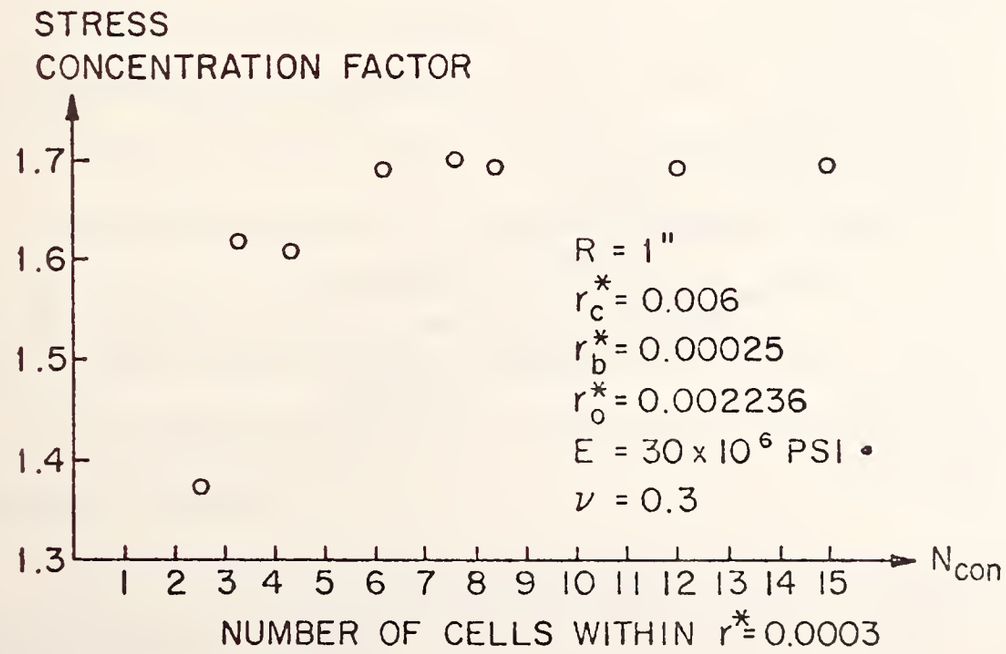

Fig. 7.8. Convergence of stress concentration with increasing number of cells.

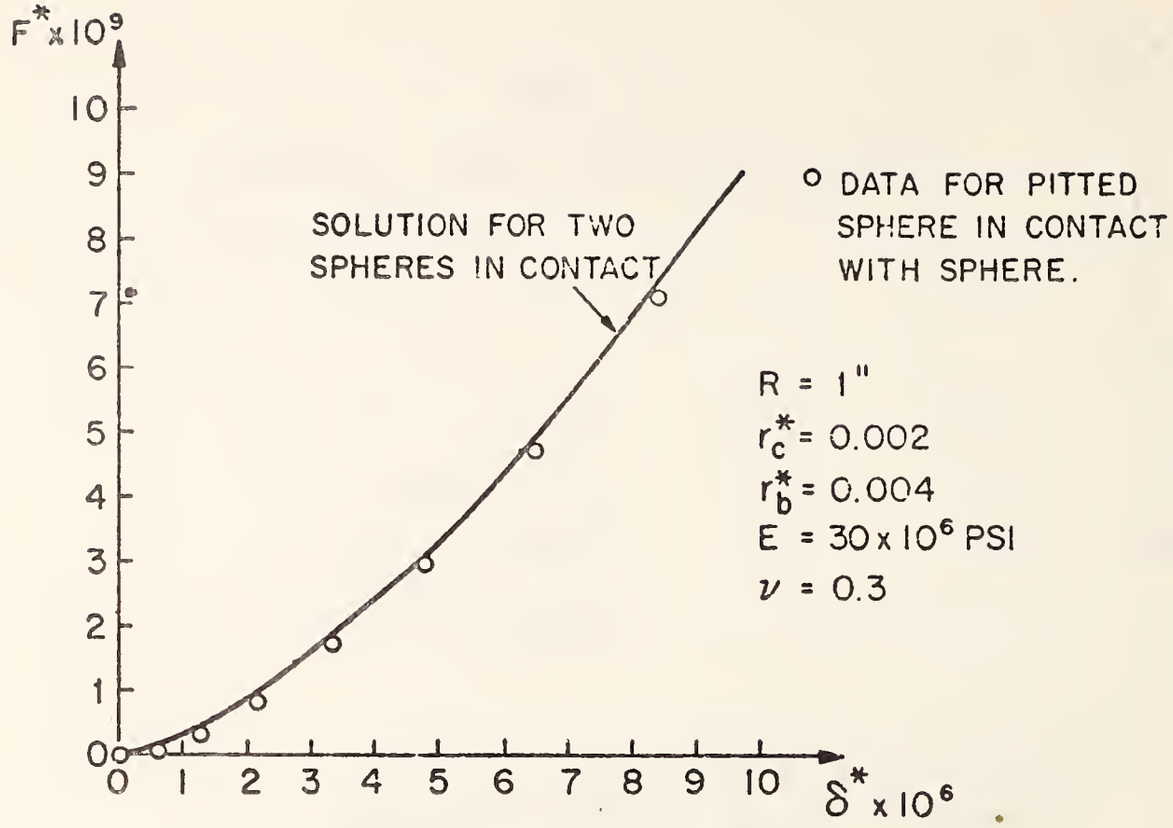

Fig. 7.9. Load-approach relationship

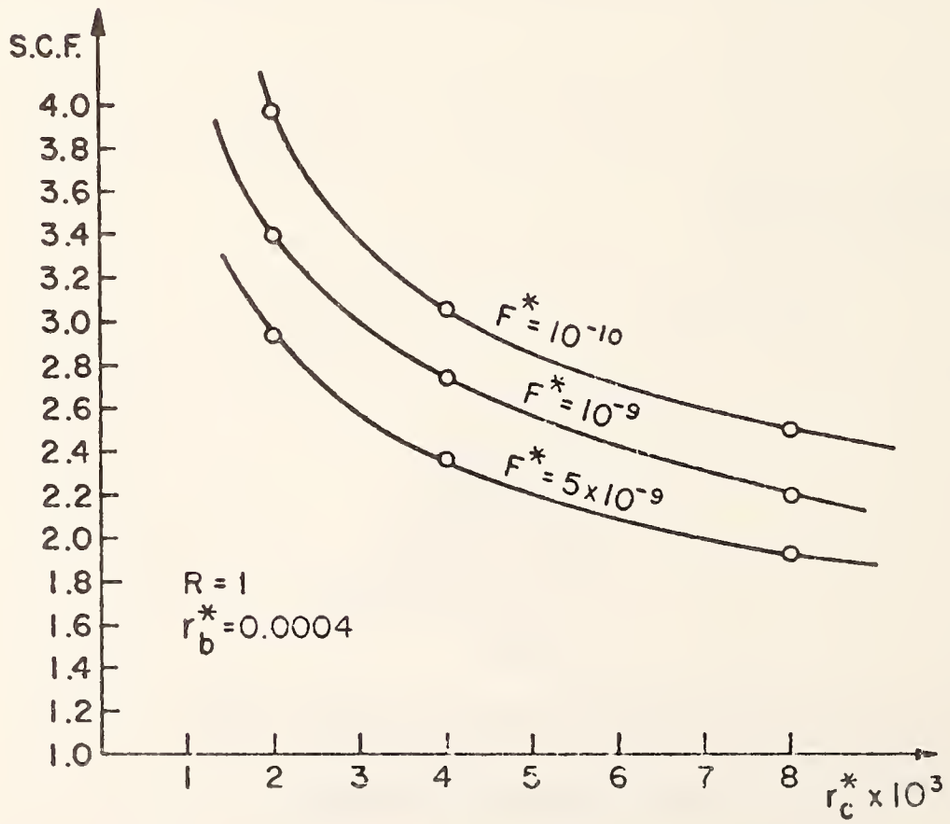

Fig. 7.10. The effect of load and r_c on stress concentration factor.

figure 7.10, required an average running time of 10 min each on the IBM/360/65 computer, corresponding to $8.33 per case, with N = 34 nodes per case.

7.6 Conclusions

A non-Hertzian elastic contact problem involving an unknown multiply-connected contact region has been solved. The example problem considered, is that of a pitted sphere in contact with an unpitted sphere. The axisymmetry of the problem enabled us to use the "simply-discretized method" with a polar coordinate grid. For problems with a lower degree of symmetry, it had been found in earlier work, that a more complicated (and less efficient) method of solution was necessary because of the numerical instability of the equations generated. It may be appropriate to describe the equation set (7.24) as "quasi-stable" because it exhibits dependence on the location of the (N + 1)th field point. Through experience and heuristic reasoning, it was established that locating the additional field point (P' in fig. 7.3) at the outside boundary yields a well-conditioned matrix.

The variation of the SCF, contact region and peak pressure P^*_{max} with changes in the pit blending radius r^*_b, and the pit edge radius r^*_c, was studied, and some numerical results were presented.

The numerical solution was shown to converge rapidly with a moderate cell density.

The principal results of this chapter have been published by the International Union of Theoretical and Applied Mechanics in

a joint paper by Woodward, Paul and Singh. To the best of our knowledge, this is the first published solution of a multiply-connected contact region problem with an a priori unknown contact boundary.

8. CONCLUSIONS

A general method of solution of three dimensional frictionless conformal contact problems has been presented. Specifically, two conformal examples were analyzed, viz., the case of an elastic sphere indenting an elastic spherical seat and the case of an elastic cylinder indenting an elastic cylindrical seat. The necessary influence functions, needed for solution of these problems, were generated numerically and validated with analytic solutions wherever possible.

The predicted values of contact stress, load, approach, and contact area for these examples is in close agreement with Hertz's solutions in the case of small loads, where small contact regions occur. For larger angles of contact, the load-approach relationship obtained for the sphere-seat problem was found to compare favorably with the experimental results. The displacement field obtained in the analysis of an elastic sphere in contact with a conformal rigid seat was found to be reproduced, with satisfactory accuracy, by a finite element model subjected to the same pressure distribution.

Therefore, it may be concluded that the solution obtained by the methods of this dissertation is the unique solution to the problem. Pressure distributions and maximum pressure obtained in the anlaysis of conformal cylinders were within 1.5 percent of the values predicted by Persson [1964]. The values of load vs. contact angle also agree with

the values computed by Persson. In reviewing the above results, it is concluded that the method presented can be used to successfully analyze three dimensional conformal contact.

In addition the non-conformal problem involving a pitted-sphere contacting a sphere was solved for a variety of pit geometries. This problem is of interest because it has a multiply connected contact region. The necessary iteration needed to converge to the true boundaries of the problem was established. The predicted values of contact stress were essentially Hertzian away from the pit location and the stress became much larger in the vicinity of the pit, as expected; the stress concentration factor was found as a function of pit geometry parameters.

In all of the above mentioned axisymmetric examples, axisymmetry was utilized to the fullest extent in the discretization process and it was discovered that all solutions were quasi-stable using the simply discretized method of Singh and Paul [1974]. This has not been observed before.

The computer costs in all cases were minimal, being at most $8.33/for the 34 field point model for the pitted sphere examples.

The principle conclusions of the foregoing results may be summarized as follows:

1. A general method of solving frictionless, three dimensional conformal contact problems has been formulated.

2. A method by which numerical influence functions may be generated is presented and validated where analytic solutions could be obtained.
3. The conformal analysis was shown to be in close agreement with the limiting cases of Hertzian contact for light loads and with other numerical, analytic and experimental analyses of conformal contact problems.
4. A problem involving a multiply connected contact region was solved.

Future research should be directed towards applying the above method to the solution of non-axisymmetric problems in conformal contact. Within the broad area of elastic contact theory, the inclusion of friction and dynamics in contact theory are needed areas of investigation.

APPENDIX A

DOMINANT SINGULARITIES IN THE STERNBERG INFLUENCE FUNCTION FOR A POINT LOAD ON A SPHERE

Consider a sphere of radius R compressed between two diametrically opposed point loads, F. The displacements u_r and u_θ, as shown in figure A.1, are derived in Luré [1964] and are given by equations (A.1) and (A.2). It will be shown in this appendix that the dominant singular terms in these displacement functions are those of the Boussinesq influence functions for a point load on a plane.

The Sternberg Influence Functions may be written as follows:

$$u_r = \frac{(m-2)F}{4G(m+1)\pi R} + \frac{F}{4\pi GR}\left\{\frac{(m-1)}{m}\left(\frac{1}{\sin\frac{\theta}{2}} + \frac{1}{\cos\frac{\theta}{2}} - 4\right)\right.$$

$$+ \frac{(m-2)^2}{m^2}\left(\log\cot\frac{\theta}{4}\cot\frac{\pi-\theta}{4} - 2\right) -$$

$$- \frac{3m^2-20m+16}{m^3}\left(\sin^2\frac{\theta}{2}\log\frac{1+\sin\frac{\theta}{2}}{\sin\frac{\theta}{2}} +\right.$$

$$\left.\left. + \cos^2\frac{\theta}{2}\log\frac{1+\cos\frac{\theta}{2}}{\cos\frac{\theta}{2}} + \frac{1}{2} - \sin\frac{\theta}{2} - \cos\frac{\theta}{2}\right)\right.$$

$$\left. + \sum_{K=1}^{\infty} A_{2K} P_{2K}(\cos\theta)\right\} \qquad (A.1)$$

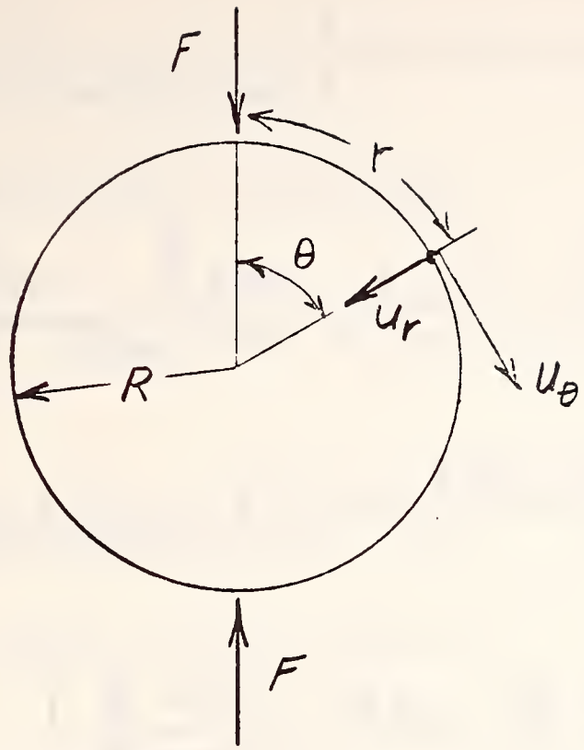

Fig. A.1. Diametrically Opposed Point Loads on a Sphere

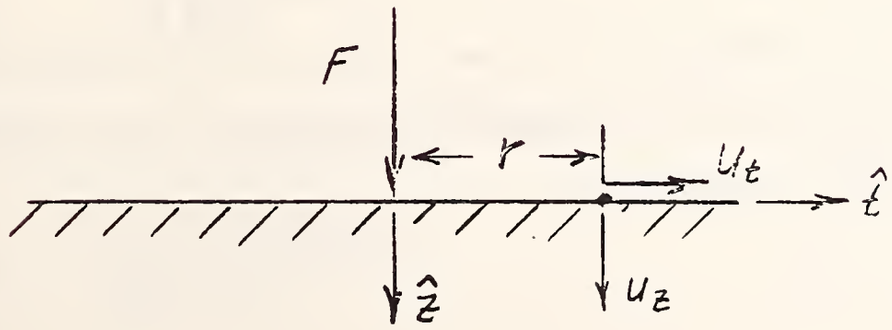

Fig. A.2. Coordinate System for a Point Load on a Plane

and

$$u_\theta = -\frac{F}{4\pi GR}\left\{\frac{(m-2)}{m}\ \frac{\cos\frac{\theta}{2}-\sin\frac{\theta}{2}}{\sin\theta}\right.$$

$$+\ \frac{m^2+8m-8}{m^2}\left[\left(1-\cos\frac{\theta}{2}-\sin\frac{\theta}{2}\right)\cot\theta\right.$$

$$\left.+\ \frac{1}{2}\sin\theta\log\cot\frac{\theta}{2}\ \frac{1+\sin\frac{\theta}{2}}{1+\cos\frac{\theta}{2}}\right]$$

$$\left.+\ \sum_{k=1}^{\infty} B_{2k}\ \frac{dP_{2k}(\cos\theta)}{d\theta}\right\} \qquad \text{(A.2)}$$

where m is the reciprocal of Poisson's ratio, G is the modulus of rigidity, $P_{2k}(\cos\theta)$ are the Legendre polynomials in $\cos\theta$ and the constants A_n and B_n are given by

$$A_n = \frac{1}{m^4(n-1)(n+1)(n+2)\Delta'}\Big[(m^4+7m^3+30m^2-64m+32)n^2$$

$$+(7m^4+22m^3-39m^2+44m-16)n$$

$$+10m^4-11m^3+9m^2+20m-16\Big] \qquad (A.3)$$

$$B_n = \frac{1}{m^3(n-1)(n+1)(n+2)\Delta'}\Big[(7m^3+11m^2-28m+16)(n+2)^2$$

$$+(-18m^3-18m^2+132m-72)(n+2)$$

$$+9(m-1)(m^2+8m-8)\Big] \qquad (A.4)$$

where

$$\Delta' = n(n-1)+(2n+1)\frac{m+1}{m} \qquad (A.5)$$

The Boussinesq displacement functions are given by

$$u_z = \frac{F(1-\nu^2)}{\pi E r} \qquad (A.6)$$

and

$$u_t = \frac{-F(1-2\nu)(1+\nu)}{2\pi E r} \qquad (A.7)$$

where ν and E are Poisson's ratio and Young's modulus respectively and u_z, u_t and r are illustrated in figure A.2. Consider the coordinate

system in figure A.1 where $r = R\theta$. As r tends to zero, r will be assumed equal to distance r along the straight boundary in figure A.2. Also θ in equations (A.1) and (A.2) will be replaced by r/R. Specifically, it will be shown that

$$\lim_{r \to 0} u_r = u_z \tag{A.8}$$

and

$$\lim_{r \to 0} u_\theta = u_t \tag{A.9}$$

Now consider the singular terms in equation (A.1). They are as follows:

$$S_1 = \frac{F}{4\pi GR} \frac{m-1}{m} \frac{1}{\sin \frac{\theta}{2}} \tag{A.10}$$

$$S_2 = \frac{F}{4\pi GR} \frac{(m-2)^2}{m^2} \log \cot \frac{\theta}{4} \cot \frac{\pi - \theta}{4} \tag{A.11}$$

$$S_3 = \frac{F}{4\pi GR} \left(\frac{-3m^2 - 20m + 16}{m^3} \right) \left(\sin^2 \frac{\theta}{2} \log \frac{1 + \sin \frac{\theta}{2}}{\sin \frac{\theta}{2}} \right) \tag{A.12}$$

It can be seen upon inspection that all other terms tend toward a finite quantity. S_1 and S_2 definitely tend toward ∞ as θ tends toward zero whereas S_3 is indeterminant at $\theta = 0$. It will be shown for the

limit of r tending to zero that

$$S_1 = u_z \tag{A.13}$$

$$\lim_{\theta \to 0} \frac{S_1}{S_2} = 0 \tag{A.14}$$

and

$$\lim_{\theta \to 0} S_3 = 0 \tag{A.15}$$

Expanding S_1, in terms of θ we find

$$S_1 = \frac{F}{4\pi GR} \frac{m-1}{m} \left(\frac{2}{\theta} + \frac{\theta}{12} + \frac{7}{2880} \theta^3 + \cdots \right) \tag{A.16}$$

As $\theta \to 0$ the only singular term is the first, which will be termed S_{10}. Now consider the $\lim_{r \to 0}$ of the ratio $\frac{S_{10}}{u_z}$. Recalling the $\theta = r/R$, $m = \frac{1}{\nu}$ and $G = \frac{E}{2(1+\nu)}$,

$$\frac{S_{10}}{u_z} = \frac{\frac{F(1-\nu^2)}{\pi E R} \frac{R}{r}}{\frac{F(1-\nu^2)}{\pi E} \frac{1}{r}} = 1 \tag{A.17}$$

Therefore the singular term S_1 corresponds directly to u_z.

Investigating the limit of the ratio S_1/S_2, where

$$\frac{S_1}{S_2} = \frac{m(m-1)}{m^2} \frac{\csc\frac{\theta}{2}}{\log\left(\cot\frac{\theta}{4}\cot\frac{\pi-\theta}{4}\right)} \tag{A.18}$$

it can be shown, using l'Hopital's rule that

$$\lim_{\theta\to 0}\frac{S_1}{S_2} = \lim_{\theta\to 0}\frac{m(m-1)}{m^2}\frac{4\cot\frac{\theta}{2}}{\csc\frac{\pi-\theta}{4}\sec\frac{\pi-\theta}{4}\sin\frac{\theta}{4}\cos\frac{\theta}{4}+1}$$

$$= \infty \tag{A.19}$$

Thus, even though the singularity S_2 is present in the displacement u_r, it is weak compared to the singularity S_1.

Finally, examining S_3, using l'Hopital's rule it can be shown that

$$\lim_{\theta\to 0} S_3 = \lim_{\theta\to 0}\frac{F}{4\pi GR}\left(\frac{-3m^2-20m+16}{m^3}\right)\frac{1}{2}\frac{\sin^2\frac{\theta}{2}}{1+\sin\frac{\theta}{2}}$$

$$= 0 \tag{A.20}$$

In other words, S_3 is not a singular term, but tends toward zero at the load.

From the above analysis it can be seen that the dominant

singularity in u_r is S_1 and furthermore, in the limit as r tends toward zero $S_1 = u_z$. Therefore, it may be concluded that in the same limit $u_r = u_z$. This is illustrated in table A.1. As θ decreases, the percent difference between u_r and u_z also decreases.

Now consider the displacements u_θ and u_t. The three terms in equation (A.2) which are singular or indeterminant are

$$T_1 = \frac{-F K_2}{\pi R}\left\{\frac{\cos\frac{\theta}{2} - \sin\frac{\theta}{2}}{\sin\theta}\right\} \tag{A.21}$$

$$T_2 = \frac{-F(m^2+8m-8)}{4\pi G R\, m^2}\left(1-\cos\frac{\theta}{2}-\sin\frac{\theta}{2}\right)\cot\theta \tag{A.22}$$

$$T_3 = \frac{-F(m^2+8m-8)}{4\pi G R\, m^2}\left(\frac{1}{2}\sin\theta \log\cot\frac{\theta}{2}\frac{1+\sin\frac{\theta}{2}}{1+\cos\frac{\theta}{2}}\right) \tag{A.23}$$

where $K_2 = \frac{(1-2\nu)(1+\nu)}{2E}$.

T_1 is singular while T_2 and T_3 are indeterminant. The other term in equation (A.2) involving $dP_{2k}(\cos\theta)/d\theta$ is known to be zero at θ equal to zero.

Examining the ratio T_1/u_t it can be shown that for $r = R\theta$

TABLE A.1

COMPARISON OF BOUSSINESQ INFLUENCE FUNCTION TO THE INFLUENCE FUNCTION FOR A POINT LOAD ON A SPHERE

θ[Deg.]	u_r[in.][a]	u_z[in.]	% Difference
10.00	1.44963	1.65964	12.654
1.00	16.4732	16.5964	0.74222
0.10	165.917	165.964	0.02806
0.01	1659.65	1659.64	-0.00179

R = 10", F = 30×10^7 lb, E = 30×10^6 psi, ν = 0.30

[a] 51 Terms taken in Legendre Polynomial

$$\frac{T_1}{u_t} = \frac{\theta\left(\cos\frac{\theta}{2} - \sin\frac{\theta}{2}\right)}{\sin\theta} \tag{A.24}$$

Using l'Hopital's rule,

$$\lim_{\theta\to 0}\frac{T_1}{u_t} = \lim_{\theta\to 0}\frac{\left(\cos\frac{\theta}{2}-\sin\frac{\theta}{2}\right)+\theta\left(-\sin\frac{\theta}{2}-\cos\frac{\theta}{2}\right)}{\cos\theta} = 1 \tag{A.25}$$

Therefore in the limit as θ, or r, tends to zero $u_t = T_1$.

Consider term T_2 in the limit as θ goes to zero, and using l'Hopital's rule

$$\begin{aligned}\lim_{\theta\to 0} T_2 &= \lim_{\theta\to 0}\frac{-F(m^2+8m-8)}{4\pi G R m^2}\,\frac{\left(1-\cos\frac{\theta}{2}-\sin\frac{\theta}{2}\right)}{\tan\theta}\\ &= \lim_{\theta\to 0} -\frac{F(m^2+8m-8)}{4\pi G R m^2}\,\frac{\left(\frac{1}{2}\sin\frac{\theta}{2}-\frac{1}{2}\cos\frac{\theta}{2}\right)}{\sec^2\theta}\\ &= \frac{F(m^2+8m-8)}{8R\pi G m^2}\end{aligned} \tag{A.26}$$

This proves that although T_2 was indeterminant it is not a singular term in the limit as θ tends to zero.

Finally, consider T_3. T_3 may be rewritten in the form

$$T_3 = \frac{-F(m^2+8m-8)}{8\pi G R m^2} \frac{\log\left(\frac{\csc\frac{\theta}{2}+1}{\sec\frac{\theta}{2}+1}\right)}{\csc\theta} \qquad \text{(A.27)}$$

which is indeterminant as θ tends to zero. Using l'Hopital's rule and reducing the results

$$\lim_{\theta\to 0} T_3 = \lim_{\theta\to 0} \frac{-F(m^2+8m-8)}{8\pi G R m^2}\left(\frac{\sin\theta\cos\frac{\theta}{2}}{\cos\theta\cos\frac{\theta}{2}(1+\sin\frac{\theta}{2})}\right.$$

$$\left. + \frac{\sin^2\theta\tan\frac{\theta}{2}}{\cos\theta(1+\cos\frac{\theta}{2})}\right) = 0 \qquad \text{(A.28)}$$

Therefore T_3 is not a singularity.

From the above analysis it was shown that the only singularity in the function u_θ is T_1 and that this is equal to u_t as θ tends to zero.

APPENDIX B

DISPLACEMENTS ON A CYLINDER UNDER TWO DIAMETRICALLY OPPOSED LINE LOADS

Consider a cylinder under two lines loads F as shown in figure B.1. Muskhelishvili [1963] has shown that for the case of plane strain the displacements in the x and y directions respectively are,

$$u_x = \frac{-F}{4\pi\mu}\left\{\frac{2(\lambda+2\mu)}{(\lambda+\mu)}\ln\frac{r_2}{r_1} + \right.$$

$$\left. +(\cos 2\alpha_1 - \cos 2\alpha_2) - \frac{2\mu\cos\phi}{(\lambda+\mu)}\frac{x}{R}\right\} \qquad (B.1)$$

$$u_y = \frac{-F}{4\pi\mu}\left\{\frac{2\mu}{\lambda+\mu}(\alpha_1+\alpha_2) - (\sin 2\alpha_1 + \sin 2\alpha_2)\right.$$

$$\left. - \frac{2\mu\cos\phi}{(\lambda+\mu)}\frac{y}{R}\right\} \qquad (B.2)$$

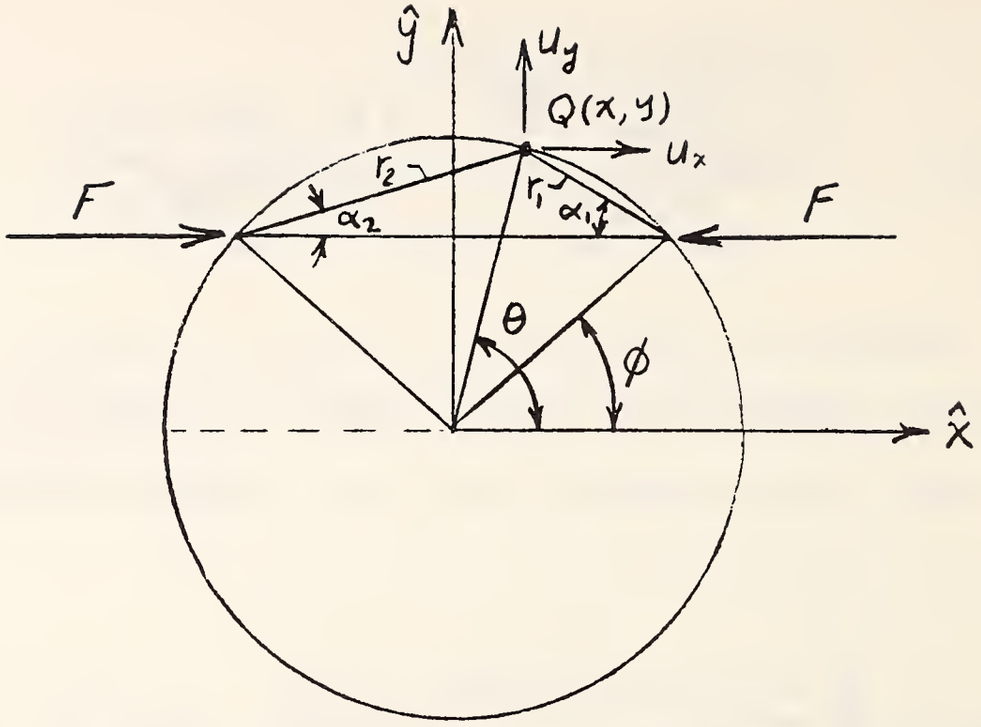

Fig. B.1. Cylinder Under Two Opposing Line Loads

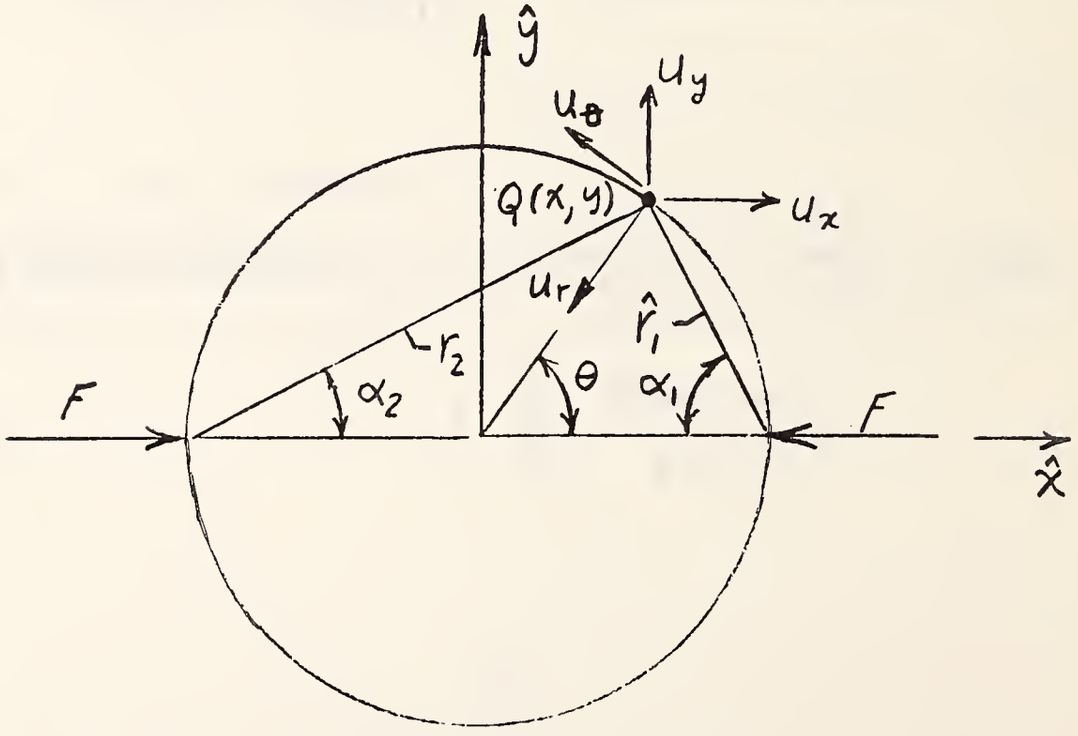

Fig. B.2. Geometry for Diametrically Opposed Line Loads on a Cylinder

where λ and μ are the Lamé constants.

Now consider the case where the two line loads are diametrically opposed (figure B.2). The following relations may be derived for the geometry illustrated in

$$\alpha_1 + \alpha_2 = \frac{\pi}{2}$$

$$\frac{r_1}{r_2} = \tan\frac{\theta}{2}$$

$$\alpha_2 = \frac{\theta}{2}$$

$$\alpha_1 = \frac{\pi}{2} - \frac{\theta}{2} \qquad \text{(B.3)}$$

$$x = R\cos\theta$$

$$y = R\sin\theta$$

Substituting in the relations of (B.2) into equations (A.1) and (A.2), the displacements u_x and u_y become,

$$u_x = F K_1 \left\{ \ln \tan\left|\frac{\theta}{2}\right| + \cos\theta \right\} \qquad \text{(B.4)}$$

$$u_y = F \left\{ K_1 \sin\theta - \frac{K_2}{\pi} \right\} \qquad \text{(B.5)}$$

where

$$K_1 = \frac{(\lambda + 2\mu)}{2\pi\mu(\lambda+\mu)} = \frac{2(1-\nu^2)}{\pi E} \tag{B.6}$$

$$K_2 = \frac{1}{4(\lambda+\mu)} = \frac{(1+\nu)(1-2\nu)}{2E} \tag{B.7}$$

E and ν are Young's modulus and Poisson's ratio respectively. In polar coordinates the radial and tangential displacements, notated u_r and u_t respectively, computed as functions of u_x and u_y are

$$u_r = -u_x \cos\theta - u_y \sin\theta \tag{B.8}$$

$$u_\theta = -u_x \sin\theta + u_y \cos\theta \tag{B.9}$$

Substituting equations (B.4) and (B.5) into equations (B.8) and (B.9), u_r and u_θ become

$$u_r = -FK_1\left\{\cos\theta \ln\tan\frac{\theta}{2} + 1\right\} + \frac{FK_2}{\pi}\sin\theta \tag{B.10}$$

and

$$U_\theta = -F K_1 \sin\theta \ln \tan\frac{\theta}{2} - \frac{F K_2}{\pi} \cos\theta \qquad \text{(B.11)}$$

APPENDIX C

SINGULARITIES IN THE INFLUENCE FUNCTIONS FOR A CYLINDER UNDER TWO DIAMETRICALLY OPPOSED LINE LOADS

Consider a cylinder, of radius R, under two diametrically opposed line loads F, as shown in figure C.1. The displacements u_r and u_θ as derived in appendix B are

$$u_r = -K_1 F\left\{\cos\theta \ln \tan\frac{\theta}{2} + 1\right\} + \frac{K_2}{\pi} F \sin\theta \qquad (C.1)$$

and

$$u_\theta = -K_1 F \sin\theta \ln \tan\frac{\theta}{2} - \frac{K_2}{\pi} F \cos\theta \qquad (C.2)$$

where

$$K_1 = \frac{2(1-\nu^2)}{\pi E} \qquad (C.3)$$

and

$$K_2 = \frac{(1+\nu)(1-2\nu)}{2E} \qquad (C.4)$$

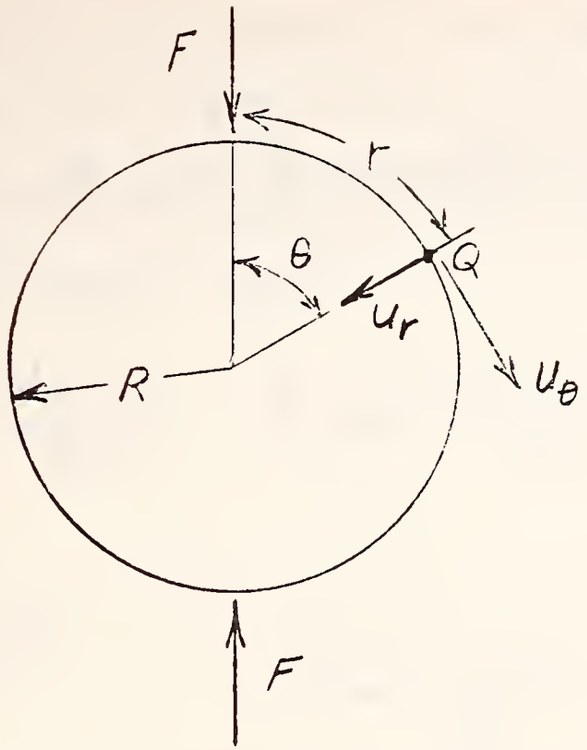

Fig. C.1. Two Diametrically Opposed Line Loads on a Cylinder

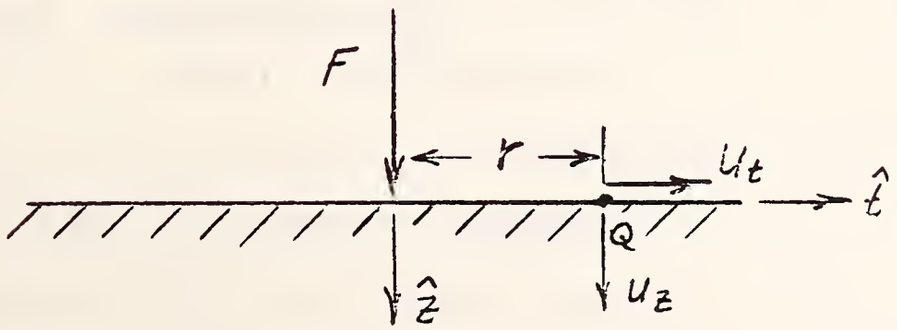

Fig. C.2. Line Load on an Elastic Half Space

E is Young's modulus and ν is Poisson's ratio. Also consider the Flamant solution for a line load acting on a half space as illustrated in figure C.2. As presented in section 4.3, the displacements u_z and u_t are

$$u_z = \frac{2F(1-\nu^2)}{\pi E} \log \frac{d}{r} - \frac{(1+\nu)F}{\pi E} \qquad (C.5)$$

and

$$u_t = -\frac{(1+\nu)(1-2\nu)F}{2E} \qquad (C.6)$$

it will be shown that the singularity in the displacement u_r is the same as that of u_z near the load. Furthermore, the limit of u_θ, as θ tends to zero, will be shown to be u_t.

As illustrated in figure C.2, r represents the distance between the applied load and the point Q where the displacements u_z and u_t are calculated. Let us define a coordinate r on figure C.1 such that $r = R\theta$. Replacing θ with $\frac{r}{R}$ in equation (C.1), it will be shown that $u_r - u_z$ as r tends toward zero. Likewise, u_θ will be shown to approach u_t as r tends to zero.

In terms of the coordinate r, the ratio u_r/u_z may be written as

$$\frac{u_r}{u_z} = \frac{-F K_1 \left\{ \cos \frac{r}{R} \ln \tan \frac{r}{2R} + 1 \right\} + \frac{K_2 F}{\pi} \sin \frac{r}{R}}{F K_1 \ln \frac{d}{r} - K_3 F} \qquad (C.7)$$

where

$$K_3 = \frac{(1+\nu)}{\pi E} \qquad (C.8)$$

Taking the limit as r tends to zero of equation (C.7) and using l'Hopital's rule,

$$\lim_{r \to 0} \frac{u_r}{u_z} = \frac{r}{R} \cot \frac{r}{R} - \frac{r}{R} \frac{K_2}{\pi K_1} \cos \frac{r}{R} -$$

$$- \frac{r}{R} \sin \frac{r}{R} \ln \tan \frac{r}{2R} \qquad (C.9)$$

The second term in (C.9) clearly goes to zero for r equal to zero while the first and third terms are indeterminant.

Expanding $\cot \frac{r}{R}$ in the first term of equation (C.9), and taking the limit as r tends to zero

$$\lim_{r\to 0} \frac{r}{R}\cot\frac{r}{R} =$$

$$= \lim_{r\to 0} \frac{r}{R}\left(\frac{R}{r} - \frac{r}{3R} - \frac{r^3}{45R^3} - \cdots\right)$$

$$= 1 \qquad (C.10)$$

Taking the limit of the third term in equation (C.9) and using l'Hopital's rule,

$$\lim_{r\to 0} -\frac{r}{R}\sin\frac{r}{R}\log\tan\left|\frac{r}{2R}\right|$$

$$= \lim_{r\to 0} \frac{\frac{1}{2}\frac{r^2}{R^2}\tan\frac{r}{2R}\sec^2\frac{r}{2R}\sin^2\frac{r}{R}}{\sin\frac{r}{R} + \frac{r}{R}\cos\frac{r}{R}}$$

$$= 0 \qquad (C.11)$$

Hence, the only nonzero term in equation (C.9) in the limit as r tends to zero is the first and it tends toward 1. Therefore in the limit as r tends to zero, $u_r = u_z$.

Now consider the limit of u_θ/u_t. Both u_θ and u_t are finite at r equal to zero. In equation (C.2), the first term can be shown to go

to zero for small r. u_θ, therefore, tends to the value $-K_2$ for small r. This is exactly the value of u_t for all r. Thus,

$$\lim_{r \to 0} \frac{u_\theta}{u_t} = 1 \qquad (C.12)$$

and $u_\theta = u_t$ when r tends to zero.

APPENDIX D

DERIVATION OF SURFACE DISPLACEMENTS FOR A CYLINDRICAL CAVITY UNDER TWO DIAMETRICALLY OPPOSED LINE LOADS

Timoshenko and Goodier [1970] derived the stress functions ψ and ϕ corresponding to an elliptic hole with uniform pressure p applied on two diametrically opposed segments. Consider a unit circle in the ζ plane and the mapping function,

$$Z = \omega(\zeta) \tag{D.1}$$

where

$$\omega(\zeta) = R\left(\zeta + \frac{m}{\zeta}\right) \tag{D.2}$$

$\omega(\zeta)$ maps the unit circle in the ζ plane into an ellipse in the Z plane with semiaxes

$$a = R(1+m)$$

$$b = R(1-m) \tag{D.3}$$

For m = 0, the mapping becomes a circle of radius R. Now consider an elliptic hole with a pressure distribution applied as shown in

figure D-1. Timoshenko has shown that the stress functions in the ζ plane, corresponding to the above loading, are

$$\frac{2\pi i}{PR}\phi(\zeta) = -\frac{4m}{\zeta}\log\sigma_1 \quad +$$

$$+\left(\zeta+\frac{m}{\zeta}\right)\log\frac{\zeta^2-\sigma_1^2}{\zeta^2-\bar{\sigma}_1^2}+\left(\sigma_1+\frac{m}{\sigma_1}\right)\log\frac{\zeta+\sigma_1}{\zeta-\sigma_1}$$

$$+\left(\frac{1}{\sigma_1}+m\sigma_1\right)\log\frac{\zeta-\bar{\sigma}_1}{\zeta+\bar{\sigma}_1} \qquad (D.4)$$

and

$$\frac{2\pi i}{PR}\psi(\zeta) = -4\log\sigma_1(1+m^2)\frac{\zeta}{\zeta^2-m} \quad +$$

$$+\left(\sigma_1+\frac{m}{\sigma_1}\right)\log\frac{\zeta-\bar{\sigma}_1}{\zeta+\bar{\sigma}_1}+\left(\frac{1}{\sigma_1}+m\sigma_1\right)\log\frac{\zeta+\sigma_1}{\zeta-\sigma_1} \qquad (D.5)$$

where σ_1, and $\bar{\sigma}_1$ correspond to the mapped points Z_1 and $\bar{Z}_1$ in the Z plane. Letting m = 0 for the case of a circular hole, the mapping function becomes

$$Z = \omega(\zeta) = R\zeta$$

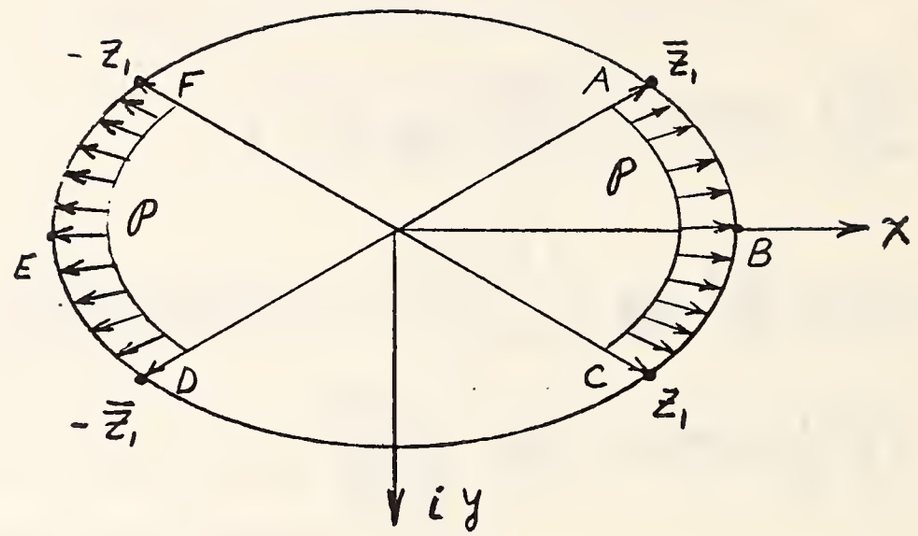

Fig. D.1. Elliptic Hole with Internal Pressure

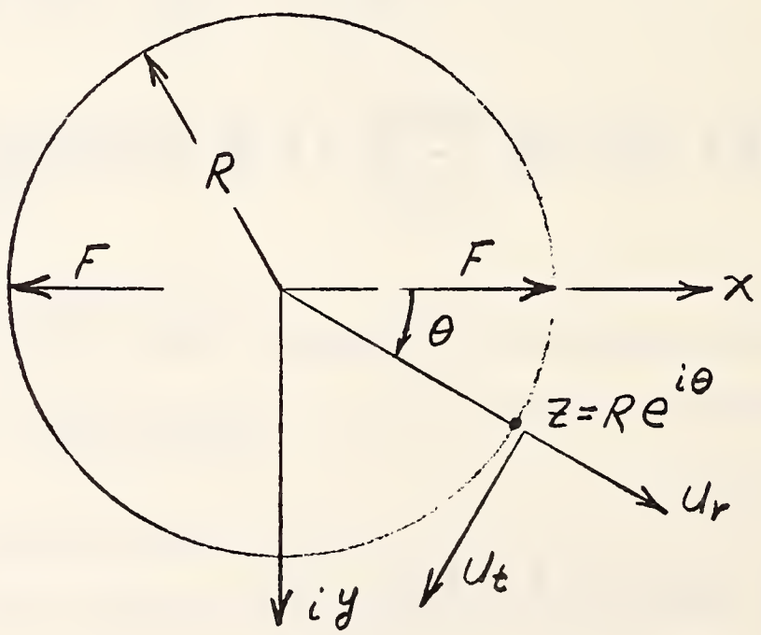

Fig. D.2. Diametrically Opposed Line Leads on a Cylindrical Cavity

and equations (D.4) and (D.5) may be written in the Z plane as

$$\frac{2\pi i}{PR}\,\phi(z) = \frac{z}{R}\log\frac{z^2 - z_1^2}{z^2 - \bar{z}_1^2} +$$

$$+ \frac{z}{R}\log\frac{z+z_1}{z-z_1} + \frac{\bar{z}_1}{R}\log\frac{z-\bar{z}_1}{z+\bar{z}_1} \qquad \text{(D.6)}$$

and

$$\frac{2\pi i}{PR}\,\psi(z) = -\frac{4R}{z}\log\frac{z_1}{R} +$$

$$+ \frac{z_1}{R}\log\frac{z-\bar{z}_1}{z+\bar{z}_1} + \frac{\bar{z}_1}{R}\log\frac{z+z_1}{z-z_1} \qquad \text{(D.7)}$$

The displacements u_r and u_θ are related to the stress functions by

$$2\mu(u_r + i u_\theta) = e^{-i\theta}\left\{\kappa\phi(z) - z\,\overline{\phi'(z)} - \overline{\psi(z)}\right\} \qquad \text{(D.8)}$$

where μ is the modulus of rigidity, ν is Poisson's ratio and

$$\kappa = \frac{3-\nu}{1+\nu} \qquad \text{(D.9)}$$

for plane stress or

$$\kappa = 3 - 4\nu \tag{D.10}$$

for plane strain. (See figure D.2.)

In order to find the correct displacements for concentrated, diametrically opposed loads, F, let p vary as $F/|Z_1 - \bar{Z}_1|$ and take the limit as $|Z_1 - \bar{Z}_1| \to 0$. Hence for concentrated loads the stress functions become

$$\frac{2\pi i}{PR}\phi = \lim_{|z_1-\bar{z}_1|\to 0}\left\{\frac{\frac{z}{R}\log\frac{z^2-z_1^2}{z^2-\bar{z}_1^2}}{|z_1-\bar{z}_1|} + \right.$$

$$\left. + \frac{\frac{z}{R}\log\frac{z+z_1}{z-z_1} - \frac{\bar{z}_1}{R}\log\frac{z+\bar{z}_1}{z-\bar{z}_1}}{|z_1-\bar{z}_1|}\right\} \tag{D.11}$$

and

$$\frac{2\pi i}{PR}\psi = \lim_{|z_1-\bar{z}_1|\to 0}\left\{\frac{-\frac{4R}{z}\log\frac{z_1}{R}}{|z_1-\bar{z}_1|} + \right.$$

$$\left. + \frac{\frac{z_1}{R}\log\frac{z-\bar{z}_1}{z+\bar{z}_1} - \frac{\bar{z}_1}{R}\log\frac{z-z_1}{z+z_1}}{|z_1-\bar{z}_1|}\right\} \tag{D.12}$$

The quantities Z, Z_1 and $\bar{Z}_1$ may be written as

$$Z = Re^{i\theta}$$

$$Z_1 = Re^{i\alpha} \qquad (D.13)$$

$$\bar{Z}_1 = Re^{-i\alpha}$$

Substituting equations (D.13) into equations (D.11) and (D.12), the functions ψ and ϕ may be written in terms of θ and α. The limit of $|Z_1 - \bar{Z}_1|$ is now the limit as $\alpha \to 0$. Taking that limit, the functions ψ and ϕ become

$$\frac{2\pi}{F}\,\phi(z) = \left\{ \frac{z_0}{R} \log \frac{z+z_0}{z-z_0} \right\} \qquad (D.14)$$

and

$$\frac{2\pi}{F}\,\psi(z) = \left\{ \frac{-2R}{z} + \frac{z_0}{R} \log \frac{z-z_0}{z+z_0} + \right.$$

$$\left. + \frac{2z z_0^2}{R(z^2-z_0^2)} \right\} \qquad (D.15)$$

where $Z_0 = \bar{Z}_0 = R$.

The displacements u_r and u_θ may be found by substituting equations (D.14) and (D.15) into equation (D.8). Separating out the real and imaginary parts, u_r and u_θ are found to be

$$u_r = \frac{-F}{4\pi\mu}\left\{(K+1)\cos\theta \log\tan\left[\frac{\theta}{2}\right] + \right.$$

$$\left. + \frac{(K-1)}{2}\pi\sin\theta \right\} \qquad (D.16)$$

and

$$u_\theta = \frac{F}{4\pi\mu}\left\{(K+1)\sin\theta \log\tan\left[\frac{\theta}{2}\right] - \right.$$

$$\left. - \frac{(K-1)}{2}\pi\cos\theta \right\} \qquad (D.17)$$

For plane strain these displacements may be written in terms of E and ν as

$$u_r = F\left\{\frac{2(1-\nu^2)}{\pi E}\cos\theta \log\tan\left[\frac{\theta}{2}\right] + \right.$$

$$\left. + \frac{(1-2\nu)(1+\nu)}{2E}\sin\theta \right\} \qquad (D.18)$$

and

$$u_\theta = F\left\{\frac{2(1-\nu^2)}{\pi E}\sin\theta \log\tan\left[\frac{\theta}{2}\right] - \right.$$

$$\left. - \frac{(1-2\nu)(1+\nu)}{2E}\cos\theta \right\} \qquad (D.19)$$

APPENDIX E

SINGULARITIES IN THE INFLUENCE FUNCTIONS FOR A CYLINDRICAL CAVITY UNDER TWO DIAMETRICALLY OPPOSED LINE LOADS

Consider a cylindrical cavity of radius R, under two diametrically opposed line loads F, as shown in figure E.1. u_r and u_θ as derived in appendix D are

$$u_r = -K_1 F \cos\theta \log \tan\frac{\theta}{2} - K_2 F \sin\theta \qquad (E.1)$$

$$u_\theta = K_1 F \sin\theta \log \tan\frac{\theta}{2} - K_2 F \cos\theta \qquad (E.2)$$

where

$$K_1 = \frac{2(1-\nu^2)}{\pi E} \qquad (E.3)$$

and

$$K_2 = \frac{(1-2\nu)(1+\nu)}{2E} \qquad (E.4)$$

E is Young's modulus and ν is Poisson's ratio. Also consider the Flamant Solution for a line load acting on a half space as illustrated in figure E.2.

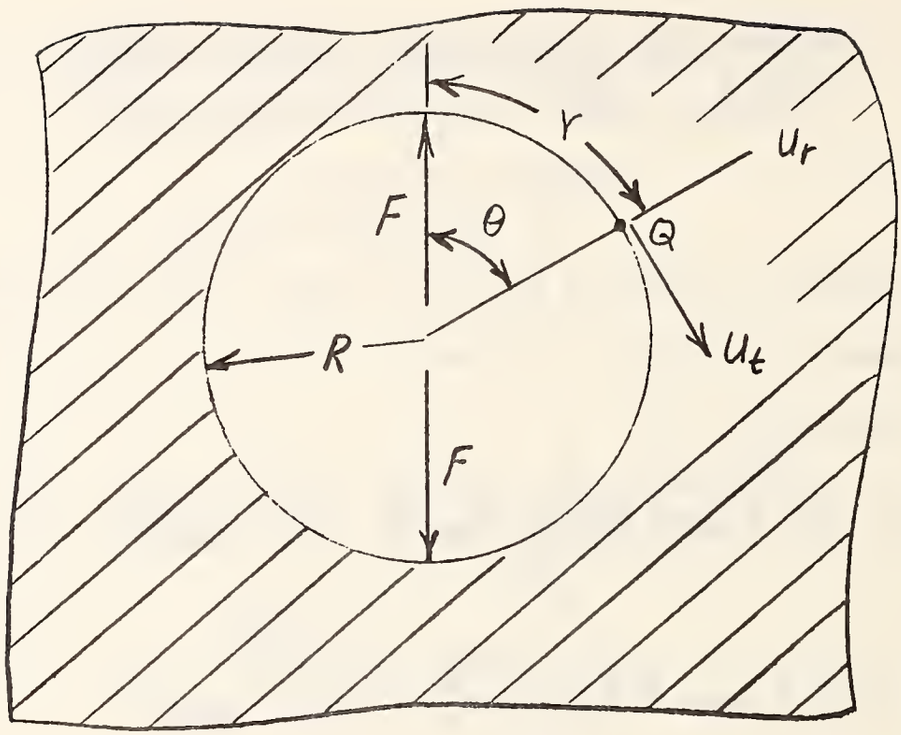

Fig. E.1. Two Diametrically Opposed Line Loads on a Cylindrical Cavity

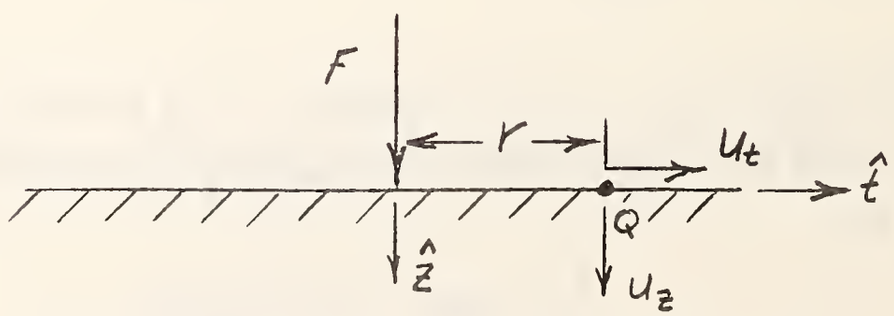

Fig. E.2. Line Load on an Elastic Half Space

As presented in section 4.3, the displacements u_z and u_t are

$$u_z = \frac{2F(1-\nu^2)}{\pi E} \log \frac{d}{r} - \frac{F(1+\nu)}{\pi E} \qquad (E.5)$$

and

$$u_t = - \frac{(1+\nu)(1-2\nu)F}{2E} \qquad (E.6)$$

It will be shown that the singularity in the displacement u_r is the same as that of u_z near the load. Furthermore, the limit of u_θ, as θ tends to zero, will be shown to be u_t.

As illustrated in figure E.2, r represents the distance between the applied load and the point Q where the displacement u_z and u_t are calculated. Let us define a coordinate r on figure E.1 such that $r = R\theta$. Replacing θ with $\frac{r}{R}$ in equation (E.1), it will be shown that $u_r = u_z$ as r tends to zero. Likewise, u_θ will be shown to approach u_t as r tends to zero.

In terms of the coordinate r, the ratio u_r/u_z may be written as

$$\frac{u_r}{u_z} = \frac{-F\left[K_1 \cos \frac{r}{R} \log \tan \frac{r}{2R} + K_2 \sin \frac{r}{R}\right]}{F\left[K_1 \log \frac{d}{r} - K_3\right]} \qquad (E.7)$$

where

$$K_3 = \frac{(1+\nu)}{\pi E} \tag{E.8}$$

Taking the limit as r tends to zero, of equation (E.7) and using l'Hopital's rule

$$\lim_{r\to 0} \frac{u_r}{u_z} = \frac{r}{R}\cot\frac{r}{R} - \frac{r}{R}\sin\frac{r}{R}\log\tan\frac{r}{2R} + \frac{r}{R}\frac{K_2}{K_1}\cos\frac{r}{R} \tag{E.9}$$

The third term in equation (E.9) clearly goes to zero as r tends to zero, while the first and second terms are indeterminant.

Expanding $\cot\frac{r}{R}$ in the first term in equation (E.9) and taking the limit as r tends to zero,

$$\lim_{r\to 0}\frac{r}{R}\cot\frac{r}{R} = \lim_{r\to 0}\frac{r}{R}\left(\frac{R}{r} - \frac{r}{3R} - \frac{r^3}{45R^3} - \cdots\right) = 1 \tag{E.10}$$

Taking the limit of the second term in equation (E.9) and using l'Hopitals rule

$$\lim_{r \to 0} \frac{r}{R} \sin \frac{r}{R} \log \tan \left| \frac{r}{2R} \right| =$$

$$= \lim_{r \to 0} \frac{\frac{1}{2} \frac{r^2}{R^2} \tan \frac{r}{2R} \sec^2 \frac{r}{2R} \sin \frac{2r}{R}}{\sin \frac{r}{R} + \frac{r}{R} \cos \frac{r}{R}} = 0 \qquad \text{(E.11)}$$

Hence the only nonzero term in equation (E.9) in the limit as r tends to zero is the first and it tends to 1. Therefore in the limit as r tends to zero, $u_r = u_z$.

Now consider the limit of u_θ/u_t. Both u_θ and u_t are finite at r equal to zero. In the first term of equation (E.2) can be shown to go to zero as r approaches zero. u_θ, therefore, tends to the value $-K_2F$ for small r. This is exactly the value of u_t for all r. Thus,

$$\lim_{r \to 0} \frac{u_\theta}{u_T} = 1 \qquad \text{(E.12)}$$

and $u_\theta = u_t$ when r equals 0.

APPENDIX F

DERIVATION OF THE PROFILE FUNCTION FOR CONFORMAL CONTACT OF A SPHERE AND SPHERICAL SEAT

Consider a sphere of radius R_1 in contact with a spherical seat of radius R_2 at a point O as illustrated in figure F.1. It is assumed that point A, located at ψ on the sphere, will contact point B on the seat, located at ϕ. The distance between A and B, denoted f, is the profile function for these points. The value of the profile function in terms of ϕ and ψ is derived below.

Vectors $\vec{r}_1$ and $\vec{r}_2$ are defined such that $\vec{r}_1$ extends from O to A and $\vec{r}_2$ extends from O to B. The quantities ω_1 and ω_2 define the angles between the x axis and $\vec{r}_1$ and $\vec{r}_2$ respectively. From geometry of isosceles triangles it can be shown that

$$\omega_1 = \frac{\psi}{2} \tag{F.1}$$

and

$$\omega_2 = \frac{\phi}{2} \tag{F.2}$$

Furthermore, from geometry

$$|\vec{r}_1| = 2R_1 \sin\frac{\psi}{2} \tag{F.3}$$

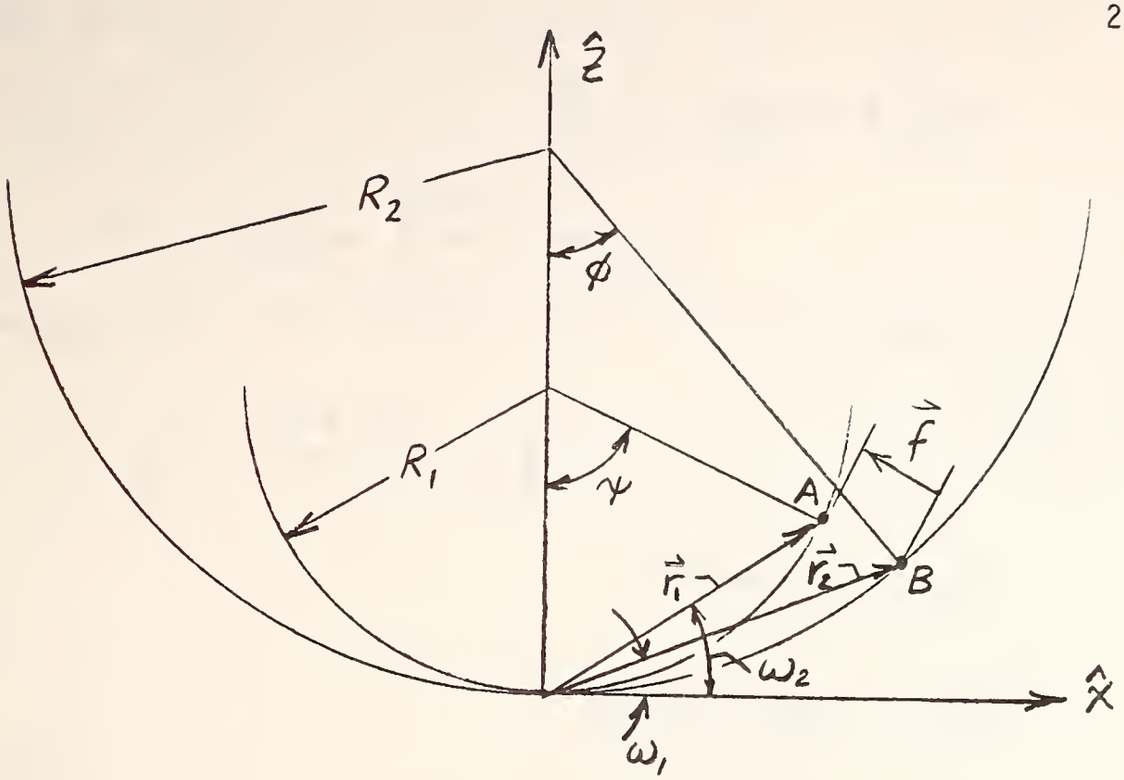

Fig. F.1. Profile function for a sphere and spherical seat

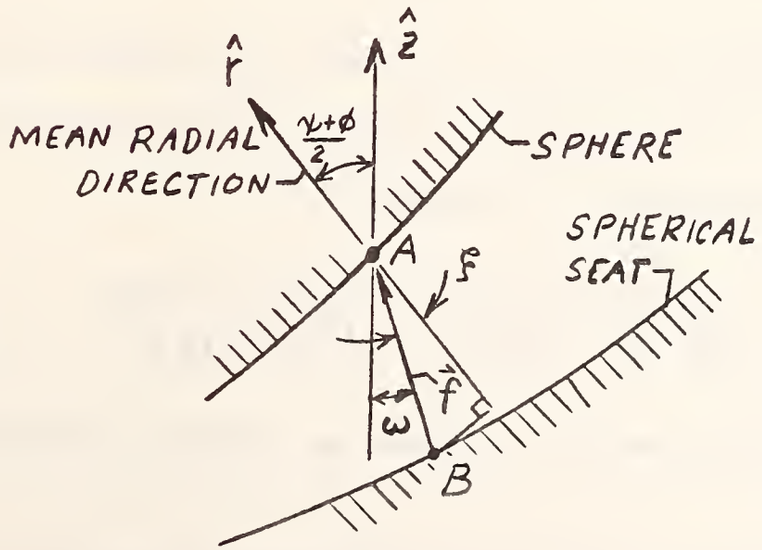

Fig. F.2. Profile function, $\vec{f}$, relative to mean radial direction, $\hat{r}$

$$|\vec{r}_2| = 2R_2 \sin\frac{\phi}{2} \tag{F.4}$$

The components in the x and z directions of $\vec{r}_1$ amd $\vec{r}_2$ may be expressed as

$$\begin{aligned} r_{1x} &= R_1 \sin\psi \\ r_{1z} &= 2R_1 \sin^2\frac{\psi}{2} \\ r_{2x} &= R_2 \sin\phi \\ r_{2z} &= 2R_2 \sin^2\frac{\phi}{2} \end{aligned} \tag{F.5}$$

The values of r_{1x}, r_{1z}, r_{2x} and r_{2z} are merely the cartesian coordinates of points A and B. The value of $|\vec{f}|$ is therefore defined by the distance between these two points or

$$|\vec{f}| = \sqrt{(r_{1x} - r_{2x})^2 + (r_{1z} - r_{2z})^2} \tag{F.6}$$

where r_{1x}, r_{2x}, r_{1z} and r_{2z} are given by relations (F.5) in terms of ψ and ϕ.

Now consider the mean radial direction which forms an acute angle of $\frac{\phi + \psi}{2}$ with the z direction as shown in figure F.2. The angle between $\overline{AB}$ and the mean radial direction is ξ while the acute angle

between $\overline{AB}$ and the z axis is labeled γ such that $\xi + \gamma = (\phi + \psi)/2$. The value of ξ may be determined using the following relations

$$\gamma = \arctan\left(\frac{r_{2x} - r_{1x}}{r_{1z} - r_{2z}}\right) \tag{F.7}$$

and

$$\xi = \frac{\phi + \psi}{2} - \gamma \tag{F.8}$$

APPENDIX G

INTEGRATION OF THE BOUSSINESQ INFLUENCE FUNCTION OVER AN ANNULAR ELEMENT

It is required to evaluate the integral

$$I(x,y) = \iint \frac{dx'dy'}{\sqrt{(x-x')^2+(y-y')^2}} \qquad (G.1)$$

over an annular element where (x,y) represents the location of a field point C along the center line of the annular segment as illustrated in figure G.1. The annular element has inner radius r_1, outer radius r_2 and the field point is located as radius r_c. The sides of the element are defined by angle θ measured from the center line.

Now consider the right triangle as shown in figure G.2. The integral in equation (G.1) over the right triangle is given in Luré [1964] as

$$I = \ell \ln \tan\left(\frac{\pi}{4} + \frac{\phi}{2}\right) \qquad (G.2)$$

This result will be used to approximate the integral in equation (G.1) over the annular region in figure G.1.

Let the annular region of figure G.1 be divided into six right triangles as shown in figure G.3. They are as follows.

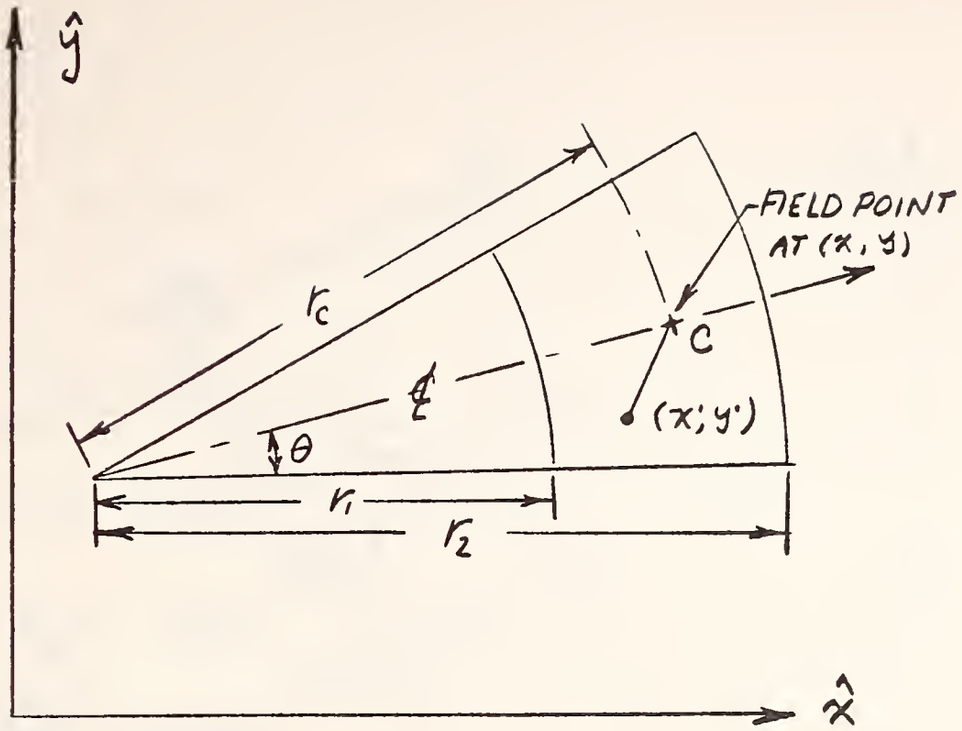

Fig. G.1. Annular Segment with Field Point along Center Line

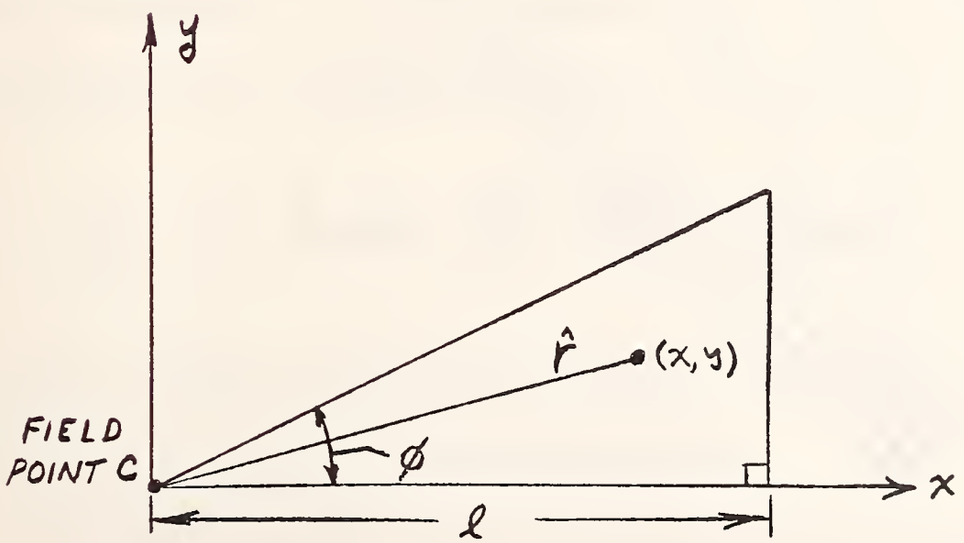

Fig. G.2. Right Triangle with Field Point as a Vertex

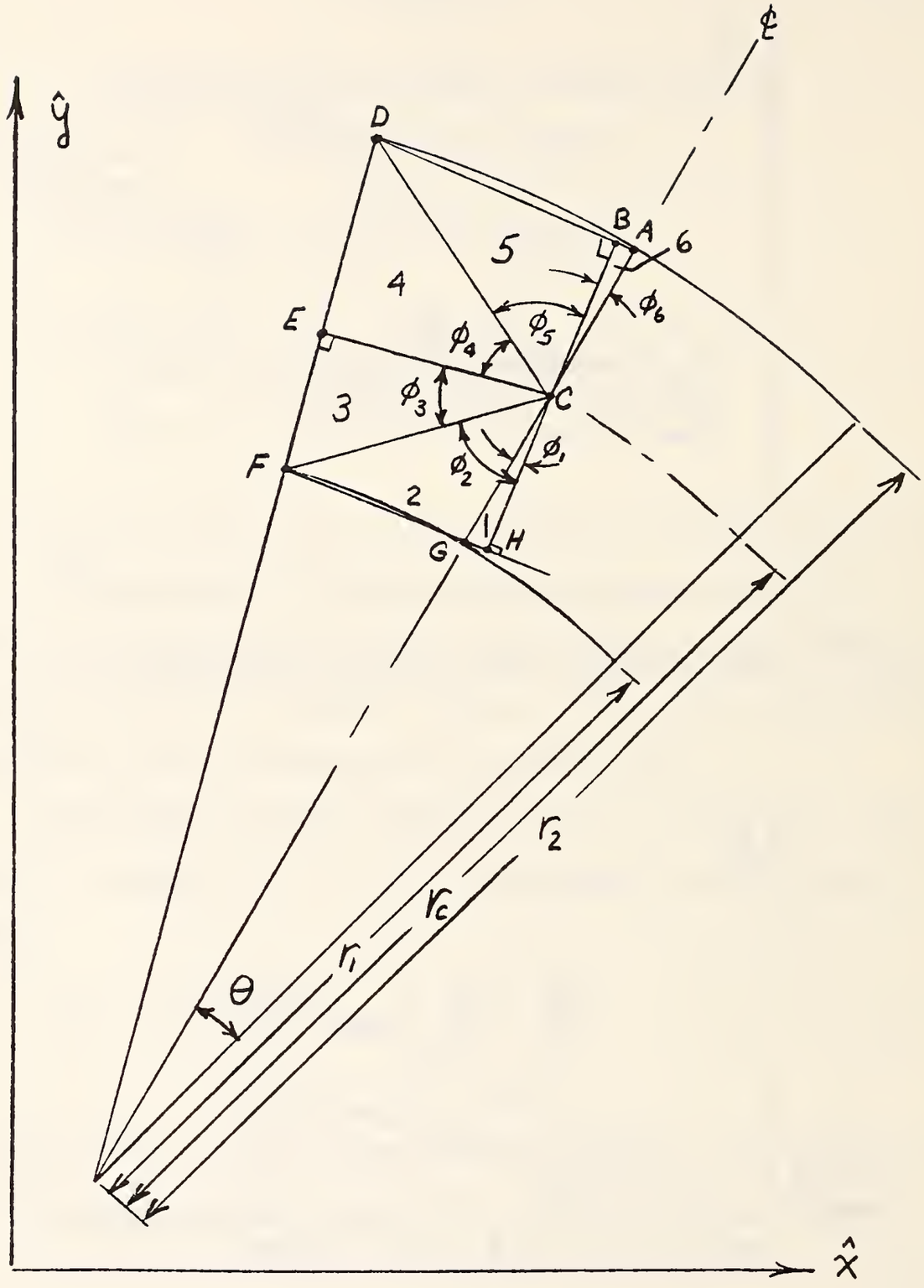

Fig. G.3. Annular Region Subdivided into Six Right Triangles

$$\Delta_1 \equiv ACB$$
$$\Delta_2 \equiv BCD$$
$$\Delta_3 \equiv DCE$$
$$\Delta_4 \equiv ECF \qquad (G.3)$$
$$\Delta_5 \equiv FCH$$
$$\Delta_6 \equiv GCH$$

The calculation of the integral (G.1) over each triangle may be performed using relation (G.2). The integrals over each of the triangles defined by relations (G.3) will be termed I_1, I_2 ····· I_6 corresponding to the integrals over triangles 1, 2 ····· 6 respectively. Thus

$$I_i = l_i \ln \tan\left(\frac{\pi}{4} + \frac{\phi_i}{2}\right) \qquad i = 1,6 \qquad (G.4)$$

where ϕ_i i = 1,6 are illustrated in figure G.3. The values of ϕ_i are all functions of r_1, r_2, r_c and θ defined below.

$$\phi_1 = \frac{\theta}{2} \qquad (G.5a)$$

$$\phi_2 = \arccos\left\{\frac{(r_c - r_i)\cos\frac{\theta}{2}}{\sqrt{r_c^2\sin^2\theta + (r_c\cos\theta - r_i)^2}}\right\} \quad \text{(G.5b)}$$

$$\phi_3 = \arctan\left\{\frac{(r_c\cos\theta - r_i)}{(r_c\sin\theta)}\right\} \quad \text{(G.5c)}$$

$$\phi_4 = \arctan\left\{\frac{(r_2 - r_c\cos\theta)}{(r_c\sin\phi)}\right\} \quad \text{(G.5d)}$$

$$\phi_5 = \frac{\pi}{2} - \frac{\phi_4}{4} - \frac{\theta}{2} \quad \text{(G.5e)}$$

$$\phi_6 = \pi - \theta_2 - \theta_3 - \theta_4 - \theta_5 + \theta_1 \quad \text{(G.5f)}$$

The values of ℓ_i can then be defined by

$$\ell_1 = \ell_2 = CH = (r_c - r_i)\cos\frac{\theta}{2} \quad \text{(G.6a)}$$

$$\ell_3 = \ell_4 = CE = r_c\sin\theta \quad \text{(G.6b)}$$

$$\ell_5 = \ell_6 = CB = \sqrt{(r_c\sin\theta)^2 + (r_2 - r_c\cos\theta)^2}\cos\phi_5 \quad \text{(G.6c)}$$

The total integral I_T over the annular element can be approximated by

$$I_T = 2\left\{\sum_{i=2}^{6} \ell_i \ln\tan\left(\frac{\pi}{4} + \frac{\phi_i}{2}\right) - \ell_1 \ln\tan\left(\frac{\pi}{4} + \frac{\phi_1}{2}\right)\right\} \quad \text{(G.7)}$$

APPENDIX H

DERIVATION OF A CONTACT CRITERION FOR CLOSELY CONFORMING SPHERES

Consider a sphere of radius R_1 interpenetrating the surface of a spherical seat of radius R_2 by an amount δ. For the problem at hand δ corresponds to the rigid body approach due to some unknown applied force F, on the sphere. Figure H.1 illustrates the sphere and seat and pertinent notations for the discussion to follow.

Point A is located on the surface of the sphere at coordinate ψ. Point B is located on the seat between point A on the sphere and O_2, the center of the seat. The radial gap between A and B, denoted by f, is equal to the sum of the elastic radial displacements w_1 and w_2, on the sphere and seat respectively, in the deformed state. From the geometry of the problem the following relationships may be stated:

$$\overline{O_2A} = \overline{O_2C} + \overline{CA} = (e+\delta)\cos\phi + R_1\cos(\psi-\phi) \tag{H.1}$$

$$\overline{O_2B} = R_2 \tag{H.2}$$

$$\overline{BA} = \overline{O_2A} - \overline{O_2B} = (e+\delta)\cos\phi + R_1\cos(\psi-\phi) - R_2 \tag{H.3}$$

where $e = R_2 - R_1$.

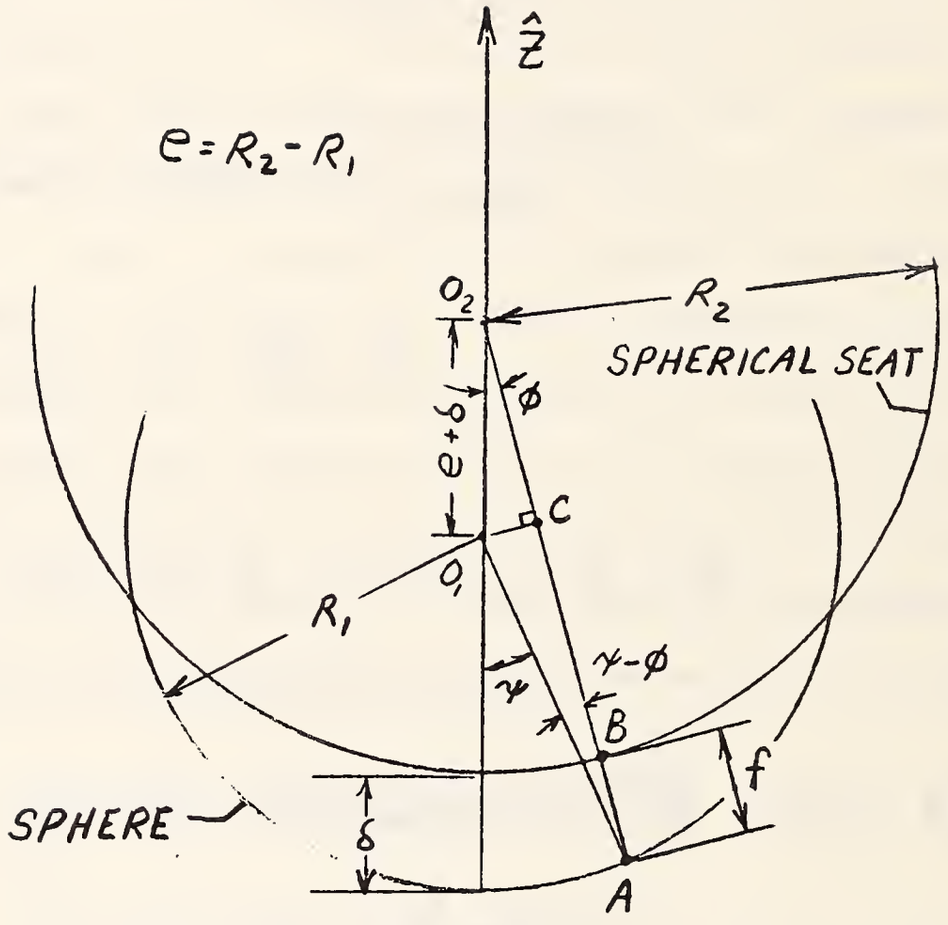

Fig. H.1. Sphere interpenetrating a spherical seat

Now consider the case where $R_2 \approx R_1$ and $\delta << R_1$, hence $\psi \approx \phi$. With these assumptions equation (H.3) may be written as

$$\overline{BA} \approx e(\cos\psi - 1) + \delta \cos\psi \qquad \text{(H.4)}$$

Recalling that $\overline{BA} = w_1 + w_2$

$$w_1 + w_2 + e(1 - \cos\psi) - \delta\cos\psi = 0 \qquad \text{(H.5)}$$

Equation (H.5) is an approximate contact criterion based on radial displacements.

APPENDIX I

RELATIONSHIP BETWEEN THE ELASTIC CONSTANTS IN PLANE STRESS AND PLANE STRAIN

Given the displacement and stress fields in a state of plane stress in terms of the elastic constants E and ν, the equivalent fields for the identical problem in plane strain may be found by substitution of $\bar{E}$ for E and $\bar{\nu}$ for ν where

$$\bar{E} = \frac{E}{1-\nu^2} \tag{I.1}$$

and

$$\bar{\nu} = \frac{\nu}{1-\nu} \tag{I.2}$$

This can be verified by substitution of (I · 1) and (I · 2) into the stress-strain relations for plane stress. The stress-strain relationships for a linear isotropic material are

$$\begin{aligned} \varepsilon_x &= \frac{1}{E}(\sigma_x - \nu\sigma_y) \\ \varepsilon_y &= \frac{1}{E}(\sigma_y - \nu\sigma_x) \\ \gamma_{xy} &= \frac{2(1+\nu)}{E}\tau_{xy} \end{aligned} \tag{I.3}$$

Substituting equations (I · 1) and (I · 2) into (I · 3) yields

$$\varepsilon_x = \frac{1}{E}\left\{(1-\nu^2)\sigma_x - \nu(1+\nu)\sigma_y\right\}$$

$$\varepsilon_y = \frac{1}{E}\left\{(1-\nu^2)\sigma_y - \nu(1+\nu)\sigma_x\right\} \qquad \text{(I.4)}$$

$$\gamma_{xy} = \frac{2(1+\nu)}{E}\tau_{xy}$$

Equations (I · 4) are the stress-strain relations for plane strain.

Similarly, a solution in plane stress may be obtained from a solution in plane strain by substituting E' for E and ν' for ν where

$$E' = E\,\frac{(1+2\nu)}{(1+\nu)^2} \qquad \text{(I.5)}$$

$$\nu' = \frac{\nu}{1+\nu} \qquad \text{(I.6)}$$

Substituting relations (I · 5) and (I · 6) into equations (I · 4) one obtains equations (I · 3) for plane stress.

APPENDIX J

HERTZIAN FORMULAS FOR A SPHERE INDENTING A SPHERICAL SEAT

For the case of a sphere of radius R_1 indenting a spherical seat of radius R_2, Hertz's theory predicts the following relationships between load F, approach δ, and the radius of the contact region a (see Timoshenko and Goodier, 1970 pp. 409-14):

$$a = \left[\frac{3\pi}{4} \frac{k R_1 R_2 F}{R_2 - R_1} \right]^{\frac{1}{3}} \tag{J.1}$$

$$\delta = \left[\frac{9\pi^2}{16} \frac{F^2 k^2 (R_2 - R_1)}{R_1 R_2} \right]^{\frac{1}{3}} \tag{J.2}$$

where

$$k = \frac{1-\nu_1^2}{\pi E_1} + \frac{1-\nu_2^2}{\pi E_2} \tag{J.3}$$

ν_1 and ν_2 are Poisson's ratio for the sphere and seat respectively and E_1 and E_2 are the respective values of Young's modulus.

The pressure at a radius of r from the center of the contact region is given by

$$P(r) = \frac{3F}{2\pi a^2} \sqrt{1 - \frac{r^2}{a^2}} \tag{J.4}$$

These formulae are only valid for contact regions which have dimensions small compared to both R_1 and R_2.

APPENDIX K

HERTZIAN FORMULAS FOR A CYLINDER INDENTING A CYLINDRICAL SEAT

For the case of a cylinder of radius R_1 indenting a cylindrical seat of radius R_2, Hertz's theory predicts the following relationships between load F per unit length and the half width of the contact region b (see Timoshenko and Goodier, 1970 pp. 418-19):

$$b = \left[\frac{4 F k R_1 R_2}{R_2 - R_1}\right]^{\frac{1}{2}} \tag{K.1}$$

$$F = \frac{b^2 (R_2 - R_1)}{4 k R_1 R_2} \tag{K.2}$$

where

$$k = \frac{1-\nu_1^2}{\pi E_1} + \frac{1-\nu_2^2}{\pi E_2} \tag{K.3}$$

ν_1 and ν_2 are the Poisson's ratio of the cylinder and seat respectively while E_1 and E_2 are the respective values of Young's modulus.

The pressure distribution at a distance of r from the center line of contact region is given by

$$p(r) = \frac{2F}{\pi b}\sqrt{1 - \frac{r^2}{b^2}} \tag{K.4}$$

These formulae are only valid for $b << R_1$. The approach for cylinders in contact or the contact of a cylindrical seat is predicted to be infinite by Hertzian theory which is clearly not possible. For an explanation of this inadequacy and the derivation of an appropriate formula for cylinlers in line contact see Singh [August 1974].

APPENDIX L

DERIVATION OF A CONTACT CRITERION FOR CONTACT OF A SPHERE AND SPHERICAL SEAT WITH A CONSTRAINED DISPLACEMENT FIELD

Consider an elastic sphere of radius R_1 indenting an elastic spherical seat of radius R_2. For a given force applied to the sphere, the bodies will approach by δ and the contact area will extend to ψ_{max} on the sphere. It will be assumed that a point located at ψ on the sphere will contact a point at ϕ on the seat and

$$\frac{R_1}{R_2} = \frac{\sin\phi}{\sin\psi} \tag{L.1}$$

This is physically equivalent to requiring points with the same x coordinates as shown in figure L.1 to contact after deformation. Only displacements in the z direction will be considered in the criterion. Consider the sphere interpenetrating the seat (although this is physically impossible) by an amount δ. The distance between points A and B is labeled f.

Noting the geometry at hand and the constraint equation (L.1) the gap f may be written as

$$f = (R_2 - R_1) + \delta + R_1\cos\psi - R_2\cos\phi \tag{L.2}$$

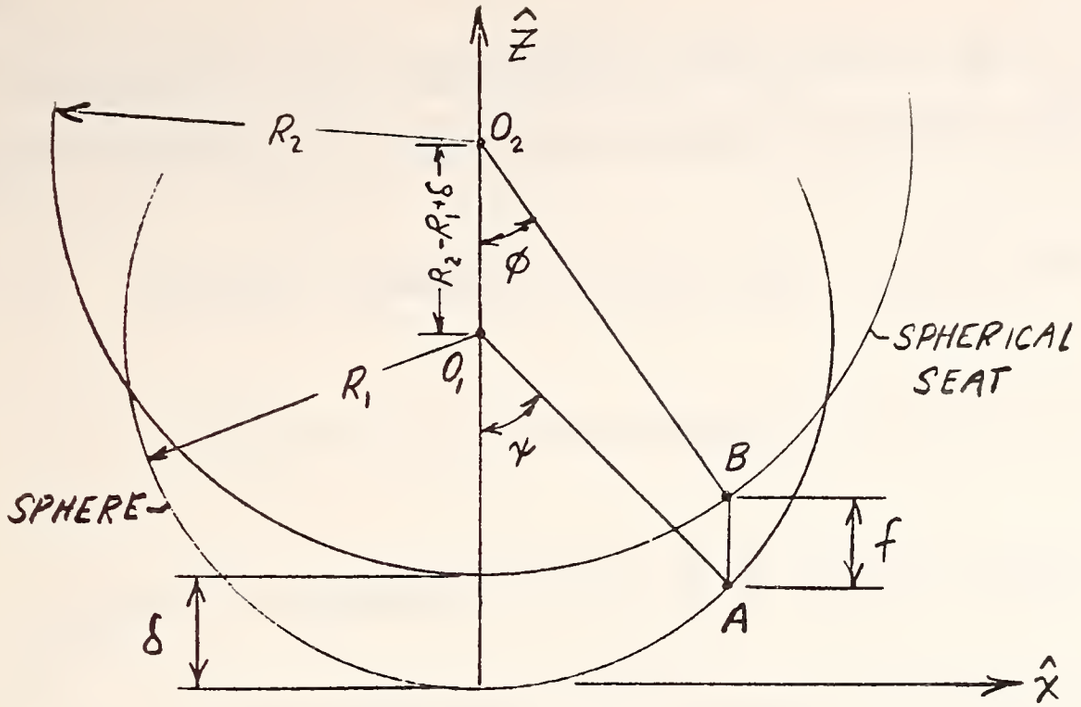

Fig. L.1. Sphere interpenetrating a spherical seat

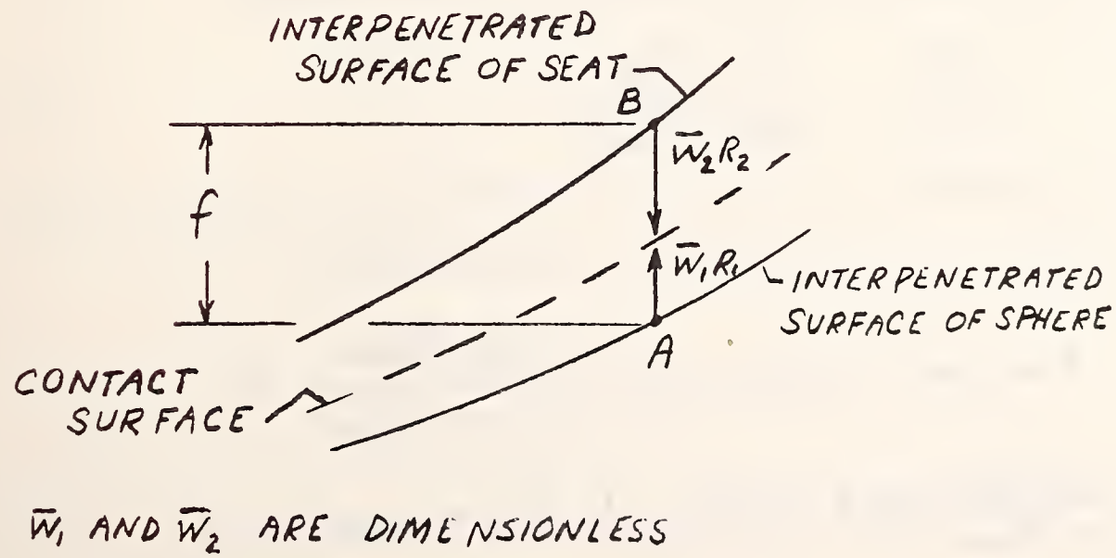

Fig. L.2. Detail of interpenetration surfaces of sphere and seat

This gap must be closed by the dimensionless elastic displacements $\bar{w}_1$ and $\bar{w}_2$ on the sphere and seat respectively. (see fig. L.2) Thus

$$R_1 W_1 + R_2 W_2 = (R_2 - R_1) + \delta - (R_2 \cos\phi - R_1 \cos\psi) \qquad (L.3)$$

Writing equation (L.3) for points on the outer boundary

$$R_1 W_1^\circ + R_2 W_2^\circ = R_2 - R_1 + \delta - (R_2 \cos\phi_{max} - R_1 \cos\psi_{max}) \qquad (L.4)$$

Equation (L.4) may be solved for δ. Substituting the resulting value of δ into equation (L.3) and rearranging terms gives

$$(\bar{W}_1 - \bar{W}_1^\circ) R_1 + (\bar{W}_2 - \bar{W}_2^\circ) R_2 =$$

$$- R_2 (\cos\phi - \cos\phi_{max}) + R_1 (\cos\psi - \cos\psi_{max}) \qquad (L.5)$$

Writing equation (L.1) for points on the outer boundary

$$\frac{R_1}{R_2} = \frac{\sin\phi_{max}}{\sin\psi_{max}} \qquad (L.6)$$

Dividing equation (L.5) by R_1 and substituting in relation (L.6) the final expression for the contact criterion becomes

$$(\bar{W}_1 - \bar{W}_1^\circ) + (W_2 - W_2^\circ) \frac{\sin\psi_{max}}{\sin\phi_{max}} =$$

$$- \frac{\sin\phi_{max}}{\sin\psi_{max}} (\cos\phi - \cos\phi_{max}) + (\cos\psi - \cos\psi_{max}) \qquad (L.7)$$

The above expression (L.7) is the contact criterion used in the analysis of Goodman and Keer [1965] who omit the bar over the dimensionless quantities $\bar{w}_1$, $\bar{w}_2$.

APPENDIX M

DERIVATION OF CONSTRAINED DISPLACEMENT FIELD FOR SURFACE POINTS OR AN ELASTIC SPHERE CONTACTING A RIGID SEAT

Consider an elastic sphere of radius R_1 in contact with a rigid spherical seat of radius R_2. It is known a priori that the contact surface will be of radius R_2. Assume that all points on the surface of the sphere move in a direction parallel to the line of the applied load. For a given contact angle ψ_{max}, the displacement field is then uniquely determined and will be derived below.

The displacement of surface points on the sphere consists of a rigid body translation δ and an elastic displacement field $u_z(\psi)$. Consider a sphere which has undergone the rigid body translation so that its surface interpenetrates the seat as illustrated in figure M.1. The elastic displacement of point A on the sphere is then defined by u_z in accordance with the given assumption. Taking vector components of $\overrightarrow{OB}$, $\overrightarrow{O'A}$ and $\overrightarrow{OO'}$ the magnitude of $\vec{u}_z$ can be derived to be

$$|\vec{u}_z| = -|\overrightarrow{OB}|\cos\psi + |\overrightarrow{OO'}| + |\overrightarrow{O'A}|\cos\phi \qquad (M.1)$$

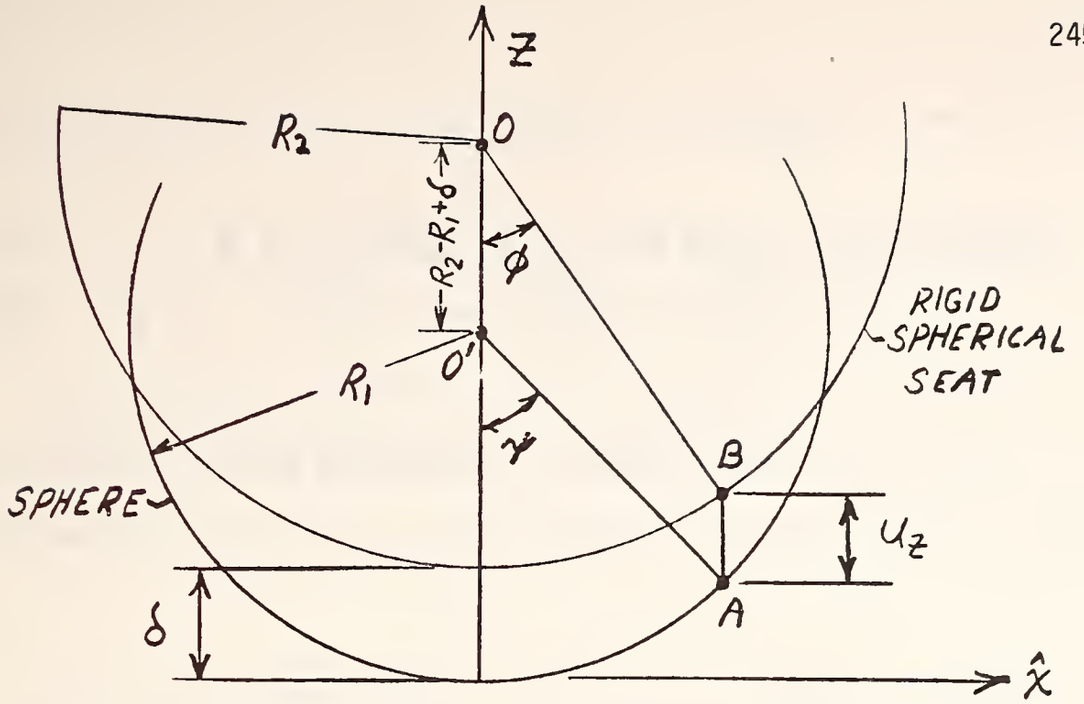

Fig. M.1. Elastic sphere interpenetrating a rigid seat

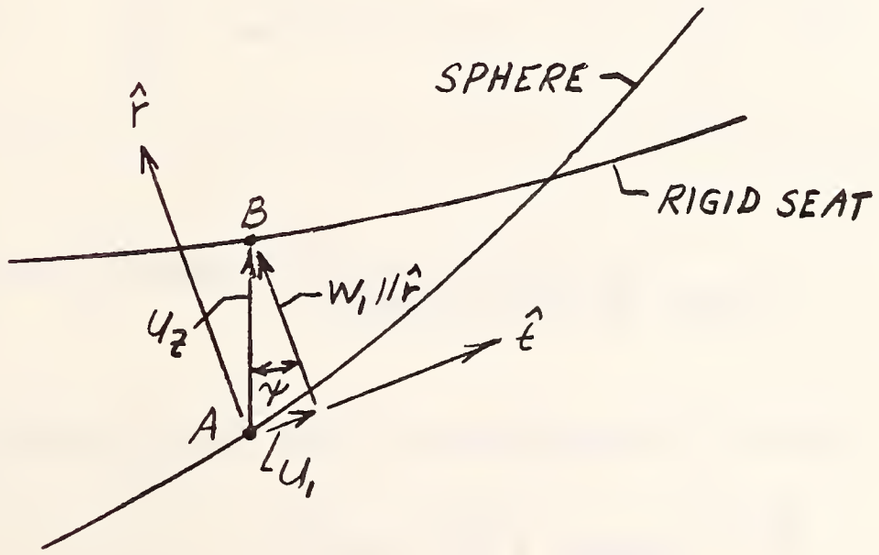

Fig. M.2. Components of surface displacement on sphere

which can be expressed as

$$|\vec{u}_z| = R_2(1-\cos\phi) - R_1(1-\cos\psi) + \delta \qquad \text{(M.2)}$$

Let a $\hat{r}$ - $\hat{t}$ coordinate system be defined at point A such that $\hat{r}$ is directed radially inward on the sphere and $\hat{t}$ is directed $\pi/2$ clockwise of $\hat{r}$. Then the components of $\vec{u}_z$, $w_1\hat{r}$ and $u_1\hat{t}$, may be computed by

$$w_1 = |\vec{u}_z| \cos\psi \qquad \text{(M.3)}$$

and

$$u_1 = |\vec{u}_z| \sin\psi \qquad \text{(M.4)}$$

The initial assumption requires A and B to be located such that

$$R_1 \sin\psi = R_2 \sin\phi \qquad \text{(M.5)}$$

thus

$$\phi = \arcsin\left(\frac{R_1}{R_2}\sin\psi\right) \qquad \text{(M.6)}$$

Combining equations (M.3), (M.4), and (M.6) one finds

$$W_1 = R_2 \left\{ 1 - \cos \left[\arcsin \left(\frac{R_1}{R_2} \sin \psi \right) \right] \right\} \cos \psi$$

$$- R_1 (1 - \cos \psi) \cos \psi + \delta \cos \psi \qquad \text{(M.7)}$$

and

$$U_1 = W_1 \tan \psi \qquad \text{(M.8)}$$

The derivative $\frac{du_1}{d\psi}$ may be expressed as

$$\frac{d U_1}{d \psi} = \frac{R_1^{\,2}}{R_2} \sin^2 \psi \cos \psi \Big/ \sqrt{1 - \left(\frac{R_1}{R_2} \sin \psi \right)^2}$$

$$- R_2 \cos \left\{ \arcsin \left(\frac{R_1}{R_2} \sin \psi \right) \right\} \cos \psi$$

$$- R_1 \sin^2 \psi + R_2 \cos \psi - R_1 (1 - \cos \psi) \cos \psi + \delta \cos \psi$$

This latter derivative is useful in computing the surface strain $\varepsilon_{\psi\psi}$.

APPENDIX N

COMPUTATION OF THE ORIENTATION OF TANGENTIAL COMPONENTS OF DISPLACEMENT ON SPHERICAL SURFACES

Consider the spherical surface of radius R illustrated in figure N.1. The surface is subjected to a load F at point B located at (ψ_B, β_B). The tangential displacement u_t, at a given point A located at $(\psi_A, 0)$, lies along the tangent to the great circle connecting A and B and is directed away from B for positive values. The angle between the positive u_t direction and the tangent at A which lies in the η_1 - γ_1 plane is defined at τ. ϕ is the angle measured between OA and OB. For purposes of integration of the tangential displacement influence function it is desired to find τ in terms of ψ_A, ψ_B and β_B.

Consider the portion of the spherical surface A M B as illustrated in figure N.2. The spherical angle at M is β_B and the opposite angle is ϕ. The adjacent angles to M are ψ_A and ψ_B. The spherical angle at A is τ. From the law of cosines for spherical trigonometry

$$\cos\theta = \cos\psi_B \cos\psi_A + \sin\psi_B \sin\psi_A \cos\beta_B \qquad (N.1)$$

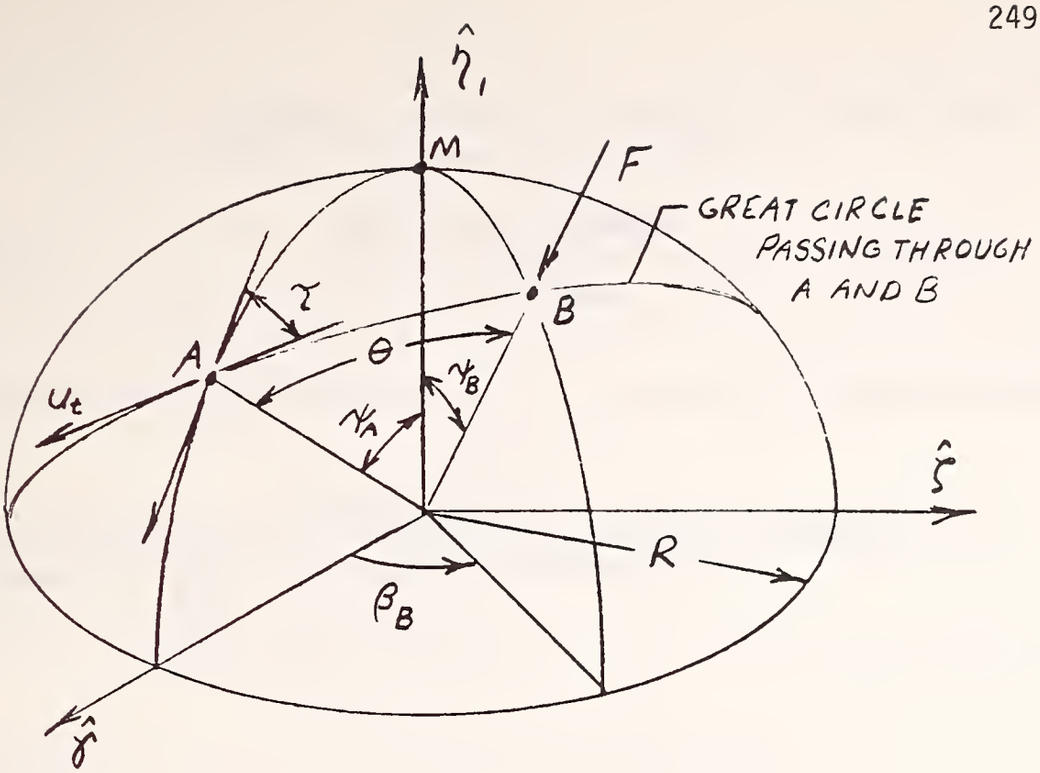

Fig. N.1. Orientation of tangential displacements due to a point load on a sphere.

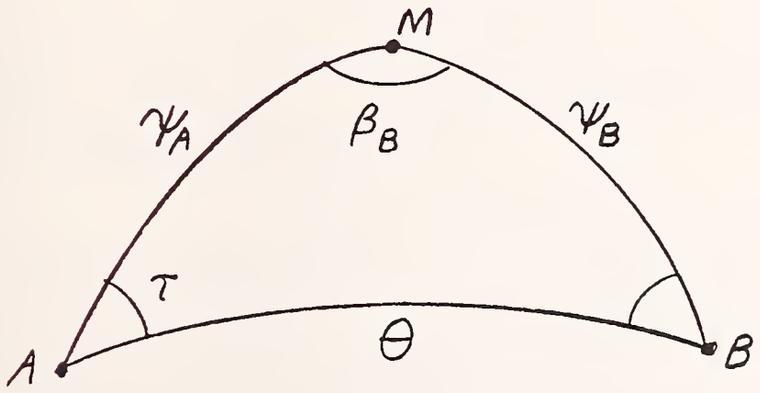

Fig. N.2. Spherical triangle

The law of sines for spherical trigonometry states:

$$\sin \tau = \frac{\sin \beta_B \sin \psi_B}{\sin \theta} \qquad \text{(N.2)}$$

combining equations (N.1) and (N.2) and taking the inverse of sin τ,

$$\tau = \arcsin \frac{\sin \beta_B \sin \psi_B}{\sin \left[\arccos (\cos \psi_B \cos \psi_A + \sin \psi_B \sin \psi_A \cos \beta_B) \right]} \qquad \text{(N.3)}$$

The above result can also be derived with cartesian vectors.

APPENDIX O

INTEGRATION OF INFLUENCE FUNCTION FOR CYLINDRICAL GEOMETRIES

The influence functions for a cylinder under two diametrically opposed line loads, normal to the surface as derived in section 4.7 are

$$G_1(\psi, \psi'; \nu_1, E_1) = -K_1' \left\{ \cos(\psi' - \psi) \ln \tan \frac{\psi' - \psi}{2} + 1 \right\} + \frac{K_2'}{\pi} \sin(\psi' - \psi) \qquad (0.1)$$

$$H_1(\psi, \psi'; \nu_1, E_1) = -K_1' \sin(\psi' - \psi) \ln \tan \frac{\psi' - \psi}{2} - \frac{K_2'}{\pi} \cos(\psi' - \psi) \qquad (0.2)$$

where G_1 $(\psi, \psi', E_1, \nu_1)$ is the influence function for the displacement of a point at ψ due to a load at ψ' $(\psi' \geq \psi)$ and H_1 $(\psi_1 \psi', E_1, \nu_1)$ is the influence function for the tangential displacement. E_1 and ν_1 are elastic constants of the cylinder and the constants K'_1 and K'_2 are given by

$$K_1^i = \frac{2(1-\nu_i^2)}{\pi E_i} \qquad (i=1,2) \qquad (0.3)$$

$$K_2^i = \frac{(1-\nu_i)(1-2\nu_i)}{2E_i} \qquad (i=1,2) \qquad (0.4)$$

Similarly for the cylindrical seat under two diametrically opposed normal line loads the influence functions as derived in section 4.8 are

$$G_2(\phi,\phi',\nu_2,E_2) = -K_1^2\cos(\phi'-\phi)\ln\tan\frac{\phi'-\phi}{2} - \\ - K_2^2\sin(\phi'-\phi) \qquad (0.5)$$

and

$$H_2(\phi,\phi',\nu_2,E_2) = K_1^2\sin(\phi'-\phi)\ln\tan\frac{\phi'-\phi}{2} \\ - K_2^2\cos(\phi'-\phi) \qquad (0.6)$$

where k_1^2 and k_2^2 are given by equations (0.3, 0.4)

G_2 represents the radial displacement influence function and H_2 is that for the tangential displacement on the cylindrical seat.

Consider the loading p (ψ') on the cylinder between ψ_1 and ψ_2 ($\psi_2 > \psi_1$) as shown in figure 0.1. p (ψ') is a constant pressure P and ψ is located such that $\psi \leq \psi_1$ (see fig. 0.1). The displacement w_1 at ψ due to p (ψ') can be computed as

$$w_1 = \int_{\psi_1}^{\psi_2} p(\psi)\, G_1(\psi,\psi',\nu_1,E_1)\, R_1\, d\psi' \\ = P R_1 \int_{\psi_1}^{\psi_2} G_1(\psi,\psi',\nu_1,E_1)\, d\psi' \qquad (0.7)$$

The tangential displacement u_1 due to load p (ψ') can be expressed as

$$u_1 = \int_{\psi_1}^{\psi_2} p(\psi)\, H_1(\psi,\psi',\nu_1,E_1)\, R_1\, d\psi' \\ = P R_1 \int_{\psi_1}^{\psi_2} H_1(\psi,\psi',\nu_1,E_1)\, d\psi' \qquad (0.8)$$

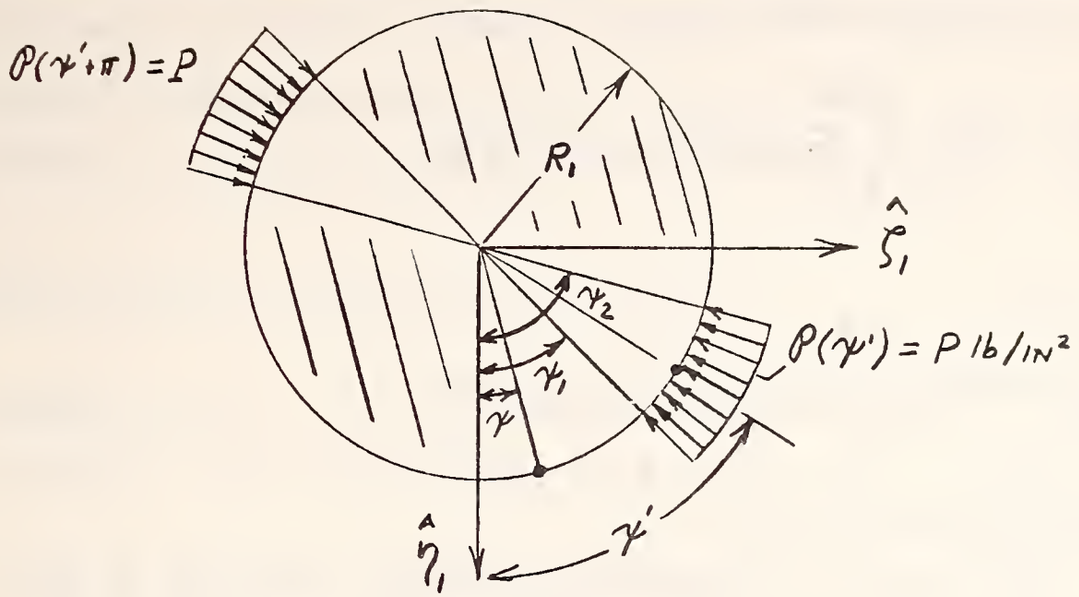

Fig. 0.1. Pressure loading on a cylinder

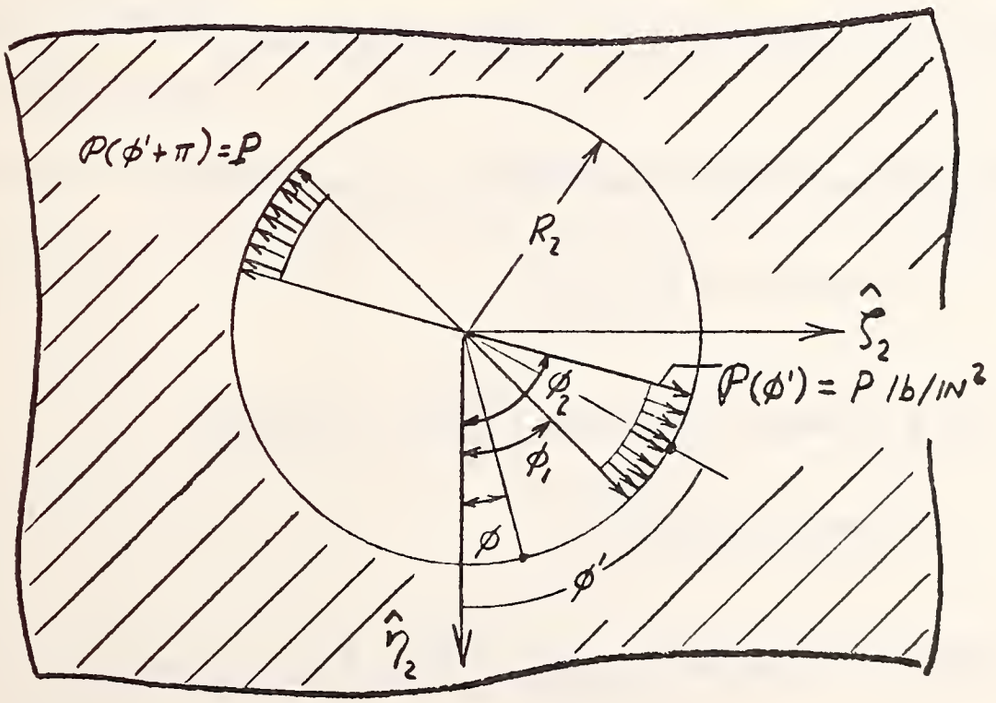

Fig. 0.2. Pressure loading on a cylindrical seat

Similarly on the cylindrical seat the radial and tangential displacements at ϕ due to p (ϕ') are

$$W_2 = PR_2 \int_{\phi_1}^{\phi_2} G_2(\phi, \phi', \nu_2, E_2)\, d\phi' \tag{0.9}$$

and

$$U_2 = PR_2 \int_{\phi_1}^{\phi_2} H_2(\phi, \phi', \nu_2, E_2)\, d\phi' \tag{0.10}$$

respectively (see fig. 0.2)

The integrals in equations (0.7), (0.8), (0.9) and (0.10) may be evaluated analytically. In each case the first term in G_1, H_1, G_2 and H_2 can be integrated by parts while the integration of the second terms is trivial. The indicated integration results in

$$W_1 = PR_1 \left[-K_1' \sin(\psi'-\psi) \ln \tan \frac{\psi'-\psi}{2} - K_2' \cos(\psi'-\psi)\right]_{\psi'=\psi_1}^{\psi'=\psi_2} \tag{0.11}$$

$$U_1 = PR_1 \left[K_1' \left(\cos(\psi'-\psi) \ln \tan\left(\frac{\psi'-\psi}{2}\right) - \ln \sin(\psi'-\psi)\right) - K_2' \sin(\psi'-\psi)\right]_{\psi'=\psi_1}^{\psi'=\psi_2} \tag{0.12}$$

$$W_2 = PR_2 \left[-K_1^2 \sin(\phi'-\phi) \ln \tan\left(\frac{\phi'-\phi}{2}\right) + K_1^2(\phi'-\phi) - K_2^2 \cos(\phi'-\phi)\right]_{\phi'=\phi_1}^{\phi'=\phi_2} \tag{0.13}$$

$$U_2 = PR_2 \left[-K_1^2 \cos(\phi'-\phi) \ln \tan \frac{\phi'-\phi}{2} + K_1^2 \ln \sin(\phi'-\phi) - K_2^2 \sin(\phi'-\phi)\right]_{\phi'=\phi_1}^{\phi'=\phi_2} \tag{0.14}$$

These expressions for u_1, u_2, w_1 and w_2 are valid for ψ_1, ψ_2, ϕ_1 and ϕ_2 less than $\frac{\pi}{2}$. In order to extend the domain of the integration to π, symmetry of the displacement fields must be considered. For ψ_1, ψ_2, ϕ_1 and ϕ_2 less than $\frac{\pi}{2}$ these conditions may be expressed as

$$W_1(\psi, \psi_1, \psi_2, P) = W_1(\psi, \pi - \psi_2, \pi - \psi_1, P) \tag{0.15}$$

$$U_1(\psi, \psi_1, \psi_2, P) = -U_1(\psi, \pi - \psi_2, \pi - \psi_1, P) \tag{0.16}$$

$$W_2(\phi, \phi_1, \phi_2, P) = W_2(\phi, \pi - \phi_2, \pi - \phi_1, P) \tag{0.17}$$

$$U_2(\phi, \phi_1, \phi_2, P) = -U_2(\phi, \pi - \phi_2, \pi - \phi_1, P) \tag{0.18}$$

The above analysis is valid only for $\psi \leq \psi_1 < \psi_2$. If $\psi \geq \psi_2 > \psi_1$ (or $\phi \geq \phi_2 > \phi_1$) then the absolute values of $\psi - \psi_i$ ($i = 1, 2$) and $\phi - \phi_i$ in equations (0.11)-(0.14) should be considered in the evaluation of w_1, w_2, u_1 and u_2. In addition to the above, the direction of u_1 and u_2 must be accounted for by considering these quantities as being $+ u_1$ (or $+ u_2$) when $\psi \leq \psi_1 < \psi$ ($\phi \leq \phi_1 < \phi_2$) and as $- u_1$ ($- u_2$) when $\psi \geq \psi_2 > \psi_1$ ($\phi \geq \phi_1 > \phi_2$).

APPENDIX P

DERIVATION OF A PLANAR APPROXIMATION TO THE ELEMENTAL AREA ON A SPHERICAL SURFACE

Consider the area ABCD on a spherical surface of radius R as shown in figure P.1. It is desired to approximate this curved area with a plane element so that the integral of the Boussinesq influence functions can be approximated for the spherical element.

The area on the sphere is bounded by $\psi' \pm \Delta$ and $\beta' \pm \Delta$ where $\Delta << 1$ radian. A cone generator is defined such that its apex N falls on the η axis and points A, B, C, and D fall on the surface of the cone (see fig. P.1). The surface ABCD on the cone closely approximates the surface on the sphere for small Δ. Let point G be located midway between A and D, and let G' be its projection on the η axis (as shown in fig. P.2). From figures P.1 and P.2, the following relations may be established:

$$AG = GD = R \sin \Delta$$

$$OG = R \cos \Delta \qquad \text{(P.1)}$$

$$NG = OG \tan \psi' = R \cos \Delta \tan \psi'$$

$$NA = NG - AG = R(\cos \Delta \tan \psi' - \sin \Delta) = \frac{R \sin(\psi' - \Delta)}{\cos \psi'}$$

$$ND = NG + AG = R(\cos \Delta \tan \psi' + \sin \Delta) = \frac{R \sin(\psi' + \Delta)}{\cos \psi'}$$

$$\rho = \frac{1}{2} \frac{\overline{G'G}\,(2\Delta)}{NG} = \Delta \cos \psi'$$

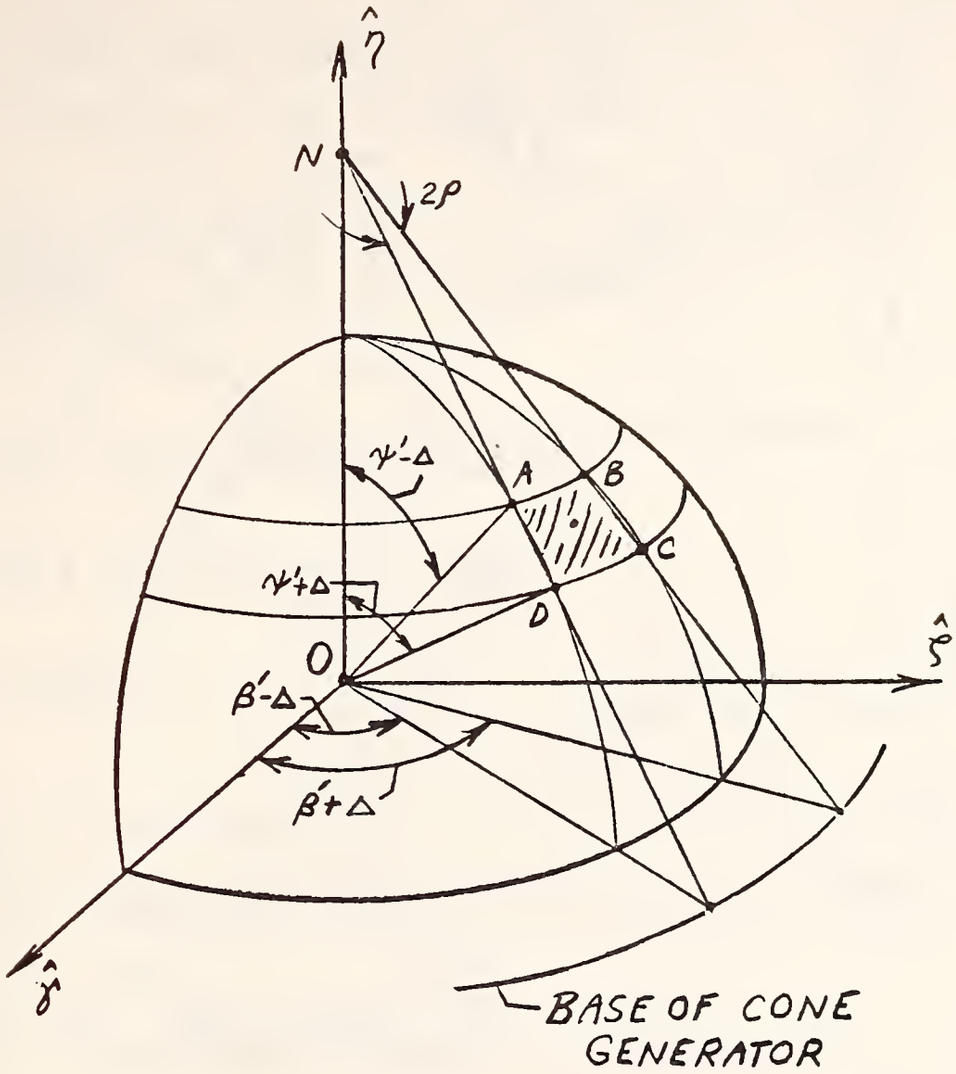

Fig. P.1. Elemental area on spherical surface

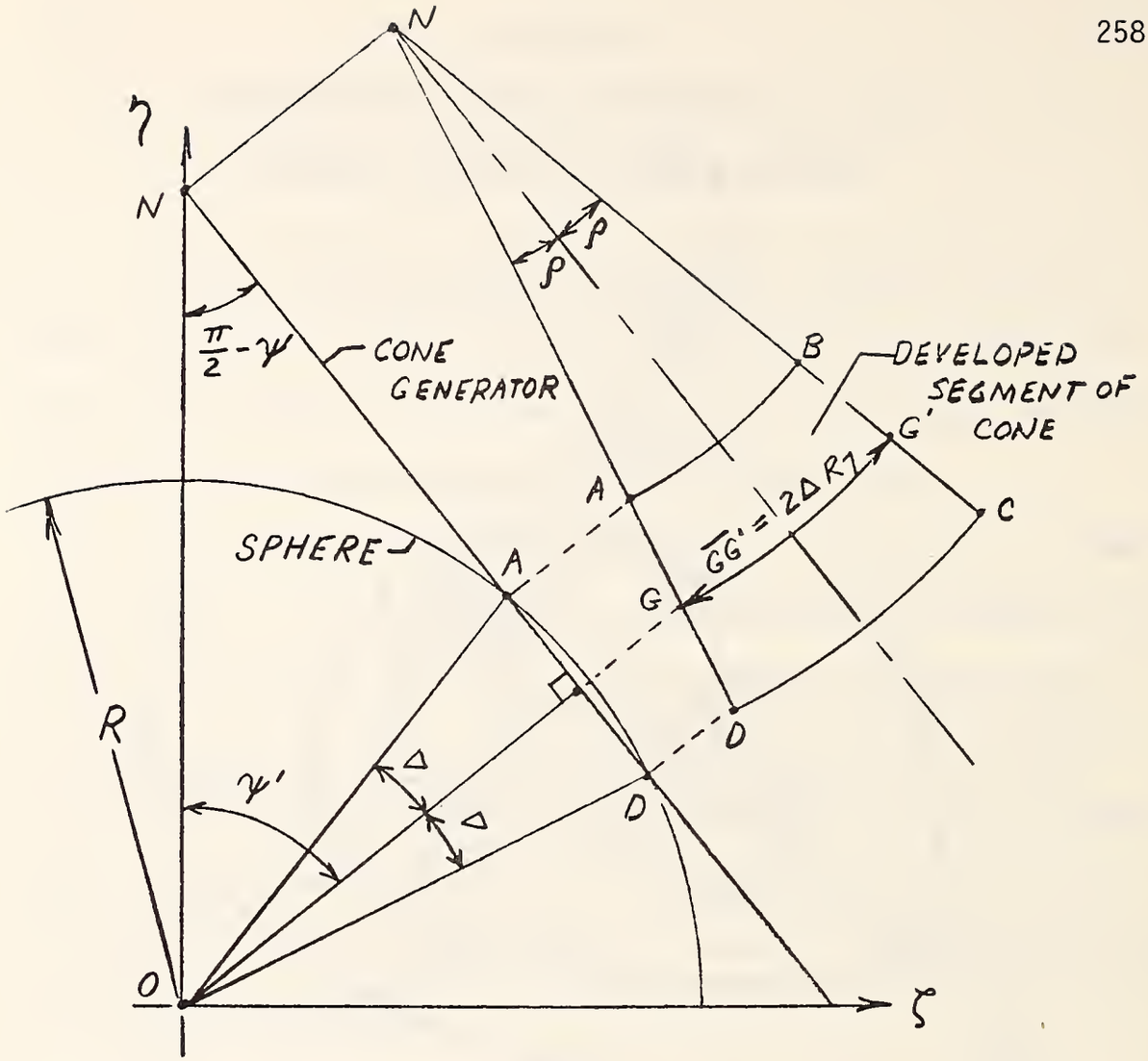

Fig. P.2. Section view of cone generator

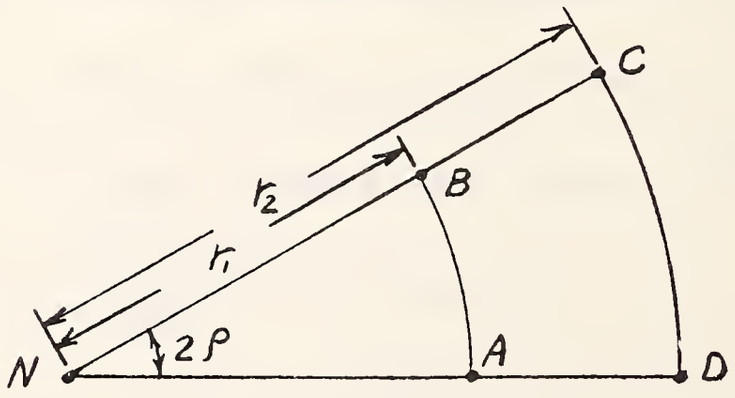

Fig. P.3. Annular segment

Finally, for small Δ, the area ABCD on the cone can be closely approximated by a planar annular element including points N, A, B, C, and D. Figure P.3 illustrates an annular segment ABCD with inner radius r_1, outer radius r_2 and half angle of ρ. In relating the equation (P.1) to the geometry of the annular element the quantities r_1, r_2 and can be described as

$$r_1 = NA = R \sin(\psi' - \Delta) / \cos \psi' \tag{P.2}$$

$$r_2 = ND = R \sin(\psi' + \Delta) / \cos \psi' \tag{P.3}$$

$$\rho = \Delta \cos \psi' \tag{P.4}$$

The corresponding areas of the original spherical element may be compared to the area of the planar annular element. For the sphere

$$\begin{aligned} A_S &= R^2 \int_{\psi'-\Delta}^{\psi'+\Delta} \sin \psi \, d\psi \int_{\beta'-\Delta}^{\beta'+\Delta} d\beta \\ &= R^2 2\Delta \left[-\cos \psi \right]_{\psi'-\Delta}^{\psi'+\Delta} \\ &= 4R^2 \Delta \sin \psi' \sin \Delta \end{aligned} \tag{P.5}$$

For the annular element

$$\begin{aligned} A_a &= \frac{2\rho}{2\pi} \pi (r_2^2 - r_1^2) \\ &= \Delta \cos \psi' \left(\frac{R^2 \sin(\psi'+\Delta) - R^2 \sin^2(\psi'-\Delta)}{\cos^2 \psi'} \right) \\ &= 4\Delta R^2 \sin \psi' \sin \Delta \cos \Delta \end{aligned} \tag{P.6}$$

For small Δ, $A_a \approx A_s$.

NOMENCLATURE

A_a	area of annular segment
A_i	area of cell i
A_{ij}	area of cell ij
A_n	coefficients defined in equations (4.20) and (A.3)
A_s	area of sector on sphere
A_{2k}	coefficients in equations (4.18) and (A.1)
a	radius of contact region in chapter 5, semi-major axis of ellipse in appendix D
a^*	non-dimensional radius of contact region
B_{ij}	coefficients defined by equation (2.12)
B_n	coefficients defined by equations (4.21) and (A.4)
B_{2k}	coefficients in equations (4.19) and (A.2)
b_{ij}	coefficients defined by equation (2.10)
b	half width of contact region in appendix K, semi-minor axis of ellipse in appendix D
c_{ijl}	distance between field point l and a point in cell s_{ij}
$\bar{c}_{ijl}$	distance between field point l and centroid of cell s_{ij}
d	hypothetical interpenetration
do	initial interpenetration of spheres
E	Young's modulus
E_i	Young's modulus of body i
E'	equivalent Young's modulus for plane stress

$\bar{E}$	equivalent Young's modulus for plane strain
e	difference in radii of curvature, R_2-R_1
F	force in context of point loads, force per unit length in context of line loads
F_i	force at node i
F^*	nondimensional force
$F_{CONSPHERE}$	force resulting from analysis by CONSPHERE
F_{Hertz}	force resulting from Hertzian analysis
$F^*_{CONSPHERE}$	nondimensional force resulting from analysis by CONSPHERE
F^*_{Hertz}	nondimensional force resulting from Hertzian analysis
f	profile function or initial separation between two points which merge after deformation
$\vec{f}$	vector describing initial spearation fo two points which merge after deformation
f_i	initial separation of field points i
f'_i	$f_{N+1} - f_i$
f_r, f_t, f_ω	components of f in $\hat{r}$, $\hat{t}$ and $\hat{\omega}$ directions respectively
f(x,y)	f evaluated at point (x,y)
$f_i(x,y)$	distance of surface i from x-y plane evaluated at (x,y)
G	modulus of rigidity
G ( )	influence function for displacements normal to a surface in a cartesian coordinate system
G ( )	influence function for displacements normal to a surface in a polar or spherical coordinate system
G_i ( )	G ( ) for body i
g ( )	nondimensional influence function

g_r ( ) — nondimensional influence function for displacements in the radial direction

g_θ ( ) — nondimensional influence function for displacements in the tangential direction

H ( ) — influence function for displacements tangential to a surface in a cartesian coordinate system

H ( ) — influence function for displacements tangential to a surface in a polar or spherical coordinate system

H_i ( ) — H( ) for body i

h_r — numerically generated nondimensional influence function for displacements in the radial direction

h_θ — numerically generated nondimensional influence function for displacements in the tangential direction

I_T — total integral over an annular segment

I_{ijl} — $\int_{S_{ij}} dA_{ij}/C_{ijl}$

K_1 — elastic parameter $\frac{2(1-\nu^2)}{\pi E}$

K_2 — elastic parameter $\frac{(1-2\nu)(1+\nu)}{2E}$

K_3 — elastic parameter $\frac{1+\nu}{\pi E}$

K_1^j — K_i evaluated for body j

k — elastic parameter $\frac{1-\nu_1^2}{\pi E} + \frac{1-\nu_2^2}{\pi E}$

k_1 — initial value of constant in point mating procedure

k_j^i — constant in point mating procedure for j^{th} solution on body i

m — inverse of Poisson's ratio in chapter 4 and appendix A, constant in mapping function in appendix D, number of equal sectors in Ω in chapter 7

N	number of cells in simply discretized solution
N_{con}	number of cells within r_{con}
$\hat{n}_i$	unit normal vector to surface of body i
P	constant pressure
P_i	constant pressure in cell i
P_{max}	maximum pressure
P_i^*	nondimensional pressure, kP_i
P^*_{max}	kP^*_{max}
$P_{2k}(\cos\theta)$	Legendre polynomial in $\cos\theta$
$p(\ )$	interfacial contact pressure in polar or spherical coordinate system
$p(x,y,z)$	interfacial contact pressure in cartesian coordinates
R	radius of curvature
R_i	radius of curvature of body i (k = 1,2)
R_m	mean radius of curvature, $\frac{2R_1R_2}{R_2+R_1}$ (note: in conformal theory $-R_2$ is substituted for R_2)
ΔR	$R_2 - R_1$
r	coordinate of generic point
r^*	nondimensional coordinate of generic point, r/R_m
$\hat{r}$	unit vector in mean radial direction
$\vec{r}$	position vector
$\vec{r}_i$	position vector to point on surface of body i
r_b	radius of blending point of pit on sphere

r_c	radius of curvature at "edge" of pit in chapter 7, radius of centroid in appendix G
r_{con}	radius used in convergence studies
r_I	radius of inner boundary of contact region
r_i	chords used in analysis of influence functions for a cylinder in chapter 4 and appendix B (i = 1,2), radius of inner boundary of i^{th} cell in chapter 7
r_o	radius of outer boundary of contact region
r_{ix}, r_{iz}	x and z components respectively of vector $\vec{r}_i$
r^*	r/R_m
r_b^*	r_b/R_m
r_c^*	r_c/R_m
Δr	length of cell
$r\Delta\phi$	width of cell
S	separation of merging field points
$\vec{S}$	separation vector of merging field points
S_r, S_t, S_ω	$\hat{r}$, $\hat{t}$, and $\hat{\omega}$ components of $\vec{S}$
S_1, S_2, S_3	singularities in influence function for radial displacements on a sphere
SCF	stress concentration factor
S_{ij}	region included in ring i between rays j and j + 1
s_i	distance along contour curve of body i (i = 1,2)
s_i^j	s_i on j^{th} solution
TOL	tolerance used to determine merging of field points
T_1, T_2, T_3	singularities in influence function for tangential displacements on a sphere
$\hat{t}$	unit vector in mean tangential directions

u	displacement tangent to surface
u_r	displacement in radial direction
u_t	displacement in tangential direction
u_z	displacement in z direction
u_θ	displacement in tangential direction
u_i	tangential displacement on body i (i = 1,2)
V_j	coefficients defined in equation (2.11)
v_i	displacement in $\hat{\omega}$ direction on body i (i = 1,2)
w	displacement normal to surface
w_i	normal displacement on body i (i = 1,2)
w_i^o	w_i at outer boundary of contact region
$\bar{w}_i$	nondimensional normal displacement w_i/R_i
(x,y,z)	coordinates of generic point in cartesian coordinate system
$(\hat{x}_i, \hat{y}_i, \hat{z}_i)$	unit vectors on body i
Z	generic vector in Z plane, $Re^{i\theta}$
Z_o	vector in $\hat{x}$ direction in Z plane
Z_1	vector in Z plane
$\bar{Z}_1$	conjugate of Z_1
z_i	value of $f_i(x,y)$
α	angle between mean radial direction and the Z axis
α_1, α_2	angles defined in figures 4.12 and B.1
β	coordinate of generic point in spherical coordinate system
β_{ij}	centroidal radius of sector S_{ij}

γ	angle between $\vec{F}$ and Z axis
$\hat{\gamma}_1, \hat{\gamma}_2$	unit vectors in cartesian coordinate systems fixed to bodies 1 and 2 respectively
γ_{xy}	shear stress
Δ'	small angle $<<$ 1 radian
Δ	constant defined in equations (4.22) and (A.5)
Δ_i	rigid body translation of body i (i = 1,2), triangle i (i = 1,6) defined in appendix G only
δ	approach
δ^*	δ/R_m
$\delta_{CONSPHERE}$	approach predicted by CONSPHERE
$\delta^*_{CONSPHERE}$	$\delta_{CONSPHERE}/R_m$
δ_{Hertz}	approach predicted by Hertzian theory
δ^*_{Hertz}	δ_{Hertz}/R_m
δ_r, δ_t	approach in the $\hat{r}$ and $\hat{t}$ directions respectively
ε	root mean square error
ε_x, ε_y	components of strain in appendix I
ε_{ij}	strain tensor (i,j = β, ψ, r, ω, ϕ)
ζ	generic vector in ζ-plane
$\hat{\zeta}_1$, $\hat{\zeta}_2$	unit vectors in cartesian coordinate system fixed on bodies 1 and 2 respectively
$\hat{\eta}_1, \hat{\eta}_2$	unit vectors in cartesian coordinate system fixed on bodies 1 and 2 respectively
θ	generic angle used in spherical and polar coordinate systems
κ	elastic parameter equal to $\frac{3-\nu}{1+\nu}$ for plane stress and $3-4\nu$ for plane strain

λ	angle between normal vector $\hat{n}_i$ and $\hat{r}$ direction
μ	modulus of rigidity, Lame's constant
ν	Poisson's ratio
ν_i	Poisson's ratio of body i (i = 1,2)
ν'	equivalent Poisson's ratio for plane stress
$\bar{\nu}$	equivalent Poisson's ratio for plane strain
ξ	angle between $\vec{f}$ and $\hat{r}$
ρ	half vertex angle of annular segment in chapter 5 and appendix P, a boundary radius (r_I or r_o) of the contact region in chapter 7
σ_x, σ_y	components of stress in appendix I
σ_1	vector in ζ-plane
$\bar{\sigma}_1$	conjugate of σ_1
τ	angle defined in equation (7.9) in chapter 7, angle describing orientation of u_t in appendix N
τ_{xy}	shear stress
υ	regularization parameter
ϕ	generic angle in spherical and polar coordinate systems fixed to body 2
ϕ_{max}	angle defining boundary of contact region on body 2
$\Delta\phi$	$2\pi/m$ in chapter 7
ψ	generic angle in spherical and polar coordinate systems fixed to body 1
ψ_{max}	angle defining boundary of contact region on body 1
$\psi(P_i)$	function which is minimized in Functional Regularization method
Ω	contact region

Ω	projection of contact region onto x-y plane in chapters 2 and 7 only
Ω_i	region of cell i in chapters 2 and 7, contact region on body i in chapters 3-6
Ω_{ij}	contact region of cell j on body i
Ω^*	candidate or tentative contact region
Ω^*_{2j}	tentative contact region of cell j on body 2
$\hat{\omega}$	unit vector defined by equation (3.3b)
$\omega(\zeta)$	mapping function
ω_i	angle between $\vec{r}_i$ and $\hat{x}$ (i = 1,2)

BIBLIOGRAPHY

Boussinesq, J. Application des Potentiels a l'Etude de l'Equilibre et des Mouvement des Solides Elastiques. Paris: Gauthier-Villars, 1885.

Carnahan, B.; Luther, H. A.; and Wilkes, J. O. Applied Numerical Methods. New York: Johy Wiley & Sons, 1969.

Chan, S. K., and Tuba, I. S. "Finite Element Method for Contact Problems of Solid Bodies--Part I. Theory and Validation--Part II. Application to Turbine Blade Fastenings." Int. J. Mech. Sci. 13 (1971): 615-39.

Chaud, R.; Haug, E. J.; and Rim. K. Solution of General Unbounded Contact Problems by Quadratic Programming and Finite Element Techniques. Interim Technical Report, U. S. Army Research Office, Durham, N. C. Contract #DAHC04-74-G-0040, April 1974.

Chiu, Y. P. "On the Contact Problem of Cylinders Containing a Shallow Longitudinal Surface Depression." Jour. of Applied Mechanics 36, Trans. of the ASME 91, ser. E, no. 4 (1969): 852-58.

Conry, T. F., and Seireg, A. "A Mathematical Programming Method for Design of Elastic Bodies in Contact." Journal of Applied Mechanics, Trans. of ASME, ser. E, 38 (January 1971): 387-92.

Flamant. Compt. Rendu. Paris: 1892, p. 1465.

Galin, L. A. Contact Problems in the Theory of Elasticity. Translated by H. Moss. Edited by I. N. Sneddon. Raleigh: North Carolina State College, School of Physical Sciences and Applied Mathematics, October 1961.

Goodman, L. E., and Keer, L. M. "The Contact Stress Problem for an Elastic Sphere Indenting an Elastic Cavity." International Journal of Solids and Structures 1 (1965): 407-15.

Gradshteyn, I. S., and Ryzhik, I. M. Table of Integrals, Series and Products. New York: Academic Press, 1965.

Guerrero, I., and Turteltaub, M. J. "The Elastic Sphere Under Arbitrary Concentrated Surface Foods." Journal of Elasticity 2, no. 1 (March 1972): 21-33.

Hadamard, J. Lectures on Cauchy's Problem in Linear Partial Differential Equations. New York: Dover Publications, 1952, pp. 33-34.

Hertz, H. Miscellaneous Papers. Translated by D. E. Jones and G. A. Schott. New York: Macmillan Co., 1896.

_____. "On the Contact of Elastic Solids." Journal Furr die Reine und Angewandte Mathematik 92 (1918): 156-71

Hildebrand, Frances B. Advanced Calculus for Applications. Englewood Cliffs, N. J.: Prentice-Hall, 1962.

_____. Methods of Applied Mathematics. 2d ed. Englewood Cliffs, N. J.: Prentice-Hall, 1965.

I. B. M. Scientific Subroutine Package, System /360 (360A-CM-03X) Vers III, Programmers Manual H20-0205-2, I.B.M. Corp., White Plains, N. Y. (1968).

Kalker, J. J. "Aspects of Contact Mechanics." IUTAM Symposium on Contact of Deformable Bodies. University of Delft Press, 1975.

_____. "On the Uniqueness of Contact Problems in the Theory of Elasticity." Kontaktnoe vzaimodeistivie tvordikh tel Izdatel 'stvo Nanka, Moscow, 1971.

Kalker, J. J., and Van Randen, Y. "A Minimum Principle for Frictionless Elastic Contact with Application to Non-Hertzian Half Space Contact Problems." Journal of Engineering Mathematics 6, no. 2 (April 1972): 193-206.

Littman, W. E., and Widner, R. L. "Propagation of Contact Fatigue from Surface and Subsurface Origin." Journal of Basic Engineering, Trans. of the ASME 88, ser. D (1966): 624-36.

Love, A. E. H. A Treatise on the Mathematical Theory of Elasticity. 4th ed. Dover, New York: 1944.

Lure, A. I. Three-Dimensional Problems of the Theory of Elasticity. Interscience: 1964.

Martin, J. A., and Eberhardt, A. D. "Identification of Potential Failure Nuclei in Rolling Contact Fatigue." Journal of Basic Engineering, Trans. of the ASME, ser. D, 80 (1967): 932-42.

Muskhelishvili. Some Basic Problems of the Mathematical Theory of Elasticity. 2d ed. of English translation by J. R. M. Rodok, Gronigen Noordhoff, 1963.

Olesiak, Z. "Annular Punch on Elastic Semi-Space." Archum Mech. Stosow 17, no. 4 (1965): 633-42.

Parlas, S. C., and Michalpoulos, C. D. "Axisymmetric Contact Problem for an Elastic Half Space with a Cylindrical Hole." Int. J. of Engrg. Science 10 (1972): 699-707.

Persson, A. "On the Stress Distribution of Cyclinderical Elastic Bodies in Contact." Ph. D. dissertation, Chalmers Tekniska Hogskola, Goteborg, Sweden, 1964.

Singh, K. P. "Contact Stresses in Elastic Bodies with Arbitrary Profiles." Ph. D. dissertation, University of Pennsylvania, 1972.

_____. "On the Inadequacy of Hertzian Solution of Two-Dimensional Line Contact Problems." Journal of the Franklin Institute 298, no. 2 (August 1974).

Singh, K. P., and Paul, B. "A Method for Solving Ill-posed Integral Equations of the First Kind." Computer Methods in Applied Mechanics and Engineering 2 (1973): 339-48.

_____. "Numerical Solution of Non-Hertzian Elastic Contact Problems." Journal of Applied Mechanics 41, Trans. of the ASME 96, ser. E, 2 (1974): 484-96.

Singh, K. P.; Paul, B.; and Woodward, W. S. "Contact Stresses for Multiply Connected Regions--The Case of Pitted Spheres." IUTAM Symposium on the Mechanics of Contact between Deformable Bodies. Edited by J. J. Kalker and K. L. Johnson, Delft University Press, June 1975.

Sjtaerman, Ja. I. Kontaktnaja Zadatja Teorii Uprugosti. Moscow, 1944.

_____. "Local Deformation in Elastic Circular Cylinders with Nearly Equal Radii Under Pressure." Comptes Rendus (Doklady), de l'Académie des Sciences de l'URSS 29, no. 3 (1940).

Sokolnikoff, I. S. Mathematical Theory of Elasticity. New York: McGraw-Hill, 1956.

Sternberg, E., and Eubanks, R. A. "On the Singularity at a Concentrated Load Applied to a Curved Surface." Proceedings at the Second U. S. National Congress of Applied Mechanics. Ann Arbor, Michigan, June 1954.

Sternberg, E.; Eubanks, R. A.; and Sadowsky, M. A. "On the Anisymmetry Problem of Elasticity Theory for a Region Bounded by Two Concentric Spheres." Proceedings of the First U. S. National Congress of Applied Mechanics. Chicago, Ill., June 1951, pp. 209-15.

Sternberg, E., and Rosenthal, F. "The Elastic Sphere Under Concentrated Loads." Journal of Applied Mechanics 19 (1952): 413-21.

Tollian, T. E. "On Competing Failure Modes in Rolling Contact." ASLE Trans. 10, no. 4 (1967): 418-35.

Timoshenko, S. P., and Goodier, J. N. Theory of Elasticity. 3d ed. New York: McGraw-Hill, 1970.

* U.S. GOVERNMENT PRINTING OFFICE : 1977 0-728-664/1265

REQUEST FOR FEEDBACK TO
The DOT Program Of University Research

DOT-TST-77-48

YES	NO	
☐	☐	Did you find the report useful for your particular needs? If so, how?
☐	☐	Did you find the research to be of high quality?
☐	☐	Were the results of the research communicated effectively by this report?
☐	☐	Do you think this report will be valuable to workers in the field of transportation represented by the subject area of the research?
☐	☐	Are there one or more areas of the report which need strengthening? Which areas?
☐	☐	Would you be interested in receiving further reports in this area of research? If so, fill out form on other side.

Please furnish in the space below any comments you may have concerning the report. We are particularly interested in further elaboration of the above questions.

Cut Out Along This Line

COMMENTS

Thank you for your cooperation. No postage necessary if mailed in the U.S.A.

RESEARCH FEEDBACK

Your comments, please . . .

This booklet was published by the DOT Program of University Research and is intended to serve as a reference source for transportation analysts, planners, and operators. Your comments on the other side of this form will be reviewed by the persons responsible for writing and publishing this material. Feedback is extremely important in improving the quality of research results, the transfer of research information, and the communication link between the researcher and the user.

FOLD ON TWO LINES, STAPLE AND MAIL.

Fold Fold

DEPARTMENT OF TRANSPORTATION
OFFICE OF THE SECRETARY
Washington, D.C. 20590

Official Business

PENALTY FOR PRIVATE USE, $300

POSTAGE AND FEES PAID
DEPARTMENT OF
TRANSPORTATION
DOT 518

Office of University Research
Office of the Secretary (TST-60)
U.S. Department of Transportation
400 Seventh Street, S.W.
Washington, D.C. 20590

Fold Fold

IF YOU WISH TO BE ADDED TO THE MAIL LIST FOR FUTURE REPORTS, PLEASE FILL OUT THIS FORM.

Name _____ Title _____
Use Block Letters or Type

Department/Office/Room _____

Organization _____

Street Address _____

City _____ State _____ Zip _____

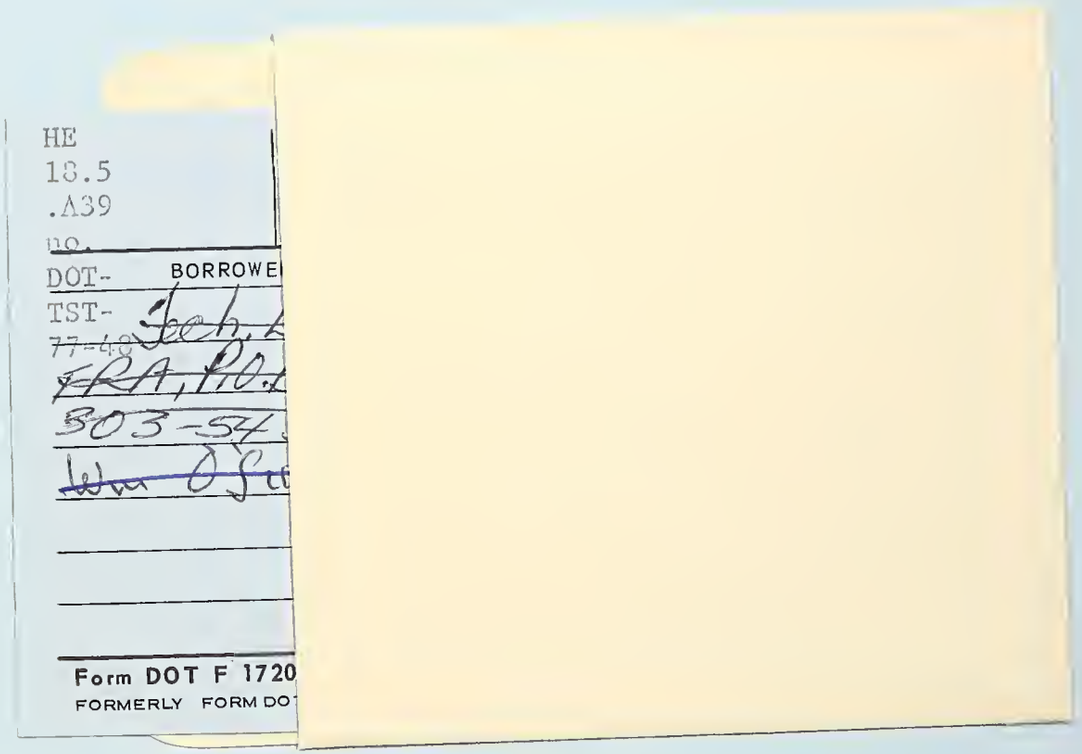

DEPARTMENT OF TRANSPORTATION
OFFICE OF THE SECRETARY
Washington, D.C. 20590

Official Business

PENALTY FOR PRIVATE USE, $300

DOT 518